The role of inclusions in ALS pathogenesis

De rol van eiwit inclusies in de ALS pathogenese

Proefschrift

Ter verkrijging van de graad van doctor aan de

Erasmus Universiteit Rotterdam

Op gezag van de rector magnificus

Prof. Dr. H.G. Schmidt

En volgens besluit van het college voor Promoties

De openbare verdediging zal plaatsvinden op

Woensdag 19 september 2012 om 15:30 uur

Door

Vera van Dis

Geboren te Rotterdam

Promotiecommissie:

Promotor:	Prof. Dr. C.I. de Zeeuw
	Prof. Dr. C.C. Hoogenraad
Overige leden:	Prof.dr. J.M. Kros
	Prof. dr. P.A.E. Sillevis Smitt
	Prof.dr. D.N. Meijer
Copromotor:	Dr. D. Jaarsma

Table of contents

Outline of this thesis

Amyotrophic lateral sclerosis (ALS) is a devastating neurodegenerative disease that primarily afflicts motor neurons, leading to paralysis and death within 3 to 5 years after diagnosis. Genetic studies have uncovered multiple genetic defects causing familial forms of ALS and mutations occurring in proteins with a variety of functions, including RNA metabolism (TDP43, FUS) and oxygen free radical homeostasis (SOD1). A commonality among all ALS forms is the presence of intracellular inclusions that primarily consist of insoluble protein aggregates. These inclusions indicate that protein aggregation is a central pathogenic event shared by multiple ALS forms. The research of the present thesis focuses on the role of protein aggregation and inclusion formation in two types of ALS: 1) ALS caused by mutations in the superoxide dismutase 1 (SOD1) gene (ALS1); and 2) ALS caused by mutations in the vesicle-associated membrane protein (VAMP)-associated protein B (VAPB) gene (ALS8).

Chapter 1 provides a general introduction on ALS. **Chapters 2-5** describe work done with SOD1-ALS mice, that develop an ALS-like disease. In **chapter 2** we show that inclusions consisting of aggregated mutant SOD1 are found in motor neurons as well as in other populations of neurons, in particular interneurons, albeit at a later time point. The data are compatible with the idea that protein aggregation retrogradely spreads from motor neurons to pre-motor neurons. In **chapter 3** we show that also astrocytes develop inclusions with aggregated SOD1 several weeks after the presence of inclusions in motor neurons. As in neurons, the presence of aggregates in astrocytes correlates with signs of cell death. To determine whether we could modify the age of first appearance of SOD1 inclusions in astrocytes by increasing proteotoxic stress, we crossed the SOD1-ALS mice with an astrocyte-specific tauopathy mouse model. This study showed that the burden of excessive levels of aggregation-prone tau did not influence the time of first appearance of SOD1-inclusions in astrocytes of SOD1-ALS mice. However, astrocytes in the double mutant mice showed an increase in both SOD1 and tau aggregation after the onset of motor neuron degeneration. The data indicate that pathology in astrocytes is secondary to pathology in motor neurons, and have a limited effect on disease progression.

In **chapter 4** we generated and characterized a transgenic mouse model with impaired retrograde axonal transport, and we crossed it with the SOD1-ALS mouse model. The mice with impaired retrograde axonal transport develop several pathological features also observed in ALS patients, but do not develop an ALS-like motor phenotype. Surprisingly, when crossed with SOD1-ALS mice, the retrograde axonal transport impairment prolonged survival in the double mutant mouse. In **chapter 5** we show that a dominant pathological hallmark of ALS, the fragmentation of the Golgi apparatus, may be linked to abnormalities in dynein-dynactin dependent trafficking, and precede many other 'early' changes in motor neurons observed in the SOD1-ALS mouse model.

In **chapter 6** we describe the generation and characterisation of transgenic mice carrying the P56S mutant form of VAPB, a small tail-anchored endoplasmatic reticulum (ER) membrane protein. Transgenic VAPB-P56S proteins develop atypical inclusions that contain smooth ER-like tubular profiles. However, despite the presence of multiple inclusions, VAPB-P56S mice do not show signs of motor neuron degeneration and muscle weakness. Instead, we obtained evidence that the VAPB inclusions represent neuroprotective structures, which concentrate ER associated degradation (ERAD).

Chapter 7 provides a general discussion of our findings on the following subjects: the role of trans-synaptic and cell-to-cell spreading of protein aggregation in ALS; the role of glial inclusions in the pathogenesis of ALS and other neurodegenerative diseases; the role of intracellular transport and sorting abnormalities in ALS pathogenesis; the role of ER stress and ER protein quality control in ALS.

The past years have shown that ALS is not a single disease, but an array of genetically, pathologically and clinically distinct disorders. The work of this thesis confirms the notion that the pathogenesis of each ALS form consist of a multifactorial process involving different cellular processes and multiple cell types that are afflicted in parallel or sequentially. Precise knowledge about the molecular and cellular deficits and the order of events will be instrumental for the design of therapeutic approaches.

General Introduction

1.1 Amyotrophic Lateral Sclerosis (ALS) is a neurodegenerative disease of motor neurons

Amyotrophic Lateral Sclerosis (ALS) is a progressive, late onset, neurodegenerative disease of motor neurons leading to paralysis of skeletal muscles and, eventually, death. The term amyotrophic lateral sclerosis indicates the combination of wasting of the muscle (amyotrophy) as a consequence of the degeneration of the α-motor neurons that innervate the skeletal muscles, and hardening of the lateral white matter of the spinal cord (lateral sclerosis), which is a consequence of the degeneration of the motor neurons in the motor cortex. Other names for ALS are Charcot's disease after the French neurologist who first described patients with ALS in 1869 (Kiernan et al., 2011), and Lou Gehrig disease after a USA baseball player who died of ALS in 1941, and motor neuron disease (Anon, 1990).

The diagnosis of ALS thus requires the degeneration of at least two populations of neurons of the motor system: 1) the α-motor neurons in the spinal cord and the brain stem that directly control the activity of muscle fibres, clinically termed lower motor neurons (LMN); and 2) neurons in the motor cortex that control the activity of the LMN, and that are termed upper motor neurons (UMN) (Lemon, 2008). Degeneration of LMN and UMN give rise to different symptoms: LMN symptoms are characterized by muscle weakness, muscle atrophy and fasciculations (small involuntary muscle contractions). UMN symptoms consist of increased muscle tone, spasticity, increased and altered reflexes, and slowness of movement (Körner et al., 2011). UMN symptoms also can be caused by degeneration of other neurons that control the activity of LMN, *i.e.* spinal interneurons and neuronal populations in the brain stem.

Symptoms usually start focally in one of the limbs, or the head and neck area (Ravits et al., 2007). Patients are grouped according to the area of onset, *i.e.* lumbar (legs), cervical (arm) or bulbar (head and neck). Patients with bulbar onset first develop problems with speech and swallowing; and patients with cervical onset start with problems in one of the hands. Usually, cervical onset patients have a shorter survival after diagnosis as compared to lumbar onset patients.

Patients also show variability in the proportion of LMN and UMN deficits. Multiple studies have questioned the relationship between UMN and LMN involvement with some studies favouring anterograde spread of pathology from UMN to LMN, and other studies favouring retrograde propagation from LMN to UMN, independent propagation of pathology in spinal cord and motor cortex, or a mixture of these events (Ravits and La Spada, 2009). The relative involvement of UMN versus LMN also may be different in different ALS forms. For instance, familial ALS caused by SOD1 mutations (ALS1, see below) is clinically known to be a LMN onset disorder (Andersen and Al-Chalabi, 2011). Accordingly, analysis of transgenic SOD1-ALS mice show that pathological changes occur first in LMN and subsequently in other populations of neurons favouring a retrograde model of disease propagation from LMN to premotor neurons (**See chapter 2**). Another finding from SOD1-ALS mice is that not all LMN are equally vulnerable: Thus the largest motor neurons innervating fast fatigable (FF) muscle fibres, are those that degenerate first, followed by smaller LMN that innervate fast fatigue-resistant (FR) fibres (Saxena et al., 2009). Instead,

smaller motor neurons that innervate slow (S) fibers are relatively spared. Data from SOD1-ALS mice also show that FR and S motor neurons display a considerable ability to reinnervate denervated muscle fibers and to compensate the initial loss of FF motor neurons (Williams et al., 2009).

ALS patients usually do not show sensory or cognitive deficits although pathological changes also may occur in non-motor areas (Geser et al., 2011). Indeed, subsets of patients develop signs of frontotemporal dementia (FTD). Furthermore, pathological and genetic evidence show a mechanistic relationship between ALS subtypes and FTD subtypes. In particular, abnormal expansion of a hexanucleotide repeat (GGGGCC) in the gene C9ORF72 has been recently shown to be the most common genetic cause of both ALS and FTD (DeJesus-Hernandez et al., 2011; Renton et al., 2011). In addition, TDP-43 inclusions are a dominant hallmark of most ALS and FTD patients (see below).

Currently, there are no effective treatment options for ALS. Riluzole, a drug with heterogeneous pharmacological properties that may inhibit neurotransmitter release, has been shown to lengthen survival by approximately 2 - 3 months, and may extend the time before a patient needs ventilation support (Miller et al., 2012). Other treatments are designed to relieve symptoms and improve the quality of life of patients, *e.g*. to ease muscle cramps and control spasticity (baclofen and diazepam), or reduce excess saliva and phlegm (trihexyphenidyl or amitriptyline).

1.2 Multiple causes of ALS

The incidence of ALS is between 0.6 and 2.4 per 100.000 per year, with a greater incidence among Caucasian compared to other ethnicities (Cronin et al., 2007). The disease generally affects adults over 40 years of age, peaking at 74 years. Men are affected slightly more than women (ratio 1.3). The mean survival time after disease onset is 32.6 months, ranging from 26.3 to 43.0 months (Worms, 2001; Cronin et al., 2007). Age of onset, region of onset and disease duration can vary between patients, even within one family (Ravits and La Spada, 2009).

Most ALS patients develop sporadic disease (sALS), *i.e.* without clear Mendelian inheritance, but in 10% the disease is familial (fALS), usually with autosomal-dominant inheritance (Andersen and Al-Chalabi, 2011). In 1993 the first genetic mutation for ALS was found in the gene encoding Cu/Zn superoxide dismutase 1 (SOD1) (Rosen et al., 1993). This is an ubiquitous expressed protein that catalyses the detoxification of superoxide radicals to oxygen and hydrogen peroxide**.**

Approximately 2.5-6 % of the ALS patients are affected by a mutation in the SOD1 gene. Little about the disease pathogenesis is understood, although many mouse models expressing mutant SOD1 have been developed to uncover some of the pathological mechanisms leading to motor neuron cell death.

Since the first discovery over 150 different mutations in the SOD1 gene have been discovered, mostly causing a single amino acid replacement, resulting in a missense phenotype. The SOD1 knock out mouse model does not develop motor neuron (MN) disease (Reaume et al., 1996), indicating that the disease is not caused by a loss of function mutation. It has been proposed that a gain of function would cause neuron toxicity, yet

there is no correlation between the pathology and the dismutase activity of the mutant SOD1 protein (Tiwari and Hayward, 2005; Turner and Talbot, 2008; Andersen and Al-Chalabi, 2011).
Different SOD1 mutations lead to different disease phenotypes. For example, the A4V mutation results in an aggressive neurodegenerative disease whereas the D90A mutation results in a slowly progressive low penetrant disease. Both in patients and in animal models, ubiquitinated aggregates of mutant SOD1 have been observed. Furthermore, mice overexpressing various forms of mutant SOD1 develop an ALS like phenotype resembling the human disease (Turner and Talbot, 2008).

Table 1.1 Major mutations causing ALS

	Gene	inheritence	(%) fALS	(%) sALS	gene function	known mutations	references
ALS/ FTD	C9 ORF72	AD ALS/FTD	39	7,6	unknown	expanded GGGGCC-repeat	1, 2
ALS 1	SOD1	AD adult typical ALS	20	2-	conversion of superoxide radicals	>150	3
ALS 10	TDP43	AD/AR ALS/FTD	5	1	DNA/RNA splicing etc	>40	4
ALS 6	FUS/ TLS	AD/AR typical ALS	4	1,5	DNA/RNA binding and transport, TDP43 homology	>30	5, 6

AD= Autosomal Dominant, AR=Autosomal Recessive. Reviewed by: (Andersen and Al-Chalabi, 2011; Ferraiuolo et al., 2011)
References: 1) DeJesus-Hernandez et al., 2011; 2) Renton et al., 2011; 3) Rosen et al., 1993; 4) Neumann et al., 2006; 5) Kwiatkowski et al., 2009; 6) Vance et al., 2009

Following SOD1, several other genes implicated in ALS were discovered (Table 1.1, 1,2 and 1.3). A milestone in ALS research was the discovery of Tar DNA-binding protein 43 (TDP-43) in inclusions of sALS and fALS patients (Neumann et al., 2006; Cohen et al., 2011). TDP43 is a protein localized in the nucleus, having an important role in RNA regulation. When pathological, it translocates to the cytoplasm where it forms ubiquitinated, hyperphosporylated aggregates of abnormally cleaved protein. In ALS patients, TDP-43 is deprived from the nucleus, suggesting a loss of function phenotype (Arai et al., 2006; Neumann et al., 2006). TDP43 aggregates were also detected in Alzheimer's disease, Lewy Body dementia, and Huntington's disease (table 1.4) (Baloh, 2011; van Blitterswijk et al., 2012). Some fALS families have TDP-43 mutations, which are all located at the c-terminal prion related domain (Wegorzewska and Baloh, 2011).
Transgenic TDP-43 overexpression (wildtype or mutant) is toxic to mouse models in a dose dependent manner, resulting in neurological abnormalities, and limited neuronal loss, mostly in cortical layer V neurons and spinal MN. However, the characteristic cytoplasmic TDP-43 inclusions are only rare in these mice (Joyce et al., 2011; Wegorzewska and Baloh, 2011), questioning the viability of these models as ALS disease models.
The Fused in Sarcoma/Translated in Lipoma (FUS/TLS) gene was found while screening for TDP-43 related genes (Kwiatkowski et al., 2009; Vance et al., 2009). Mutations in FUS/TLS are linked to other neurodegenerative diseases like FTD (table 1.1) (Andersen

and Al-Chalabi, 2011). Patient pathology is characterized by cytoplasmic ubiqutinated FUS/TLS inclusions. Overexpressing mutant FUS in rats results in a neurodegenerative phenotype characterized by ubiquitinated FUS positive aggregates (Huang et al., 2011), recapitulating some features of patients with ALS and FTD.

A recent major finding was the GGGGCC repeat expansion between intron 1 and 2 in the chromosome 9 open reading frame 72 (C9ORF72) gene, that was recently linked to ALS (DeJesus-Hernandez et al., 2011; Renton et al., 2011). It was found to cause up to 39% of fALS and 7.6% of sALS (Smith et al., 2012). Also this repeat is highly associated with FTD, and it is particularly found in patients with an ALS/FTD phenotype.

Other mutations are rare and result in non-classical ALS (Table 1.2 and 1.3). In 2002, a mutation is the Alsin gene was found (Yang et al., 2001). This protein is a guanine-nucleotide exchange factor for GTPases, involved in endosome trafficking.

Some mutations are involved in RNA processing: For example Angiogenin (Greenway et al., 2004), and senataxin (Chen et al., 2004), both associated with juvenile ALS. Others have a role in cellular trafficking. A mutation in the $P150^{glued}$ subunit of the dynein/dynactin complex, mediating minus end-directed transport (Münch et al., 2004), is also associated with LMN disease (Puls et al., 2003). Moreover, mutations in Vesicle-associated membrane protein (VAMP) – associated protein B (VAPB), an ER protein involved in membrane trafficking, are linked to ALS (Nishimura et al., 2004).

More recently, other mutations in small groups of patients were found to have a link with ALS pathogenesis (table 1.2 and 1.3). Mutations in Optineurin, a protein important in Golgi maintenance and membrane trafficking (Maruyama et al., 2010) and Polyphosphoinositide phosphatase 4 (FIG 4) mutations, a phosphoinositide 5-phosphatase, regulating PI(3,5)P2, a protein regulating trafficking of endosomal vesicles to the trans Golgi. Patients with mutations in this gene mostly develop corticospinal tract pathology and bulbar onset ALS (Chow et al., 2009).

Very recent a mutation in Profilin 1 was found. This gene is important in the conversion from (monomeric) G-actin to (filamentous) F-actin. Mutant Profilin 1 alters actin dynamics and inhibits axonal outhgrowth (Wu et al., 2012).

Another set of gene mutations are found in proteins involved in protein degradation pathways: ubiquilin 2, an ubiquitin like protein regulation protein degradation (Deng et al., 2011) and Valosin-containing protein (VCP), an AAA+-ATPase, extracting ubiquitin dependent substrates to the proteasome (Johnson et al., 2010).

An expanded repeat in the Ataxin 2 gene, a RNA helicase gene, is linked to ALS. Previously Ataxin 2 mutations were linked to spinocerebellar ataxia type 2 (SCA2), a disease characterized by cerebellar ataxia and slow saccades of the eye (Imbert et al., 1996; Pulst et al., 1996; Sanpei et al., 1996). More than 34 CAG repeats in this gene are linked to SCA2, whereas 24 and 34 repeats are linked to ALS. Normal repeat length is 22 or 23 repeats (Elden et al., 2010).

1.3 Inclusions and protein aggregation in ALS

ALS and other neurodegenerative diseases are characterized by insoluble aggregates of misfolded proteins. Examples are Alpha-synuclein deposits in Parkinson's

disease (Spillantini et al., 1997; Saiki et al., 2012), Beta-amyloid plaques in Alzheimer's disease (Anand et al., 2012; Goate and Hardy, 2012) and tau deposits in tauopathies such as Pick's disease, progressive supranuclear palsy, corticobasal degeneration, and Alzheimer's disease (Ittner et al., 2011).
Aggregates are observed in various shapes. Most of them can be double-labelled with ubiquitin, targeting misfolded proteins for degradation, or the ubiquitin-binding protein P62, which plays an important role in the proteasomal and/or autophagic clearance of misfolded and aggregation-prone proteins. Immunoreactivity for P62, however, not only characterizes pathological proteinaceous inclusions.

Table 1.2: ALS genes and risk factors

	gene	inheritence	(%) fALS	(%) sALS	gene function	known mutations	references
ALS 3	?	AD					
ALS 7	?	AD					
ALS 8	VAPB	AD heterogenous disease	<1	/	ER membrane protein	P56S and T26I	1,2
ALS 9	Angio-genin	AD typical ALS	<1	/	angiogenic factor	>15	3
ALS 14	VCP	AD typical ALS	1-2	<1	ER associated degragdation	5	4
ALS 13	Ataxin2	AD typical ALS	<1	<1	interaction with stress granule components	Expanded CAG repeat	5
ALS 11	FIG4	AD typical ALS	2	<1	phosphoinositide 5-phosphatase	10	6
ALS 5	Spatac-sin	AR juvenile slowly progressive			Unknowm	12	7

AD= Autosomal Dominant, AR=Autosomal Recessive. Reviewed by: (Andersen and Al-Chalabi, 2011; Ferraiuolo et al., 2011)
References: 1) Nishimura et al., 2004; 2) Chen et al., 2010; *3)* Greenway et al., 2004; 4) Johnson et al., 2010; 5) Elden et al., 2010; 6) Chow et al., 2009; 7) Orlacchio et al., 2010

Because mutations in SOD1 were first discovered, most research was done on this gene. Both post-mortem patient material and mutant SOD1 overexpressing mouse models show similar neuronal pathology (Turner and Talbot, 2008). Examples of inclusions found in ALS are: ubiquitinated, skein like aggregates, which are composed of loosly arranged filamentous material (figure 1.1A) and eosinophilic ubiquitin-negative bunina bodies (figure 1.1C), which are small eosinophilic inclusions, that are found in the cytoplasm of MN (Okamoto et al., 2008). And another form of inclusions seen in ALS are small round inclusion bodies or hyaline Lewy body like aggregates (figure 1.1B), consisting of large, round inclusions (Kato et al., 2001). Axonal spheroids are detected in the axon, consisting of accumulation of neurofilaments (King et al., 2011). Recently SOD1 positive aggregates were detected in sALS cases as well (Guareschi et al., 2012).

In other genetic forms of ALS similar pathological features have been described (table 1.5). However, there are subtle differences. In **chapter 2** and **chapter 3** we show that pathology usually starts in MNs and subsequently spreads to interneurons and glia. Different cell types develop different inclusions. Table 1.4 shows how one protein mutation can lead to different pathology in various diseases. Table 1.5 shows that beside neurons, also glial cells are often affected in ALS.

Astrogliosis and mutant SOD1 aggregates in astrocytes are found in late disease stages in mutant SOD1-ALS mice (**chapter 3**). However, their effect on disease progression is poorly understood.
How these aggregates affect the cell is not completely known. The cell can utilize various mechanisms against protein misfolding. One mechanism is ER stress. This process aims to properly fold the proteins and otherwise target the misfolded proteins for degradation by the ubiquitin proteasome pathways. Aggregates can overload the proteasome, which leads to inhibition of the proteasome and MN pathology, leading eventually to apoptosis (Urushitani et al., 2002; Kabashi et al., 2012).

Table 1.3: atypical ALS forms

	gene	inheritence	(%) FALS	(%) SALS	gene function	known mutations	references
ALS 2	ALSIN	AR juvenile, slowly progressive UMN	<1	/	GEF for Rab5 and Rac1	19	1
ALS 12	Optineurin	AD/AR relative slowly progressive	1-2	<0,5	membrane trafficking/golgi maintenance	5	2
ALS 4	Senataxin	AD juvenile, slowly progressive	<1	/	DNA/RNA metabolism	9	3
ALS	DCTN1	AD heterogenous disease	<1	/	dynein/dynactin subunit	3	4
ALS	Profillin 1	AD limb-onset ALS	?	?	Conversion of G-actin to F-actin	4	5
ALS	Ubiquilin	x-linked typical juvenile and adult ALS	<1	/	protein degradation	>5	6

AD= Autosomal Dominant, AR=Autosomal Recessive. Reviewed by: (Andersen and Al-Chalabi, 2011; Ferraiuolo et al., 2011)
References: 1) Yang et al., 2001; 2) Maruyama et al., 2010; 3) Chen et al., 2004; 4) Münch et al., 2004; 5) Wu et al., 2012; 6) Deng et al., 2011

Furthermore, the MN phenotype in SOD1-ALS-mouse models is correlated with the amount of mutant SOD1 aggregates (Turner and Talbot, 2008). Similar, in Alzheimer's disease a correlation between the amount of Amyloid β plaques and cognitive decline has been observed (Nelson et al., 2012), indicating that these aggregates are indeed a pathological feature of neurodegenerative disease.

In our mutant VAPB mice (**chapter 6)** it appears that the aggregates are of a different kind. These aggregates seem to be contained in an ER compartment, shielding the mutant VAPB from the rest of the cell (**chapter 6**). This is also true for other aggregate prone proteins. Miller and colleagues show that the amount of mutant Huntingtin inclusions, the causative gene of Huntington's disease, is related to the longer survival of cells, by reducing concentration of free mutant Huntingtin in the cytosol (Arrasate et al., 2004; Vukosavic et al., 1999; Nelson et al., 2012)

Table 1.4: TDP-43 pathology in neurodegenerative disease

disease	aggregate type	references
ALS	skein like, round and lewy-body like ubiquitin positive inclusions	1, 2, 3
Frontotemporal dementia	ubiquitin positive, tau negative. Pick bodies, lentiform, round and intranuclear inclusions	1, 2
Alzheimer's disease	cytoplasmic neurofibrillary tangles, lewy bodies, tau positive cytoplasmic inclusions	4, 5, 6 , 7
Corticobasal Dementia	thread or coil like structures	7, 8
Lewy-body dementia	cytosolic inclusions lewy bodies , α-synuclein positive	4, 5, 6
Huntington's disease	cytosolic inclusions.	9
Progressive supranuclear palsy	rounded inclusions and irregular shaped cytoplasmic inclusions	8
Parkinson's disease	cytoplasmic neurofibrillary tangles, lewy bodies.	7

References: 1) Arai et al., 2006; 2) Neumann et al., 2007; 3) Geser et al., 2008; 4) Amador-Ortiz et al., 2007; 5) Higashi et al., 2007; 6) Nakashima-Yasuda et al., 2007; 7) Uryu et al., 2008; 8) Yokota et al., 2010; 9) Schwab et al., 2008

1.4 Disrupted organelles in ALS

MN are very large neurons, with their axons reaching up to one meter in length. Therefore, active intracellular transport is very important. Looking closely at the disease models, we observe that the large neurons are the first affected, *e.g.* the fast fatigable neurons (Saxena et al., 2009).

Intracellular transport is a strictly regulated process. Microtubules in the axon are highly organized with their plus-tip towards the synapse and the minus end back towards the cell body. Anterograde axonal transport towards the plus tip of the microtubule, is regulated by a family of proteins called kinesins. Retrograde axonal transport, *i.e.* transport towards the minus end of the microtubule, is regulated by dynein motors in the dynein/dynactin complex. In neurodegenerative diseases a slowing of cellular transport has been described, either direct via a $p150^{glued}$ mutation (Münch et al., 2004), a subunit of the dynein/dynactin complex, or via other, unknown mechanisms. The slowing of intracellular transport is extensively described in SOD1 mouse models (De Vos et al., 2008).

In ALS the axonal transport is slowed, both in the anterograde and the retrograde direction. How this leads to MN disease is not entirely clear. Inhibiting retrograde transport using transgenic mice expressing the $P150^{glued}$ mutation G59S can induce MN disease (Puls et al.,

2003; Münch et al., 2004; Lai et al., 2007). Also mice with a targeted disruption of the retrograde transport develop MN disease (LaMonte et al., 2002; Hafezparast et al., 2003). However, as shown in **chapter 4**, transgenic animals with diminished retrograde trafficking do not necessarily develop MN cell death (Teuling et al., 2008). Furthermore, crossing a mouse model with a SOD1 mutation with a mouse model with impaired trafficking, results in a longer survival of the double transgenic animals (Kieran et al., 2005; Teuling et al., 2008).

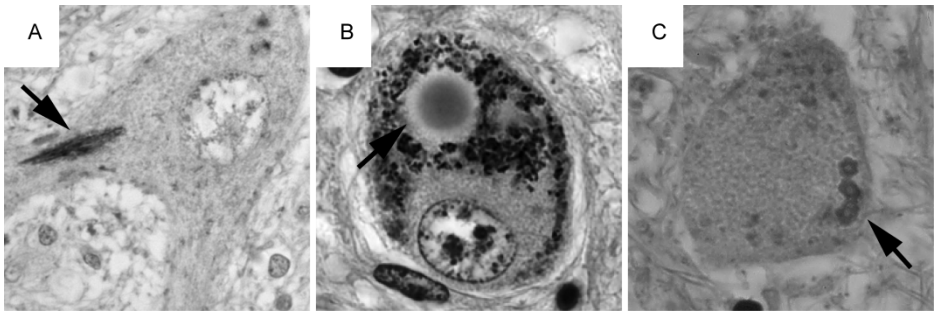

Figure 1.1; different types of inclusion bodies in ALS.
(A) A skein like inclusion (arrow). (B) Lewy body like inclusion (arrow) Also note the eccentric nuclei (C) Bunina bodies (arrow).

Cellular organelles are affected by neurodegenerative disease. For example, the Golgi apparatus (GA), that sorts and targets proteins from the endoplasmic reticulum (ER) to the cytosol and cell surface, will become fragmented. Proteins move through the GA from the cis-golgi site to the trans-golgi. During their transport through the GA, proteins are glycosylated, which probably has regulatory, folding, transport and sorting purposes. The shape of the GA depends on microtubules, microtubule depolymerization results in Golgi fragmentation (GF) (Burkhardt et al., 1997). Fragmentation of the GA, i.e. the transformation from a network of linear profiles to dispersed smaller elements, is a major feature in motor neurons of ALS patients and SOD1-ALS mice (Mourelatos et al., 1990, 1994, 1996; Gonatas et al., 1992; Stieber et al., 2000). GF is also correlated with TDP-43 aggregation and redistribution from the nucleus to cytoplasm (Fujita et al., 2008). To understand this phenotype we tried to link GF to other pathological features of the mutant SOD1 mouse model in **chapter 5.** We found that cells with GF are able to transport the beta subunit of cholera toxin, retrograde to the cell soma. Furthermore we observed increased GF when retrograde transport is inhibited.
Another organelle affected in ALS is the ER. Which is responsible for the proper folding of proteins. Protein misfolding induces ER stress, the unfolded protein response. The aim of this process is to suppress further protein translation and induce ER chaperones to assist in protein folding. If this fails, it results in apoptosis. ER associated degradation (ERAD) is a process where the misfolded proteins are targeted and transported to the cytosol towards the proteasome for degradation (Kanekura et al., 2009). It is shown that mutant SOD1 can induce ER stress in the area of MN degeneration (Kikuchi et al., 2006). The ER membrane

protein VAPB was first linked to ALS in a Brazilian family (Nishimura et al., 2004). VAPB is a member of the VAP proteins (VAMP associated proteins) (Skehel et al., 1995), consisting of VAPA, VAPB and VAPC (Nishimura et al., 1999). VAPB is 60% homologous to VAPA. VAPC is a splice variant of VAPB, lacking the TMD and the coiled coil. VAPB is believed to function in binding two phenylalanines in an acidic tract (FFAT-motif) (Loewen and Levine, 2005), neurotransmitter release (Skehel et al., 1995), neuromuscular junction formation (Pennetta et al., 2002), and ER stress pathways (Kanekura et al., 2006).

Table 1.5: aggregate morphology in ALS

protein	Aggregates	primary constituent	Ubi-quitin	Glia	remarks	references
SOD1	skeins, bunina bodies, hyaline lewy body like, axonal spheroids	SOD1	+	+	UMN <LMN	1, 2, 3, 4
TDP43	cytoplasmic skeins, dense round inclusions. Rarely intranuclear inclusions	TDP-43	+	+ curved or bullit shaped	linked with FTD and sporadic ALS	5, 6, 7
C9ORF72	granular, filamentous or compact Lewy-body like	TDP-43	+	+	linked with FTD/ALS and sporadic ALS	8, 9, 10, 11
FUS/TLS	basophilic inclusion bodies in the cytosol	FUS/TLS	+	+	Juvenile diseae onset: round FUS inclusions. Adult onset disease: tangles and oligendendrocyte inclusions	12
VAPB	insoluble round inclusions	VAPB?	+	?	heterogenoous disease	13, 14
sporadic ALS no known causative gene	bunina bodies, lewy-hyaline and skein like inclusions	TDP-43, optineurin	+	+		15, 16, 17
VCP	bunina bodies	TDP-43	+	?	heterogenous disease	18
Optineurin	round, skein like and lewy body like inclusions	TDP-43	+	+		15
FIG4	cytoplasmic inclusions	LC3-II, p62, LAMP-2	+	+	cognitive defects	19, 20
Ataxin 2	skeins, filamentous inclusions	TDP-43	+	?		21
Ubiquilin	compact skein like inclusions	TDP-3, p62, FUS, optineurin	+	?		22, 23, 24
Senataxin	axonal speroids	SMI-32	+	?	young onset, slowly progressive	25

table continues on next page

Table 1.5: aggregate morphology in ALS; continued						
protein	Aggregates	primary constituent	Ubi-quitin	Glia	Remarks	references
ALSIN	?	?	?	?	UMN>LMN young onset, slowly progressive	26
spatacsin	round hyaline inclusion	?	?	?		27
Angio-genin	skein like inclusions in the cytoplasm and nucleus	cytoplasm: TDP-43, nuclear: angiogenin	+	+		28

Review by (Andersen and Al-Chalabi, 2011)

References: 1) Leigh et al., 1991; 2) Okamoto et al., 1993; 3) Okamoto et al., 2008; 4) Kato et al., 1997; 5) Arai et al., 2006; 6) Neumann et al., 2007; 7) Geser et al., 2011; 8) Al-Sarraj et al., 2011; 9) Bigio et al., 2012; 10) Brettschneider et al., 2012; 11) Hsiung et al., 2012; 12) Mackenzie et al., 2011; 13) Nishihira et al., 2008;14) Chen et al., 2010; 15) Hortobágyi et al., 2011; 16) Sasaki, 2011; 17) Stewart et al., 2012; 18) Johnson et al., 2010; 19) Chen et al., 2004; 20) Ferguson et al., 2009; 21) Hart et al., 2012; 22) Deng et al., 2011; 23) Brettschneider et al., 2012; 24) Williams et al., 2012; 25) (Rabin et al., 1999; 26) Yang et al., 2001; 27) Orlacchio et al., 2010; 28) Seilhean et al., 2009

Mutant VAPB aggregates are present in disorganized stretches of ER in vitro and in animal models. Their pathological role is not yet determined. In **chapter 6** we describe the actions of mutant VAPB in MN of transgenic mice overexpressing mutant VAPB specifically in neurons. The mutant VAPB overexpressing mice developed characteristic ER aggregates that include endogenous VAPB in a dominant-negative manner (Teuling et al., 2007). However a minority of mice developed signs of muscle weakness: in their MN we observed that the ER aggregates disappeared. Further testing using ERAD markers led us to belief the mutant VAPB aggregates are a protective cluster of ER.

References

Al-Sarraj S, King A, Troakes C, Smith B, Maekawa S, Bodi I, Rogelj B, Al-Chalabi A, Hortobágyi T, Shaw CE (2011) p62 positive, TDP-43 negative, neuronal cytoplasmic and intranuclear inclusions in the cerebellum and hippocampus define the pathology of C9orf72-linked FTLD and MND/ALS. Acta neuropathologica 122:691–702.

Amador-Ortiz C, Lin W-L, Ahmed Z, Personett D, Davies P, Duara R, Graff-Radford NR, Hutton ML, Dickson DW (2007) TDP-43 immunoreactivity in hippocampal sclerosis and Alzheimer's disease. Annals of neurology 61:435–445.

Anand R, Kaushal A, Wani WY, Gill KD (2012) Road to Alzheimer's disease: the pathomechanism underlying. Pathobiology : journal of immunopathology, molecular and cellular biology 79:55–71.

Andersen PM, Al-Chalabi A (2011) Clinical genetics of amyotrophic lateral sclerosis: what do we really know? Nature reviews Neurology 7:603–615.

Anon (1990) Dementia and motoneurone disease. Lancet 335:1250–1252.

Arai T, Hasegawa M, Akiyama H, Ikeda K, Nonaka T, Mori H, Mann D, Tsuchiya K, Yoshida M, Hashizume Y, Oda T (2006) TDP-43 is a component of ubiquitin-positive tau-negative inclusions in frontotemporal lobar degeneration and amyotrophic lateral sclerosis. Biochemical and biophysical research communications 351:602–611.

Arrasate M, Mitra S, Schweitzer ES, Segal MR, Finkbeiner S (2004) Inclusion body formation reduces levels of mutant huntingtin and the risk of neuronal death. Nature 431:805–810

Baloh RH (2011) TDP-43: the relationship between protein aggregation and neurodegeneration in amyotrophic lateral sclerosis and frontotemporal lobar degeneration. The FEBS journal 278:3539–3549.

Bigio EH, Weintraub S, Rademakers R, Baker M, Ahmadian SS, Rademaker A, Weitner BB, Mao Q, Lee K-H, Mishra M, Ganti RA, Mesulam M-M (2012) Frontotemporal lobar degeneration with TDP-43

proteinopathy and chromosome 9p repeat expansion in C9ORF72: clinicopathologic correlation. Neuropathology : official journal of the Japanese Society of Neuropathology.

Brettsc3hneider J, Van Deerlin VM, Robinson JL, Kwong L, Lee EB, Ali YO, Safren N, Monteiro MJ, Toledo JB, Elman L, McCluskey L, Irwin DJ, Grossman M, Molina-Porcel L, Lee VM-Y, Trojanowski JQ (2012) Pattern of ubiquilin pathology in ALS and FTLD indicates presence of C9ORF72 hexanucleotide expansion. Acta neuropathologica 123:825–839.

Burkhardt JK, Echeverri CJ, Nilsson T, Vallee RB (1997) Overexpression of the dynamitin (p50) subunit of the dynactin complex disrupts dynein-dependent maintenance of membrane organelle distribution. The Journal of cell biology 139:469–484.

Chen H-J, Anagnostou G, Chai A, Withers J, Morris A, Adhikaree J, Pennetta G, de Belleroche JS (2010) Characterization of the properties of a novel mutation in VAPB in familial amyotrophic lateral sclerosis. The Journal of biological chemistry 285:40266–40281.

Chen Y-Z, Bennett CL, Huynh HM, Blair IP, Puls I, Irobi J, Dierick I, Abel A, Kennerson ML, Rabin BA, Nicholson GA, Auer-Grumbach M, Wagner K, De Jonghe P, Griffin JW, Fischbeck KH, Timmerman V, Cornblath DR, Chance PF (2004) DNA/RNA helicase gene mutations in a form of juvenile amyotrophic lateral sclerosis (ALS4). American journal of human genetics 74:1128–1135.

Chow CY, Landers JE, Bergren SK, Sapp PC, Grant AE, Jones JM, Everett L, Lenk GM, McKenna-Yasek DM, Weisman LS, Figlewicz D, Brown RH, Meisler MH (2009) Deleterious variants of FIG4, a phosphoinositide phosphatase, in patients with ALS. American journal of human genetics 84:85–88.

Cohen TJ, Lee VMY, Trojanowski JQ (2011) TDP-43 functions and pathogenic mechanisms implicated in TDP-43 proteinopathies. Trends in molecular medicine 17:659–667.

Cronin S, Hardiman O, Traynor BJ (2007) Ethnic variation in the incidence of ALS: a systematic review. Neurology 68:1002–1007.

De Vos KJ, Grierson AJ, Ackerley S, Miller CCJ (2008) Role of axonal transport in neurodegenerative diseases. Annual review of neuroscience 31:151–173.

DeJesus-Hernandez M et al. (2011) Expanded GGGGCC hexanucleotide repeat in noncoding region of C9ORF72 causes chromosome 9p-linked FTD and ALS. Neuron 72:245–256.

Deng H-X et al. (2011) Mutations in UBQLN2 cause dominant X-linked juvenile and adult-onset ALS and ALS/dementia. Nature 477:211–215.

Elden AC et al. (2010) Ataxin-2 intermediate-length polyglutamine expansions are associated with increased risk for ALS. Nature 466:1069–1075.

Ferguson CJ, Lenk GM, Meisler MH (2009) Defective autophagy in neurons and astrocytes from mice deficient in PI(3,5)P2. Human molecular genetics 18:4868–4878.

Ferraiuolo L, Kirby J, Grierson AJ, Sendtner M, Shaw PJ (2011) Molecular pathways of motor neuron injury in amyotrophic lateral sclerosis. Nature reviews Neurology 7:616–630.

Fujita Y, Mizuno Y, Takatama M, Okamoto K (2008) Anterior horn cells with abnormal TDP-43 immunoreactivities show fragmentation of the Golgi apparatus in ALS. Journal of the neurological sciences 269:30–34.

Geser F, Brandmeir NJ, Kwong LK, Martinez-Lage M, Elman L, McCluskey L, Xie SX, Lee VM-Y, Trojanowski JQ (2008) Evidence of multisystem disorder in whole-brain map of pathological TDP-43 in amyotrophic lateral sclerosis. Archives of neurology 65:636–641.

Geser F, Stein B, Partain M, Elman LB, McCluskey LF, Xie SX, Van Deerlin VM, Kwong LK, Lee VM-Y, Trojanowski JQ (2011) Motor neuron disease clinically limited to the lower motor neuron is a diffuse TDP-43 proteinopathy. Acta neuropathologica 121:509–517.

Goate A, Hardy J (2012) Twenty years of Alzheimer's disease-causing mutations. Journal of neurochemistry 120 Suppl 1:3–8.

Gonatas NK, Stieber A, Mourelatos Z, Chen Y, Gonatas JO, Appel SH, Hays AP, Hickey WF, Hauw JJ (1992) Fragmentation of the Golgi apparatus of motor neurons in amyotrophic lateral sclerosis. The American journal of pathology 140:731–737.

Greenway MJ, Alexander MD, Ennis S, Traynor BJ, Corr B, Frost E, Green A, Hardiman O (2004) A novel candidate region for ALS on chromosome 14q11.2. Neurology 63:1936–1938.

Guareschi S, Cova E, Cereda C, Ceroni M, Donetti E, Bosco DA, Trotti D, Pasinelli P (2012) An over-oxidized form of superoxide dismutase found in sporadic amyotrophic lateral sclerosis with bulbar onset shares a toxic mechanism with mutant SOD1. Proceedings of the National Academy of Sciences of the United States of America 109:5074–5079.

Hafezparast M et al. (2003) Mutations in dynein link motor neuron degeneration to defects in retrograde transport. Science (New York, NY) 300:808–812.

Hart MP, Brettschneider J, Lee VMY, Trojanowski JQ, Gitler AD (2012) Distinct TDP-43 pathology in ALS patients with ataxin 2 intermediate-length polyQ expansions. Acta neuropathologica 124:221–230.

Higashi S, Iseki E, Yamamoto R, Minegishi M, Hino H, Fujisawa K, Togo T, Katsuse O, Uchikado H, Furukawa Y, Kosaka K, Arai H (2007) Concurrence of TDP-43, tau and alpha-synuclein pathology in brains of Alzheimer's disease and dementia with Lewy bodies. Brain research 1184:284–294.

Hortobágyi T, Troakes C, Nishimura AL, Vance C, van Swieten JC, Seelaar H, King A, Al-Sarraj S, Rogelj B, Shaw CE (2011) Optineurin inclusions occur in a minority of TDP-43 positive ALS and FTLD-TDP cases and are rarely observed in other neurodegenerative disorders. Acta neuropathologica 121:519–527.

Hsiung G-YR, DeJesus-Hernandez M, Feldman HH, Sengdy P, Bouchard-Kerr P, Dwosh E, Butler R, Leung B, Fok A, Rutherford NJ, Baker M, Rademakers R, Mackenzie IRA (2012) Clinical and pathological features of familial frontotemporal dementia caused by C9ORF72 mutation on chromosome 9p. Brain : a journal of neurology 135:709–722.

Huang C, Zhou H, Tong J, Chen H, Liu Y-J, Wang D, Wei X, Xia X-G (2011) FUS transgenic rats develop the phenotypes of amyotrophic lateral sclerosis and frontotemporal lobar degeneration. PLoS genetics 7:e1002011.

Imbert G, Saudou F, Yvert G, Devys D, Trottier Y, Garnier JM, Weber C, Mandel JL, Cancel G, Abbas N, Dürr A, Didierjean O, Stevanin G, Agid Y, Brice A (1996) Cloning of the gene for spinocerebellar ataxia 2 reveals a locus with high sensitivity to expanded CAG/glutamine repeats. Nature genetics 14:285–291.

Ittner A, Ke YD, van Eersel J, Gladbach A, Götz J, Ittner LM (2011) Brief update on different roles of tau in neurodegeneration. IUBMB life 63:495–502.

Johnson JO et al. (2010) Exome sequencing reveals VCP mutations as a cause of familial ALS. Neuron 68:857–864.

Joyce PI, Fratta P, Fisher EMC, Acevedo-Arozena A (2011) SOD1 and TDP-43 animal models of amyotrophic lateral sclerosis: recent advances in understanding disease toward the development of clinical treatments. Mammalian genome : official journal of the International Mammalian Genome Society 22:420–448.

Kabashi E, Agar JN, Strong MJ, Durham HD (2012) Impaired proteasome function in sporadic amyotrophic lateral sclerosis. Amyotrophic lateral sclerosis : official publication of the World Federation of Neurology Research Group on Motor Neuron Diseases 13:367–371.

Kanekura K, Nishimoto I, Aiso S, Matsuoka M (2006) Characterization of amyotrophic lateral sclerosis-linked P56S mutation of vesicle-associated membrane protein-associated protein B (VAPB/ALS8). The Journal of biological chemistry 281:30223–30233.

Kanekura K, Suzuki H, Aiso S, Matsuoka M (2009) ER stress and unfolded protein response in amyotrophic lateral sclerosis. Molecular neurobiology 39:81–89.

Kato S, Hayashi H, Nakashima K, Nanba E, Kato M, Hirano A, Nakano I, Asayama K, Ohama E (1997) Pathological characterization of astrocytic hyaline inclusions in familial amyotrophic lateral sclerosis. The American journal of pathology 151:611–620.

Kato S, Sumi-Akamaru H, Fujimura H, Sakoda S, Kato M, Hirano A, Takikawa M, Ohama E (2001) Copper chaperone for superoxide dismutase co-aggregates with superoxide dismutase 1 (SOD1) in neuronal Lewy body-like hyaline inclusions: an immunohistochemical study on familial amyotrophic lateral sclerosis with SOD1 gene mutation. Acta neuropathologica 102:233–238.

Kieran D, Hafezparast M, Bohnert S, Dick JRT, Martin J, Schiavo G, Fisher EMC, Greensmith L (2005) A mutation in dynein rescues axonal transport defects and extends the life span of ALS mice. The Journal of cell biology 169:561–567.

Kiernan MC, Vucic S, Cheah BC, Turner MR, Eisen A, Hardiman O, Burrell JR, Zoing MC (2011) Amyotrophic lateral sclerosis. Lancet 377:942–955.

Kikuchi H, Almer G, Yamashita S, Guégan C, Nagai M, Xu Z, Sosunov AA, McKhann GM, Przedborski S (2006) Spinal cord endoplasmic reticulum stress associated with a microsomal accumulation of mutant superoxide dismutase-1 in an ALS model. Proceedings of the National Academy of Sciences of the United States of America 103:6025–6030.

King AE, Dickson TC, Blizzard CA, Woodhouse A, Foster SS, Chung RS, Vickers JC (2011) Neuron-glia interactions underlie ALS-like axonal cytoskeletal pathology. Neurobiology of aging 32:459–469.

Körner S, Kollewe K, Fahlbusch M, Zapf A, Dengler R, Krampfl K, Petri S (2011) Onset and spreading patterns of upper and lower motor neuron symptoms in amyotrophic lateral sclerosis. Muscle & nerve 43:636–642.

Kwiatkowski TJ et al. (2009) Mutations in the FUS/TLS gene on chromosome 16 cause familial amyotrophic lateral sclerosis. Science (New York, NY) 323:1205–1208.

Lai C, Lin X, Chandran J, Shim H, Yang W-J, Cai H (2007) The G59S mutation in p150(glued) causes dysfunction of dynactin in mice. The Journal of neuroscience : the official journal of the Society for Neuroscience 27:13982–13990.

LaMonte BH, Wallace KE, Holloway BA, Shelly SS, Ascaño J, Tokito M, Van Winkle T, Howland DS, Holzbaur ELF (2002) Disruption of dynein/dynactin inhibits axonal transport in motor neurons causing late-onset progressive degeneration. Neuron 34:715–727.

Leigh PN, Whitwell H, Garofalo O, Buller J, Swash M, Martin JE, Gallo JM, Weller RO, Anderton BH (1991) Ubiquitin-immunoreactive intraneuronal inclusions in amyotrophic lateral sclerosis. Morphology, distribution, and specificity. Brain : a journal of neurology 114 (Pt 2):775–788.

Lemon RN (2008) Descending pathways in motor control. Annual review of neuroscience 31:195–218.

Loewen CJR, Levine TP (2005) A highly conserved binding site in vesicle-associated membrane protein-associated protein (VAP) for the FFAT motif of lipid-binding proteins. The Journal of biological chemistry 280:14097–14104.

Mackenzie IRA, Ansorge O, Strong M, Bilbao J, Zinman L, Ang L-C, Baker M, Stewart H, Eisen A, Rademakers R, Neumann M (2011) Pathological heterogeneity in amyotrophic lateral sclerosis with FUS mutations: two distinct patterns correlating with disease severity and mutation. Acta neuropathologica 122:87–98.

Maruyama H et al. (2010) Mutations of optineurin in amyotrophic lateral sclerosis. Nature 465:223–226.

Miller RG, Mitchell JD, Moore DH (2012) Riluzole for amyotrophic lateral sclerosis (ALS)/motor neuron disease (MND). Cochrane database of systematic reviews (Online) 3:CD001447.

Mourelatos Z, Adler H, Hirano A, Donnenfeld H, Gonatas JO, Gonatas NK (1990) Fragmentation of the Golgi apparatus of motor neurons in amyotrophic lateral sclerosis revealed by organelle-specific antibodies. Proceedings of the National Academy of Sciences of the United States of America 87:4393–4395.

Mourelatos Z, Gonatas NK, Stieber A, Gurney ME, Dal Canto MC (1996) The Golgi apparatus of spinal cord motor neurons in transgenic mice expressing mutant Cu,Zn superoxide dismutase becomes fragmented in early, preclinical stages of the disease. Proceedings of the National Academy of Sciences of the United States of America 93:5472–5477.

Mourelatos Z, Hirano A, Rosenquist AC, Gonatas NK (1994) Fragmentation of the Golgi apparatus of motor neurons in amyotrophic lateral sclerosis (ALS). Clinical studies in ALS of Guam and experimental studies in deafferented neurons and in beta,beta'-iminodipropionitrile axonopathy. The American journal of pathology 144:1288–1300.

Münch C, Sedlmeier R, Meyer T, Homberg V, Sperfeld AD, Kurt A, Prudlo J, Peraus G, Hanemann CO, Stumm G, Ludolph AC (2004) Point mutations of the p150 subunit of dynactin (DCTN1) gene in ALS. Neurology 63:724–726.

Nakashima-Yasuda H et al. (2007) Co-morbidity of TDP-43 proteinopathy in Lewy body related diseases. Acta neuropathologica 114:221–229.

Nelson PT et al. (2012) Correlation of Alzheimer disease neuropathologic changes with cognitive status: a review of the literature. Journal of neuropathology and experimental neurology 71:362–381.

Neumann M, Kwong LK, Truax AC, Vanmassenhove B, Kretzschmar HA, Van Deerlin VM, Clark CM, Grossman M, Miller BL, Trojanowski JQ, Lee VM-Y (2007) TDP-43-positive white matter pathology in frontotemporal lobar degeneration with ubiquitin-positive inclusions. Journal of neuropathology and experimental neurology 66:177–183.

Neumann M, Sampathu DM, Kwong LK, Truax AC, Micsenyi MC, Chou TT, Bruce J, Schuck T, Grossman M, Clark CM, McCluskey LF, Miller BL, Masliah E, Mackenzie IR, Feldman H, Feiden W, Kretzschmar HA, Trojanowski JQ, Lee VM-Y (2006) Ubiquitinated TDP-43 in frontotemporal lobar degeneration and amyotrophic lateral sclerosis. Science (New York, NY) 314:130–133.

Nishihira Y, Tan C-F, Onodera O, Toyoshima Y, Yamada M, Morita T, Nishizawa M, Kakita A, Takahashi H (2008) Sporadic amyotrophic lateral sclerosis: two pathological patterns shown by analysis of distribution of TDP-43-immunoreactive neuronal and glial cytoplasmic inclusions. Acta neuropathologica 116:169–182.

Nishimura AL, Mitne-Neto M, Silva HCA, Richieri-Costa A, Middleton S, Cascio D, Kok F, Oliveira JRM, Gillingwater T, Webb J, Skehel P, Zatz M (2004) A mutation in the vesicle-trafficking protein VAPB causes late-onset spinal muscular atrophy and amyotrophic lateral sclerosis. American journal of human genetics 75:822–831.

Nishimura Y, Hayashi M, Inada H, Tanaka T (1999) Molecular cloning and characterization of mammalian homologues of vesicle-associated membrane protein-associated (VAMP-associated) proteins. Biochemical and biophysical research communications 254:21–26.

Okamoto K, Hirai S, Amari M, Watanabe M, Sakurai A (1993) Bunina bodies in amyotrophic lateral sclerosis immunostained with rabbit anti-cystatin C serum. Neuroscience letters 162:125–128.

Okamoto K, Mizuno Y, Fujita Y (2008) Bunina bodies in amyotrophic lateral sclerosis. Neuropathology : official journal of the Japanese Society of Neuropathology 28:109–115.

Orlacchio A, Babalini C, Borreca A, Patrono C, Massa R, Basaran S, Munhoz RP, Rogaeva EA, St George-Hyslop PH, Bernardi G, Kawarai T (2010) SPATACSIN mutations cause autosomal recessive juvenile amyotrophic lateral sclerosis. Brain : a journal of neurology 133:591–598.

Pennetta G, Hiesinger PR, Fabian-Fine R, Meinertzhagen IA, Bellen HJ (2002) Drosophila VAP-33A directs bouton formation at neuromuscular junctions in a dosage-dependent manner. Neuron 35:291–306.

Puls I, Jonnakuty C, LaMonte BH, Holzbaur ELF, Tokito M, Mann E, Floeter MK, Bidus K, Drayna D, Oh SJ, Brown RH, Ludlow CL, Fischbeck KH (2003) Mutant dynactin in motor neuron disease. Nature genetics 33:455–456.

Pulst SM, Nechiporuk A, Nechiporuk T, Gispert S, Chen XN, Lopes-Cendes I, Pearlman S, Starkman S, Orozco-Diaz G, Lunkes A, DeJong P, Rouleau GA, Auburger G, Korenberg JR, Figueroa C, Sahba S

(1996) Moderate expansion of a normally biallelic trinucleotide repeat in spinocerebellar ataxia type 2. Nature genetics 14:269–276.
Rabin BA, Griffin JW, Crain BJ, Scavina M, Chance PF, Cornblath DR (1999) Autosomal dominant juvenile amyotrophic lateral sclerosis. Brain : a journal of neurology 122 (Pt 8):1539–1550.
Ravits J, Paul P, Jorg C (2007) Focality of upper and lower motor neuron degeneration at the clinical onset of ALS. Neurology 68:1571–1575.
Ravits JM, La Spada AR (2009) ALS motor phenotype heterogeneity, focality, and spread: deconstructing motor neuron degeneration. Neurology 73:805–811.
Reaume AG, Elliott JL, Hoffman EK, Kowall NW, Ferrante RJ, Siwek DF, Wilcox HM, Flood DG, Beal MF, Brown RH, Scott RW, Snider WD (1996) Motor neurons in Cu/Zn superoxide dismutase-deficient mice develop normally but exhibit enhanced cell death after axonal injury. Nature genetics 13:43–47.
Renton AE et al. (2011) A hexanucleotide repeat expansion in C9ORF72 is the cause of chromosome 9p21-linked ALS-FTD. Neuron 72:257–268.
Rosen DR, Siddique T, Patterson D, Figlewicz DA, Sapp P, Hentati A, Donaldson D, Goto J, O'Regan JP, Deng HX (1993) Mutations in Cu/Zn superoxide dismutase gene are associated with familial amyotrophic lateral sclerosis. Nature 362:59–62.
Saiki S, Sato S, Hattori N (2012) Molecular pathogenesis of Parkinson's disease: update. Journal of neurology, neurosurgery, and psychiatry 83:430–436.
Sanpei K et al. (1996) Identification of the spinocerebellar ataxia type 2 gene using a direct identification of repeat expansion and cloning technique, DIRECT. Nature genetics 14:277–284.
Sasaki S (2011) Autophagy in spinal cord motor neurons in sporadic amyotrophic lateral sclerosis. Journal of neuropathology and experimental neurology 70:349–359.
Saxena S, Cabuy E, Caroni P (2009) A role for motoneuron subtype-selective ER stress in disease manifestations of FALS mice. Nature neuroscience 12:627–636.
Schwab C, Arai T, Hasegawa M, Yu S, McGeer PL (2008) Colocalization of transactivation-responsive DNA-binding protein 43 and huntingtin in inclusions of Huntington disease. Journal of neuropathology and experimental neurology 67:1159–1165.
Seilhean D, Cazeneuve C, Thuriès V, Russaouen O, Millecamps S, Salachas F, Meininger V, Leguern E, Duyckaerts C (2009) Accumulation of TDP-43 and alpha-actin in an amyotrophic lateral sclerosis patient with the K17I ANG mutation. Acta neuropathologica 118:561–573.
Skehel PA, Martin KC, Kandel ER, Bartsch D (1995) A VAMP-binding protein from Aplysia required for neurotransmitter release. Science (New York, NY) 269:1580–1583.
Smith BN et al. (2012) The C9ORF72 expansion mutation is a common cause of ALS+/-FTD in Europe and has a single founder. European journal of human genetics : EJHG.
Spillantini MG, Schmidt ML, Lee VM, Trojanowski JQ, Jakes R, Goedert M (1997) Alpha-synuclein in Lewy bodies. Nature 388:839–840.
Stewart H, Rutherford NJ, Briemberg H, Krieger C, Cashman N, Fabros M, Baker M, Fok A, DeJesus-Hernandez M, Eisen A, Rademakers R, Mackenzie IRA (2012) Clinical and pathological features of amyotrophic lateral sclerosis caused by mutation in the C9ORF72 gene on chromosome 9p. Acta neuropathologica 123:409–417.
Stieber A, Gonatas JO, Collard J, Meier J, Julien J, Schweitzer P, Gonatas NK (2000) The neuronal Golgi apparatus is fragmented in transgenic mice expressing a mutant human SOD1, but not in mice expressing the human NF-H gene. Journal of the neurological sciences 173:63–72.
Teuling E, Ahmed S, Haasdijk E, Demmers J, Steinmetz MO, Akhmanova A, Jaarsma D, Hoogenraad CC (2007) Motor neuron disease-associated mutant vesicle-associated membrane protein-associated protein (VAP) B recruits wild-type VAPs into endoplasmic reticulum-derived tubular aggregates. The Journal of neuroscience : the official journal of the Society for Neuroscience 27:9801–9815.
Teuling E, van Dis V, Wulf PS, Haasdijk ED, Akhmanova A, Hoogenraad CC, Jaarsma D (2008) A novel mouse model with impaired dynein/dynactin function develops amyotrophic lateral sclerosis (ALS)-like features in motor neurons and improves lifespan in SOD1-ALS mice. Human molecular genetics 17:2849–2862.
Tiwari A, Hayward LJ (2005) Mutant SOD1 instability: implications for toxicity in amyotrophic lateral sclerosis. Neuro-degenerative diseases 2:115–127.
Turner BJ, Talbot K (2008) Transgenics, toxicity and therapeutics in rodent models of mutant SOD1-mediated familial ALS. Progress in neurobiology 85:94–134.
Urushitani M, Kurisu J, Tsukita K, Takahashi R (2002) Proteasomal inhibition by misfolded mutant superoxide dismutase 1 induces selective motor neuron death in familial amyotrophic lateral sclerosis. Journal of neurochemistry 83:1030–1042.
Uryu K, Nakashima-Yasuda H, Forman MS, Kwong LK, Clark CM, Grossman M, Miller BL, Kretzschmar HA, Lee VM-Y, Trojanowski JQ, Neumann M (2008) Concomitant TAR-DNA-binding protein 43 pathology

is present in Alzheimer disease and corticobasal degeneration but not in other tauopathies. Journal of neuropathology and experimental neurology 67:555–564.

van Blitterswijk M, van Es MA, Hennekam EAM, Dooijes D, van Rheenen W, Medic J, Bourque PR, Schelhaas HJ, van der Kooi AJ, de Visser M, de Bakker PIW, Veldink JH, van den Berg LH (2012) Evidence for an oligogenic basis of amyotrophic lateral sclerosis. Human molecular genetics.

Vance C et al. (2009) Mutations in FUS, an RNA processing protein, cause familial amyotrophic lateral sclerosis type 6. Science (New York, NY) 323:1208–1211.

Vukosavic S, Dubois-Dauphin M, Romero N, Przedborski S (1999) Bax and Bcl-2 interaction in a transgenic mouse model of familial amyotrophic lateral sclerosis. J Neurochem 73:2460–2468.

Wegorzewska I, Baloh RH (2011) TDP-43-based animal models of neurodegeneration: new insights into ALS pathology and pathophysiology. Neuro-degenerative diseases 8:262–274.

Williams AH, Valdez G, Moresi V, Qi X, McAnally J, Elliott JL, Bassel-Duby R, Sanes JR, Olson EN (2009) MicroRNA-206 delays ALS progression and promotes regeneration of neuromuscular synapses in mice. Science (New York, NY) 326:1549–1554.

Williams KL, Warraich ST, Yang S, Solski JA, Fernando R, Rouleau GA, Nicholson GA, Blair IP (2012) UBQLN2/ubiquilin 2 mutation and pathology in familial amyotrophic lateral sclerosis. Neurobiology of aging.

Worms PM (2001) The epidemiology of motor neuron diseases: a review of recent studies. Journal of the neurological sciences 191:3–9.

Wu C-H et al. (2012) Mutations in the profilin 1 gene cause familial amyotrophic lateral sclerosis. Nature.

Xiao S, McLean J, Robertson J (2006) Neuronal intermediate filaments and ALS: a new look at an old question. Biochimica et biophysica acta 1762:1001–1012.

Yang Y, Hentati A, Deng HX, Dabbagh O, Sasaki T, Hirano M, Hung WY, Ouahchi K, Yan J, Azim AC, Cole N, Gascon G, Yagmour A, Ben-Hamida M, Pericak-Vance M, Hentati F, Siddique T (2001) The gene encoding alsin, a protein with three guanine-nucleotide exchange factor domains, is mutated in a form of recessive amyotrophic lateral sclerosis. Nature genetics 29:160–165.

Yokota O, Davidson Y, Bigio EH, Ishizu H, Terada S, Arai T, Hasegawa M, Akiyama H, Sikkink S, Pickering-Brown S, Mann DMA (2010) Phosphorylated TDP-43 pathology and hippocampal sclerosis in progressive supranuclear palsy. Acta neuropathologica 120:55–66.

Chapter 2

Spinal Inhibitory Interneuron Pathology Follows Motor Neuron Degeneration Independent of Glial Mutant Superoxide Dismutase 1 Expression in SOD1-ALS Mice

Hossaini, Mehdi PhD; Cano, Sebastian Cardona MD, MSc; van Dis, Vera MSc; Haasdijk, Elize D. BSc; Hoogenraad, Casper C. PhD; Holstege, Jan C. PhD, MD; Jaarsma, Dick PhD

From the Department of Neuroscience (MH, SCC, VvD, EDH, JCH, DJ), Erasmus Medical Centre, Rotterdam; and Department of Cell Biology (CCH), Faculty of Science, Utrecht University, Utrecht, The Netherlands.

Published: J Neuropathol Exp Neurol, August 2011, Vol. 70, No. 8 pp. 662-677

Abstract

Motor neuron degeneration and skeletal muscle denervation are hallmarks of amyotrophic lateral sclerosis (ALS), but other neuron populations and glial cells are also involved in ALS pathogenesis. We examined changes in inhibitory interneurons in spinal cords of the ALS model low-copy Gurney G93A-SOD1 (G1del) mice and found reduced expression of markers of glycinergic and GABAergic neurons, that is, glycine transporter 2 (*GlyT2*) and glutamic acid decarboxylase (*GAD65/67*), specifically in the ventral horns of clinically affected mice. There was also loss of *GlyT2* and *GAD67* messenger RNA-labeled neurons in the intermediate zone. Ubiquitinated inclusions appeared in interneurons before 20 weeks of age, that is, after their development in motor neurons but before the onset of clinical igns and major motor neuron degeneration, which starts from 25 weeks of age. Because mutant superoxide dismutase 1 (SOD1) in glia might contribute to the pathogenesis, we also examined neuron-specific G93A-SOD1 mice; they also had loss of inhibitory interneuron markers in ventral horns and ubiquitinated interneuron inclusions. These data suggest that, in mutant SOD1-associated ALS, pathological changes may spread from motor neurons to interneuronsin a relatively early phase of the disease, independent of the presence of mutant SOD1 in glia. The degeneration of spinal inhibitory interneurons may in turn facilitate degeneration of motor neurons and contribute to disease progression.

Introduction

Amyotrophic lateral sclerosis (ALS) is a neurodegenerative disease, characterized by late-onset progressive degeneration of motor neurons resulting in paralysis of limb, facial, and respiratory muscles and usually leading to death within 5 years after diagnosis. In most patients, the disease is sporadic, whereas approximately 10% of cases have a monogenetic inherited form (1). Mutations associated with ALS have been identified in the gene for superoxide dismutase 1 (SOD1) (2) and, more recently, in genes encoding the DNA/RNA binding proteins, TAR-DNA-binding protein-43 (TDP-43) and FUS/TLS (1, 3). In addition, mutations in optineurin, VAPB, angiogenin, DCTN1, FIG4, senataxin, and alsin are associated with some ALS cases and ALS-like disorders (1, 4). Nuclear-to-cytoplasmic redistribution, aberrant processing and aggregation of TDP-43 are prominent pathological features in most ALS patients, independent of the presence of TDP-43 mutations (3, 5, 6). SOD1-associated ALS (SOD1-ALS) and FUS/TLS-ALS patients instead develop aggregates of SOD1 (2, 7, 8) and FUS/TLS (3, 9, 10), respectively. These and additional data point to an important role for protein aggregation in the pathogenesis of ALS, but the relationships between protein aggregation, neuronal degeneration, and clinical manifestations in different types of ALS are poorly understood (3, 7, 8, 11).

Hypotheses on ALS pathogenesis usually focus on toxic mechanisms that primarily affect motor neurons; their vulnerability has been linked to their large size, long axons, high metabolic activity, specialized physiological properties, and their dependence on skeletal muscle- and glia-derived factors (12, 13). Although motor neuron degeneration and skeletal muscle denervation represent hallmarks of ALS, cell loss and degenerative changes also occur in other neuron populations throughout the nervous system, particularly in the motor cortex and in glia (14-21). The involvement of multiple cell types favors disease models in which abnormalities in non-motor neurons or non-neuronal cells occur concurrently or sequentially with motor neuron degeneration and raises questions about the relationship between the degeneration of different cell types. For example, multiple clinicopathological studies have investigated the relationship between degeneration of spinal motor neurons and cortical (upper) motor neurons that underlie lower and upper motor neuron manifestations, respectively. These studies have provided variable results that suggest independent degeneration of cortical motor neurons and spinal motor neurons, anterograde propagation of disease from motor cortex to spinal cord, or retrograde progression of disease from spinal cord to motor cortex (14, 22-26). A linkage between upper and lower motor signs in initial stages of disease has been suggested, that is, when there are focal manifestations; this linkage may be lost in later stages of disease as neurodegeneration and clinical manifestations spread independently in the cortex and spinal cord (27). Taken together, clinicopathological studies indicate that neurons interconnected or contiguous to affected regions develop degenerative changes more readily than other cells and point to the occurrence of disease mechanisms that mediate or facilitate spreading of disease to neighboring or interconnected neurons (14).

Considerable attention has been devoted to the role of glia in SOD1-ALS (28). For example, SOD1 aggregates are present in astrocytes in the spinal cords of SOD1-ALS

patients and transgenic mouse models (29). Other evidence pointing to a role of glial abnormalities in SOD1-ALS comes from studies with mutant SOD1 transgenic mice that express no or reduced levels of mutant SOD1 in glia. These mice show slower disease progression and prolonged survival compared with ubiquitous mutant SOD1-expressing mice, although disease onset is unaltered (30-33). On the other hand, expression of mutant SOD1 in neurons determines disease onset and is sufficient to cause an ALS-like disease in mice, indicating that mutant SOD1 in glia does not contribute to disease initiation but rather to disease propagation (28, 34). How mutant SOD1 in glia contributes to disease progression remains to be defined.

The intermediate zone of the spinal cord (Rexed laminae IV-VIII) contains several neuron types that play important roles in controlling the activities of motor neurons, for example, in reflexive and patterned movements and the maintenance of muscle tone (35, 36). Abnormalities in 1 or more populations of interneurons may cause overexcitation or overinhibition of motor neurons and possibly causing them excitotoxic stress (37). There are reports of loss of intermediate zone interneurons in the spinal cord of ALS patients (17, 38) and mutant-SOD1 transgenic mice (39, 40). Furthermore, abnormalities in inhibitory interneurons or inhibitory synapses may occur before motor neuron degeneration in mutant-SOD1 transgenic mice (41-43). We previously showed that spinal interneurons in a low-copy line of G93A-mutant SOD1 mice (G1del mice) (44) start to express the stress transcription factors c-Jun and ATF3 from 20 weeks of age (45, 46). This is several weeks later than the onset of c-Jun and ATF3 activation in motor neurons (at 14-15 weeks), but before the onset of motor manifestations, which starts after the age of 25 weeks in these mice (13, 45). To explore the role of non-motor neuron abnormalities in ALS further, we studied degeneration of spinal inhibitory interneurons in mutant SOD1-ALS mice.

Materials and Methods

Transgenic Mice

Ubiquitous G93A-SOD1 mice were originally derived from Gurney G1 mice, but because of a reduction in the transgene copy number (8 instead of ~20 transgene copy numbers per haploid genome), they show a delayed disease onset and are termed G1del mice (34, 44). The G1del mice were maintained under standard housing conditions in a FVB/N background by mating hemizygote males with nontransgenic females. Nontransgenic offspring served as controls (34). Neuron-specific G93A-hSOD1 mice carrying the complementary DNA (cDNA) of G93A-mutant hSOD1 cloned into the Thy1.2 expression cassette were generated as described (34). Data from this study were obtained from homozygotes of the T3 line (T3T3 mice) generated by intercrossing T3 hemizygotes and from T3hSOD1 double transgenic mice generated by crossing T3 mice with line N29 wild-type hSOD1-overexpressing mice (34). Onset of clinical disease was determined on the basis of weight, the ability to extend the hind limbs, and the ability to hang upside down on a grid for 1 minute (34). Mice reached end-stage disease when they could not right themselves within 5 seconds when placed on their back, when they lost more than 30% of their maximal weight, or when they developed infection of 1 eye. End-stage mice also were

unable to hang in the hanging grid test, which predominantly depends on performance of forelimb muscles.

GlyT2-GFP transgenic mice bred in the C57BL6/J background (47) were obtained from Dr Hanns Ulrich Zeilhofer (Institute of Pharmacology Toxicology, University of Zurich). All animal experiments were approved by the Erasmus University animal care committee and performed in accordance with the guidelines of the Principles of Laboratory Animal Care (National Institutes of Health Publication No. 86-23) and the European Community Council Directive (86/609/EEC).

Immunohistochemistry

Mice were anesthetized with pentobarbital and perfused transcardially with 4% paraformaldehyde. The lumbar and cervical spinal cord were carefully dissected, embedded in gelatin blocks, and sectioned at 40 µm with a freezing microtome, as described (48). Free-floating sections were processed for immunohistochemistry using a standard avidin-biotin-immunoperoxidase complex method (ABC; Vector Laboratories, Burlingame, CA) with diaminobenzidine (0.05%) as the chromogen (48). Guinea pig anti-glycine transporter 2 (*GlyT2*; Millipore, Billerica, MA; 1:10000) and rabbit anti-glutamic acid decarboxylase (*GAD65/67*; Millipore; 1:4000) were used as primary antibodies to label glycinergic and GABAergic nerve terminals, respectively. Other primary antibodies were rabbit anti-ATF3 (Santa Cruz Biotechnology, Santa Cruz, CA; 1:1000), rabbit anticalbindin (Swant, Marly, Switzerland; 1:10000), goat anti-choline acetyl transferase (ChAT; Millipore; 1:500), rat anti-Mac2 (Cedarlane, Burlington, Ontario, Canada; 1:2000), rabbit anti-phospho-c-Jun (Ser63; Cell Signaling, Beverly, MA; 1:1000), mouse antiparvalbumin (Swant; 1:10000), mouse antiubiquitin (clone FK2; Affinity BioReagents, Golden, CO; 1:2000), and rabbit antiubiquitin (Dako, Glostrup, Denmark; 1:2000). Immunoperoxidase-stained sections were analyzed and photographed using a Leica DM-RB microscope and a Leica DC300 digital camera.

To examine the relative intensity of glycine transporter 2 (*GlyT2*) and *GAD65/67* immunoperoxidase staining, lumbar L3-L5 sections were photographed using a 5× objective, and optical densities were determined from TIFF files using MetaMorph image analysis software (Molecular Devices, Sunnyvale, CA). Optical densities were determined in rectangular areas of 200 × 250 µm and 100 × 400 µm for the ventral and dorsal horns, respectively. To minimize variability resulting from the sectioning and staining procedures, these analyses were performed with spinal cord specimens embedded in a single gelatin block and processed in the same run. Gelatin blocks typically contained 12 cervical C5-C8 or lumbar L3-L5 specimens from G1del mice of 3 different ages or disease stages (*e.g.* 20 weeks, 30 weeks, end-stage disease, n = 3 per group) and nontransgenic littermates aged 20 to 30 weeks (n = 3). Other blocks contained specimens from 40-week-old T3T3 mice (n = 3), symptomatic (70-100 weeks old, n = 3), and 2-year-old nontransgenic or T3 hemizygote littermates (34).

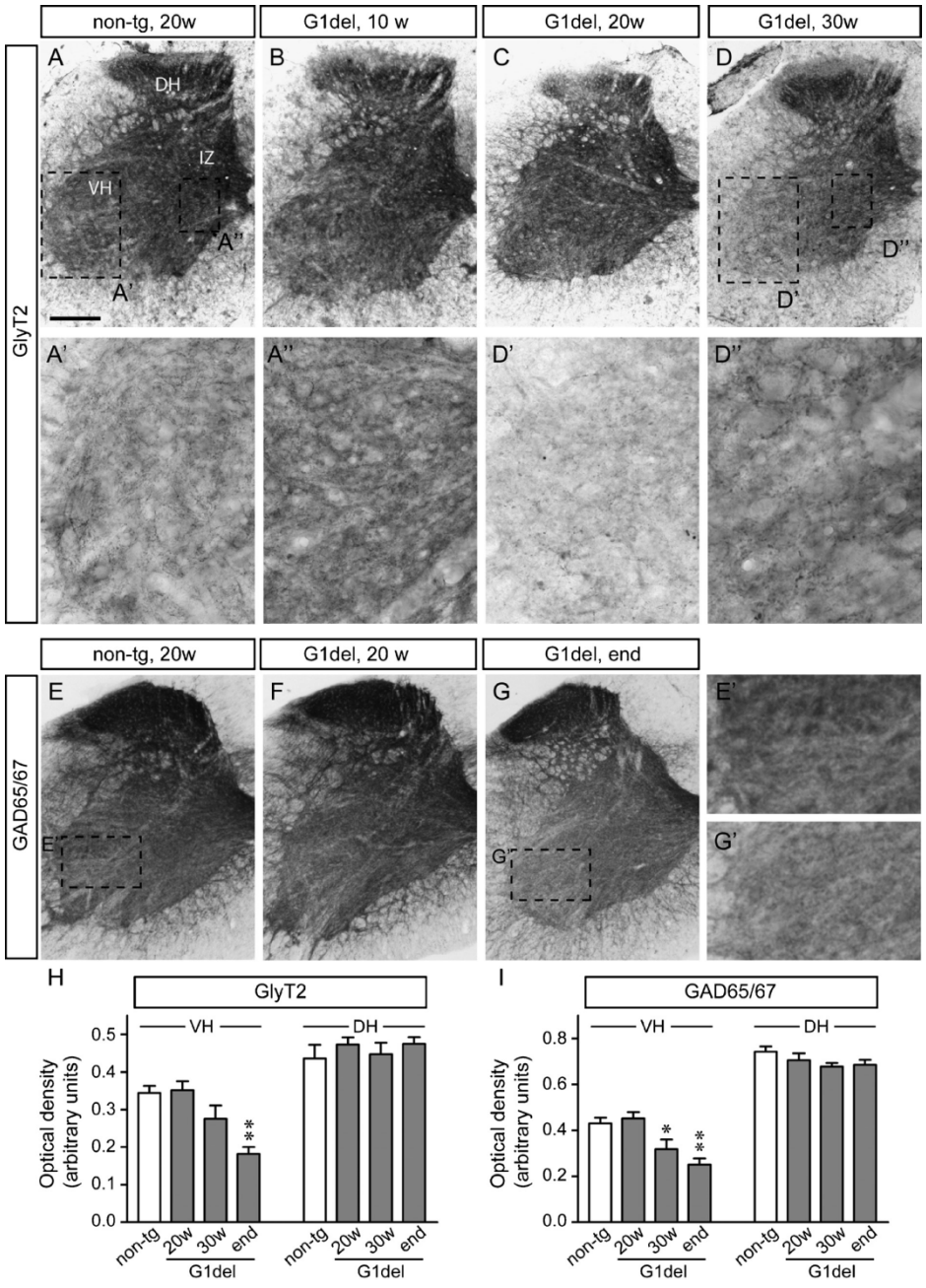

Figure 2.1. Loss of glycine transporter 2 (*GlyT2*) and glutamic acid decarboxylase (*GAD65/67*) immunoreactivity in the ventral horn of spinal cord of symptomatic G1del mice.

Figure 2.1. Loss of glycine transporter 2 (*GlyT2*) and glutamic acid decarboxylase (*GAD65/67*) immunoreactivity in the ventral horn of spinal cord of symptomatic G1del mice. (A-D) Immunohistochemistry of *GlyT2* in L4 spinal cord of nontransgenic mice (A, A', A") and G1del mice aged 10 (B), 20 (C), or 30 (D, D', D") weeks. There is prominent loss of immunoreactivity in the ventral horn (VH), a mild change in the intermediate zone (IZ), and no change in immunoreactivity in the dorsal horn (DH) of the 30-week-old G1del mouse spinal cord. (E-G) *GAD65/67* in C7 spinal cord of a nontransgenic mouse (E, E'), 20-week-old (B), and end-stage (G, G') G1del mice. There is loss of immunoreactivity in the ventral horn of the end-stage G1del mouse spinal cord. (H,I) Bar graphs of optical densities of *GlyT2* (H) and *GAD65/67* (I) immunostaining in ventral and dorsal horn. Values represent mean ± SE (n = 3 per bar with 4 sections analyzed per mouse). Data were obtained from sections incubated in a single gelatin block and processed in a single immunostaining procedure. *, $p < 0.05$; **, $p < 0.01$; 1-way analysis of variance with the Tukey multiple comparison test. Scale bar = 200 µm (A).

In Situ Hybridization

In situ hybridization (ISH) was performed on free-floating 4% paraformaldehyde-fixed 30-µm-thick frozen sections using digoxigenin-labeled RNA probes, as described (49). Sense and antisense probes were transcribed from linearized plasmid constructs containing the partial *GlyT2* or *GAD67* cDNA sequences using a digoxigenin labeling kit (Roche, Indianapolis, IN). Sections were incubated overnight at 65°C with the probes diluted at 200 ng/mL. After hybridization, the digoxigenin-labeled RNA-RNA complex was detected by using alkaline phosphatase-conjugated sheep-antidigoxigenin (Roche; diluted 1:4000, incubated 48 hours at 4°C), with 5-bromo-4-chloro-3-indolyl phosphate and nitro-blue tetrazolium as substrate and chromogen, respectively.

Alkaline phosphatase-stained sections were analyzed and photographed using a Leica DM-RB microscope and a Leica DC300 digital camera. For quantitative analysis of the number of *GlyT2* and *GAD67* messenger RNA (mRNA)-labeled cells, lumbar L3-L5 sections were examined with an Olympus microscope fitted with a Lucivid miniature monitor coupled to StereoInvestigator software (version 4.37; MicroBrightField, Colchester, VT). The sections were systematically sampled across the spinal cord (each 10th section). The counting fields, 350 µm apart, were 0.0225 mm2; cells in contact with the left and lower boundaries of the counting fields were excluded. The area of the gray matter multiplied by the number of cells per squared millimeter gave the number of cells per section. Sections used for this analysis were produced in a single staining run to avoid variability in staining intensities and numbers of labeled cells resulting from differences in staining conditions between runs.

To combine *GlyT2* or *GAD67* ISH with immunofluorescence, hybridized digoxigenin complementary RNA was visualized using a tyramide amplification method with fluorescein isothiocyanate-labeled tyramide (50). After hybridization, sections were incubated with biotinylated-sheep antidigoxigenin antibody (Roche) (1:500; 48 hours at 4°C in phosphate-buffered saline [PBS], 2% milk powder, and 0.5% Triton X-100), followed by incubation with avidin-biotin-peroxidase complex (Vector Laboratories) and subsequently reacted with fluorescein isothiocyanate-tyramide conjugate (4 µg/mL) in the presence of H2O2 (0.001%) in PBS containing 0.1 mol/L imidazole, pH 7.6 (51). Thereafter, the sections were washed in PBS and processed for immunofluorescence with rabbit anti-ATF3 and rabbit antiubiquitin as the primary antibodies and Cy3-labeled donkey-anti-rabbit (1:200; Jackson ImmunoResearch, Bar Harbor, ME) as the secondary

antibody. Double-labeled sections were analyzed with a Zeiss LSM 510 confocal laser scanning microscope using 40×/1.3 and 63×/1.4 oil-immersion objectives.

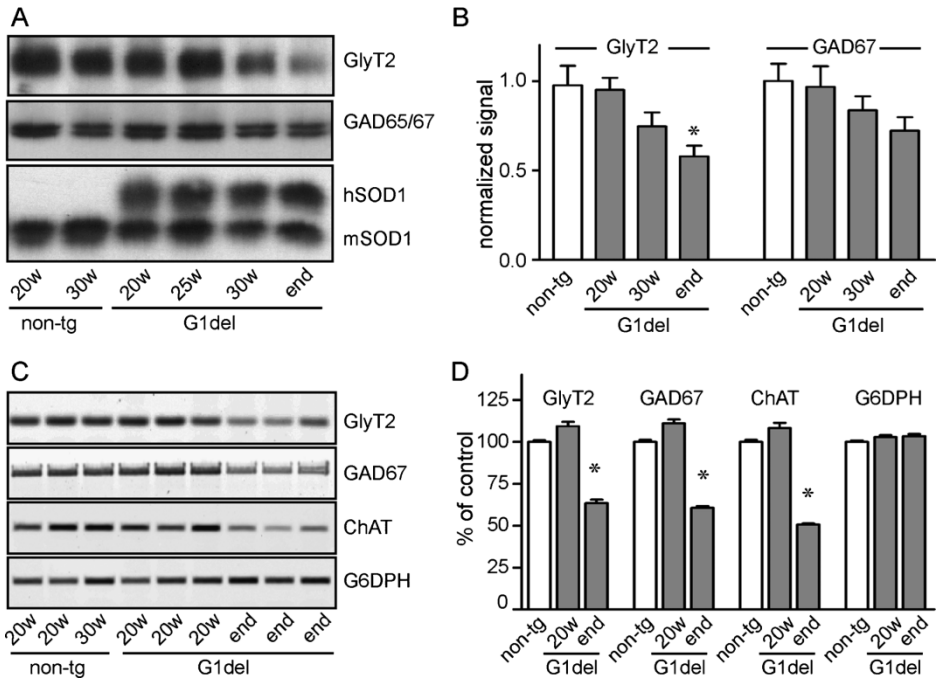

Figure 2.2. Loss of glycine transporter 2 (*GlyT2*) and glutamic acid decarboxylase (*GAD65/67*) protein and mRNA levels in the spinal cord of symptomatic G1del mice. (A, B) Representative results (A) and quantification (B) of Western blot analysis of *GlyT2* and *GAD65/67* in spinal cord homogenate of nontransgenic and G1del mice show reduced *GlyT2* and a trend to reduced *GAD65/67* signal in end-stage G1del mice. Values in bar graph are mean ± SEM (n = 3). *, $p < 0.05$ versus nontransgenic mice and 20-week-old G1del mice. (C, D) Reverse transcription-PCR analysis of relative *GlyT2*, *GAD67*, ChAT, and G6DPH mRNA concentrations in cDNA samples from nontransgenic and G1del mouse spinal cord homogenates. Values in bar graph are mean ± SEM (n = 3). *, $p < 0.01$ versus nontransgenic mice and 20-week-old G1del mice. One-way analysis of variance, Tukey multiple comparison test for B and D

Western Blot

Spinal cord specimens were homogenized and sonicated in 20 volumes of PBS containing 0.5% Nonidet P-40 (NP-40) and protease inhibitors cocktail (Sigma) and centrifuged at 800 × g for 5 minutes at 4°C, and protein concentrations of the supernatants (S1) were determined. Samples containing 2 to 10 µg protein were electrophoresed on 8% or 10% SDS-PAGE gels and blotted on polyvinylidene fluoride membranes (Millipore). The membranes were blocked with 5% nonfat dry milk in PBS with 0.05% Tween 20, incubated in primary antibody, diluted in PBS with 0.05% Tween 20 with 1% dry milk followed by an incubation in peroxidase-conjugated secondary antibody, incubated in chemiluminescence reagent (Amersham, Piscataway, NJ), and exposed to film or a Kodak Image station. Primary antibodies used for Western blot included mouse antiactin (Millipore; 1:4000), guinea pig anti-*GlyT2* (Millipore; 1:5000), rabbit anti-*GAD65/67*

(1:5000), and rabbit antimurine SOD1 (SOD101; Stressgen, Victoria, British Columbia, Canada; 1:8000).

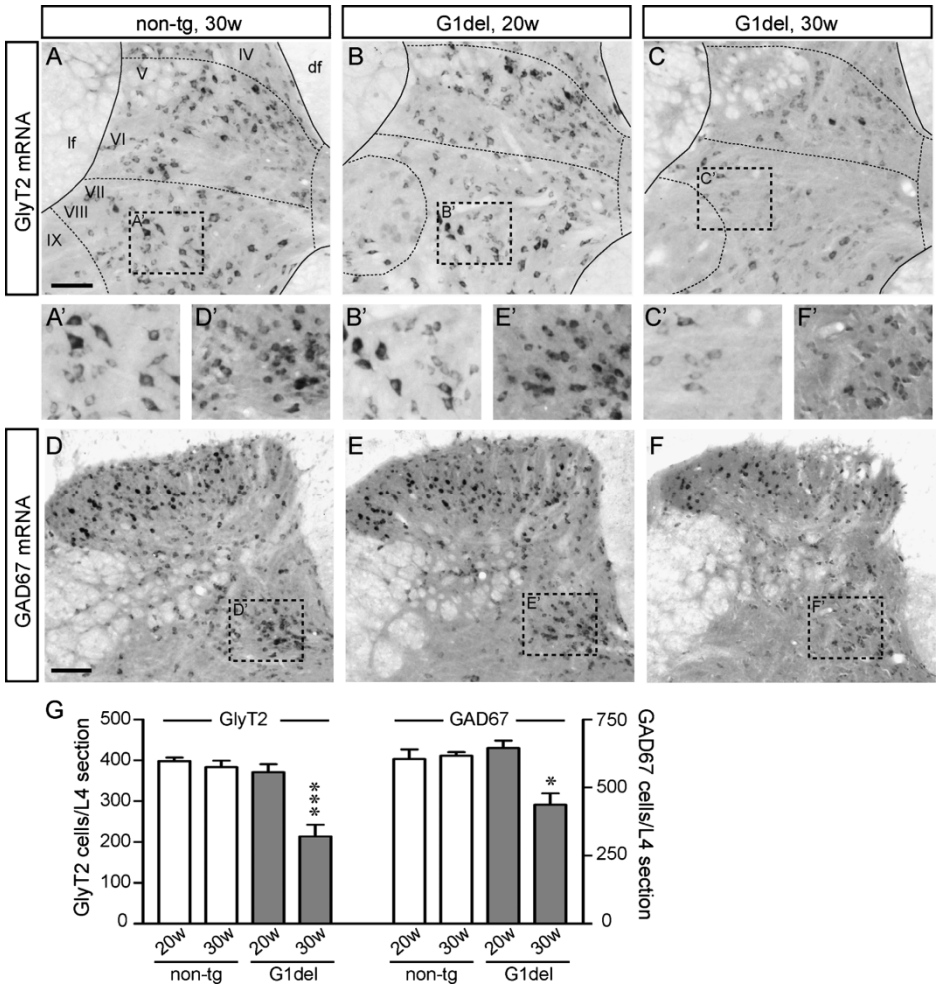

Figure 2.3. Decrease of *GlyT2* and *GAD67* mRNA in situ hybridization in symptomatic G1del mice. (A-G) Photomicrographs (A-F) and quantitative analysis (G) of *GlyT2* (A-C, G) or *GAD67* (D-F, G) mRNA in L4 spinal cord sections showing reduced numbers of stained cells in symptomatic (30 weeks) G1del mice. Data in G are mean ± SEM (n = 3 mice/bar). *, $p < 0.05$; ***, $p < 0.001$ versus nontransgenic mice and 20-week-old G1del mice. One-way analysis of variance, Tukey multiple comparison test. Scale bars= 100 µm (A, D)

Reverse Transcription-Polymerase Chain Reaction

Semiquantitative reverse transcription-polymerase chain reaction (PCR) was performed as previously described (52). Total RNA was extracted from spinal cord tissue using TRIzol and treated with DNAse. The RNA (5 µg) was converted into cDNA using oligo(dT) primer and reverse transcriptase in a total reaction volume of 20 µl. Polymerase chain reaction was performed with 0.1 µL of the reverse transcriptase reaction mixture in a reaction volume of 25 µl. Primers used were as follows: ChAT, 5'-GCGAATCGTTGGTATGACAAGTC-3' (forward) and 5'-

TTGAAGTTTCTCTGCCGAGGAG-3' (backward); G6dph, 5'-TTTGGACCCATCTGGAATCG-3' and 5'-CACTTTGACCTTCTCATCACGGAC-3'; *GAD67*, 5'-TACGGGGTTCGCACAGGTC-3' and 5'-CCCCAGGCAGCATCCACAT-3'; *GlyT2*, 5'-TACCGCTACCCTAACTGGTCCATGG-3' and 5'-ATCCACACGAC TGGACTAGCACTGA; *GlyT2*A, 5' ACTCTACGGTT CAATCTGTTGTCC-3' and 5'-GGTCCTAGGTGCACGAGGACTATCCCGG-3'. The number of PCR cycles and quantity of cDNA were determined to be within the linear range of the reactions. For quantification, the PCR products were electrophoresed on a 2% agarose gel, stained with ethidium bromide, and scanned on a Molecular Dynamics Typhoon instrument

Statistical Analysis

Statistical analyses were done using GraphPad Prism software (San Diego, CA). Means from different age groups and different transgenic mouse lines were compared using 1-way analysis of variance and the Tukey post test.

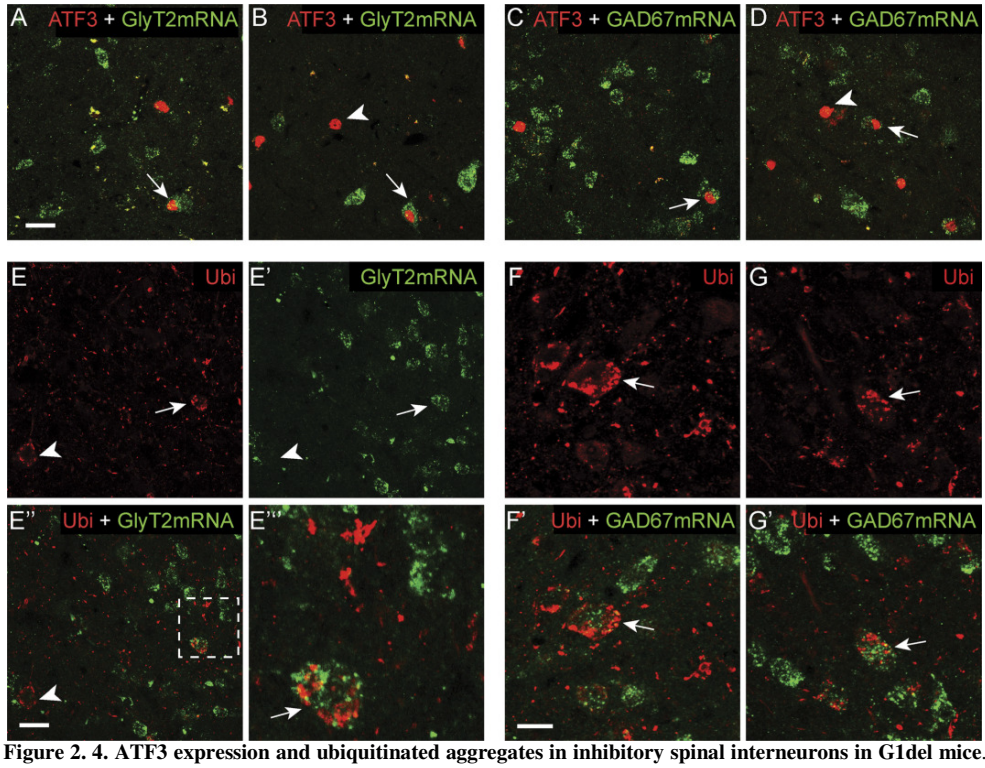

Figure 2. 4. ATF3 expression and ubiquitinated aggregates in inhibitory spinal interneurons in G1del mice. (A-D) Double-labeling confocal microscopy of ATF3 immunoreactivity and *GlyT2* (A, B) or *GAD67* (C, D) mRNA in situ hybridization in L4 spinal cord intermediate zone of 30-week-old (A, C) and end-stage (B, D) G1del mice. Single ATF3-labeled cells are indicated by arrowheads; double-labeled cells are indicated by small arrows. (E-G) Double labeling of ubiquitin immunoreactivity and *GlyT2* (E, F) or *GAD67* (G) mRNA showing ubiquitinated aggregates in *GlyT2* (arrows in E, F) and *GAD67* (arrow in G) mRNA-positive neurons. The frequent ubiquitin-immunoreactive structures that are not associated with neuronal somata represent aggregates in neurites and glia (34, 45).

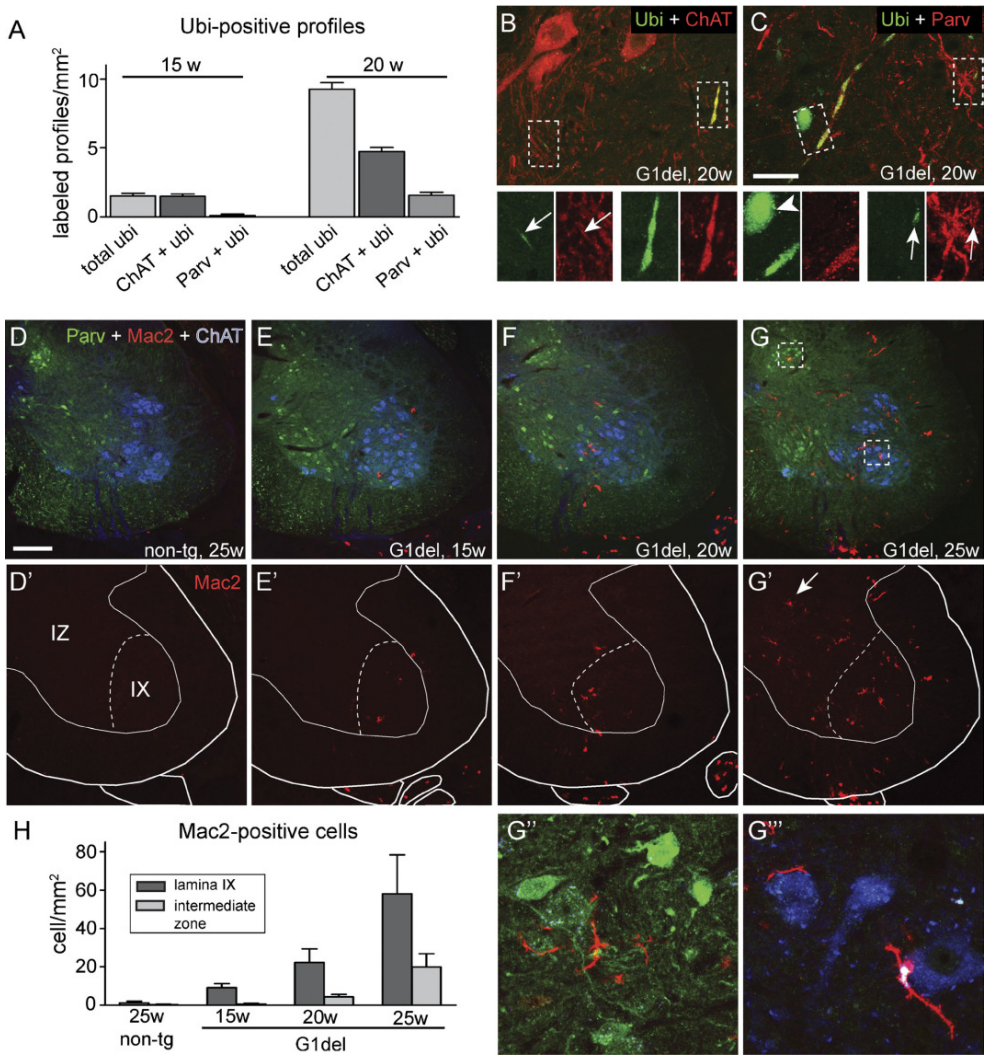

Figure 2.5. Early dendritic ubiquitin pathology and microglia activation in the spinal intermediate zone in G1del mice. (A-C) Choline acetyl transferase (ChAT)-ubiquitin (B) and parvalbumin-ubiquitin (C), double-labeling confocal immunofluorescence of lumbar spinal cord sections from a 20-week-old G1del mouse shows double labeling in ChAT (B)- or parvalbumin (C)-positive dendrites in the ventral horn (B) and intermediate zone (C), respectively. In C, there is a single-labeled ubiquitinated dendritic profile (arrowhead). Bar graph in A shows the number (mean ± SEM, n = 4 mice) of ubiquitin-positive dendritic profiles in L4 lumbar spinal cord sections of 15- and 20-week-old G1del mice. (D-H) Triple-labeling confocal immunofluorescence showing activated microglia cells (Mac2), motor neurons (ChAT), and parvalbumin (Parv)-positive interneurons in lumbar L4 spinal cord sections of nontransgenic (D, D') and presymptomatic G1del mice at 15 (E, E'), 20 (F, F'), and 25 (G, G') weeks of age. There is an age-related increase of activated microglia in ventral horns of G1del spinal cords and the appearance of activated microglia in the spinal intermediate zone of a 25-week-old G1del mouse (arrow in G). (G'', G''') High magnifications illustrating Mac2-positive microglia in close apposition of parvalbumin-positive interneurons and motor neurons, respectively. Scale bars = 25 µm (C), 200 µm (D).

Results

Reduced *GlyT2* and *GAD65/67* Protein and mRNA Levels in the Spinal Cord of Symptomatic G1del Mice

G1del (also termed G1slow or low-copy G1) mice ubiquitously express G93A-mutant SOD1; they develop weakness in 1 or more limbs from age 24 to 30 weeks and die of fatal paralysis between 32 and 40 weeks of age (48, 53). Early pathological and molecular changes in motor neurons include swelling and vacuolization of a subset of mitochondria starting before 3 weeks (53), the appearance of ubiquitinated pathology, Golgi fragmentation, endoplasmic reticulum stress, and ATF3 activation starting from 13 to 15 weeks (13, 45). These changes precede neuromuscular denervation, loss of motor neurons, and astrogliosis and microgliosis. Abnormalities in interneurons (ATF3 and phospho-c-Jun expression) occur after 20 weeks (45). In this study, we examined G1del mice at ages 10 to 15 weeks (early presymptomatic), 20 to 25 weeks (late presymptomatic), and 30 weeks (symptomatic) and mice that had reached disease end stage.

To identify inhibitory interneurons, we used the expression of *GlyT2* and *GAD* as markers for glycinergic and GABAergic neurons, respectively (49, 54, 55). Immunohistochemistry showed that *GlyT2* was expressed throughout the spinal cord gray matter except for the most superficial part of the dorsal horn (Figs. 2.1A-D). At high magnification, labeling was distributed in punctae, consistent with a predominant localization in nerve terminals (Figs. 2.1A-D) and in accord with previous studies (54). The distribution of *GlyT2* immunoreactivity in spinal cords of 10- and 20-week-old G1del mice was indistinguishable from that in nontransgenic mice (Figs. 2.1B, C), whereas in symptomatic and end-stage G1del mice, there was a marked reduction of *GlyT2* immunoreactivity, particularly in the ventral horn motor neuronal cell groups (Figs. 2.1D, H). *GlyT2* immunoreactivity was not altered in the dorsal horn (Figs. 2.1D, H). Reduced *GlyT2*-immunoreactivity in the ventral horn occurred in both cervical and lumbar cord but, in general, was more prominent in the latter.

GABAergic interneurons were labeled with an antibody that binds both *GAD67*, the predominant *GAD* isoform in the ventral horn, and *GAD65* that is expressed in a more restricted set of GABAergic interneurons and terminals (55, 56). *GAD65/67* immunoreactivity was present throughout the spinal cord gray matter with more prominent labeling in the dorsal horn compared with that of *GlyT2* (Fig. 2.1E). As with *GlyT2*, no change in overall staining occurred in spinal cord sections from 10- and 20-week-old G1del mice (Figs. 2.1F, I). There was reduced *GAD65/67* immunoreactivity in the ventral horn of symptomatic G1del mice (Figs. 2.1G, I).

Western blot showed reduced *GlyT2* and *GAD65/67* immunoreactivity in spinal cord homogenates of symptomatic and end-stage G1del mice (Figs. 2.2A, B). In addition, we performed semiquantitative reverse transcription-PCR analysis to examine changes at the mRNA level. Consistent with the immunohistochemistry and Western blotting, *GlyT2* and *GAD67* mRNA levels in the spinal cord of 20-week-old G1del mice were the same as in the spinal cord of nontransgenic mice, whereas *GlyT2* and *GAD67* mRNA levels were reduced in symptomatic and end-stage G1del mice (Figs. 2.2C, D). In the end-stage disease mice, *GlyT2* and *GAD67* mRNA levels were reduced by approximately 50%, which was

comparable to the loss of ChAT mRNA, which is predominantly produced by motor neurons.

We studied *GlyT2* and *GAD67* mRNA expression using ISH. Consistent with previous reports (49, 54), *GlyT2* mRNA-labeled cells were predominantly localized in the deep dorsal horn and the intermediate zone (Rexed laminae V-VIII), whereas they were detected at a low frequency in the motor columns in the ventral horn (Rexed laminae IX) (Fig. 2.3A) and the superficial dorsal horn. Labeled cells were small- to medium-sized (15-25 μm in diameter) and showed varying labeling intensities. The distribution of *GlyT2* mRNA was the same as in nontransgenic mice in 10- and 20-week-old G1del mice, whereas 30-week-old symptomatic G1del mice showed a reduction of *GlyT2* mRNA, which was due to both reduced numbers of *GlyT2* mRNA-labeled cells and reduced staining intensities in remaining cells (Figs. 2.3A-C). Quantitative analysis indicated a 50% loss of *GlyT2* mRNA-labeled cells in lumbar L3-L5 sections of 30-week-old G1del mice compared with controls and 20-week-old G1del mice (Fig. 2.3G).

GAD67 mRNA labeling was most prominent in dorsal lamina of the spinal cord with a high density of small intensely stained cells in Rexed laminae II-III (Fig. 2.3D). Labeled cells in other lamina usually were less intensely detected, whereas a very low number of *GAD67* mRNA-positive cells were present in the motor columns. As with *GlyT2* mRNA, there was reduced *GAD67* mRNA in 30-week-old and end-stage G1del mice (Fig. 2.3F). Neurons in superficial dorsal horn seemed relatively spared. Quantitative analysis indicated 30% to 40% loss of labeled cells in lumbar L3-L5 sections of 30-week-old G1del mice versus control and 20-week-old G1del mice (Fig. 2.3G).

ATF3 Expression and Ubiquitinated Aggregates in Inhibitory Spinal Interneurons

To determine whether ATF3 was associated with inhibitory interneurons, we combined fluorescent ISH of *GlyT2* or *GAD67* mRNA with ATF3 immunofluorescence. Double labeling with ATF3 revealed multiple *GlyT2* mRNA/ATF3-and *GAD67* mRNA/ATF3 double-labeled neurons in the intermediate zone and deep dorsal horn of 30-week-old and end-stage G1del mice (Figs. 2.4A-D).

Systematic analysis of lumbar L3-L5 sections of 30-week-old G1del mice indicated that 27% ± 5% (mean ± SE, n = 3 animals, 30-40 ATF3 cells analyzed per mouse) of ATF3-positive cells were *GlyT2* mRNA-positive, whereas 33% ± 5% were *GAD67* mRNA-positive. A subset of double-labeled neurons showed eccentric nuclei (Figs. 2.4A, C, D) (suggesting pathologic alteration), consistent with previous observations (45).

To determine whether spinal inhibitory interneurons also develop ubiquitinated SOD1 aggregates, we double-stained for *GlyT2* or *GAD67* mRNA and polyubiquitinated epitopes. Multiple *GlyT2* or *GAD67* mRNA-stained neurons containing ubiquitin-immunoreactive structures were identified in the spinal cords of symptomatic G1del mice (Figs. 2.4E-G). The mRNA staining did not overlap with that of ubiquitin. In lumbar L3-L5 sections (2 mice, 3 sections per mouse), approximately 50% (14/26) of intermediate zone neurons with ubiquitin immunopositivity also stained for *GlyT2* mRNA. Similarly, in *GAD67* mRNA/ubiquitin-stained sections, approximately 50% (12/27) of ubiquitinated neurons stained for *GAD67* mRNA. These data indicate that G1del mice show loss of spinal

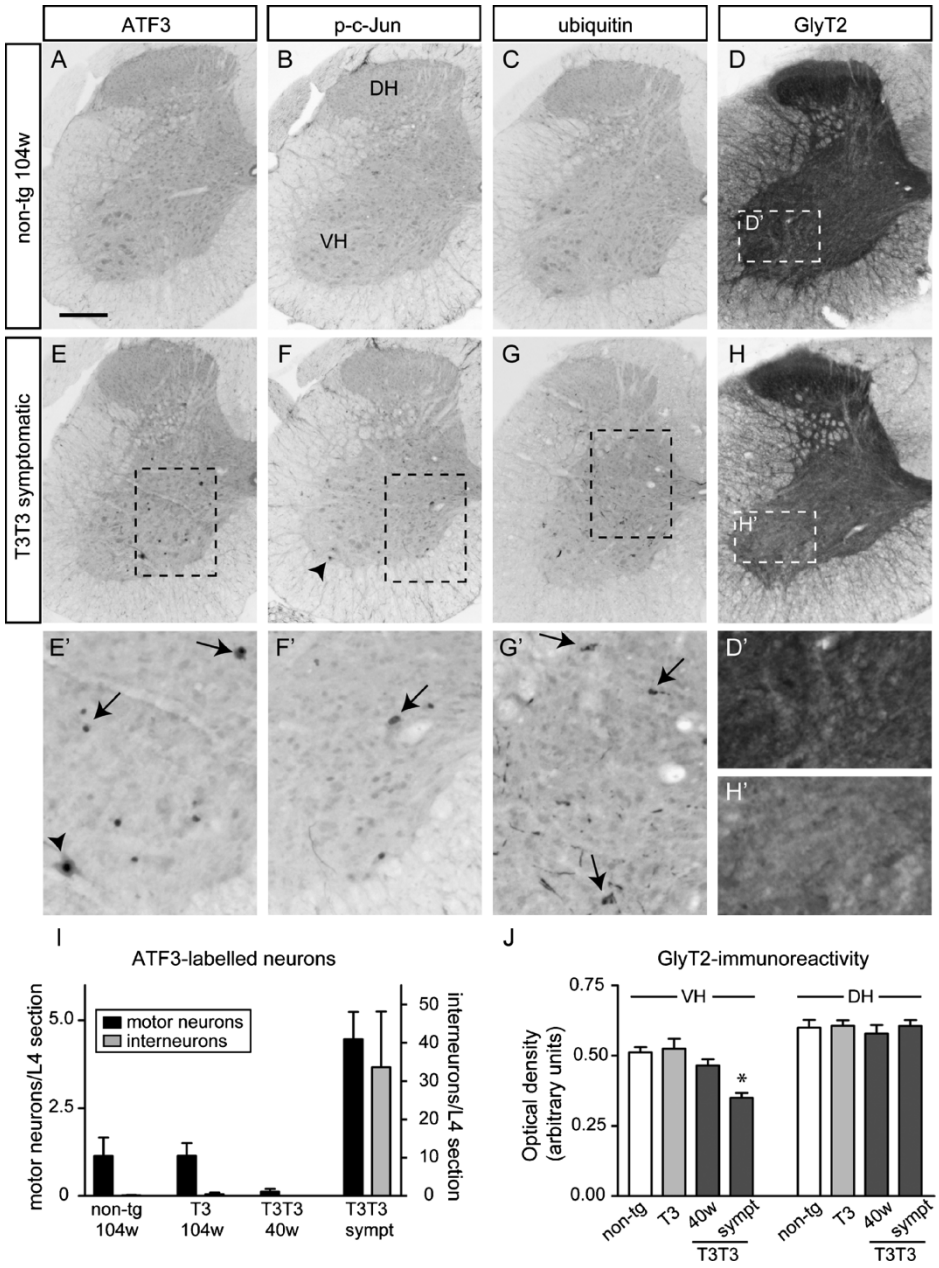

Figure 2.6. Interneuron abnormalities in T3T3 neuron-specific G93A-SOD1 mice. (A-H) Immunohistochemistry of ATF3 (A, E, E'), phospho (ser63)-c-Jun (B, F, F'), ubiquitin (C, G, G'), and glycine transporter 2 (*GlyT2*) (D, D', H, H') in L4 (A-C, E-G) and C6 (D,H) spinal cord sections of an aged nontransgenic mouse (A-D) and a symptomatic T3T3 (E-H) mouse. There are ATF3-, phospho (ser63)-c-Jun-, and ubiquitin-positive interneurons (arrows in E-G) in addition to motor neurons (arrowheads). Symptomatic T3T3 mice also show loss of *GlyT2* immunoreactivity in the ventral horn (VH; compare D' and H') but not the dorsal horn. (I) Bar graphs of the number (mean ± SEM, n = 4 mice) of ATF3-labeled motor neurons and interneurons in T3T3 and nontransgenic mice. (J) Optical densities of *GlyT2* immunostaining in ventral and dorsal horn of C6 cervical spinal cord sections of nontransgenic, T3, and T3T3 transgenic mice. Values represent means ± SE (n = 3 per bar with 4 sections analyzed per mouse). *,p< 0.001 versus 104-week-old nontransgenic and T3 mice and p < 0.05 versus 40-

week-old T3T3 mice. One-way analysis of variance, Tukey multiple comparison test. sympt indicates symptomatic. Scale bar = 200 µm (A).

inhibitory interneurons, which is preceded by ATF3 expression and the appearance of ubiquitinated aggregates, 2 key pathological hallmarks that also precede motor neuron loss.

Early Dendritic Ubiquitin Pathology in Inhibitory Interneurons in G1del Spinal Cord

Ubiquitinated aggregates in motor neurons of G1del mice occur initially and more frequently in dendrites than in the cell soma (34, 45). These aggregates are strongly immunoreactive for human SOD1 and first appear at 13 to 15 weeks and only in the motor columns (45). Double labeling with ChAT showed that at 15 weeks, essentially all ubiquitinated dendrites were immunoreactive for ChAT (Figs. 2.5A, B). However, a proportion of ubiquitinated dendrites was ChAT-negative and also occurred in the intermediate zone in 20-week-old and older mice (Fig. 2.5A). Thus, ubiquitin pathology also occurred in dendrites of non-motor neurons in older mice

To determine whether non-motor neuron dendritic ubiquitin pathology also occurs in the dendrites of inhibitory interneurons, we double stained for ubiquitin and parvalbumin (Figs. 2.5A, C). Parvalbumin, a small calcium binding protein, was used as a substitute marker instead of *GlyT2* or *GAD*65 because staining for *GlyT2* and *GAD67* protein or mRNA does not outline the dendritic compartment of interneurons. Parvalbumin is reported to be present in the somatodendritic compartment of a subset of inhibitory interneurons that project to motor neurons (57). Accordingly, we obtained evidence in *GlyT2*-GFP transgenic mice that more than 90% of parvalbumin-positive neurons in the intermediate zone and ventral horn of spinal cord are glycinergic (47) (Figure, Supplemental Digital Content 1, http://links.lww.com/NEN/A250). Double labeling for ubiquitin and parvalbumin showed that at 20 weeks, but not at 15 weeks, a subset of ubiquitinated neurites were parvalbumin positive (Figs. 2.5A, C). Parvalbumin-positive ubiquitinated dendrites were preferentially localized in the intermediate zone, although sometimes they occurred in the motor columns. Triple staining for ubiquitin, ChAT, and parvalbumin showed that parvalbumin was only present in a subset of ChAT-negative ubiquitinated dendrites, indicating the presence of ubiquitin in dendrites of other populations of spinal interneurons. Of note, we never observed ChAT and parvalbumin double- stained neurons and neurites, thereby excluding the possibility that parvalbumin-positive dendrites were from motor neurons.

Early Microglial Activation in the Intermediate Zone in G1del Mice

There was a low density of activated microglia, identified using an antibody against Mac2 (58), in the motor columns of 15-week-old G1del mice, whereas higher densities of Mac2-positive microglia were seen in the motor columns at older ages (Figs. 2.5E-H). Activated microglia appeared in the intermediate zone between 20 and 25 weeks. Activated microglia in motor columns were usually in close apposition with motor neurons. Sections from 25-week-old G1del mice stained for both Mac2 and parvalbumin revealed multiple examples of Mac2-positive microglia contacting parvalbumin-positive interneurons (Fig. 2.5G). Together, these data further support the relatively early

pathological alterations of spinal interneurons, including a subclass of parvalbumin-positive cells.

Interneuron Abnormalities in Neuron-Specific G93A-SOD1 Mice

To determine whether neuron-specific mutant SOD1 expression also is sufficient to trigger interneuron abnormalities, we examined homozygous T3T3 mice that express G93A-mutant SOD1 in neurons throughout the CNS, including spinal motor neurons and interneurons (34). Hemizygote T3 mice do not develop clinical and pathological signs of motor abnormalities up to 2 years, whereas homozygous T3T3 mice develop a motor neuron disease strongly resembling that in G1del mice. The age of onset in T3T3 mice is higher (>54 weeks) and considerably more variable (54 to >104 weeks) than in G1del mice, likely because of lower mutant SOD1 expression levels in motor neurons (34). ATF3 immunohistochemistry revealed ATF3-immunoreactive motor neurons and interneurons in spinal cord of symptomatic (n = 2) and end-stage (n = 5) T3T3 mice (Figs. 2.5A, E, I). ATF3 staining was also observed in the spinal cord of 2-year-old presymptomatic T3T3 mice (n = 2) but not in 40-week-old T3T3 mice (n = 4). Hemizygote T3 mice and nontransgenic mice showed ATF3 staining in some motor neurons at 2 years (Fig. 2.6) but not at 40 and 70 weeks (not shown). Old T3 and nontransgenic mice did not show ATF3-positive interneurons (Fig. 2.6).

Immunostaining with an anti-phospho (ser63)-c-Jun antibody resulted in motor neuron and interneuron staining patterns that strongly resembled those obtained with anti-ATF3 antibody. Thus, phospho-c-Jun-positive motor neurons and interneurons occurred in spinal cord of 2-year-old, symptomatic, and end-stage T3T3 mice, whereas no or sporadic-labeled motor neurons occurred in spinal cord of nontransgenic, T3, and 40-week-old T3T3 mice (Figs. 2.6B, F). Immunohistochemistry showed the presence of intensely ubiquitin-immunoreactive dendrites and cell bodies in the spinal cord of symptomatic T3T3 mice and 2-year-old but not 40-week-old T3T3 presymptomatic mice. Ubiquitinated dendrites were in both the ventral horn and the intermediate zone, indicating that the ubiquitinated aggregates were in interneurons in addition to motor neurons (Fig. 2.6G). Direct evidence for death of interneurons in T3T3 mice was obtained by reanalyzing sections stained with a silver degeneration staining method that outlines dying neurons and their processes (34). This analysis revealed multiple argyrophilic interneurons (Figure, Supplemental Digital Content 2, http://links.lww.com/NEN/A251).

Symptomatic T3T3 mice showed reduced levels of *GlyT2* immunoreactivity in the ventral horn but not in the dorsal horn (Fig. 2.6H). No changes in *GlyT2* immunoreactivity occurred in spinal cord of 40-week-old T3T3 mice or T3 mice up to 2 years, indicating that reduced *GlyT2* immunoreactivity correlated with the occurrence of other degenerative changes and clinical manifestations.

As in G1del mice, all symptomatic T3T3 mice showed ubiquitin-parvalbumin double-labeled dendrites and cell bodies (Figs. 2.7A, B), as well as parvalbumin-immunoreactive neurons with nuclear ATF3 staining (Fig. 2.7D). We also combined ubiquitin with *GlyT2* staining, which enabled us to examine whether motor neurons with ubiquitinated aggregates were contacted by glycinergic boutons (Figs. 2.7B, C). Most ubiquitin-positive motor neurons (15/17 identified in lumbar sections from symptomatic T3T3 mice) were

surrounded by *GlyT2*-immunoreactive boutons (Fig. 2.7C), whereas ubiquitinated motor neurons in lumbar sections from 20- to 25-week-old G1del mice generally showed a normal pattern of *GlyT2*-immunoreactive boutons (not shown). Quantitative analyses to identify subtle losses of *GlyT2*-immunoreactive boutons (as previously demonstrated for high copy G1 mice [41) were beyond the scope of this study.

Dendritic Ubiquitin Pathology and Microglia Activation in the Intermediate Zone After the Ventral Horn in Neuron-Specific G93A Mice

As indicated above, no ubiquitin pathology was observed in spinal cord of 40-week-old T3T3 mice, whereas in presymptomatic and symptomatic T3T3 mice, ubiquitinated aggregates were always in both motor neurons and interneurons. Thus, it was not possible to determine whether ubiquitin pathology appeared at an earlier time point in motor neurons than in interneurons, as in G1del mice (Fig. 2.5A). To address this question, we used T3hSOD1 mice, which develop a considerably more predictable disease phenotype (34). The T3hSOD1 mice take advantage of the fact that coexpression of high levels of wild-type SOD1 (via a yet poorly understood mechanism) facilitates onset an progression of disease, and lowers the threshold of the concentration of mutant SOD1 required to cause disease within the normal lifespan of mice (48, 59, 60). T3hSOD1 mice develop signs of muscle weakness starting from 1 year of age, but dendrites with ubiquitinated aggregates appear before the age of 20 weeks, long before clinical onset (34). Double labeling of ChAT and ubiquitin showed that the large majority of these ubiquitinated dendrites were cholinergic (Figs. 2.7E, G), whereas only a few dendrites were ChAT-negative (Figs. 2.7F, G). A higher level of ChAT-negative ubiquitinated dendrites occurred in a later presymptomatic stage at 35 weeks (Fig. 2.7G). These data indicate that in T3 neuron-specific G93A mice (as in G1del mice), dendritic ubiquitin pathology occurs first only in motor neurons, and later, albeit still in a presymptomatic stage, also in spinal interneurons. Similarly, as in G1del mice, neuron-specific G93A mice show microglia activation first in the motor columns and subsequently in the intermediate zone (Figs. 2.7H-K). Taken together, these data indicate that neuron-specific and ubiquitous G93A-SOD1 mice develop similar interneuronal pathological features, specifically after the onset of the disease in motor neurons.

Discussion

We have shown that SOD1-ALS transgenic mice expressing G93A mutant SOD1 lose the markers of glycinergic and GABAergic inhibitory neurons *GlyT2* and *GAD65/67* mRNA and protein in the spinal cord, indicating their involvement in the disease. These interneurons develop 2 key pathological hallmarks that also characterize degenerating motor neurons: ubiquitinated inclusions and expression of the stress transcription factor ATF3. These findings complement previous studies showing the degeneration of spinal interneurons in sporadic ALS patients and in transgenic SOD1-ALS mice (17, 38, 39, 61). We also show that ubiquitin pathology appears first in motor neurons (before 15 weeks of

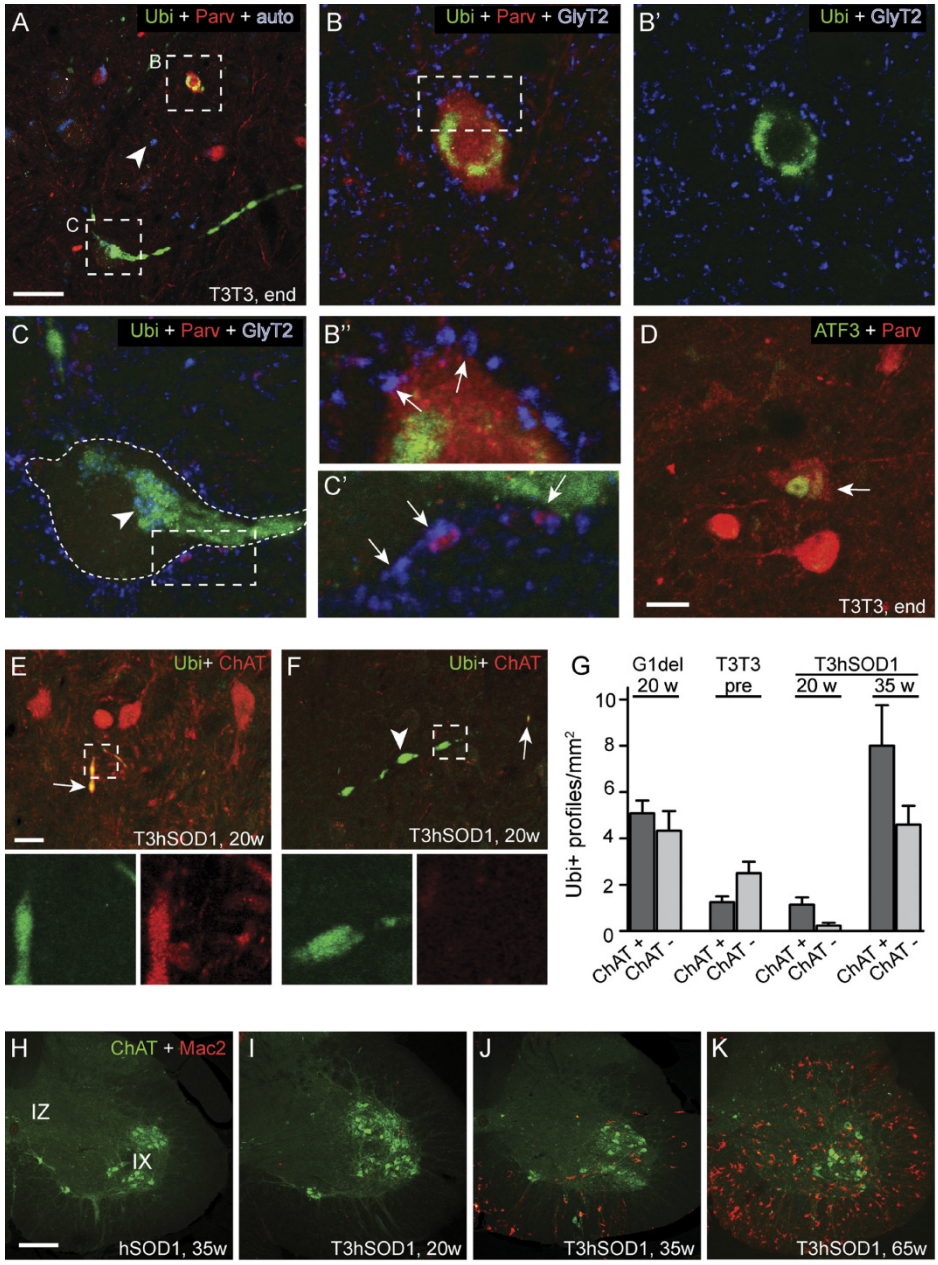

Figure 2.7. Ubiquitinated aggregates and ATF3 expression in motor neurons and parvalbumin-positive interneurons in neuron-specific G93A mice (A-C) Confocal immunofluorescence of C6 cervical section from an end-stage T3T3 mouse triple stained for ubiquitin (Ubi), parvalbumin (Parv), and glycine transporter 2 (*GlyT2*). The *GlyT2* signal is not shown in the overview image in A to outline autofluorescence (auto; arrowhead). There is prominent ubiquitin immunoreactivity in the cell body and a dendrite of a large motor neuron (A, C) and in the cell body of a parvalbumin-positive interneuron lying close to the motor column (A, B). There are *GlyT2*-immunoreactive boutons surrounding these neurons (B, C). (D) Double labeling of ATF3 and parvalbumin in the intermediate zone of C6 cervical spinal cord section of an end-stage T3T3 mouse showing ATF3 expression in a parvalbumin-positive neuron. (E-G) Double-labeling confocal immunofluorescence showing ubiquitin immunoreactivity in choline acetyl transferase (ChAT)-positive dendritic profiles in the ventral horn (E) and

ChAT-negative profiles in the intermediate zone (F) of lumbar spinal cord sections from a 20-week-old T3hSOD1 mouse. Bar graph (G) shows the number (mean ± SE) of ChAT-positive and ChAT-negative profiles labeled for ubiquitin in L4 lumbar spinal cord of 20-week-old G1del mice (n = 4), presymptomatic 2-year-old T3T3 mice (n = 2), 20-week-old T3hSOD1 mice (n = 4), and 35-week-old T3hSOD1 mice (n = 3). Values were obtained inChAT-ubiquitin double-labeled sections (4 sections per mouse). (H-K) Double-labeling confocal immunofluorescence showing activated microglia (Mac2-positive) and motor neurons (ChAT-positive) in lumbar L4 spinal cord sections of wild-type hSOD1 transgenic mice at 35 weeks of age (H) and T3hSOD1 double-transgenic mice aged 20 (I), 35 (J), or 65 (K) weeks. Note the absence of activated microglia in spinal cord of hSOD1 and 20-week-old T3hSOD1 mice, a low density of activated microglia in the ventral horn of 35-week-old T3hSOD1 mice, and numerous activated microglia throughout the ventral horn and intermediate zone of symptomatic 65-week-old T3hSOD1 mice (K). Scale bars = 50 µm (A), 25 µm (D, E), 200 µm (H).

age), and subsequently in interneurons (onset between 15 and 20 weeks of age). This is consistent with the sequential expression of ATF3 in motor neurons and interneurons in G93A-SOD1 mice (45).

Because ubiquitin aggregates occur first and more frequently in dendrites rather than in the cell soma of neurons (34, 45) and because *GlyT2* and *GAD67* mRNA and protein are not present in dendrites, we used parvalbumin as a substitute marker for the dendrites of inhibitory interneurons. Although there is compelling evidence that parvalbumin in spinal cord intermediate zone is predominantly associated with inhibitory neurons (Figure, Supplemental Digital Content 1, http://links.lww.com/NEN/A250) (57), it cannot be excluded that some parvalbumin-immunoreactive dendrites in the intermediate zone belong to excitatory neurons. Nevertheless, our data show that in 15-week-old G1del mice, ubiquitin staining is only associated with motor neuronal somata and dendrites (identified by ChAT staining),while at 20 weeks, approximately half of the ubiquitin-stained dendrites are ChAT-negative and are located in the intermediate zone, indicating that they are not of motor neurons. In view of our data that at least 50% of the ubiquitin-immunoreactive intermediate zone neurons express *GlyT2* or *GAD67* mRNA in a later phase of disease, it is likely that a significant proportion of the non-motor neuron ubiquitinated dendrites at 20 weeks belong to inhibitory interneurons.

The onset of degenerative changes in interneurons precedes the onset of behavioral motor manifestations and most of the motor neuron degeneration (45), raising the question as to whether interneuron degeneration contributes to further degeneration and motor signs. Our data indicate that the overall level of *GlyT2* and *GAD* immunoreactivity in the ventral horn is unaltered at 20 weeks, but subtle changes at inhibitory synapses on individual motor neurons cannot be excluded. Several studies suggest that changes in synaptic inputs to motor neurons contribute to motor neuron degeneration and motor manifestations of ALS (42, 62-65). Two recent studies also indicate that there are subtle losses of inhibitory synapses innervating motor neurons in presymptomatic high-copy G1 mice (41, 43), and compensatory sprouting of inhibitory glycinergic axons may also occur (41). These and our present data support the notion that early degenerative changes in inhibitory interneurons may contribute to the degeneration of motor neurons in SOD1-ALS mice, for example, by facilitating excitotoxic stress, one of the potential factors contributing to motor neuron degeneration in SOD1-ALS (28, 37, 42).

Ubiquitin pathology and ATF3 expression appeared in interneurons several weeks after their appearance in motor neurons. This raises the possibility that interneuron degenerative

changes somehow are a consequence of motor neuron degeneration. A linkage between interneuron and motor neuron degeneration is also suggested by the fact that *GlyT2* and *GAD67* immunoreactivity is specifically reduced in the ventral horn, indicating the selective involvement of inhibitory interneurons innervating motor neurons. Longitudinal analyses of muscle denervation in SOD1-ALS mice have shown that large motor neurons that innervate type IIB muscle fibers and form the forceful fast-fatigable (FF) units degenerate before clinical onset (66, 67). The time of appearance of ubiquitin pathology and the onset of ATF3 expression (at 13-15 weeks) coincide with the onset of early molecular changes in FF motor neurons, as identified in gene profiling experiments of motor neuron subtypes (13). Instead, fast fatigue-resistant and slow motor neurons become involved in later phase of disease (13, 66, 67). Together, these data indicate that the disease in SOD1-ALS mice starts in FF motor neurons and subsequently involves other motor neurons and at the same time spinal interneurons.

The appearance of interneuron abnormalities after the onset of motor neuron degeneration, combined with evidence that mutant SOD1 in glia contributes to disease progression after initiation of disease in motor neurons, may indicate that mutant SOD1 in glia plays an important role of the spreading of disease to interneurons. However, we found that neuron-specific G93A-SOD1 mice develop the same interneuronal abnormalities as in ubiquitous mutant SOD1-expressing G1del mice, indicating that glial mutant SOD1 expression is dispensable for triggering spinal interneuron degeneration. One proposed glial mechanism is that microglial activation triggered by motor neuron degeneration could cause or facilitate the degeneration of other neurons (28, 68). Some evidence suggests that toxic microglial actions requires microglial mutant SOD1 expression (31, 69), but mutant SOD1-independent actions of activated microglia may also occur; indeed, deleterious actions of microglia have been proposed for multiple neurodegenerative conditions (70). However, a major role of activated microglia in triggering early interneuron alterations in SOD1-ALS mice seems unlikely in view of our data that microglial activation is still limited at the time of the first appearance of interneuron dendritic ubiquitin pathology (*i.e.* between 15 and 20 weeks in ubiquitous G1del mice and 20 and 35 weeks in neuron-specific T3hSOD1 mice).

An alternative mechanism that could explain the appearance of interneuronal pathology subsequent to motor neuronal pathology is transcellular transmission of protein aggregation by seeds of aggregated species (71). Recent evidence indicates that such a mechanism may contribute to the spreading of pathology in neuronal protein aggregation disorders, including synucleinopathies and tauopathies (71). Furthermore, seeding-like properties have been demonstrated for mutant SOD1 (72). Hence, a possible scenario that is compatible with our data would be that mutant SOD1 aggregates released by degenerating motor neurons are taken up by interneuronal nerve endings and retrogradely transported to their parent cell to trigger or facilitate further SOD1 aggregation leading to the ubiquitinated inclusions and, eventually, cell death.

The availability of SOD1 transgenic mice models has enabled the precise dissection of the pathological progression of disease, indicating the involvement of different cell types at different disease stages as well as different cell autonomous and non-cell autonomous disease mechanisms. A central question is whether similar mechanisms also operate in sporadic ALS, which is predominantly characterized by TDP43 aggregates. The recent

availability of new mouse models, such as TDP43 transgenic mice that reproduce aspects of this TDP43 pathology (73-76), may help resolve this question and further unravel the disease mechanisms underlying ALS.

Acknowledgments

The authors thank Drs N. Nelson and N.J.K. Tillakaratne for *GlyT2* and *GAD67* cDNA constructs and Dr H.U. Zeilhofer for providing *GlyT2*-GFP transgenic mice.

References

1. Dion PA, Daoud H, Rouleau GA. Genetics of motor neuron disorders: New insights into pathogenic mechanisms. Nature Rev 2009:10;769-82
2. Andersen PM. Amyotrophic lateral sclerosis associated with mutations in the CuZn superoxide dismutase gene. Cur Neurol Neurosci Rep 2006:6;37-46
3. Mackenzie IR, Rademakers R, Neumann M. TDP-43 and FUS in amyotrophic lateral sclerosis and frontotemporal dementia. Lancet Neurol 2010:9;995-1007
4. Maruyama H, Morino H, Ito H, et al. Mutations of optineurin in amyotrophic lateral sclerosis. Nature 2010:465;223-26
5. Van Deerlin VM, Leverenz JB, Bekris LM, et al. TARDBP mutations in amyotrophic lateral sclerosis with TDP-43 neuropathology: A genetic and histopathological analysis. Lancet Neurol 2008:7;409-16
6. Neumann M, Sampathu DM, Kwong LK, et al. Ubiquitinated TDP-43 in Frontotemporal lobar degeneration and amyotrophic lateral sclerosis. Science 2006:314;130-33
7. Shaw BF, Valentine JS. How do ALS-associated mutations in superoxide dismutase 1 promote aggregation of the protein? Trends Biochem Sci 2007:32;78-85
8. Bergemalm D, Forsberg K, Srivastava V, et al. Superoxide dismutase-1 and other proteins in inclusions from transgenic amyotrophic lateral sclerosis model mice. J Neurochem 2010:114;408-18
9. Vance C, Rogelj B, Hortobagyi T, et al. Mutations in FUS, an RNA processing protein, cause familial amyotrophic lateral sclerosis type 6. Science 2009:323;1208-11 10. Kwiatkowski TJ Jr, Bosco DA, Leclerc AL, et al. Mutations in the FUS/TLS gene on chromosome 16 cause familial amyotrophic lateral sclerosis. Science 2009:323;1205-8
11. Johnson BS, McCaffery JM, Lindquist S, et al. A yeast TDP-43 proteinopathy model: Exploring the molecular determinants of TDP-43 aggregation and cellular toxicity. Proc Natl Acad Sci U S A 2008:105;6439-44
12. Van Damme P, Robberecht W. Recent advances in motor neuron disease. Curr Opin Neurol 2009:22;486-92
13. Saxena S, Cabuy E, Caroni P. A role for motoneuron subtype-selective ER stress in disease manifestations of FALS mice. Nat Neurosci 2009:12;627-36
14. Ravits JM, La Spada AR. ALS motor phenotype heterogeneity, focality, and spread: Deconstructing motor neuron degeneration. Neurology 2009:73;805-11
15. Piao YS, Wakabayashi K, Kakita A, et al. Neuropathology with clinical correlations of sporadic amyotrophic lateral sclerosis: 102 autopsy cases examined between 1962 and 2000. Brain Pathol 2003:13;10-22
16. Maekawa S, Al-Sarraj S, Kibble M, et al. Cortical selective vulnerability in motor neuron disease: A morphometric study. Brain 2004:127;1237-51
17. Stephens B, Guiloff RJ, Navarrete R, et al. Widespread loss of neuronal populations in the spinal ventral horn in sporadic motor neuron disease. A morphometric study. J Neurol Sci 2006:244;41-58
18. Kikuchi H, Doh-ura K, Kawashima T, et al. Immunohistochemical analysis of spinal cord lesions in amyotrophic lateral sclerosis using microtubule-associated protein 2 (MAP2) antibodies. Acta Neuropathol (Berl) 1999:97;13-21
19. Nishihira Y, Tan CF, Onodera O, et al. Sporadic amyotrophic lateral sclerosis: Two pathological patterns shown by analysis of distribution of TDP-43-immunoreactive neuronal and glial cytoplasmic inclusions. Acta Neuropathol 2008:116;169-82

20. Geser F, Brandmeir NJ, Kwong LK, et al. Evidence of multisystem disorder in whole-brain map of pathological TDP-43 in amyotrophic lateral sclerosis. Arch Neurol 2008:65;636-41
21. Geser F, Stein B, Partain M, et al. Motor neuron disease clinically limited to the lower motor neuron is a diffuse TDP-43 proteinopathy. Acta Neuropathol 2011:121;509-17
22. Kobayashi Z, Tsuchiya K, Arai T, et al. Clinicopathological characteristics of FTLD-TDP showing corticospinal tract degeneration but lacking lower motor neuron loss. J Neurol Sci 2010:298;70-77
23. Attarian S, Vedel JP, Pouget J, et al. Progression of cortical and spinal dysfunctions over time in amyotrophic lateral sclerosis. Muscle Nerve 2008:37;364-75
24. Eisen A, Weber M. The motor cortex and amyotrophic lateral sclerosis. Muscle Nerve 2001:24;564-73
25. Chou SM, Norris FH. Amyotrophic lateral sclerosis: Lower motor neuron disease spreading to upper motor neurons. Muscle Nerve 1993:16;864-69
26. Brooks BR. The role of axonal transport in neurodegenerative disease spread: A meta-analysis of experimental and clinical poliomyelitis compares with amyotrophic lateral sclerosis. Can J Neurol Sci 1991:18;435-38
27. Ravits J, Paul P, Jorg C. Focality of upper and lower motor neuron degeneration at the clinical onset of ALS. Neurology 2007:68;1571-75
28. Ilieva H, Polymenidou M, Cleveland DW. Non-cell autonomous toxicity in neurodegenerative disorders: ALS and beyond. J Cell Biol 2009:187;761-72
29. Kato S, Takikawa M, Nakashima K, et al. New consensus research on neuropathological aspects of familial amyotrophic lateral sclerosis with superoxide dismutase 1 (SOD1) gene mutations: Inclusions containing SOD1 in neurons and astrocytes. Amyotroph Lateral Scler Other Motor Neuron Disord 2000:1;163-84
30. Beers DR, Henkel JS, Xiao Q, et al. Wild-type microglia extend survival in PU.1 knockout mice with familial amyotrophic lateral sclerosis. Proc Natl Acad Sci U S A 2006:103;16021-26
31. Boillee S, Yamanaka K, Lobsiger CS, et al. Onset and progression in inherited ALS determined by motor neurons and microglia. Science 2006:312;1389-92
32. Wang L, Sharma K, Grisotti G, et al. The effect of mutant SOD1 dismutase activity on non-cell autonomous degeneration in familial amyotrophic lateral sclerosis. Neurobiol Dis 2009:35;234-40
33. Yamanaka K, Chun SJ, Boillee S, et al. Astrocytes as determinants of disease progression in inherited amyotrophic lateral sclerosis. Nat Neurosci 2008:11;251-53
34. Jaarsma D, Teuling E, Haasdijk ED, et al. Neuron-specific expression of mutant superoxide dismutase is sufficient to induce amyotrophic lateral sclerosis in transgenic mice. J Neurosci 2008:28;2075-88
35. Jankowska E. Spinal interneuronal networks in the cat: Elementary components. Brain Res Rev 2008:57;46-55
36. Grillner S, Thomas MJ. Measured motion: Searching for simplicity in spinal locomotor networks. Curr Opin Neurobiol 2009:19;572-86
37. Van Den Bosch L, Van Damme P, Bogaert E, et al. The role of excitotoxicity in the pathogenesis of amyotrophic lateral sclerosis. Biochim Biophys Acta 2006:1762;1068-82
38. Oyanagi K, Ikuta F, Horikawa Y. Evidence for sequential degeneration of the neurons in the intermediate zone of the spinal cord in amyotrophic lateral sclerosis: A topographic and quantitative investigation. Acta Neuropathol 1989:77;343-49
39. Morrison BM, Janssen WG, Gordon JW, et al. Time course of neuropathology in the spinal cord of G86R superoxide dismutase transgenic mice. J Comp Neurol 1998:391;64-77
40. Martin LJ, Liu Z, Chen K, et al. Motor neuron degeneration in amyotrophic lateral sclerosis mutant superoxide dismutase-1 transgenic mice: Mechanisms of mitochondriopathy and cell death. J Comp Neurol 2007:500;20-46
41. Chang Q, Martin LJ. Glycinergic innervation of motoneurons is deficient in amyotrophic lateral sclerosis mice: A quantitative confocal analysis. Am J Pathol 2009:174;574-85
42. Jiang M, Schuster JE, Fu R, et al. Progressive changes in synaptic inputs to motoneurons in adult sacral spinal cord of a mouse model of amyotrophic lateral sclerosis. J Neurosci 2009:29;15031-38
43. Pullen AH, Athanasiou D. Increase in presynaptic territory of C-terminals on lumbar motoneurons of G93A SOD1 mice during disease progression. Eur J Neurosci 2009:29;551-61
44. Gurney ME. The use of transgenic mouse models of amyotrophic lateral sclerosis in preclinical drug studies. J Neurol Sci 1997:152;S67-S73

45. Vlug AS, Teuling E, Haasdijk ED, et al. ATF3 expression precedes death of spinal motoneurons in amyotrophic lateral sclerosis-SOD1 transgenic mice and correlates with c-Jun phosphorylation, CHOP expression, somato-dendritic ubiquitination and Golgi fragmentation. Eur J Neurosci 2005:22;1881-94
46. Jaarsma D, Holstege JC, Troost D, et al. Induction of c-Jun immunoreactivity in spinal cord and brainstem neurons in a transgenic mouse model for amyotrophic lateral sclerosis. Neurosci Lett 1996:219;179-82
47. Zeilhofer HU, Studler B, Arabadzisz D, et al. Glycinergic neurons expressing enhanced green fluorescent protein in bacterial artificial chromosome transgenic mice. J Comp Neurol 2005:482;123-41
48. Jaarsma D, Haasdijk E, Grashorn JAC, et al. Cu/Zn superoxide dismutase (SOD1) overexpression in mice causes mitochondrial degeneration, axonal degeneration and premature motoneuron death, and accelerates the development of motoneuron disease in mice expressing fALS-mutant SOD1. Neurobiol Dis 2000:7;623-43
49. Hossaini M, French PJ, Holstege JC. Distribution of glycinergic neuronal somata in the rat spinal cord. Brain Res 2007:1142;61-69
50. Speel EJ, Hopman AH, Komminoth P. Tyramide signal amplification for DNA and mRNA in situ hybridization. Methods Mol Biol 2006:326;33-60
51. Hopman AH, Ramaekers FC, Speel EJ. Rapid synthesis of biotin-, digoxigenin-, trinitrophenyl-, and fluorochrome-labeled tyramides and their application for In situ hybridization using CARD amplification. J Histochem Cytochem 1998:46;771-77
52. Maatkamp A, Vlug A, Haasdijk E, et al. Decrease of Hsp25 protein expression precedes degeneration of motoneurons in ALS-SOD1 mice. Eur J Neurosci 2004:20;14-28
53. Jaarsma D, Rognoni F, Van Duijn W, et al. CuZn superoxide dismutase (SOD1) accumulate in vacuolated mitochondria in transgenic mice expressing amyotrophic lateral sclerosis (ALS)-linked SOD1 mutations. Acta Neuropathol 2001:102;293-305
54. Zafra F, Aragon C, Olivares L, et al. Glycine transporters are differentially expressed among CNS cells. J Neurosci 1995:15;3952-69
55. Mackie M, Hughes DI, Maxwell DJ, et al. Distribution and colocalisation of glutamate decarboxylase isoforms in the rat spinal cord. Neuroscience 2003:119;461-72
56. Ma W, Behar T, Chang L, et al. Transient increase in expression of *GAD*65 and *GAD67* mRNAs during postnatal development of rat spinal cord. J Comp Neurol 1994:346;151-60
57. Alvarez FJ, Jonas PC, Sapir T, et al. Postnatal phenotype and localization of spinal cord V1 derived interneurons. J Comp Neurol 2005:493;177-92
58. Rotshenker S, Reichert F, Gitik M, et al. Galectin-3/MAC-2, Ras and PI3K activate complement receptor-3 and scavenger receptor-AI/II mediated myelin phagocytosis in microglia. Glia 2008:56;1607-13
59. Deng HX, Shi Y, Furukawa Y, et al. Conversion to the amyotrophic lateral sclerosis phenotype is associated with intermolecular linked insoluble aggregates of SOD1 in mitochondria. Proc Natl Acad Sci U S A 2006:103;7142-47
60. Prudencio M, Durazo A, Whitelegge JP, et al. An examination of wild-type SOD1 in modulating the toxicity and aggregation of ALS-associated mutant SOD1. Hum Mol Genet 2010:19;4774-89
61. Stephens B, Navarrete R, Guiloff RJ. Ubiquitin immunoreactivity in presumed spinal interneurones in motor neurone disease. Neuropathol Appl Neurobiol 2001:27;352-61
62. Schutz B. Imbalanced excitatory to inhibitory synaptic input precedes motor neuron degeneration in an animal model of amyotrophic lateral sclerosis. Neurobiol Dis 2005:20;131-40
63. Vucic S, Cheah BC, Kiernan MC. Defining the mechanisms that underlie cortical hyperexcitability in amyotrophic lateral sclerosis. Exp Neurol 2009:220;177-82
64. Attarian S, Pouget J, Schmied A. Changes in cortically induced inhibition in amyotrophic lateral sclerosis with time. Muscle Nerve 2009:39;310-17
65. Raynor EM, Shefner JM. Recurrent inhibition is decreased in patients with amyotrophic lateral sclerosis. Neurology 1994:44;2148-53
66. Hegedus J, Putman CT, Tyreman N, et al. Preferential motor unit loss in the SOD1 G93A transgenic mouse model of amyotrophic lateral sclerosis. J Physiol 2008:586;3337-51
67. Pun S, Santos AF, Saxena S, et al. Selective vulnerability and pruning of phasic motoneuron axons in motoneuron disease alleviated by CNTF. Nat Neurosci 2006:9;408-19
68. Henkel JS, Beers DR, Zhao W, et al. Microglia in ALS: The good, the bad, and the resting. J Neuroimmune Pharmacol 2009:4;389-98

69. Beers DR, Ho BK, Siklos L, et al. Parvalbumin overexpression alters immune-mediated increases in intracellular calcium, and delays disease onset in a transgenic model of familial amyotrophic lateral sclerosis. J Neurochem 2001:79;499-509
70. Perry VH, Nicoll JA, Holmes C. Microglia in neurodegenerative disease. Nat Rev Neurol 2010:6;193-201
71. Aguzzi A, Rajendran L. The transcellular spread of cytosolic amyloids, prions, and prionoids. Neuron 2009:64;783-90
72. Chia R, Tattum MH, Jones S, et al. Superoxide dismutase 1 and tgSOD1 mouse spinal cord seed fibrils, suggesting a propagative cell death mechanism in amyotrophic lateral sclerosis. PLoS One 2010:5;e10627
73. Xu YF, Gendron TF, Zhang YJ, et al. Wild-type human TDP-43 expression causes TDP-43 phosphorylation, mitochondrial aggregation, motor deficits, and early mortality in transgenic mice. J Neurosci 2010:30;10851-59
74. Stallings NR, Puttaparthi K, Luther CM, et al. Progressive motor weakness in transgenic mice expressing human TDP-43. Neurobiol Dis 2010:40;404-14
75. Wils H, Kleinberger G, Janssens J, et al. TDP-43 transgenic mice develop spastic paralysis and neuronal inclusions characteristic of ALS and frontotemporal lobar degeneration. Proc Natl Acad Sci U S A 2010:107;3858-63
76. Wegorzewska I, Bell S, Cairns NJ, et al. TDP-43 mutant transgenic mice develop features of ALS and frontotemporal lobar degeneration. Proc Natl Acad Sci U S A 2009:106;18809-14

Supplementary Data

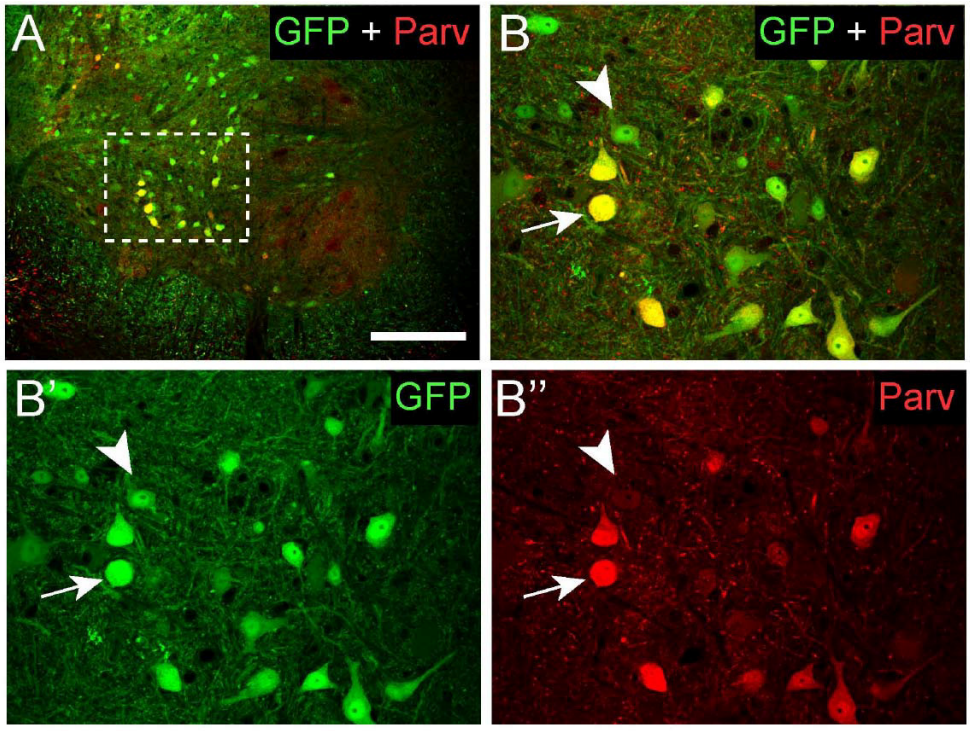

Figure S1. The majority of parvulbumin-positive spinal intermediate zone interneurons are glycinergic. Low and high magnification confocal fluorescent image showing green fluorescent protein (GFP) signal and parvalbumin immunoreactivity in a lumbar L4 section of a bacterial artificial chromosome (BAC) transgenic mouse which specifically express GFP under the control of the promotor of *GlyT2* gene, resulting in intense GFP signal in glycinergic neurons (Zeilhofer et al., 2005, J Comp Neurol. 482:123-141).The far majority of parvalbumin-positive intermediate zone neurons were GFP-positive (e.g arrow in B), indicating that they are glycinergic. Of 500 randomly selected parvalbumin-positive intermediate zone interneurons 468 (= 94%) were GFP-positive. Vice-versa many GFP-positive cells are parvalbumin negative or very weakly parvalbumin positive (arrow head in B). This indicates that parvalbumin-immunoreactivity outlines only a subset of glycinergic neurons in spinal cord.
Scale bar, 200 µm.

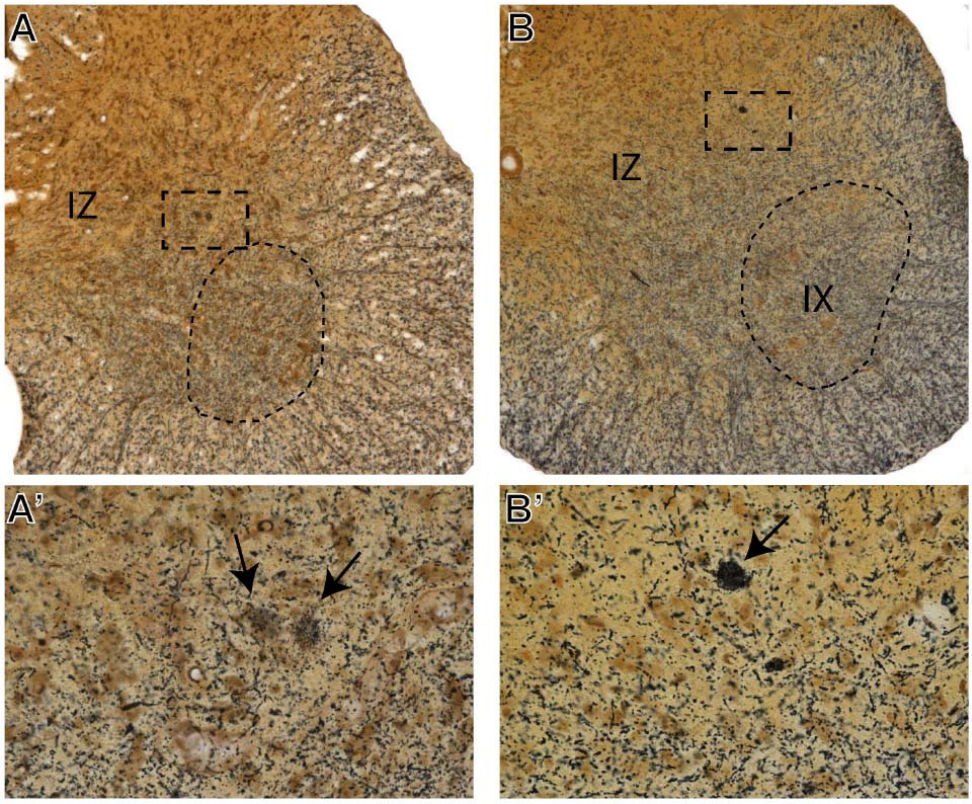

Figure S2. Silver degeneration staining reveals dying neurons in intermediate zone of spinal cord of neuron-specific SOD1-G93A transgenic mice Light-photomicrographs of spinal cord sections of symptomatic neuron-specific G93A-SOD1 mice (T3T3 line; Jaarsma et al., 2008, J Neurosci 28:2075-2088) stained with a silver degeneration staining method that produces black staining in dying neurons and their processes, and light brown staining in other cells. Note abundant argyrophylic staining in motor columns (IX) and the intermediate zone (IZ) adjacent to the motor columns. Most argyrophylic staining is associated with neuronal processes. Occasionally stained cell bodies indicative of dying interneurons (arrows) can be identified.

Chapter 3

The formation of pathological tau species in GFAP-tau overexpressing astrocytes in an environment of degenerating neurons

Vera van Dis[1], Karin Boekhoorn[1], Elize D. Haasdijk[1], Casper C. Hoogenraad[1], Mark S. Forman[2], Dick Jaarsma[1]

1. Dept of Neuroscience, Erasmus MC, Rotterdam; 2. Dept of Pathology and Laboratory Medicine, Univ. of Pennsylvania School of Medicine, Philadelphia

Abstract

Mutations in the superoxide dismutase 1 (SOD1) gene cause a form of amyotrophic lateral sclerosis (ALS). Transgenic mice expressing mutant SOD1 develop an ALS-like disease, and like SOD1-ALS patients, develop micrometer-scale aggregates in both neurons and astrocytes. The time of appearance and distribution of SOD1 aggregates in astrocytes indicate that they arise in a late phase of disease secondarily to motor neuron degeneration. In this study we show that when SOD1-ALS mice are crossed with transgenic mice expressing a high level of human tau protein in astrocytes (GFAP-tau mice) double transgenic mice develop tau hyperphosphorylation and aggregation in astrocytes. At disease endstage the tau aggregates occurred in the majority of astrocytes, a subset of whom also showed SOD1 aggregates. Together the data indicate that astrocytes show increased vulnerability to aggregation prone proteins in the context of neuronal degeneration, and support the notion that protein aggregation disorders like SOD1-ALS and tauopathies may spread from neurons to glia.

Introduction

Protein aggregation is a hallmark of various neurodegenerative diseases. Such as Alpha-synuclein deposits in Parkinson's disease (Spillantini et al., 1997), Beta-amyloid plaques in Alzheimer's disease (Masters et al., 1985) and TDP43 in Amyotrophic Lateral Sclerosis (ALS). Besides damage to neurons, also surrounding astroglia are affected in these diseases (for review see (Maragakis and Rothstein, 2006).

Amyotrophic Lateral Sclerosis (ALS) is a late onset disease of the motor neurons, leading to progressive paralysis. Death occurs typically within one to five years after diagnosis. There is no effective treatment for this disease. Most cases of ALS are caused by aggregates of TAR DNA binding protein 43 (TDP-43) (Neumann et al., 2006) However, 2-5% is caused by mutations in the Cu/Zn superoxide dysmutase 1 (SOD1) (Rosen et al., 1993). This protein converts toxic superoxide to water and hydrogen peroxide. There are over 114 known mutations in the SOD1 gene, which all cause clinical disease (Boillee et al., 2006a). Mouse models overexpressing mutant SOD1 develop an ALS-like disease. Mutant SOD1 is prone to aggregation, however, the precise mechanism why these aggregates lead to neuronal disease is not known.

Mutant SOD1 pathology is not only present in neurons, but also in surrounding glial cells (Bruijn et al., 1997; Kato et al., 1997). In patients and in mouse models, astrocyte activation is observed in the spinal cord. (Pasinelli and Brown, 2006) Furthermore, a diminished glutamate transport has been reported in affected tissues, and levels of EAAT2, an astrocyte specific glutamate transporter, are reduced in the motor cortex and spinal cord of ALS patients (Boillee et al., 2006a). What is the contribution of the astrocyte pathology to the neurodegenerative disease?

We hypothesize that glial cells are not sensitive to mutant SOD1 expression, however when in the context of neurodegeneration, they will develop SOD1 pathology. And because of the increased SOD1 pathology the glial cells will be less able to perform their normal tasks, accelerating neuronal cell death

To further elucidate the role of astrocyte pathology in ALS, we want to stress the astrocytes in SOD1 G93A (G1del) mice by crossing them to transgenic mice that express another aggregate prone protein, tau protein, in astrocytes (Forman et al., 2005). These mice develop an age-dependent accumulation of tau pathology in astrocytes (GFAP-tau mice). Tau is a microtubule associated protein (MAP) that is primarily found in axons. Tau regulates the assembly and stability of microtubules and plays an important role in the maintenance of cell structure and transport (Lin et al., 2003).

The astrocyte pathology in the homozygous mice is associated with various abnormalities, including reduced glutamate reuptake, disruption of the blood brain barrier and neuronal abnormalities (Dabir et al., 2006). These pathological events are all hallmarks of a group of neurodegenerative diseases known as tauopathies, such as Pick's disease (PiD), progressive supranuclear palsy (PSP), corticobasal degeneration (CBD), and Alzheimer's disease (AD). Tauopathies are characterized by tau hyperphosphorylation and aggregation.

Table 3.1 clinical disease and pathology in both motor neurons and astrocytes in the transgenic genotypes								
mice	clinical disease		motor neurons		Astrocytes			
	onset	death	ubiquitn pathology	death	increased GFAP	Hspb1	ubiquitin pathology	AT8
G1del	25-39	30-40	>10-15	<20-25	>20-25	>20-25	symptomatic/ end stage	-
GFAP-tau	>70-90	-	-	-	from birth	from birth	-	>70-90 w
G1del/GFAP-tau	25-38	27-40	>10-15	<20-25	from birth	from birth	Symptomatic/ end stage	symptomatic/ end stage

All ages are displayed in weeks

What we want to know is whether the tau pathology in astrocytes is influenced by the neuronal pathology in G1del mice. We hypothesise that the tau pathology of the GFAP-tau mice will develop at an earlier age in the double transgenic mice. Furthermore we expect that the SOD1 pathology will be accelerated in the affected astrocytes. Finally we expect that the increased astrocyte pathology accelerates the disease progression in G1del mice.

Materials and Methods

Animals

Human G93A-SOD1 mice (G1del) descendent from the Gurney G1del line carry approximately eight transgene copy numbers per haploid genome (compared to 24 in the original G1 mice) were housed and handled in accordance with the *Principles of Laboratory Animal Care* (National Institutes of Health publication No. 86–23) and the guidelines approved by the Erasmus University animal care committee. These mice develop weakness in one or more limbs from age 25–38 weeks, and reach end-stage disease 1–10 weeks after the onset of limb weakness.

GFAP-tau transgenic mice were generated by Forman et al. (Forman et al., 2005). These mice were created using a cDNA construct that contained the T34 human tau isoform linked to the GFAP promoter (glial cell specific). T34 human tau is one of the most abundant tau isoforms in humans, containing exon 2 and exon 10. The GFAP-tau mice were kept at the same standards as the G1del mice.

The GFAP-tau transgenic mice and the G1del mice were crossed to create double transgenic G1del/GFAP-tau mice. The heterozygous GFAP-tau and non-transgenic littermates were used as control. Genotyping of the transgenic mice was done using tail-pcr. Mice of all genotypes were weekly subjected to various behavioral tests starting from 10 weeks of age. Onset of symptoms was determined on the basis of the onset of weight loss. The inability to normally extend one of the hind limbs was used to determine the progression of paralysis. Motor strength was tested by the ability to normally perform in the hanging grid test, where mice have to hang upside down on a grid for 60 seconds.

The ability to perform for a maximum of 300 s on the accelerating rotarod (4-40 rpm, in 5 minutes; model 7650, Ugo Basile Biological Research Apparatus, Varese, Italy) was used to test for motor function. At 10 weeks of age the mice were subjected to a test trail on two

consecutive days. From 11 weeks of age mice were tested weekly. All mice were tested 3 times during each session, with 5-10 minutes rest. Their latency to fall was recorded during each run with a maximum of 300 s and the average of the 3 runs was calculated.
Mice reached end-stage disease when they could not right themselves within 5 s when placed on their back, lost more than 30% of their maximal weight, or developed infection of one of the eyes (Jaarsma et al., 2008).

Antibodies

Primary antibodies {immunohistochemistry (IHC), immunofluorescence (IF), western blottin (WB)} reported in this study are as follows: mouse anti-αB-crystallin (Stressgen Biotechnologies, San Diego, CA; IHC and IF, 1:1000, 1:2000), rabbit anti-activating transcription factor 3 (ATF3; Santa Cruz Biotechnology, Santa Cruz, CA; IHC and IF, 1:1000); mouse anti-AT8 (pSer396/pThr205; IHC, 1:1000; IF 1:5000; WB 1:1000) rabbit anti-cleaved caspase 3 (Asp175; Cell Signaling Technology, Beverly, MA; IHC, 1:200), rabbit anti-calcitonin gene-related peptide (CGRP; Calbiochem, La Jolla, CA; IHC and IF, 1:10000); goat anti-choline acetyltransferase (ChAT; Millipore, Billerica, MA; IHC and IF, 1:500); rabbit anti-GFAP (Dako, Carpinteria, CA; IHC, 1:10,000; IF, 1:5000; 1:5000); rabbit anti-glutamate transporter 1 (GLT1; from Dr. N. J. Maragakis, Johns Hopkins University, Baltimore, MD; 1:10,000); rabbit anti-heat shock protein 25 (Hspb1; Stressgen; IF, 1:2000; WB, 1:4000); rat anti-mac2 (Cedarlane IHC, 1:2000) sheep anti-hSOD1 (Calbiochem; IHC, 1:500; IF, 1:5000); mouse anti-ubiquitine (clone FK2; Affinity BioReagents, Golden, CO; IF, 1:2000); Mouse anti-tau1 (Chemicon MAB3420; IHC, 1:8000; IF, 1:2000; WB 1:2000)

Immunocytochemistry and immunofluorescence

For immunocytochemistry and immunofluorescence mice were anaesthetized with pentobarbital and perfused transcardially with 4% paraformaldehyde. The brain, the lumbar and cervical spinal cord were carefully dissected out and postfixed for 1h in 4% paraformaldehyde. Routinely, spinal cord tissue was embedded in gelatin blocks (Jaarsma et al., 2000), sectioned at 40 µm with a freezing microtome, and sections were processed, free-floating, employing a standard avidin–biotin–immunoperoxidase complex method (ABC, Vector Laboratories, USA) with 3,3-diaminobenzidine tetra chloride (0.05%) as the chromogen, or single-, double- and triple-labelling immunofluorescence (Jaarsma et al., 2000). In addition, a selected number of frozen sections were processed for a silver staining procedure that selectively labels dying neurons and their processes (Jaarsma et al., 2000).
Immunoperoxidase-stained sections were analyzed and photographed using a Leica (Nussloch, Germany) DM-RB microscope and a Leica DC300 digital camera. Sections stained for immunofluorescence were analyzed with a Zeiss (Oberkochen, Germany) LSM 510 confocal laser scanning microscope using 10x/0.3 air objective, 40x/1.3 and 63x/1.4 oil-immersion objectives.

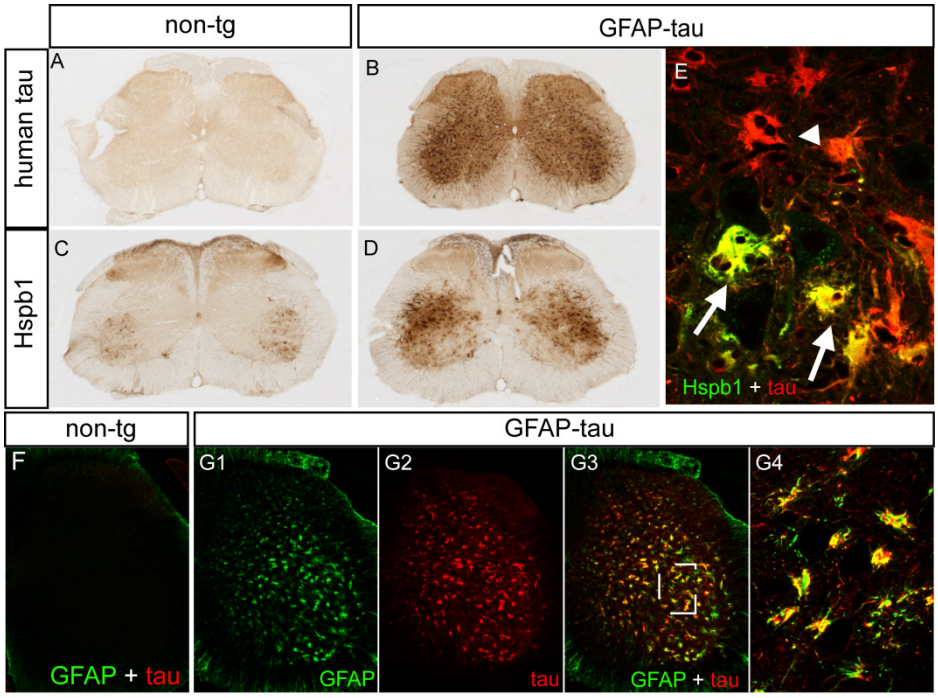

Figure 3.1. In GFAP-tau mice, a heterogenous population of astrocytes show an increase of GFAP and Heat shock protein b1 (Hspb1) expression. We stained lumbar spinal cords of a non-transgenic mouse (A and C) and a GFAP-tau mouse (B and D) for a human tau isoform (A and B) and for Hspb1 (C and D) expression. The GFAP-tau mouse expresses human tau in the grey matter of the spinal cord. Hspb1is upregulated in the motorneuron area of the GFAP-tau mouse. However this is only present in a subset of the astrocytes (E) (arrows). The arrowhead marks a tau positive astrocyte that does not express Hspb1.Double labeling of tau and GFAP in lumbar spinal cords (F-G) shows a very clear GFAP upregulation (G1) as compared to the non transgenic mice (F). At a larger magnification it is clear that GFAP positive cells also express human tau protein (J). (A-D magnification 4x, E magnification 40x, F-I magnification 10x, J magnification 63x)

Western blotting

Mice were decapitated and cerebellum, cortex, brainstem and spinal cord were dissected and immediately frozen on dry ice and stored in -80°C until use. Spinal cord tissue was homogenized in 10 volumes of PBS containing 0.5% Nonidet P-40 and 1x protease inhibitor cocktail (Complete, Roche), sonicated and centrifuged at 800*g* for 15 min, and protein concentrations of the supernatants (S1) were determined using the BCA method (Pierce, Rockford, IL, USA). For the preparation of detergent-insoluble extracts, S1 supernatants were centrifuged at 15 000*g* for 15 min. After the collection of supernatants (S2), pellets were thoroughly washed five times with PBS-0.5% Nonidet P-40 and then resuspended in sample buffer for SDS–PAGE electrophoresis and western-blotting. To blot tau aggregates a protocol adopted from (Forman et al., 2005) was used.

Tissues are homogenized in HS-TBS (50 mM Tris (pH 7.6), 750 mM NaCl, 1mM EGTA, 0.5 mM MgSO4, 100 µM EDTA) supplemented with protease inhibitors (1:25) and, if necessary, phospatase inhibitors (1:100), using 10µl/gr starting tissue. Centrifuged at 100,000 x *g* for 30 min at 4°C and than the supernatant is boiled for 5 min and centrifuged

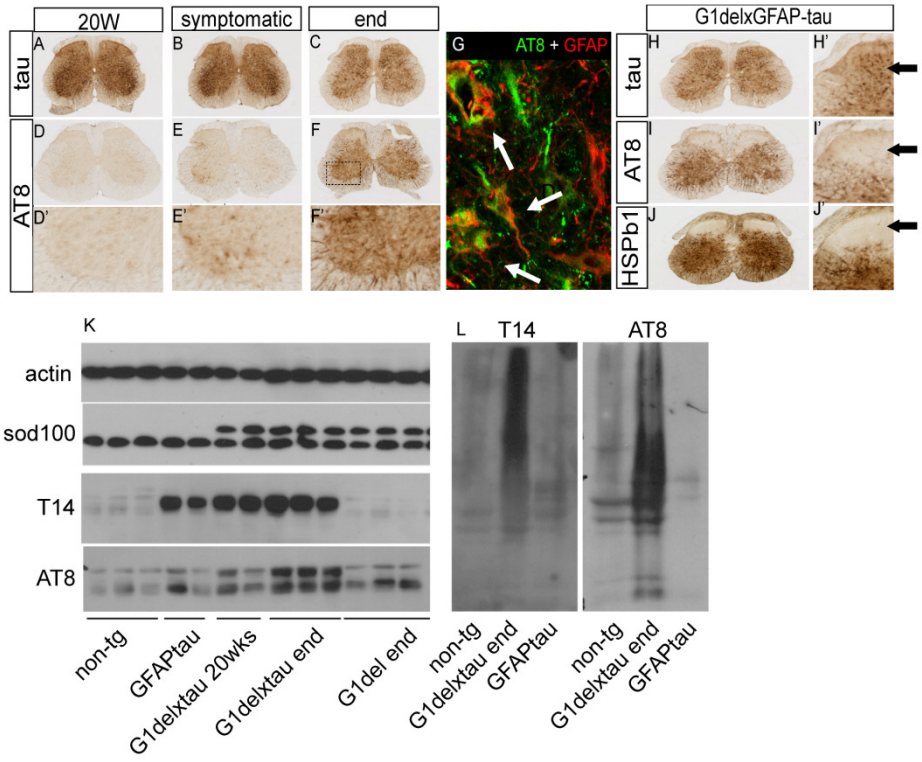

at

Figure 3.2. Tau hyperphosporylation (AT8 epitope) and Hspb1 expression are present in the motorneuron area after onset of neurodegeneration.

G1del/GFAP-tau mice expresses human tau throughout life (A-C). However, phospo-tau is only expressed from onset of disease (D-F). This is shown in detail below. Another feature we noticed was the expression of Hspb1 (H-J, right panel for detail). This is only expressed in areas of motor degeneration (arrow for detail). (A-F magnification 10x, D'-F' magnification 63x, E-M magnification 4x)

G1del/GFAP-tau mouse develops an abnormal hyperphosporylation of tau in in astrocytes (A-F, D'-F for detail). The G1del and the G1del/GFAP-tau mice show a GFAP increase, suggestive of astrogliosis. Which is colocalized with AT8 (G). The westernblot (K): Actin is used as a loading control SOD100 shows endogenous (lower bar) and transgenic SOD (upper bar). T14 shows transgenic human tau in the GFAP-tau expressing mice. AT8 shows an upregulation in the endstage disease G1del/GFAP-tau animals. (L) Both T14 and AT8 form smears in the insoluble fraction in endstage disease G1del/GFAP-tau mice.

at 15,000 x *g* for 20 min at 4°C resulting in the s1 fraction. To remove myelin and associated lipids the insoluble pellets reextracted with 1M sucrose in HS-TBS and centrifuged at 100,000 x *g* for 30 min at 4°C. The resulting pellets are homogenized in immunoprecipitation assay buffer (50 mM Tris pH 8.0, 150 mM NaCl, 5 mM EDTA, 0.5% sodium deoxycholate, 1% NP-40, 0.1% SDS) supplemented with protease inhibitors (100 ul) and centrifuge as before. The supernatant are the detergent-soluble samples, (which containe only low levels of tau protein). The detergent-insoluble pellets are extracted with 100 ul 70% formic acid and disrupted with sonication. FA is evaporated in an Automatic Environmental Speed-Vac system. The dried pellets are resuspended in SDS sample buffer. Samples containing 50-100 µg starting tissue were electrophoresed on 8-12% SDS–PAGE gels and blotted on PVDF membranes (Millipore). The membranes were blocked with 5%

non-fat dry milk (Bio-Rad) in PBS with 0.05% Tween20 (PBST), incubated in primary antibody, diluted in PBST with 1% dry milk (ON) followed by an incubation in secondary antibody, incubated in chemiluminescence reagent (ECL, Amersham), exposed to film on a Kodak Image station.

Statistics

Statistical analysis was done using GraphPad Prism 4.0 software. T-test, one way ANOVA and repeated measures ANOVA were used for analysis.

Results

Astrocytes in GFAP-tau mice over express GFAP and Hspb1 in the motorneuron area

GFAP-tau mice were perfused at 20, 40 and 70 weeks of age and lumbar spinal cord sections were processed for immunhistochemistry as described. Tau-expression was labeled with antibodies for human tau and immunofluorescent double labeled with GFAP. Homozygous GFAP-tau mice as described by Forman et al., express human tau in astrocytes throughout life in the gray matter of the spinal cord. This is accompanied by a GFAP increase and morphological changes in astrocytes. We observed the same in our heterozygous GFAP-tau mice. The tau expression colocalizes very well with a GFAP staining using immunofluorescent techniques (Fig 3.1F-G).

To address the pathological properties of the tau overexpression, we double labeled tau and heat shock protein b1 (Hspb1). We observed an increase of Hspb1 expression from birth, suggesting astrocyte pathology. Interestingly this is only expressed in the ventral spinal cord, the area of motorneurons (Fig 3.1A-E). By double labeling Hspb1 and tau we surprisingly found that not all tau positive astrocytes expressed Hspb1, suggesting a heterogeneous astrocyte population (Fig 3.1).

GFAP-tau/G1del mice develop hyperphosporylation of tau in astrocytes after onset of neurodegeneration

A pathological hallmark of tauopathies is the hyperphosphorylation and aggregation of tau. To evaluate this phenomenon in our mice we used immunohistochemical approaches using antibodies against specific phosphoepitopes (pSer396/pThr205) of the tau protein (AT8). Hyperphosporylated tau (phospho-tau) is observed by Forman et al. from 12 months of age in the homozygous GFAP-tau transgenic mice. However in our heterozygous GFAP-tau mice we observe a slight accumulation of phospo-tau over 70 months of age, *i.e.* the oldest age examined. Interestingly we only found phospho-tau in areas of neuronal degeneration.

In our double transgenic G1del/GFAP-tau mice we observed phospho-tau from about 25 weeks of age. This coincides with disease onset and start of neurodegeneration (Fig 3.2A). To confirm this we used westernblotting of the spinal cord of various types of G1del/GFAP-tau mice. At 20 weeks of age, before onset of symptoms, there is a slight increase of AT8. However at endstage disease there is a large increase in the AT8 (Fig 3.2K). The insoluble fraction shows both in the T14 and AT8 form a smear in the

symptomatic G1del/tau mice, indication aggregated forms of hyperphosphorylated tau (Fig 3.2L).

Phospho-tau does not codistribute with hSOD1 aggregates in astrocytes

It is shown that alpha-synuclein is able to promote fibrilization of tau via an interaction of the two proteins (Giasson et al., 2003; Riedel et al., 2009). Whether mutant SOD1 could facilitate the fibrilization of the overexpressed tau protein, or whether the over expressed tau is able to promote hSOD1 aggregation was examined using immunofluorescent triple labeling of human SOD1, ubiquitin and human tau.

The G1del/GFAP-tau mice do not show more SOD1 aggregates in astrocytes than their G1del littermates (Fig 3.3A, B). SOD1 aggregates in the G1del and in the G1del/GFAP-tau mice are very strong colocalized with ubiquitin, a protein associated with SOD1 aggregates. Ubiquitin poorly colocalizes with the phospo-tau positive cells. Suggesting that the GFAP-tau transgene does not influence the mutant SOD1 pathology and that aggregation of both proteins is caused via separate pathways (Fig 3.3).

Tau pathology could be a burden to the affected astrocytes. Doublelabeling of phospo-tau and caspase 3, an apoptotic marker, is used to examine this question. There are some positive cells expressing both phospo-tau and caspase 3. However, there are caspase 3 expressing neurons observed as well. There is no increase in apoptotic marker expression when cells overexpress tau protein (Fig 3.3C).

GFAP-tau does not influence survival of G1del mice.

By crossing the GFAP-tau mice with the G1del mice we developed a model where we can study the effect of astrocyte pathology in the ALS-like disease of the G1del mice. We anticipated that the tau-induced pathology would interfere with the normal astrocyte function and consequently facilitate neuronal cell dead. Resulting in an increased disease progression in G1del mice. This hypothesis was tested using various disease parameters: The rotarod to test motor behavior, the hanging wire test for muscle strength, the hind limb spread test and weight decline as a measure of disease progression. There is no significant effect of the overexpression of tau in astrocytes in the G1del mice on disease onset, disease duration or life span ($p>0.05$) (Fig 3.4). Even though there is no significant result, it seems that the doubletransgenic mice are performing worse than the non-transgenic and the GFAP-tau mice in all tests. Furthermore, we noticed that on the rotarod, the G1del mice and the G1del/GFAP-tau are never performing as well as the non-transgenic and GFAP-tau mice. Suggesting an early effect of SOD1 G93A expression in these mice.

As described earlier the GFAP-tau mice express Hspb1 from birth as do the G1del/GFAP-tau mice. The G1del mice express Hspb1 as well, but only from symptomatic disease (table 3.1).

As described in literature, both the G1del mice (Bruijn et al., 1997) and the GFAP-tau mice (Dabir et al., 2006) have a dimished glutamate transport, resulting from a decrease in GLT1 expression. GLT1 is an astrocyte specific glutamate transporter. It is well known that astrocytes are key players in the glutamate homeostasis. No difference in GLT1 expression was observed using immunofluorescence between the G1del mice and the G1del/GFAP-tau mice (data not shown).

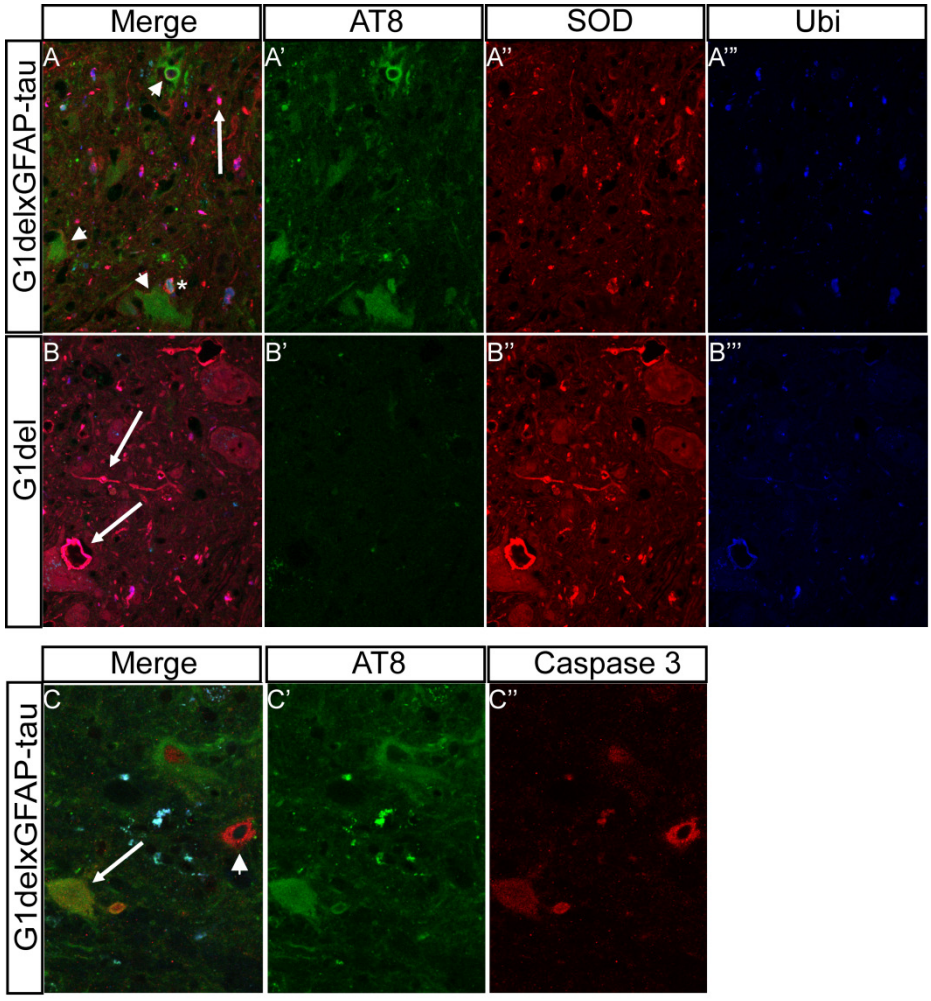

Figure 3.3. Hyperphosporylated tau and mutant SOD1 poorly colocalize in G1del/GFAP-tau mice
In the G1del mouse (B) ubiquitinated SOD1 aggregates (arrow) are formed during symptomatic disease. This also happens in the G1del/GFAP-tau mouse (A-D) (arrow). However, the phospo tau (AT8 eptitope) poorly colocalizes with the hSOD1 and with ubiquitine (arrowheads). Sometimes we do see colocalization of SOD, ubiquitin and AT8 (asterix). (magnification 40x) (Human SOD1 A'' and B'', ubiquitine A'' and B''', Phospho-tau A' and B) (C) An increase of Caspase 3 was noticed in the AT8 expressing astrocytes (arrow), although not every caspase3 positive cell expresses AT8 (arrowhead).

Discussion

By stressing the astrocytes in G1del mice we wanted to determine the role of astrocyte pathology in an ALS mouse model. Forman et al. made homozygous GFAP-tau mice expressing aggregate prone tau protein in astrocytes. These mice develop pathology from 12 months of age (Forman et al., 2005). As the GFAP-tau mice develop an age-dependent accumulation of tau it is expected that they can serve as a model for astrocyte pathology. The GFAP-tau mice we used for this research were heterozygous. Because of the lower expression of tau in the astrocytes, they did not develop pathology up to 70 weeks of age.

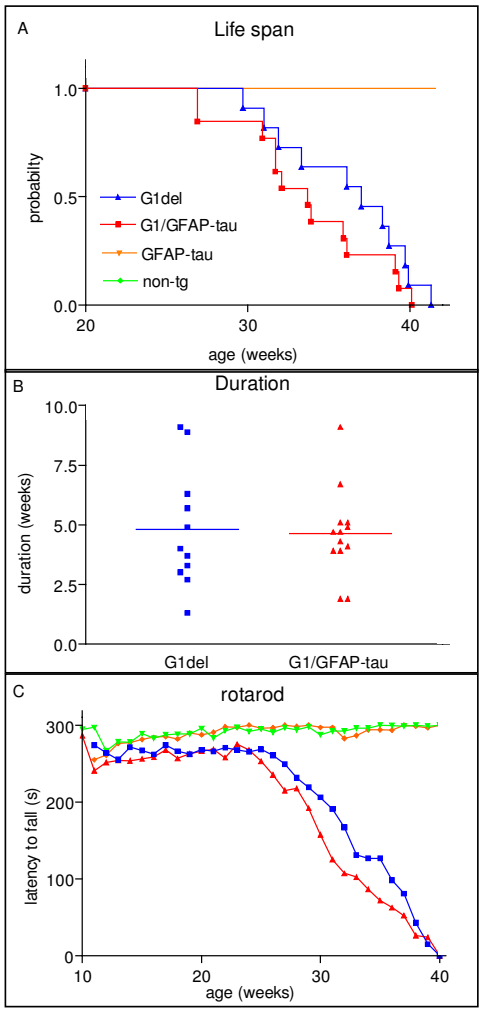

Figure 3.4. The GFAP-tau transgene does not influence the SOD1-ALS like disease in G1del mice
Life span (A) and duration of disease (B) are not significantly different. (C) Mice were tested weekly on an accelarated rottarod

By crossing the G1del mouse with the GFAP-tau mouse we made a model to test the hypothesis that astrocytes are sensitive for neuronal pathology. We expected this to be very important, because there is emerging evidence of the involvement of glial cell pathology in neurodegenerative diseases.

In literature, recent work describes that neuronal expression of human SOD1 G93A in mice is sufficient to induce a late onset form of neurodegenerative disease in mice (Jaarsma et al., 2008). In these mice, glial cells were affected at end stage disease. Furthermore an astrocyte specific expression of mutant SOD1 G85R was not sufficient to induce ALS-like disease. Only astrogliosis was described in these mice (Gong et al., 2000).

Other researchers described a role of astrocytes (Clement et al., 2003; Di Giorgio et al., 2007; Nagai et al., 2007) and microglia (Beers et al., 2006; Boillee et al., 2006b) on disease progression.

Research on microglia pathology in SOD1-ALS demonstrated that mice with a diminished SOD1 expression in microglia display a slower disease progression (Beers et al., 2006; Boillee et al., 2006b).

Studies of chimeric mice, expressing mutant SOD1 either in neurons or non-neuronal cells showed an important role of astrocytes in disease progression. In this experiment it is observed that motor neurons only displayed degeneration when surrounded by SOD1 containing non -neuronal cells (Clement et al., 2003; Yamanaka et al., 2008a).

Furthermore (Yamanaka et al., 2008b) described that deleting mutant SOD1 in astrocytes did not change onset of disease, but they observed a significant increase in disease duration. (Di Giorgio et al., 2007) and (Nagai et al., 2007) described that non-transgenic neurons plated on an astrocyte layer expressing mutant SOD1 *in vitro*, show less neuron growth, more neuronal death and a pathological morphology of the neurons. Additionally, mutant SOD1 expressing neurons are rescued when cultured on a non-transgenic astrocyte layer.

In G1del mice a GFAP increase, suggestive of astrocyte activation is observed after onset of symptoms. Furthermore expression of Heat Shock proteins, such as HSPb1 and αβ-crystallin are observed at symptomatic disease stage in areas of motorneuron degeneration. Concluding that neuronal pathology does influence the pathology present in the astrocytes.
The signs of astrocyte pathology from birth in the GFAP-tau mice are suggestive of a pathological effect of the tau protein. There is an increase of GFAP expression, which is a sign of astrocytosis. This is partly confirmed by the double labeling with Hspb1. However, not all astrocytes seem to have the same reaction to the pathological expression of tau, because not all tau-expressing astrocytes express Hspb1. Even though the appearance of phospho-tau in astrocytes in the heterozygous GFAP-tau mice is at a very late age (>70 weeks), in our double-transgenic G1del/GFAP-tau mice the astrocytic phospho-tau is already present at symptomatic disease, 25 to 28 weeks. In the G1del mice we never observe phospo-tau expession.
The appearance of phospho tau in the doubletransgenic mice seems to be associated with the start of neuronal degeneration. The phospo tau is, despite tau expression throughout the grey matter, only present in the motorneuron area. Because of this we could say that disease is initiated in neurons and spreads to the astrocytes at a late disease stage. The astrocytes become more vulnerable to aggregate prone protein. The phospho tau does not activate the apoptotic pathway in the astrocytes, because caspase 3 is not increasingly observed in phospho tau positive cells than in other cells.
Since alpha-synuclein and tau protein can promote the fibrillization of each other (Giasson et al., 2003), we wanted to see whether tau is able to promote SOD1 aggregation in astrocytes. However, since phospo-tau and SOD1 weakly colocalize in the lumbar spinal cord, it is not expected that the two proteins interact with each other. Furthermore we did not observe an increase in SOD1 aggregates. Phospho-tau does not colocalize with ubiquitine. The strong colocalization of mutant SOD1 aggregates and ubiquitine are suggestive of a different pathological pathway of aggregation than for the phospho-tau aggregates.
Yamanaka et al., and others found an effect of pathology in non neuronal cells on the disease course (Clement et al., 2003; Lepore et al., 2008; Yamanaka et al., 2008a; Yamanaka et al., 2008b). Most researchers found an effect on disease progression, where onset of disease remained the same. This implies that disease starts in neurons and then spreads to the astrocytes, activating them. In our research the pathology occurs at a very late stage of disease and it only appears after the onset of neuronal degeneration. Supporting the findings of others. The SOD1 pathology is not affected because of the tau over expression, suggesting that the tau pathology is not severe enough to interfere with astrocyte function.

The data above supports a model where disease is initiated in neurons and spreads to other cell types as neurons are degenerating. Astrocytes are affected by the degenerating neurons; however, they do not worsen further disease.

References

Beers DR, Henkel JS, Xiao Q, Zhao W, Wang J, Yen AA, Siklos L, McKercher SR, Appel SH (2006) Wild-type microglia extend survival in PU.1 knockout mice with familial amyotrophic lateral sclerosis. Proc Natl Acad Sci U S A 103:16021-16026.

Boillee S, Vande Velde C, Cleveland DW (2006a) ALS: a disease of motor neurons and their nonneuronal neighbors. Neuron 52:39-59.

Boillee S, Yamanaka K, Lobsiger CS, Copeland NG, Jenkins NA, Kassiotis G, Kollias G, Cleveland DW (2006b) Onset and progression in inherited ALS determined by motor neurons and microglia. Science 312:1389-1392.

Bruijn LI, Becher MW, Lee MK, Anderson KL, Jenkins NA, Copeland NG, Sisodia SS, Rothstein JD, Borchelt DR, Price DL, Cleveland DW (1997) ALS-linked SOD1 mutant G85R mediates damage to astrocytes and promotes rapidly progressive disease with SOD1-containing inclusions. Neuron 18:327-338.

Clement AM, Nguyen MD, Roberts EA, Garcia ML, Boillee S, Rule M, McMahon AP, Doucette W, Siwek D, Ferrante RJ, Brown RH, Jr., Julien JP, Goldstein LS, Cleveland DW (2003) Wild-type nonneuronal cells extend survival of SOD1 mutant motor neurons in ALS mice. Science 302:113-117.

Dabir DV, Robinson MB, Swanson E, Zhang B, Trojanowski JQ, Lee VM, Forman MS (2006) Impaired glutamate transport in a mouse model of tau pathology in astrocytes. J Neurosci 26:644-654.

Di Giorgio FP, Carrasco MA, Siao MC, Maniatis T, Eggan K (2007) Non-cell autonomous effect of glia on motor neurons in an embryonic stem cell-based ALS model. Nat Neurosci 10:608-614.

Forman MS, Lal D, Zhang B, Dabir DV, Swanson E, Lee VM, Trojanowski JQ (2005) Transgenic mouse model of tau pathology in astrocytes leading to nervous system degeneration. J Neurosci 25:3539-3550.

Giasson BI, Forman MS, Higuchi M, Golbe LI, Graves CL, Kotzbauer PT, Trojanowski JQ, Lee VM (2003) Initiation and synergistic fibrillization of tau and alpha-synuclein. Science 300:636-640.

Gong YH, Parsadanian AS, Andreeva A, Snider WD, Elliott JL (2000) Restricted expression of G86R Cu/Zn superoxide dismutase in astrocytes results in astrocytosis but does not cause motoneuron degeneration. J Neurosci 20:660-665.

Jaarsma D, Teuling E, Haasdijk ED, De Zeeuw CI, Hoogenraad CC (2008) Neuron-specific expression of mutant superoxide dismutase is sufficient to induce amyotrophic lateral sclerosis in transgenic mice. J Neurosci 28:2075-2088.

Jaarsma D, Haasdijk ED, Grashorn JA, Hawkins R, van Duijn W, Verspaget HW, London J, Holstege JC (2000) Human Cu/Zn superoxide dismutase (SOD1) overexpression in mice causes mitochondrial vacuolization, axonal degeneration, and premature motoneuron death and accelerates motoneuron disease in mice expressing a familial amyotrophic lateral sclerosis mutant SOD1. Neurobiol Dis 7:623-643.

Kato S, Hayashi H, Nakashima K, Nanba E, Kato M, Hirano A, Nakano I, Asayama K, Ohama E (1997) Pathological characterization of astrocytic hyaline inclusions in familial amyotrophic lateral sclerosis. Am J Pathol 151:611-620.

Lepore AC, Dejea C, Carmen J, Rauck B, Kerr DA, Sofroniew MV, Maragakis NJ (2008) Selective ablation of proliferating astrocytes does not affect disease outcome in either acute or chronic models of motor neuron degeneration. Exp Neurol.

Lin WL, Lewis J, Yen SH, Hutton M, Dickson DW (2003) Ultrastructural neuronal pathology in transgenic mice expressing mutant (P301L) human tau. J Neurocytol 32:1091-1105.

Maragakis NJ, Rothstein JD (2006) Mechanisms of Disease: astrocytes in neurodegenerative disease. Nat Clin Pract Neurol 2:679-689.

Masters CL, Simms G, Weinman NA, Multhaup G, McDonald BL, Beyreuther K (1985) Amyloid plaque core protein in Alzheimer disease and Down syndrome. Proc Natl Acad Sci U S A 82:4245-4249.

Nagai M, Re DB, Nagata T, Chalazonitis A, Jessell TM, Wichterle H, Przedborski S (2007) Astrocytes expressing ALS-linked mutated SOD1 release factors selectively toxic to motor neurons. Nat Neurosci 10:615-622.

Neumann M, Sampathu DM, Kwong LK, Truax AC, Micsenyi MC, Chou TT, Bruce J, Schuck T, Grossman M, Clark CM, McCluskey LF, Miller BL, Masliah E, Mackenzie IR, Feldman H, Feiden W, Kretzschmar HA, Trojanowski JQ, Lee VM (2006) Ubiquitinated TDP-43 in frontotemporal lobar degeneration and amyotrophic lateral sclerosis. Science 314:130-133.

Pasinelli P, Brown RH (2006) Molecular biology of amyotrophic lateral sclerosis: insights from genetics. Nat Rev Neurosci 7:710-723.

Riedel M, Goldbaum O, Richter-Landsberg C (2009) alpha-Synuclein Promotes the Recruitment of Tau to Protein Inclusions in Oligodendroglial Cells: Effects of Oxidative and Proteolytic Stress. J Mol Neurosci.

Rosen DR, Siddique T, Patterson D, Figlewicz DA, Sapp P, Hentati A, Donaldson D, Goto J, O'Regan JP, Deng HX, et al. (1993) Mutations in Cu/Zn superoxide dismutase gene are associated with familial amyotrophic lateral sclerosis. Nature 362:59-62.

Spillantini MG, Schmidt ML, Lee VM, Trojanowski JQ, Jakes R, Goedert M (1997) Alpha-synuclein in Lewy bodies. Nature 388:839-840.

Yamanaka K, Boillee S, Roberts EA, Garcia ML, McAlonis-Downes M, Mikse OR, Cleveland DW, Goldstein LS (2008a) Mutant SOD1 in cell types other than motor neurons and oligodendrocytes accelerates onset of disease in ALS mice. Proc Natl Acad Sci U S A 105:7594-7599.

Yamanaka K, Chun SJ, Boillee S, Fujimori-Tonou N, Yamashita H, Gutmann DH, Takahashi R, Misawa H, Cleveland DW (2008b) Astrocytes as determinants of disease progression in inherited amyotrophic lateral sclerosis. Nat Neurosci.

Chapter 4

A novel mouse model with impaired dynein/dynactin function develops amyotrophic lateral sclerosis (ALS)-like features in motor neurons and improves lifespan in SOD1-ALS mice

Eva Teuling [1], Vera van Dis [1], Phebe S. Wulf [1], Elize D. Haasdijk [1], Anna Akhmanova [2], Casper C. Hoogenraad [1] and Dick Jaarsma [1]

1 Department of Neuroscience, 2 Department of Cell Biology and Genetics, Erasmus MC, P.O. Box 2040, 3000CA, Rotterdam, The Netherlands.

Published: Human Molecular Genetics, 2008, Vol. 17, No. 18 2849–2862

Abstract

Amyotrophic lateral sclerosis (ALS) is a fatal neurodegenerative condition characterized by progressive motor neuron degeneration and muscle paralysis. Genetic evidence from man and mouse has indicated that mutations in the dynein/dynactin motor complex are correlated with motor neuron degeneration. In this study, we have generated transgenic mice with neuron specific expression of Bicaudal D2 N-terminus (BICD2-N) to chronically impair dynein/dynactin function. Motor neurons expressing BICD2-N showed accumulation of dynein and dynactin in the cell body, Golgi fragmentation, and several signs of impaired retrograde trafficking: the appearance of giant neurofilament swellings in the proximal axon, reduced retrograde labelling by tracer injected in the muscle, and delayed expression of the injury transcription factor ATF3 after axon transection. Despite these abnormalities, BICD2-N mice did not develop signs of motor neuron degeneration and motor abnormalities. Interestingly, the BICD2-N transgene increased life span in 'low copy' SOD1-G93A ALS transgenic mice. Our findings indicate that impaired dynein/dynactin function can explain several pathological features observed in ALS-patients, but may be beneficial in some forms of ALS.

Introduction

Amyotrophic lateral sclerosis (ALS) is a clinically and genetically heterogeneous disease characterized by late-onset progressive degeneration of motor neurons resulting in paralysis of limb, facial and respiratory muscles (1,2). Pathologically, the disease in most instances is characterized by protein aggregates that contain TDP-43, a protein involved in mRNA metabolism (3). A minority of ALS patients (10%) show Mendelian inheritance, a subset of who have mutations in the Cu/Zn superoxide dismutase (SOD1) gene resulting in SOD1 aggregates in motor neurons and glia (1,2,4). More recently, mutations in a variety of other genes have been identified in patients with ALS and ALS-like diseases (2,5–7). In a family with a slowly progressive motor neuron disease, a missense (G59S) mutation was found in the p150Glued subunit of dynactin (DCTN1) (8) and subsequently other p150Glued mutations have been reported in ALS patients (9). Recently, it was reported that heterozygous knock-in and transgenic mice expressing mutant p150Glued-G59S develop motor neuron abnormalities and degeneration (10–12). Dynactin is a multiprotein complex that regulates microtubule-based motility of the cytoplasmic dynein motor complex by increasing processivity and efficiency of the motor (13,14). A direct link between impaired dynactin/dynein function and motor neuron disease was first demonstrated by the overexpression of the dynactin subunit p50, also named dynamitin, which disrupts the dynactin/dynein complex and causes a late-onset motor neuron disease in transgenic mice (15). In addition, heterozygous missense mutations in the cytoplasmic dynein heavy chain 1 gene were found in two mouse models with late-onset motor neuron degeneration, Legs at odd angles (Loa) and Cramping 1(Cra1) (16,17), suggesting that abnormalities in both dynein and dynactin may play a role in pathogenesis of ALS (18,19).

Given the role of the dynein/dynactin complex in retrograde transport of cargoes such as endosomes, signalling complexes, degradation products and neurofilaments (19–25), it is likely that alteration in dynactin/dynein function could influence several critical cellular processes within various compartments of the motor neuron. Potential consequences of disrupted dynein/dynactin function in ALS pathology are the reported abnormalities in axonal neurofilament distribution (10,15,24, 26–28), fragmentation of the Golgi apparatus (29–31) and impaired retrograde trafficking (15,18,19). However, the precise relationship between disrupted dynein/dynactin function and the pathological features observed in ALS patients is unclear. It is not known which pathological abnormalities in motor neurons are directly related to impaired dynein/dynactin and whether a loss- or gain-of-function mechanism is the primary cause of motor neuron degeneration.

To determine the cellular and pathological effects of dynein/dynactin inhibition in motor neurons, we have generated transgenic mice with neuron-specific expression of the N-terminus of Bicaudal D2 (BICD2-N). Previous studies have shown that Bicaudal D is an evolutionarily conserved motor-adaptor protein, which is involved in dynein-mediated transport in Drosophila and mammals by linking the dynein motor complex to various cargoes (32–36). When deleting the C-terminal cargo-binding region, the N-terminus of BICD2 strongly binds the dynein/dynactin complex and impairs dynein/dynactin function

(32,33). Thus, BICD2-N overexpression is a powerful tool for dissecting the roles of dynein and dynactin in motor neurons.
Here we show that the expression of BICD2-N in motor neurons impairs dynein/dynactin function and causes Golgi fragmentation, axonal neurofilament swellings and reduced retrograde transport. Despite these changes, we found no evidence of motor neuron degeneration up to 2 years of age. Furthermore, we show that impaired dynein/dynactin function increases the lifespan of transgenic mice that express an ALS-linked SOD1 mutation. We also observed the accumulation of dynein and p150Glued in SOD1 aggregates in SOD1-G93A ALS mice, suggesting that dynein/dynactin trapped in intracellular inclusions might be beneficial to the disease phenotype in SOD1-linked ALS.

Materials and Methods

BICD2-N and SOD1-G93A transgenic mice

Animals were housed and handled in accordance with the Principles of Laboratory Animal Care (NIH publication No. 86-23) and the guidelines approved by the Erasmus University animal care committee. To generate Thy1.2-GFP-BICD2-N mice, a GFP-BICD2-N construct (32) was cloned into the XhoI site of the Thy1.2 expression vector and injected into fertilized oocytes, using standard techniques. Three lines, BN1, BN3 and BN4, were selected for further study. Transgenic lines were maintained into FVB background by crossing hemizygote males with non-transgenic females. Transgenic offspring was genotyped by PCR. A selected group of all lines was allowed to age for 2 years. These mice were weighed and inspected for signs of muscle weakness once a week, using a set of simple tests: mice were examined for their ability to extend their hind limbs when suspended in the air by their tail and their ability to hang upside down on a grid for 60 s. In addition, at specific ages, grip strength was measured using a grid attached to a force gauge (Bioseb, Chaville, France).
Other mice used in this study were G1del mice that carry a genomic hSOD1 construct with the G93A mutation and that develop progressive muscle weakness from age 24–30 weeks, reaching end-stage disease 3–10 weeks after the first symptoms (49,61). Double-transgenic mice carrying the G1del and the GFP-BICD2-N transgenes were generated by crossing hemizygous G1del mice with hemizygous BN1 or BN3 mice. The onset of symptoms was determined on the basis of the onset weight loss, the inability to normally extend one of the hind limbs or the inability to normally perform in the grid hanging test. Mice reached end-stage disease when they could not right themselves within 5 s when placed on their back, lost more than 30% of their maximal weight or developed infection of one of the eyes (4).

Antibodies

Primary antibodies [supplier; applications (IHC, immunohistochemistry; IF, immunofluorescence; WB, western blot) and dilutions] reported in this study are mouse-anti-actin (Millipore, WB 1:10 000), mouse-anti-Arp1 (Sigma, WB 1:2000), rabbit anti-ATF3 (Santa Cruz; IHC and IF 1:1000), rabbit-anti-BICD2 [(32), WB 1:1000], goat-anti-

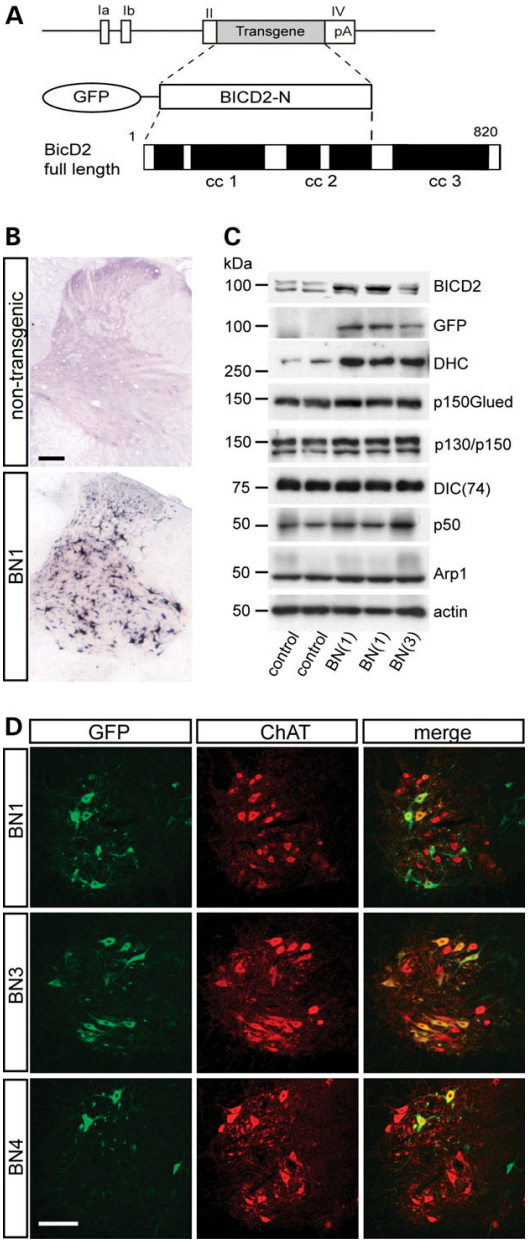

Figure 4.1: Generation of Thy1.2-BICD2-N transgenic mice. (A) The Thy1.2-GFP-BICD2-N construct was generated by cloning the N-terminal part of BICD2 (amino acid 1–637) coupled to GFP into the Thy1.2 vector. (B) In situ hybridization signal of antisense digoxigenin-labelled BICD2 cRNA on spinal cord sections from a non-transgenic and a Thy1.2-BICD2-N transgenic mouse (BN1 line). (C) Western blot analysis of spinal cord homogenate of non-transgenic, BN1 and BN3 mice shows differences in transgene expression between BN1 and BN3 mice (upper left panels), and an increase in DHC immunoreactivity in the spinal cord of BN1 and BN3 mice. (D) Confocal fluorescence of GFP-BICD2-N (green) and the motor neuronal marker ChAT (red) in L4 lumbar spinal cord sections of BN1, BN3 and BN4 mice showing the differences in proportion of transgenic motor neurons and transgene expression levels between the three lines. Bars: 100 µm.

choline acetyltransferase (ChAT, Chemicon, IF 1:500), rabbit-anti-CGRP (Calbiochem, IF 1:10 000), rat anti-CR3 receptor (clone 5C6; Serotec, IHC 1:500), rabbit-anti-dynein heavy chain (Santa Cruz, IF 1:500; WB 1:1000), mouse-anti-DIC74 (Millipore, WB 1:1000), rabbit anti-GFAP (DAKO, IF 1:5000), rabbit-anti-GFP (Abcam, WB 1:1000), mouse-anti-GM130 (BD Biosciences, IF 1:1000), rabbit anti-Hsp25 (Stessgen, IF 1:2000), rabbit-anti-KIF5A (Abcam, IF 1:2000), rat-anti-muscarinic M2-receptor (Millipore, IF 1:200),

chicken-anti-NF-M (Millipore, IF 1:4000), mouse- anti-NF-M (Sigma, IF 1:10 000), mouse-anti-p150Glued (BD Biosciences, WB 1:1000; IF 1:500), rabbit-anti-p150glued (Santa Cruz, WB 1:1000), mouse-anti-p50 (BD Biosciences, WB, 1:1000), rabbit-anti-peripherin (Millipore, IHC 1:1000), rabbit-anti- SOD1 (AbSOD100, Stressgen, WB: 1:1000), rabbit-anti-murine SOD1 (AbSOD101, Stressgen, WB 1:1000), sheep-anti-SOD2 (Calbiochem, IF 1:5000), rabbit anti-ubiquitin (Dako; IHC and IF 1:2000); mouse anti-ubiquitin (clone FK2, Affiniti; IF 1:2000); goat anti-VAChT (Chemicon, IF 1:1000).
Secondary antibodies: For avidin–biotin–peroxidase immunocytochemistry, biotinylated secondary antibodies from Vector Laboratories diluted 1:200 were used. FITC-, Cy3- and Cy5-conjugated secondary antibodies raised in donkey (Jackson Immunoresearch, USA), and Alexa488, 568 or 633 conjugated antibodies raised in goat, were used for immunofluorescence. For western blots, HRP-conjugated goat-anti- mouse or goat-anti-rabbit IgG (DAKO) was used at 1:5000.

GFP-BICD2-N and GFP-p50 expression constructs

GFP-BICD2-N and GFP-p50 constructs have been described before (32). For expression in hippocampal neurons, GFP-BICD2 and GFP-p50 were subcloned into pGW1 expression vectors.

Primary neuron cultures and transfection

Primary rat hippocampal neurons were plated at a density of 75 000 on 15 mm glass coverslips and transfected at DIV13 with GFP, GFP-BICD2-N or GFP-p50 using Lipofectamine- 2000 (Qiagen) as described previously (62). After 2 days of transfection, neurons were fixed and stained with the antibodies indicated. Representative cells were imaged using a confocal microscope. The appearance of the Golgi apparatus was investigated. p150Glued fluorescence intensities were measured with Metamorph software and differences between control and transfected neurons were analysed using Student's t-test.

Western blotting

Spinal cord tissue was homogenized in 10 volumes of PBS containing 0.5% Nonidet P-40 and 1× protease inhibitor cocktail (Complete, Roche), sonicated and centrifuged at 800g for 15 min, and protein concentrations of the supernatants (S1) were determined using the BCA method (Pierce, Rockford, IL, USA). For the preparation of detergent-insoluble extracts, S1 supernatants were centrifuged at 15 000g for 15 min. After the collection of supernatants (S2), pellets were thoroughly washed five times with PBS-0.5% Nonidet P-40 and then resuspended in sample buffer for SDS–PAGE electrophoresis and western-blotting. Samples containing 1–10 µg protein were electrophoresed on SDS–PAGE gels and blotted on PVDF membranes (Millipore). The membranes were blocked with 5% non-fat dry milk (Bio-Rad) in PBS with 0.05% Tween20 (PBST), incubated in primary antibody, diluted in PBST with 1% dry milk followed by an incubation in secondary antibody, incubated in chemiluminescence reagent (ECL, Amersham), exposed to film or a Kodak Image station and analysed with ImageQuant 2.2 software (4).

Immunohistochemical and histopathological procedure

For immunocytochemistry and immunofluorescence, mice were anaesthetized with pentobarbital and perfused transcardially with 4% paraformaldehyde. The lumbar and cervical spinal cord were carefully dissected out and post-fixed overnight in 4% paraformaldehyde. Routinely, spinal cord tissue was embedded in gelatin blocks, sectioned at 40 µm with a freezing microtome and sections were processed, free floating, employing a standard avidin–biotin–immunoperoxidase complex method (ABC, Vector Laboratories, USA) with diaminobenzidine (0.05%) as the chromogen, or single-, double- and triple-labelling immunofluorescence (4). In addition, a selected number of frozen sections were processed for a silver staining procedure that selectively labels dying neurons and their processes. Immunoperoxidase-stained sections were analysed and photographed using a Leica DM-RB microscope and a Leica DC300 digital camera. Sections stained for immunofluorescence were analysed with a Zeiss LSM 510 confocal laser scanning microscope. Quantitative analyses of motor neurons were performed as described before (50) on serial lumbar 4 (L4) sections immunoperoxidase-stained for ChAT or CGRP.
For the analysis of neuromuscular denervation, medial gastrocnemius muscle from 4% paraformaldehyde-fixed mice was dissected, embedded into gelatin blocks and sectioned at 80 µm with a freezing microtome. Sections were immunolabelled, free floating, for goat-anti-VAChT and chicken- anti-NFM, and motor endplates were labelled with FITC-bungarotoxin (1:500, Molecular Probes). Sections were examined for neuromuscular denervation under a Leica DM-RB fluorescence microscope as described (4).

mRNA in situ hybridization

In situ hybridization was performed on 30 µm-thick free-floating sections using standard methods with digoxigenin-labelled cRNA probes (63). Sense and antisense digoxigenin-labelled cRNAs were transcribed from linearized plasmids containing BICD2-cDNA.

Fluorogold retrograde tracing

To determine retrograde axonal transport, we have used retrograde tracing with fluorogold (FluoroChrome, Denver, CO, USA) (15). Briefly, anaesthetized 30-week-old non-transgenic and BN1 mice received four microinjections of fluorogold (1 µl, 2% in 0.9% saline) into the gastrocnemic muscle. After 48 h, mice were perfused transcardially with 4% paraformaldehyde, sectioned, mounted and analysed with Leica DM-RB epifluorescence microscope and a Zeiss LSM 510 META confocal laser scanning microscope with 63× Plan-apo oil immersion objective. Fluorogold signal was detected using a 405 nm laser and a META detector.

Axotomy of the sciatic nerve

Twenty-week-old BN1 and non-transgenic animals were anaesthetized, the sciatic nerve was exposed, bound with suture and cut just above the division of the sciatic nerve into the tibial and common peroneal nerves. A 2 mm piece of the nerve was removed. Animals were left to recover for 12 or 24 h. Following transection, animals were perfused

transcardially with 4% paraformaldehyde and processed for immunohistochemistry as described before with antibodies against ATF3.

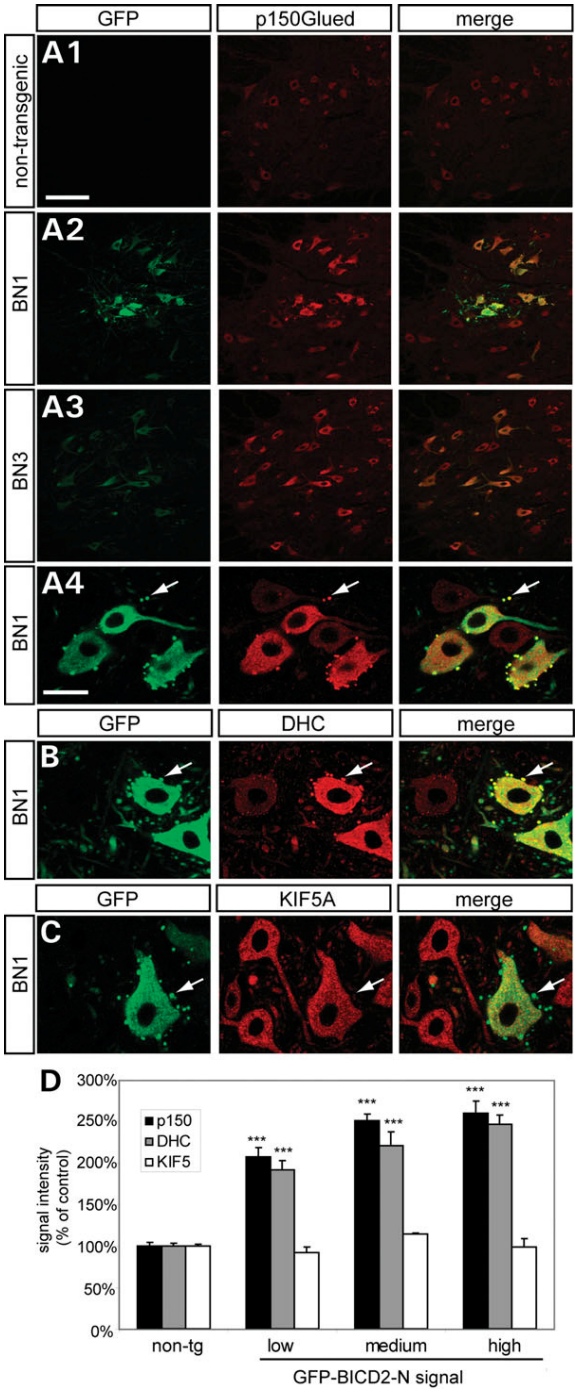

Figure 4.2: BICD2-N causes somato-dendritic accumulation of dynein/dynactin in motor neurons *in vivo*. (A–C) Confocal fluorescence of GFP-BICD2-N (green) and p150Glued (A), dynein heavy chain (DHC, B) and KIF5A (C) in L4 spinal cord sections of non-transgenic (A1), BN1 (A2, A4, B and C) and BN3 (A3) mice showing a large increase of p150Glued and dynein heavy chain immunoreactivity in transgenic motor neurons. Note that many GFP-BICD2-N neurons are surrounded by spherical structures that display intense GFP signal, p150Glued and dynein heavy chain immunoreactivity, but are immunonegative for KIF5A (arrows in A4, B and C). (D) Bar graph showing relative fluorescent signal as a function of GFP-BICD2-N expression. Motor neurons are grouped into 'low', 'medium' and 'high' expressors on the basis of GFP signal intensities as described in Material and Methods. Values for each bar are based on 20–25 cells. ***$P < 0.001$ compared with control neurons (one-way ANOVA, Tukey's multiple comparison test). Bars: A1, 100 µm; A4, 25 µm.

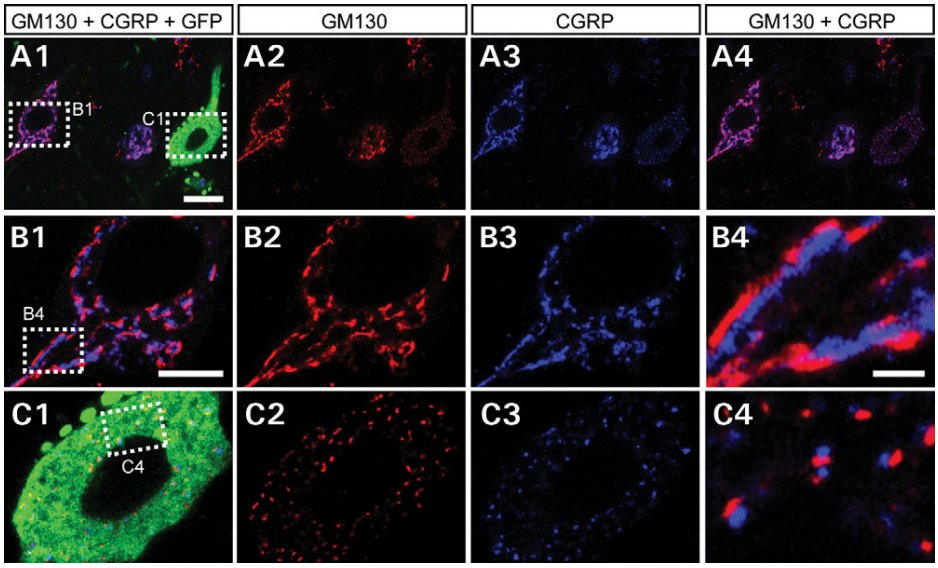

Figure 4.3: High levels of BICD2-N cause Golgi fragmentation in motor neurons. Confocal fluorescence of GFP-BICD2-N (green), cis-Golgi marker GM130 (red) and CGRP (blue) in lumbar motor neurons of a BN1 mouse shows that the Golgi apparatus in neurons expressing high levels of GFP-BICD2-N is fragmented into dispersed small elements that contain both cis- (GM130) and trans-Golgi (CGRP) elements (C). Bars: A1, 25 µm; B1, 10 µm; B4, 2 µm.

Analysis of immunofluorescence signal intensities

Analyses of GFP-BICD2-N, fluorogold or immunofluorescence signal intensities were performed with sections from spinal cord specimen from non-transgenic and transgenic mice embedded in a single-gelatin block to minimize variability due to sectioning and staining procedures. Images were taken using a Zeiss LSM 510 confocal laser scanning microscope using 40× or 63× Plan apo oil immersion objectives. Laser and detector settings were chosen to avoid saturation of the signal. Fluorescent intensities were determined using Metamorph image analysis software. For some analyses, GFP-BICD2-N-positive motor neurons were grouped according to GFP signal intensity into low (25–100), medium (100–175) and high (175–250) intensities. Therefore, all GFP-BICD2-N images were taken using the same confocal and laser settings in all material. Statistical analyses were done with GraphPad Software (Prism, San Diego, CA, USA).

Electron microscopy

For electron microscopy, mice were perfused transcardially with 4% paraformaldehyde with 0.1% (pre-embedding immunoperoxidase electron microscopy) or 1% glutaraldehyde (standard electron microscopy). Specimens were sectioned with a Vibratome and further processed using standard methods as described before (50). Vibratome sections (50–60 µm thick) were post-fixed in 1% osmium, dehydrated and embedded in Durcupan. Ultrathin (50–70 nm) sections were contrasted with uranyl acetate and lead citrate and analysed in a Phillips CM100 electron microscope at 80 kV.

Results

BICD2-N causes accumulation of dynein/dynactin in motor neuron cell bodies

To examine the effect of BICD2-N expression in motor neurons in vivo, we generated transgenic mice by cloning GFP-BICD2-N into the Thy1.2 expression cassette (Fig. 4.1A), which drives postnatal transgene expression in motor neurons and other neuron populations throughout the brain (37,38). Transgenic lines were screened on the basis of GFP-BICD2-N levels as identified by in situ hybridization (Fig. 4.1B), western blot analysis (Fig. 4.1C) and GFP signal in motor neurons as identified by ChAT-immunostaining (Fig. 4.1D). Three lines with different transgene expression levels in motor neurons were selected for further study. None of the lines showed transgene expression in all motor neurons. Quantitative analysis revealed that lines BN1 and BN4 have relatively high GFP-BICD2-N expression in ~50–60 and 30% of the spinal motor neurons, respectively, whereas line BN3 has relatively low GFP-BICD2-N expression in ~70% of the motor neurons (Fig. 4.1D). Furthermore, all lines show transgene expression throughout the brain, predominantly in the deep lamina of the cortex and the hippocampus (data not shown). Onset of transgene expression was between post-natal days 4–6. Most analyses were performed with multiple lines, but unless otherwise stated the data presented are from line BN1.

We first tested whether Thy1.2-GFP-BICD2-N expression affects dynein/dynactin expression. Western blot analysis showed increased levels of dynein heavy chain in the spinal cord of BN1 and BN3 mice compared with non-transgenic mice, whereas other dynein/dynactin components were unaltered (Fig. 4.1C). Confocal immunofluorescence analysis revealed a robust increase of p150Glued and dynein heavy chain immunoreactivity in the cell bodies and proximal dendrites in BICD2-N-expressing motor neurons (Fig. 4.2A, B and D). GFP-negative motor neurons in Thy1.2-GFP-BICD2-N mice showed the same levels of dynein/dynactin immunoreactivity as neurons from non-transgenic mice, indicating that the accumulation of dynein/dynactin components in the cell body is specifically caused by the presence of BICD2-N. Increased dynein/dynactin immunoreactivity was evident at the onset of transgene expression at post-natal days 4–6. The increased staining was specific for dynein/dynactin, as no change in labelling was observed for other markers examined, such as KIF5A (Fig. 4.2C and D) and KIF5C (not shown), neurofilament proteins (NF-M, Fig. 4.4C; SMI32, not shown), neuron-specific class III beta-tubulin (TuJ1, not shown), MAP2 (not shown), ChAT (Fig. 4.1D) and the small heat shock protein Hsp25 (not shown).

These data were confirmed by experiments in cultured hippocampal neurons; GFP-BICD2-N expression increases dynein and dynactin staining in the cell body and proximal dendrites (Supplementary Material, Fig. S1A and C). In contrast, overexpression of p50, which also inhibits dynein- dependent transport (29), shows a normal distribution of dynein/dynactin in neurons (Supplementary Material, Fig. S1A and C). These data suggest that p50 and BICD2-N inhibit dynein/dynactin via distinct mechanisms: overexpression of p50 disassembles the dynactin complex (39), whereas BICD2-N binds dynein/dynactin and causes the accumulation of the complex in the cell body.

Detailed analysis of GFP-BICD2-N expression indicates that it is diffusely expressed over the somato-dendritic compartment of motor neurons, but absent in motor axons in the ventral roots and sciatic nerve. Also, axons of other populations of neurons expressing GFP-BICD2-N such as layer V cortical neurons were devoid of GFP-BICD2-N. Remarkably, a subset of neurons that express GFP-BICD2-N at relatively high levels were surrounded by spherical structures, 0.5–2 μm in diameter, that displayed high levels of GFP signal (Fig. 4.2). These structures were also intensely immunoreactive for p150Glued and dynein heavy chain, but not for other investigated markers, such as KIF5A and MAP2 (Fig. 4.2; data not shown). Confocal analysis with an antibody against the muscarinic M2-receptor that outlines the cell membrane of motor neurons indicated that in most instances these spheres were attached to the motor neuron via thin processes (Supplementary Material, Fig. S2A). This was confirmed by electron microscopic analysis of serial sections (Supplementary Material, Fig. S2B and C). Electron microscopy also showed that the membrane protrusions were filled with electron dense material, but did not contain synaptic specializations such as post-synaptic densities, and were not contacted by presynaptic boutons. Although the significance of the membrane protrusions is not clear, we hypothesize that the structures may result from high dynein/dynactin concentration that may alter the cortical cytoskeleton, or drive outward movement of microtubules to initiate protrusions as reported recently (40); accordingly, microtubules were found in the neck of the protrusions (Supplementary Material, Fig. S2C).

BICD2-N causes Golgi fragmentation in motor neurons

Previous studies showed that the loss of dynein function or BICD2-N overexpression causes fragmentation of the Golgi apparatus (32,33,41). Accordingly, GFP-BICD2-N and GFP-p50 overexpression caused Golgi fragmentation in cultured hippocampal neurons (Supplementary Material, Fig. S1B and D). Analysis of Golgi apparatus in spinal cord of Thy1.2-GFP-BICD2-N mice with an antibody against the cis-Golgi protein GM130 (42) revealed motor neurons with fragmented Golgi in BN1 and BN4, but not BN3 mice (Fig. 4.3). The fragmentation was characterized by the transformation of the Golgi apparatus from a network of linear profiles into dispersed smaller elements (Fig. 4.3C). Double-labelling with antibodies against CGRP, a peptide that is present in the trans-Golgi and secretory granules of most large motor neurons (43), indicated that the fragmented Golgi consisted of mini-stacks containing all Golgi elements (Fig. 4.3A and C). In BN1 mice, the percentage of GFP-BICD2-N-expressing motor neurons with fragmented Golgi was 1–2% at 20 weeks of age and 7–15% at 100 weeks of age, indicating that the frequency of motor neurons with fragmented Golgi increased with ageing. Golgi fragmentation was predominantly present in high-GFP-BICD2-N-expressing motor neurons and was never observed in GFP-BICD2-N-negative motor neurons (Fig. 4.3A and B), nor in motor neurons of non-transgenic mice of any age. All motor neurons with fragmented Golgi showed a normal appearance. No consistent change in the densities of mitochondria (SOD2 staining) or endoplasmic reticulum (calreticulin staining) was observed in GFP-BICD2-N motor neurons (Supplementary Material, Fig. S3).

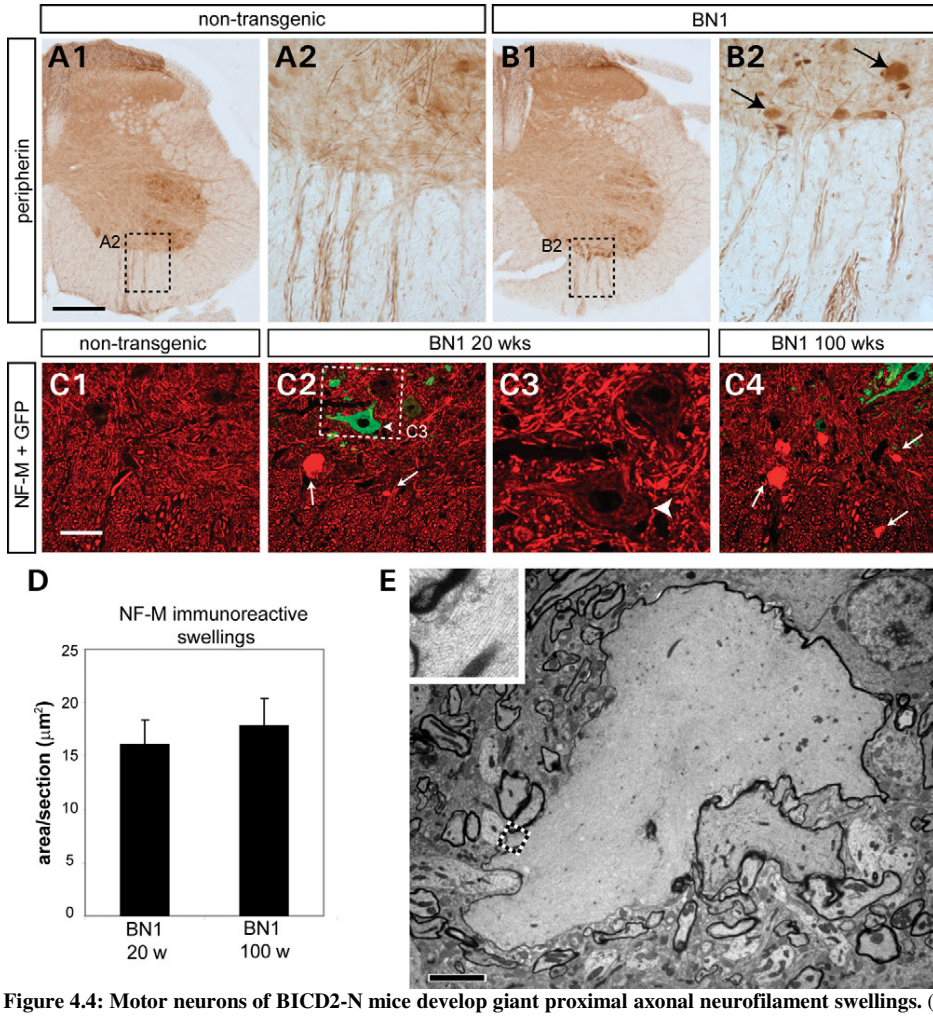

Figure 4.4: Motor neurons of BICD2-N mice develop giant proximal axonal neurofilament swellings. (A and B) Immunohistochemical staining of peripherin in L4 spinal cord sections shows that BN1 mice develop large immunoreactive structures in the ventral grey matter, where motor axons enter the white matter (arrows in B2). (C) Confocal immunofluorescence of neurofilament-M showed that these structures also were immunoreactive for neurofilament (arrows in C2 and C4). GFP-BICD2-N expression did not alter neurofilament staining in the cell bodies (arrow head in C3). (D) Quantification of the surface occupied by these neurofilament-M-labelled structures per lumbar L4 section showed that similar amounts occurred in young adult (20w) and old (100w) BN1 mice. (E) Electron microscopy showed that these structures consisted of swollen myelinated axons filled with ordered filament arrays. Bars: A1, 250 µm; C1, 50 µm; D, 2 µm.

BICD2-N causes giant proximal neurofilament swellings in motor axons

Impaired dynein/dynactin function in cultured neurons may lead to neurofilament accumulations in the proximal or distal axon (28). Therefore, in Thy1.2-GFP-BICD2-N mice, we studied the distribution of neurofilament proteins as well as peripherin, an intermediate filament protein that is expressed at high levels in motor axons. No major change in neurofilament-M and peripherin immunoreactivity occurred in motor nerve endings at the neuromuscular junctions. However, analysis of spinal cord sections revealed intense peripherin and neurofilament-M immunoreactive structures in the most ventral

aspect of the grey matter, where the motor axons enter the white matter to course to the ventral roots (Fig. 4.4A–C). In some instances, these structures also were identified in motor axons crossing the white matter, as well as in the proximal aspect of the ventral roots. The structures were also intensely labelled with antibodies against the SMI31 and SMI32 epitopes representing phosphorylated and non-phosphorylated neurofilament, respectively. Further analysis by electron microscopy showed that these structures consisted of swollen myelinated axons with a diameter reaching up to 20 µm that were filled with filamentous material (Fig. 4.4E), and strongly resembled proximal giant filamentous axonal swellings reported in ALS patients (26,27). Comparison of spinal cord sections from different transgenic lines showed that the giant axonal neurofilament swellings occurred in both BN1 and BN4 lines, but not in mice from the low expressing BN3 line. Comparison of BN1 mice over different ages (4, 20 and 104 weeks) revealed that axonal swellings did not occur at 4 weeks, but were present at 20 and 104 weeks in equal number (Fig. 4.4D). These data indicate that axonal swellings are a relatively early phenomenon after dynein/dynactin impairment.

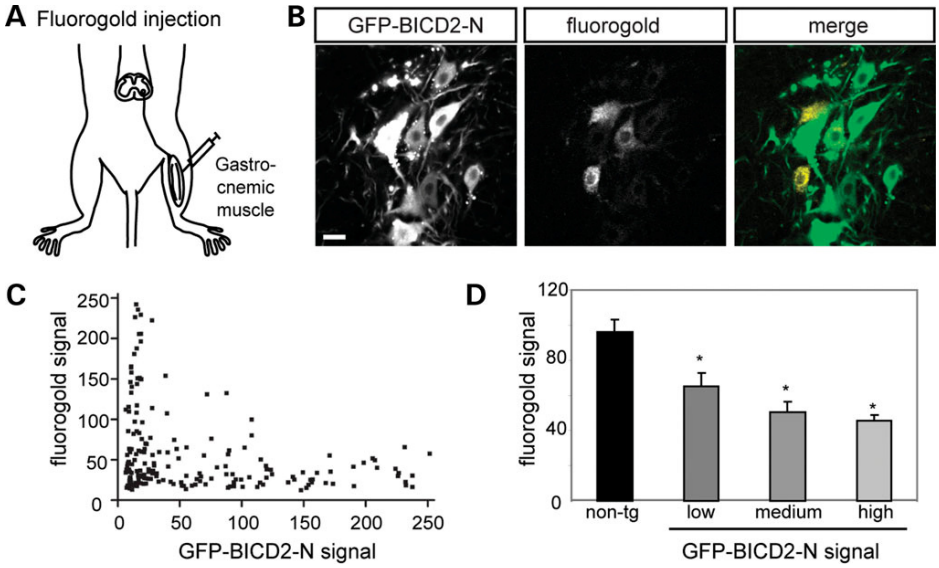

Figure 4.5: BICD2-N causes reduced retrograde fluorogold labelling. (A and B) Confocal fluorescence of L4 lumbar motor neurons of a 30-week-old BN1 mouse (B) 48 h after fluorogold injections (4 × 1 µl) in the gastrocnemic muscle (A). Transgenic motor neurons show no or reduced labelling compared with non-transgenic motor neurons (B). (C and D) Scatter plot and bar graph showing that fluorogold signal intensities negatively correlate with the GFP-BICD2-N expression levels. *P < 0.01 (one-way ANOVA, post-test for linear trend). Bar: 25 µm.

BICD2-N expression reduces retrograde axonal transport

To examine whether motor neurons expressing BICD2-N show reduced retrograde axonal transport, we performed tracing experiments with the retrograde tracer fluorogold (15). With our transgenic lines, we can take advantage of the chimeric expression of the GFP-BICD2-N transgene, in particular, the BN1 line that expresses the transgene in 50–60% of the motor neurons, with the remaining motor neurons serving as controls. Fluorogold was

injected in the gastrocnemic muscle of BN1 mice, and 48 h post-injection, lumbar L4–L5 sections were examined for fluorogold and GFP signals. As shown in Figure 5, the amount of fluorogold labelling negatively correlated with the level of GFP signal, indicating that BICD2-N expression diminishes retrograde fluorogold transport.

Axonal injury activates a number of retrograde signalling pathways to reorganize gene expression and initiate repair programmes in the injured neuron (25). To examine whether BICD2-N expression has an effect on retrograde injury signalling, we have studied ATF3 expression after sciatic nerve transection in BN1 mice and non-transgenic littermates, as ATF3 is one of the transcription factors that is strongly induced in axotomized motor neurons (44). No nuclear ATF3 labelling is present in lumbar spinal cord sections of non-axotomized BN1 and control mice. Twelve hours post-axotomy of the left sciatic nerve, weak nuclear ATF3 staining was observed in ipsi-lateral sciatic nerve motor neurons, which are localized in the dorso-lateral aspect of the L4–L5 spinal cord (Fig. 4.6A–C), and more intense labelling occurred at later time points. Quantitative analysis of ATF3 levels in axotomized BN1 mouse spinal cord showed that at 12 h post-axotomy, high-level BICD2-N-expressing motor neurons showed reduced ATF3 expression compared with BICD2-N-negative motor neurons (Fig. 4.6D and E). No difference in ATF3-labelling intensities was observed between BICD2-N-positive and negative sciatic nerve motor neurons at 24 h post-axotomy (Fig. 4.6D and E). These data show that inhibition of dynein/dynactin delays retrograde injury signalling.

BICD2-N mice do not develop motor abnormalities and motor neuron loss

To determine whether impaired dynein/dynactin function influences viability of motor neurons, BN1 mice were tested for the development of motor abnormalities up to the age of 2 years and subsequently analysed for degenerative changes in the neuromuscular system. BN1 mice did not show evidence of weight loss (Fig. 4.7A) or reduced muscle strength, as determined by a hanging wire test (Fig. 4.7B) and grip strength measurement (not shown). Furthermore, the size of the cell bodies and nuclei was the same in GFP-BICD2-N and control motor neurons (Fig. 4.7C). Counting the number of motor neurons showed that 2-year-old BN1 mice contain the same amount of L4 spinal cord motor neurons as 2-year-old non-transgenic mice and 20-week-old BN1 mice (Fig. 4.7D), and that the number of GFP-BICD2-N motor neurons was the same in 20-week- and 2-year-old BN1 mice (Fig. 4.7D). In addition, a silver staining method that visualizes degenerating neurons and their processes, did not produce argyrophilic staining in spinal cord from 2-year-old BN1 mice. Consistent with the absence of neurodegenerative changes, 2-year-old BN1 mice did not show evidence of increased astrocytosis and microgliosis compared with non-transgenic controls (Fig. 4.7F and G). Also, the neuromuscular junctions of the gastrocnemic muscle of 2-year-old BN1 mice did not show increased levels of denervated neuromuscular junctions compared with controls (Fig. 4.7E). Together these data indicate that impairment of dynein/dynactin by BICD2-N at levels that cause neurofilament and Golgi abnormalities does not necessarily cause the premature loss of motor neurons.

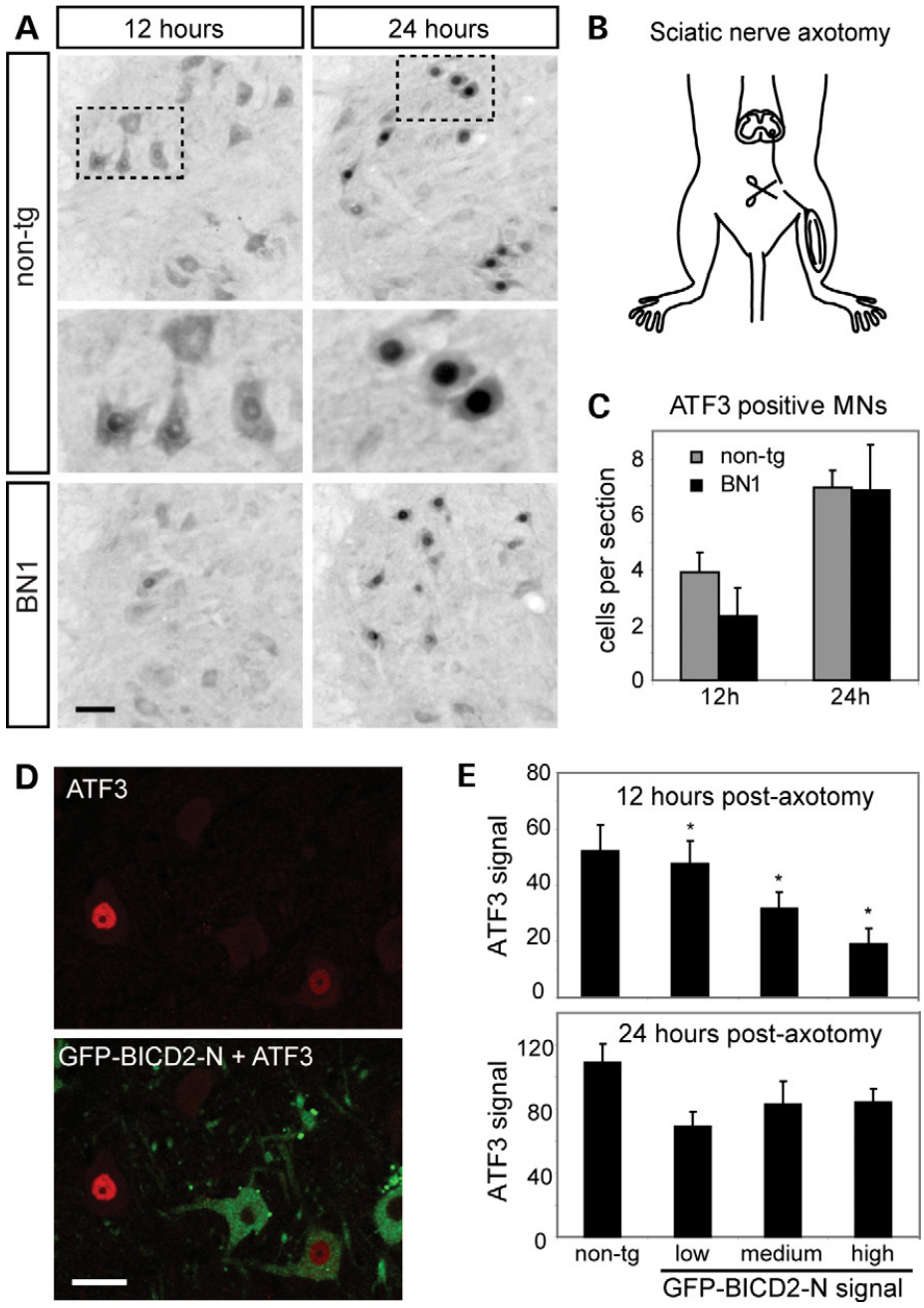

Figure 4.6: Reduced retrograde injury signalling in GFP-BICD2-N mice after axotomy. (A–C) Representative images (A) and bar graph (C) showing that transection of the sciatic nerve (B) triggers moderate and high levels of ATF3 expression in sciatic motor neurons after 12 and 24 h, respectively, as revealed immunohistochemically. (D and E) Confocal image and bar graphs showing that 12 h post-axotomy ATF3 expression is lower in GFP-BICD2-N-positive motor neurons compared with non-transgenic neurons. However, ATF3 labelling was not different at 24 h post-axotomy. *$P < 0.01$ (one-way ANOVA, post-test for linear trend). Bars: 50 µm.

BICD2-N expression increases survival of SOD1-G93A ALS mice

The pathological mechanisms that cause motor neuron degeneration in SOD1-ALS suggest that disruptions in axonal transport may play a significant role (18,24,45–47), possibly via a direct interaction of mutant SOD1 with dynein (48). To examine whether the inhibition of dynein/dynactin function by BICD2-N affects disease progression and lifespan in SOD1-ALS, we crossed our BICD2-N transgenic mice with G1del mice, a transgenic ALS mouse model that expresses human SOD1 with the G93A mutation and develops a fatal progressive motor neuron disease (49,50). Unexpectedly, double-transgenic BN1/G1del mice showed a delayed onset of motor symptoms compared with G1del mice (225 ± 8, versus 189 ± 6 day, respectively), and increased survival (271 ± 8 versus 237 ± 5 day, respectively; Fig. 4.8A and B). Accordingly, also, crossing of G1del mice with the BN3 line, which express BICD2-N at lower levels though in a higher percentage of motor neurons (as described earlier), resulted in increased survival (256 ± 8 versus 236 ± 5 day; Fig. 4.8A and B). Western blot analysis of spinal cord homogenates showed that expression levels of the mutant SOD1 protein in each BN1/G1del mice was the same as in G1del mice (Fig. 4.8C), indicating that the difference in disease phenotype cannot be explained by altered mutant SOD1 expression levels. End-stage BN1/G1del mice showed similar levels of motor neuron loss compared with G1del mice. Furthermore, the loss of GFP-BICD2-N-expressing motor neurons was proportional to the loss of motor neurons labelled for CGRP (a peptide that is expressed in a subset of predominantly large motor neurons), indicating that BICD2-N expression delayed but not prevented motor neuron degeneration.

Dynein/dynactin accumulates in dendritic ubiquitinated SOD1 aggregates in SOD1-G93A ALS mice

Dendritic ubiquitinated SOD1 aggregates represent an early pathological feature preceding motor neuron loss in G1del mice (4,50). Ultrastructurally, these aggregates consist of disorganized filaments, amorphous electron dense material and vesicular structures (4,50). Systematic ultrastructural analysis of pre-embedding ubiquitin immunoperoxidase-stained ultrathin sections from BN1/G1del spinal cord showed that all ubiquitinated dendritic aggregates identified in this material (n = 27) had the same morphological features as aggregates previously identified in G1del mice (Fig. 4.8E). Confocal immunofluorescence further showed that ubiquitinated dendritic aggregates occurred in both GFP-BICD2-N-expressing and GFP-BICD2-N-negative motor neurons in double-transgenic G1del/BN1 mice. Consistent with the notion that mutant SOD1 interacts with dynein/dynactin (48), we observed that the dendritic aggregates were immunoreactive for p150Glued (Fig. 4.8F) and dynein heavy chain (not shown). Aggregates in GFP-BICD2-N-positive dendritic profiles showed higher levels of p150Glued and dynein heavy chain immunoreactivity compared with GFP-BICD2-N-negative profiles (Fig. 4.8F).

Furthermore, also, GFP-BICD2-N was present in the ubiquitinated SOD1 aggregates. The increased dynein/dynactin levels in dendritic SOD1 aggregates in GFP-BICD2-N-expressing neurons raise the possibility that dynein/dynactin trapped in intracellular inclusions might be beneficial to the disease phenotype in SOD1-linked ALS.

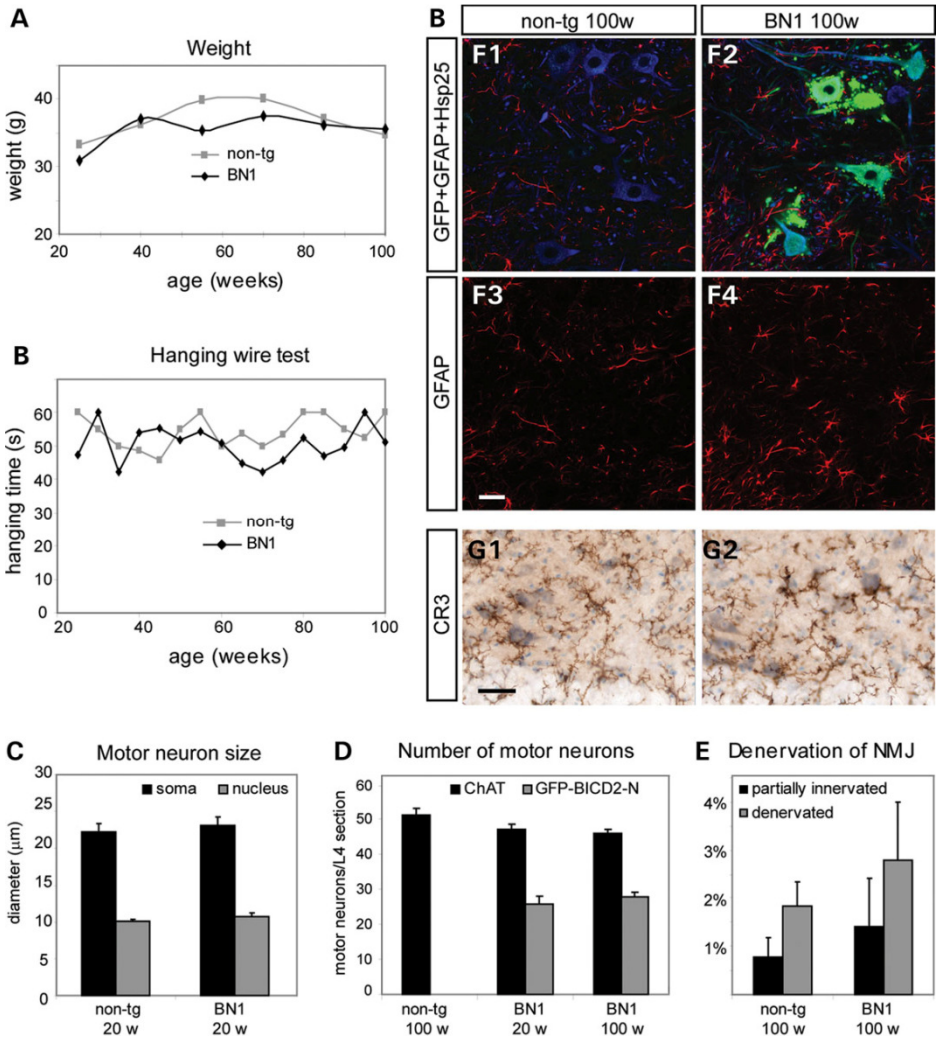

Figure 4.7: Thy1.2-BICD2-N mice do not show motor neuron degeneration up to 2 years of age. (A) Male BN1 mice show the same average weight as non-transgenic mice up to 2 years of age (data represent means of 4 male mice). (B) Performance in a hanging wire test is not different in BN1 mice compared with non-transgenic mice (data represent means of 4 male mice). (C) Diameter of motor neurons (black bars) and motor neuron nuclei (grey bars) is the same in non-transgenic and BN1 mice. (D) Bar graph showing the total number (ChAT, black bars) and transgenic (GFP, grey bars) motor neurons in L4 sections of young and old BN1 mice compared with non-transgenic mice. (E) A slight (non-significant) increase in partially innervated and denervated neuromuscular junctions (NMJs) in 100-week-old BN1 mice compared with control mice. (F) Confocal fluorescence of GFP-BICD2-N, GFAP (red) and Hsp25 (blue) in the lumbar ventral horns of 100-week-old BN1 (F2 and F4) and non-transgenic mice (F1 and A3) showing that old BN1 mice do not develop signs of astrocytosis, characterized by increased GFAP immunoreactivity. Accordingly, astrocytes in old BN1 mice as in non-transgenic mice do not stain for Hsp25, which is expressed in activated astrocytes in the spinal cord (4). (G) Immunoperoxidase-staining of the microglial protein complement receptor 3 (CR3) reveals no reactive microglia in old non-transgenic (G1) and BN1 mice (G2). Bars: 50 µm.

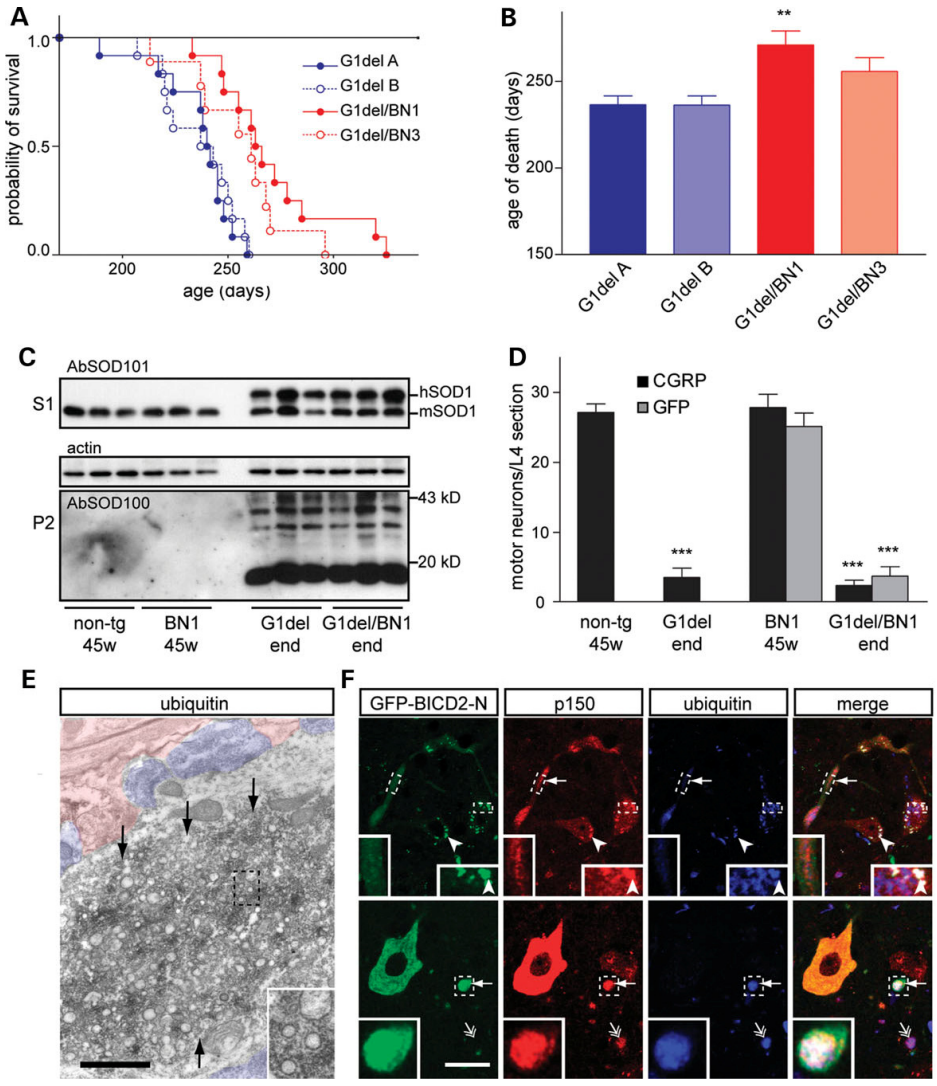

Figure 4.8: BICD2-N prolongs survival of SOD1-ALS mice. (A and B) Kaplan–Meier plot (A) and bar graph (B) showing that the age of death of G1del mice that carry the BN1 or BN3 transgene is delayed compared with single-transgenic littermates (G1delA and G1delB, respectively). **P < 0.01 compared with G1delA and G1delB (unpaired two-tailed Student's t-tests; n = 12 for the G1delA, G1delB and G1del/BN1 groups and n = 9 for the G1del/BN3 group). (C) Western blot analysis of SOD1 expression in total homogenate (S1) and NP-40-insoluble fraction (P2) shows that G1del/BN1 double-transgenic mice express similar levels of transgenic human SOD1 in spinal cord homogenate compared with non-transgenic littermates and develop similar levels of NP40-insoluble and multimeric mutant SOD1 species. SOD100, human SOD1-preferring antibody; SOD101, murine SOD1-preferring antibody that also immunoreact with high levels of human SOD1. (D) End-stage G1del/BN1 and G1del mice show similar losses of motor neurons stained for CGRP, which is expressed in a subset of large motor neurons. Loss of GFP-BICD2-N-positive neurons is comparable with the loss of CGRP immunoreactive cells. Values in the bar graphs represent mean ± SE; n = 3. ***P < 0.001 compared with non-transgenic and BN1 littermates (ANOVA with Tukey's multiple comparison test). (E) Transmission electron photomicrograph of a dendrite (surrounding neuropil in pink, presynaptic boutons in blue) in a G1del/BN1 mouse with a dendritic aggregate immunoperoxidase stained for ubiquitin (dark electron dense material). Ultrastructurally, aggregates in G1del/BN1 mice are similar to those in G1del mice and usually contain high levels of vesicular structures. (F) Confocal fluorescence of GFP-BICD2-N, p150Glued (red) and ubiquitin (blue) in the lumbar ventral horns of end-

stage G1del/BN1 mouse shows that GFP-BICD2-N and p150Glued accumulate in ubiquitinated aggregates in dendrites of GFP-BICD2-N motor neurons (arrows). Also, aggregates in GFP-BICD2-N-negative neurons are immunoreactive for p150Glued (double-headed arrow). Many neurons have accumulated autofluorescent material that gives a strong signal in all channels (arrow heads). Bars: E, 25 µm; F, 1 µm.

Discussion

In the present study, we have generated a new mouse model with impaired dynein/dynactin function by taking advantage of the properties of dynein/dynactin-interacting protein BICD2 (32,33). We show that BICD2-N causes accumulation of the dynein motor complex in the neuronal cell body and impairs retrograde axonal transport. Accordingly, the BICD2-N mice develop giant neurofilament swellings in the proximal axon, a feature that is consistent with reduced dynein/dynactin function (19,28). Despite the accumulation of dynein/dynactin components in the perykaryon and proximal dendrites, motor neurons expressing BICD2-N also develop abnormalities in this compartment, i.e. fragmentation of the Golgi apparatus. Golgi fragmentation is a well-established consequence of dynein/dynactin inhibition (29,41,51), but here we show for the first time that it can be induced via dynein/dynactin inhibition in neurons in vivo. Our data indicate that only motor neurons expressing relatively high levels of BICD2-N showed Golgi fragmentation, and that the frequency of neurons with fragmented Golgi increased with ageing. These data suggest that Golgi fragmentation is a phenomenon that requires a certain threshold of dynein/dynactin inhibition to occur. Golgi abnormalities have not been reported for other mutant mouse models with dynein/dynactin abnormalities. However, embryonic fibroblasts from mice homozygous for the Loa mutation in the dynein heavy chain gene show impaired Golgi restoration after Golgi fragmentation induced by the microtubule depolymerizing agent nocodazole (16).

We have generated the Thy1.2-GFP-BICD2-N mice as a dynein/dynactin loss-of-function mouse model to study the pathological aspects of ALS and related motor neuron diseases. Accordingly, our mice develop well-established features of ALS motor neurons, i.e. giant proximal neurofilamentous axonal swellings (26,27) and Golgi fragmentation (30,31). However, despite these abnormalities, our mice up to the age of 2 years did not develop motor abnormalities or signs of motor neuron degeneration. Even the motor neurons with fragmented Golgi did not show signs of illness. Thus, our data indicate that axonal neurofilament abnormalities and Golgi fragmentation are ALS phenomena that can be explained by impaired dynein/dynactin function, but that are not necessarily linked to neuronal degeneration. In contrast to our data, LaMonte et al. (15) have shown that disruption of dynein/dynactin function in neurons by dynamitin p50 overexpression causes a late-onset progressive motor neuron disease that has been linked to dynein-based axonal transport deficits (15,19). The motor neuron disease phenotype in these mice may be explained by a higher level of dynein/dynactin inhibition owing to very high levels of p50 expression. Accordingly, ‘low’ expressor p50 mice show a much milder phenotype (15).

Alternatively, the inhibition of dynein/dynactin function by p50 is caused by dynactin disruption (39), which may differentially affect long-term motor neuron survival. Data from other dynein/dynactin mouse models have indicated that subtle specialized defects may underlie motor neuron abnormalities in these mice. For instance, comparison of mouse

models carrying p150Glued with the G59S mutation has shown that the development of progressive motor neuron degeneration correlates with the formation of p150Glued aggregates (10–12), which is in accord with data from patients (52) and cultured motor neurons (53). In addition, data from another transgenic line indicate that G59S-p150Glued may induce abnormalities in motor neuronal lysosomal pathways, axonal calibre and neuromuscular junction morphology in the absence of retrograde axonal transport defects (12). Retrograde axonal transport as measured by the movements of a fluorescent tetanus toxin fragment was also reported to be normal in embryonic motor neurons from heterozygous Loa mice that carry a dynein heavy chain mutation and develop mild motor neuron degeneration at a progressed age (16,54). Recently, it has been shown that heterozygous Loa mice, as well as mice carrying another mutant allele of dynein heavy chain, termed Sprawling (Swl), exhibit significant prenatal degeneration of sensory proprioceptive dorsal root ganglion neurons (55). However, Swl mice, in contrast to Loa and Cra1 mice (i.e. another dynein heavy chain mutant), do not show late-onset motor neuron loss, indicating that this phenotype depends on a feature shared by the Loa and Cra1 dynein heavy chain mutants but not the Swl mutant and supporting the notion that motor neurons are vulnerable to specific abnormalities in dynein/dynactin function (16,17,55). Precise comparison of dynein/dynactin dependent-transport defects and pathological abnormalities between dynein/dynactin mouse models, including our BICD2-N mice, may help uncovering dynein/dynactin defects that contribute to motor neuron pathology.
In this study, we also show that the BICD2-N transgene increased lifespan of 'low-copy' G93A-SOD1 mice that develop an ALS-like motor neuron disease. This finding is consistent with the demonstration that also G93A-SOD1 mice carrying the Loa and Cra1 dynein heavy chain alleles show increased lifespan (54–56). Furthermore, the disease phenotype of SOD1-ALS mice that were heterozygous for G59S-mutant p150Glued or Swl-mutant dynein heavy chain was unaltered (10,55), indicating that interfering with dynein/dynactin function in SOD1-ALS mice is either beneficial or neutral. These data challenge the notion that the inhibition of dynein/dynactin-dependent processes is a contributing factor in SOD1-ALS pathogenesis (18,57). It has been proposed that Loa and Cra-mutant dyneins compensate or counteract axonal transport abnormalities triggered by mutant SOD1 (17,18,54). Alternatively, dynein/dynactin inhibition may attenuate functions that are potentially harmful to mutant SOD1-expressing motor neurons such as retrograde transport of axonal debris or protein aggregates (22,23), or deleterious retrograde signalling (25,58,59). Motor neurons in SOD1-ALS mice show early expression of axonal injury factors, including ATF3 (4,50,60). As BICD2-N-expressing motor neurons show attenuated axonal injury ATF3 response, a delay of ATF3 expression could contribute to the beneficial effect of BICD2-N in SOD1-ALS mice. We also observed an increased accumulation of dynein heavy chain and p150Glued in SOD1 aggregates in BICD2-N/SOD1-ALS mice, suggesting that trapping dynein/dynactin complexes at intracellular inclusions could restrain deleterious retrograde signalling.

Together the data from distinct dynein/dynactin mouse models, including our BICD2-N mice, indicate that partial inhibition of dynein/dynactin functions does not necessarily lead to motor neuron death, but is rather beneficial in some forms of motor neuron disease, such

as SOD1-linked ALS. On the other hand, specific mutations in dynein/dynactin components may trigger preferential degeneration of motor neurons via specific gained properties such as the formation of aggregates.

Funding

This work is supported by Prinses Beatrix Fonds and Hersenstichting Nederland grants to C.C.H and D.J. Work in the laboratory of C.C.H. is supported by the Netherlands Organization for Scientific Research (NWO-VIDI), European Science Foundation [European Young Investigators (EURYI) Award] and ALS Association (ALSA).

Acknowledgements

We thank S.A. Spangler and N. Keijzer for preparing primary neuronal cultures, Dr J.C. Holstege for assisting with fluorogold tracing and A. Hossaini for assisting with in situ hybridization experiments.

References

1. Boillee, S., Vande Velde, C. and Cleveland, D.W. (2006) ALS: a disease of motor neurons and their nonneuronal neighbors. Neuron, 52, 39–59.
2. Pasinelli, P. and Brown, R.H. (2006) Molecular biology of amyotrophic lateral sclerosis: insights from genetics. Nat. Rev. Neurosci., 7, 710–723.
3. Kwong, L.K., Neumann, M., Sampathu, D.M., Lee, V.M. and Trojanowski, J.Q. (2007) TDP-43 proteinopathy: the neuropathology underlying major forms of sporadic and familial frontotemporal lobar degeneration and motor neuron disease. Acta Neuropathol., 114, 63–70.
4. Jaarsma, D., Teuling, E., Haasdijk, E.D., De Zeeuw, C.I. and Hoogenraad, C.C. (2008) Neuron-specific expression of mutant superoxide dismutase is sufficient to induce amyotrophic lateral sclerosis in transgenic mice. J. Neurosci., 28, 2075–2088.
5. Van Deerlin, V.M., Leverenz, J.B., Bekris, L.M., Bird, T.D., Yuan, W., Elman, L.B., Clay, D., Wood, E.M., Chen-Plotkin, A.S., Martinez-Lage, M. et al. (2008) TARDBP mutations in amyotrophic lateral sclerosis with TDP-43 neuropathology: a genetic and histopathological analysis. Lancet Neurol., 7, 409–416.
6. Sreedharan, J., Blair, I.P., Tripathi, V.B., Hu, X., Vance, C., Rogelj, B., Ackerley, S., Durnall, J.C., Williams, K.L., Buratti, E. et al. (2008) TDP-43 mutations in familial and sporadic amyotrophic lateral sclerosis. Science, 319, 1668–1672.
7. Kabashi, E., Valdmanis, P.N., Dion, P., Spiegelman, D., McConkey, B.J., Vande Velde, C., Bouchard, J.P., Lacomblez, L., Pochigaeva, K., Salachas, F. et al. (2008) TARDBP mutations in individuals with sporadic and familial amyotrophic lateral sclerosis. Nat. Genet., 40, 572–574.
8. Puls, I., Jonnakuty, C., LaMonte, B.H., Holzbaur, E.L., Tokito, M., Mann, E., Floeter, M.K., Bidus, K., Drayna, D., Oh, S.J. et al. (2003) Mutant dynactin in motor neuron disease. Nat. Genet., 33, 455–456.
9. Munch, C., Sedlmeier, R., Meyer, T., Homberg, V., Sperfeld, A.D., Kurt, A., Prudlo, J., Peraus, G., Hanemann, C.O., Stumm, G. et al. (2004) Point mutations of the p150 subunit of dynactin (DCTN1) gene in ALS. Neurology, 63, 724–726.
10. Lai, C., Lin, X., Chandran, J., Shim, H., Yang, W.J. and Cai, H. (2007) The G59S mutation in p150(glued) causes dysfunction of dynactin in mice. J. Neurosci., 27, 13982–13990.
11. Laird, F.M., Farah, M.H., Ackerley, S., Hoke, A., Maragakis, N., Rothstein, J.D., Griffin, J., Price, D.L., Martin, L.J. and Wong, P.C. (2008) Motor neuron disease occurring in a mutant dynactin mouse model is characterized by defects in vesicular trafficking. J. Neurosci., 28, 1997–2005.

12. Chevalier-Larsen, E.S., Wallace, K.E., Pennise, C.R. and Holzbaur, E.L. (2008) Lysosomal proliferation and distal degeneration in motor neurons expressing the G59S mutation in the p150Glued subunit of dynactin. Hum. Mol. Genet., 17, 1946–1955.
13. Schroer, T.A. (2004) Dynactin. Annu. Rev. Cell Dev. Biol., 20, 759–779.
14. Vallee, R.B., Williams, J.C., Varma, D. and Barnhart, L.E. (2004) Dynein: an ancient motor protein involved in multiple modes of transport. J. Neurobiol., 58, 189–200.
15. LaMonte, B.H., Wallace, K.E., Holloway, B.A., Shelly, S.S., Ascano, J., Tokito, M., Van Winkle, T., Howland, D.S. and Holzbaur, E.L. (2002) Disruption of dynein/dynactin inhibits axonal transport in motor neurons causing late-onset progressive degeneration. Neuron, 34, 715–727.
16. Hafezparast, M., Klocke, R., Ruhrberg, C., Marquardt, A., Ahmad-Annuar, A., Bowen, S., Lalli, G., Witherden, A.S., Hummerich, H., Nicholson, S. et al. (2003) Mutations in dynein link motor neuron degeneration to defects in retrograde transport. Science, 300, 808–812.
17. Banks, G.T. and Fisher, E.M. (2008) Cytoplasmic dynein could be key to understanding neurodegeneration. Genome Biol., 9, 214.
18. Strom, A.L., Gal, J., Shi, P., Kasarskis, E.J., Hayward, L.J. and Zhu, H. (2008) Retrograde axonal transport and motor neuron disease. J. Neurochem, published online doi 10.1111/j.1471–4159.2008.05393.x.
19. Levy, J.R. and Holzbaur, E.L. (2006) Cytoplasmic dynein/dynactin function and dysfunction in motor neurons. Int. J. Dev. Neurosci., 24, 103–111.
20. Ibanez, C.F. (2007) Message in a bottle: long-range retrograde signalling in the nervous system. Trends Cell Biol., 17, 519–528.
21. Roy, S., Zhang, B., Lee, V.M. and Trojanowski, J.Q. (2005) Axonal transport defects: a common theme in neurodegenerative diseases. Acta Neuropathol., 109, 5–13
22. Johnston, J.A., Illing, M.E. and Kopito, R.R. (2002) Cytoplasmic dynein/ dynactin mediates the assembly of aggresomes. Cell Motil. Cytoskeleton, 53, 26–38.
23. Ravikumar, B., Acevedo-Arozena, A., Imarisio, S., Berger, Z., Vacher, C., O'Kane, C.J., Brown, S.D. and Rubinsztein, D.C. (2005) Dynein mutations impair autophagic clearance of aggregate-prone proteins. Nat. Genet., 37, 771–776.
24. Rao, M.V. and Nixon, R.A. (2003) Defective neurofilament transport in mouse models of amyotrophic lateral sclerosis: a review. Neurochem. Res., 28, 1041–1047.
25. Hanz, S. and Fainzilber, M. (2006) Retrograde signaling in injured nerve—the axon reaction revisited. J. Neurochem., 99, 13–19.
26. Hirano, A., Donnenfeld, H., Sasaki, S. and Nakano, I. (1984) Fine structural observations of neurofilamentous changes in amyotrophic lateral sclerosis. J. Neuropathol. Exp. Neurol., 43, 461–470.
27. Delisle, M.B. and Carpenter, S. (1984) Neurofibrillary axonal swellings and amyotrophic lateral sclerosis. J. Neurol. Sci., 63, 241–250.
28. Motil, J., Dubey, M., Chan, W.K. and Shea, T.B. (2007) Inhibition of dynein but not kinesin induces aberrant focal accumulation of neurofilaments within axonal neurites. Brain Res., 1164, 125–131.
29. Burkhardt, J.K., Echeverri, C.J., Nilsson, T. and Vallee, R.B. (1997) Overexpression of the dynamitin (p50) subunit of the dynactin complex disrupts dynein-dependent maintenance of membrane organelle distribution. J. Cell Biol., 139, 469–484.
30. Gonatas, N.K., Stieber, A. and Gonatas, J.O. (2006) Fragmentation of the Golgi apparatus in neurodegenerative diseases and cell death. J. Neurol. Sci., 246, 21–30.
31. Fujita, Y., Mizuno, Y., Takatama, M. and Okamoto, K. (2008) Anterior horn cells with abnormal TDP-43 immunoreactivities show fragmentation of the Golgi apparatus in ALS. J. Neurol. Sci., 269, 30–34.
32. Hoogenraad, C.C., Akhmanova, A., Howell, S.A., Dortland, B.R., De Zeeuw, C.I., Willemsen, R., Visser, P., Grosveld, F. and Galjart, N. (2001) Mammalian Golgi-associated Bicaudal-D2 functions in the dynein–dynactin pathway by interacting with these complexes. EMBO J., 20, 4041–4054.
33. Hoogenraad, C.C., Wulf, P., Schiefermeier, N., Stepanova, T., Galjart, N., Small, J.V., Grosveld, F., de Zeeuw, C.I. and Akhmanova, A. (2003) Bicaudal D induces selective dynein-mediated microtubule minus end-directed transport. EMBO J., 22, 6004–6015.
34. Matanis, T., Akhmanova, A., Wulf, P., Del Nery, E., Weide, T., Stepanova, T., Galjart, N., Grosveld, F., Goud, B., De Zeeuw, C.I. et al. (2002) Bicaudal-D regulates COPI-independent Golgi-ER transport by recruiting the dynein–dynactin motor complex. Nat. Cell Biol., 4, 986–992.

35. Grigoriev, I., Splinter, D., Keijzer, N., Wulf, P.S., Demmers, J., Ohtsuka, T., Modesti, M., Maly, I.V., Grosveld, F., Hoogenraad, C.C. et al. (2007) Rab6 regulates transport and targeting of exocytotic carriers. Dev. Cell, 3, 305–314.
36. Bullock, S.L. and Ish-Horowicz, D. (2001) Conserved signals and machinery for RNA transport in Drosophila oogenesis and embryogenesis. Nature, 414, 611–616.
37. Caroni, P. (1997) Overexpression of growth-associated proteins in the neurons of adult transgenic mice. J. Neurosci. Methods, 71, 3–9.
38. Feng, G., Mellor, R.H., Bernstein, M., Keller-Peck, C., Nguyen, Q.T., Wallace, M., Nerbonne, J.M., Lichtman, J.W. and Sanes, J.R. (2000) Imaging neuronal subsets in transgenic mice expressing multiple spectral variants of GFP. Neuron, 28, 41–51.
39. Maier, K.C., Godfrey, J.E., Echeverri, C.J., Cheong, F.K. and Schroer, T.A. (2008) Dynamitin mutagenesis reveals protein–protein interactions important for dynactin structure. Traffic, 9, 481–491.
40. Dehmelt, L., Nalbant, P., Steffen, W. and Halpain, S. (2006) A microtubule-based, dynein-dependent force induces local cell protrusions: implications for neurite initiation. Brain Cell Biol., 35, 39–56.
41. Harada, A., Takei, Y., Kanai, Y., Tanaka, Y., Nonaka, S. and Hirokawa, N. (1998) Golgi vesiculation and lysosome dispersion in cells lacking cytoplasmic dynein. J. Cell Biol., 141, 51–59.
42. Nakamura, N., Rabouille, C., Watson, R., Nilsson, T., Hui, N., Slusarewicz, P., Kreis, T.E. and Warren, G. (1995) Characterization of a cis-Golgi matrix protein, GM130. J. Cell Biol., 131, 1715–1726.
43. Caldero, J., Casanovas, A., Sorribas, A. and Esquerda, J.E. (1992) Calcitonin gene-related peptide in rat spinal cord motoneurons: subcellular distribution and changes induced by axotomy. Neuroscience, 48, 449–461
44. Tsujino, H., Kondo, E., Fukuoka, T., Dai, Y., Tokunaga, A., Miki, K., Yonenobu, K., Ochi, T. and Noguchi, K. (2000) Activating transcription factor 3 (ATF3) induction by axotomy in sensory and motoneurons: a novel neuronal marker of nerve injury. Mol. Cell. Neurosci., 15, 170–182.
45. Williamson, T.L. and Cleveland, D.W. (1999) Slowing of axonal transport is a very early event in the toxicity of ALS-linked SOD1 mutants to motor neurons. Nat. Neurosci., 2, 50–56.
46. De Vos, K.J., Chapman, A.L., Tennant, M.E., Manser, C., Tudor, E.L., Lau, K.F., Brownlees, J., Ackerley, S., Shaw, P.J., McLoughlin, D.M. et al. (2007) Familial amyotrophic lateral sclerosis-linked SOD1 mutants perturb fast axonal transport to reduce axonal mitochondria content.
Hum. Mol. Genet., 16, 2720–2728.
47. Ligon, L.A., LaMonte, B.H., Wallace, K.E., Weber, N., Kalb, R.G. and Holzbaur, E.L. (2005) Mutant superoxide dismutase disrupts cytoplasmic dynein in motor neurons. Neuroreport, 16, 533–536.
48. Zhang, F., Strom, A.L., Fukada, K., Lee, S., Hayward, L.J. and Zhu, H. (2007) Interaction between familial amyotrophic lateral sclerosis (ALS)-linked SOD1 mutants and the dynein complex. J. Biol. Chem., 282, 16691–16699.
49. Gurney, M.E., Pu, H., Chiu, A.Y., Dal Canto, M.C., Polchow, C.Y., Alexander, D.D., Caliendo, J., Hentati, A., Kwon, Y.W., Deng, H.X. et al. (1994) Motor neuron degeneration in mice that express a human Cu,Zn superoxide dismutase mutation. Science, 264, 1772–1775.
50. Vlug, A.S., Teuling, E., Haasdijk, E.D., French, P., Hoogenraad, C.C. and Jaarsma, D. (2005) ATF3 expression precedes death of spinal motoneurons in amyotrophic lateral sclerosis-SOD1 transgenic mice and correlates with c-Jun phosphorylation, CHOP expression, somato-dendritic ubiquitination and Golgi fragmentation. Eur. J. Neurosci., 22, 1881–1894.
51. Allan, V.J., Thompson, H.M. and McNiven, M.A. (2002) Motoring around the Golgi. Nat. Cell Biol., 4, E236–E242.
52. Puls, I., Oh, S.J., Sumner, C.J., Wallace, K.E., Floeter, M.K., Mann, E.A., Kennedy, W.R., Wendelschafer-Crabb, G., Vortmeyer, A., Powers, R. et al. (2005) Distal spinal and bulbar muscular atrophy caused by dynactin mutation. Ann. Neurol., 57, 687–694.
53. Levy, J.R., Sumner, C.J., Caviston, J.P., Tokito, M.K., Ranganathan, S., Ligon, L.A., Wallace, K.E., LaMonte, B.H., Harmison, G.G., Puls, I. et al. (2006) A motor neuron disease-associated mutation in p150Glued perturbs dynactin function and induces protein aggregation. J. Cell Biol., 172, 733–745.
54. Kieran, D., Hafezparast, M., Bohnert, S., Dick, J.R., Martin, J., Schiavo, G., Fisher, E.M. and Greensmith, L. (2005) A mutation in dynein rescues axonal transport defects and extends the life span of ALS mice. J. Cell Biol., 169, 561–567.

55. Chen, X.J., Levedakou, E.N., Millen, K.J., Wollmann, R.L., Soliven, B. and Popko, B. (2007) Proprioceptive sensory neuropathy in mice with a mutation in the cytoplasmic dynein heavy chain 1 gene. J. Neurosci., 27, 14515–14524.
56. Teuchert, M., Fischer, D., Schwalenstoecker, B., Habisch, H.J., Bockers, T.M. and Ludolph, A.C. (2006) A dynein mutation attenuates motor neuron degeneration in SOD1(G93A) mice. Exp. Neurol., 198, 271–274.
57. Chevalier-Larsen, E. and Holzbaur, E.L. (2006) Axonal transport and neurodegenerative disease. Biochim. Biophys. Acta, 1762, 1094–1108.
58. Carson, C., Saleh, M., Fung, F.W., Nicholson, D.W. and Roskams, A.J. (2005) Axonal dynactin p150Glued transports caspase-8 to drive retrograde olfactory receptor neuron apoptosis. J. Neurosci., 25, 6092–6104.
59. Cavalli, V., Kujala, P., Klumperman, J. and Goldstein, L.S. (2005) Sunday Driver links axonal transport to damage signaling. J. Cell Biol., 168, 775–787.
60. Lobsiger, C.S., Boillee, S. and Cleveland, D.W. (2007) Toxicity from different SOD1 mutants dysregulates the complement system and the neuronal regenerative response in ALS motor neurons. Proc. Natl Acad. Sci. USA, 104, 7319–7326.
61. Jaarsma, D., Rognoni, F., Van Duijn, W., Verspaget, H., Haasdijk, E.D. and Holstege, J.C. (2001) CuZn superoxide dismutase (SOD1) accumulate in vacuolated mitochondria in transgenic mice expressing amyotrophic lateral sclerosis (ALS)-linked SOD1 mutations. Acta Neuropathol., 102, 293–305.
62. Hoogenraad, C.C., Milstein, A.D., Ethell, I.M., Henkemeyer, M. And Sheng, M. (2005) GRIP1 controls dendrite morphogenesis by regulating EphB receptor trafficking. Nat. Neurosci., 8, 906–915.
63. Hossaini, M., French, P.J. and Holstege, J.C. (2007) Distribution of glycinergic neuronal somata in the rat spinal cord. Brain Res., 1142, 61–69.

Supplementary Data

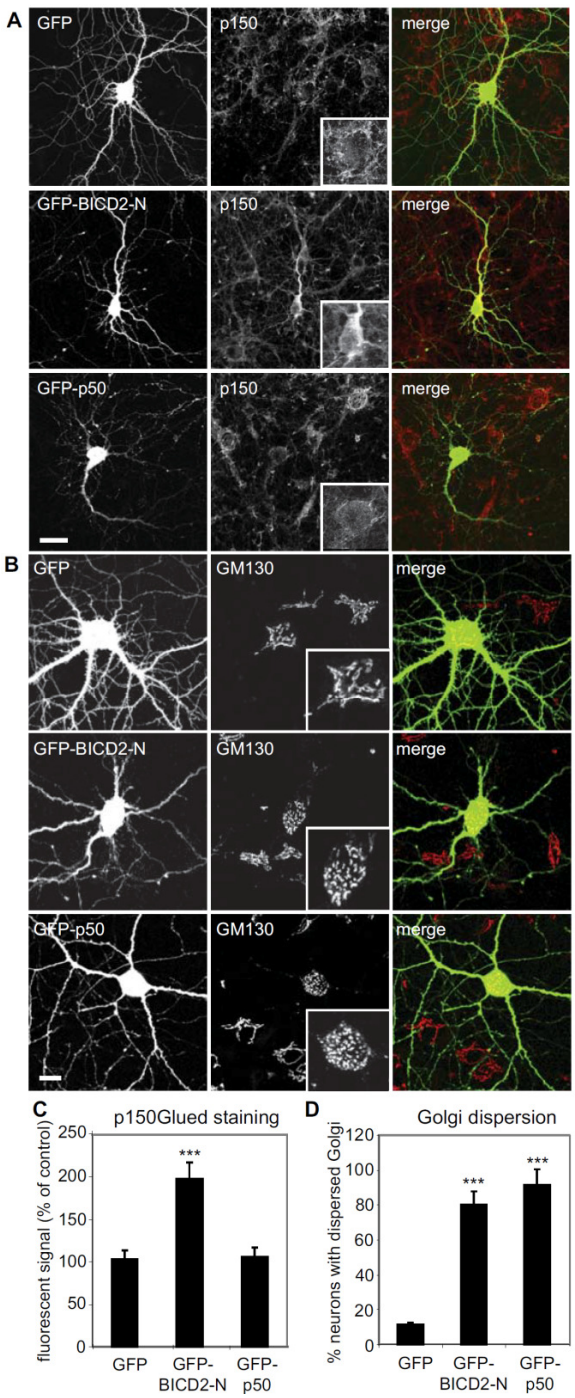

Supplementary Figure 1. BICD2-N causes Golgi fragmentation and dynein/dynactin accumulation in primary neurons A) Primary neurons expressing GFP, GFPBICD2-N and GFP-p50 for 2 days, fixed and stained with antibodies against p150Glued (red), show an increased p150Glued labelling in the somata of GFP-BICD2-N, but not in GFP, and GFP-p50 transfected neurons. Inset shows enlargement of soma. B) Expression of GFP-p50 and GFPBICD2-N, but not GFP in neurons leads to fragmentation of the Golgi apparatus as seen with antibodies against cis-Golgi marker GM130 (A,E). C) Bar graph showing intensities of p150Glued-immunoreactivity in the neuronal cell body in GFP, GFP-BICD2-N and GFPp50 expressing neurons relative to control neurons in the same image. ***, $p<0.001$ compared to GFP and GFP-p50 transfected neurons (unpaired two-tailed Student *t*-test). D) Percentage of neurons with dispersed Golgi apparatus relative to control neurons. ***, $p<0.001$ compared to GFP transfected neurons (unpaired two-tailed Student t-test). Bars: A, 20 μm; B, 10 μm.

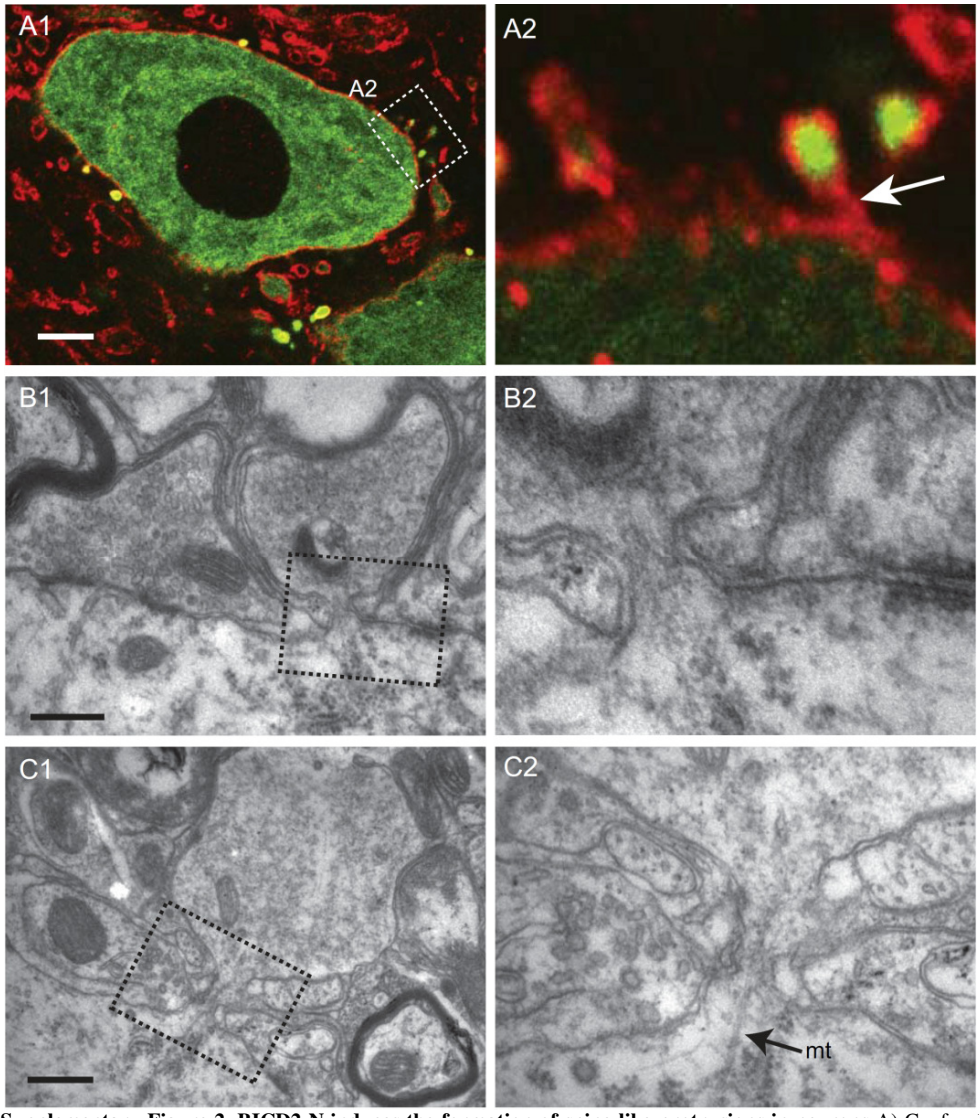

Supplementary Figure 2. BICD2-N induces the formation of spine-like protrusions in neurons A) Confocal fluorescence of GFP-BICD2-N (green) and muscarinic M2 receptor (red) of lumbar motor neuron of BN1 mouse shows that spherical structures surrounding GFP-BICD2-N neurons show high levels of GFP-signal, and usually are outlined by muscarinic M2 receptor immunoreactivity. In many occasions M2-immunoreactivity also outlines a thin stalk (arrow in A2) that connects the spherical structures to the soma. B, C) Electron microscopy shows that spherical structure are spine like protrusions that are filled with electron dense material and are usually devoid of synaptic specialisations. A higher magnification of the connecting stalk is shown in B2 and C2. Note the microtubule (mt) in the stalk in C2. Bars: A, 10 μm; B1 and C1, 500 nm.

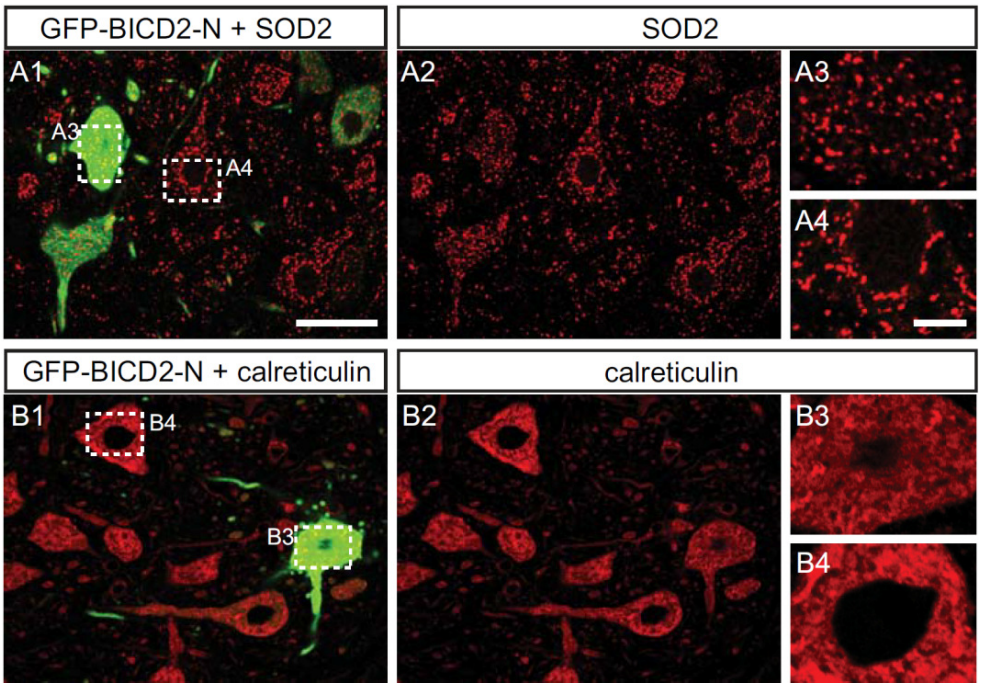

Supplementary Figure 3. BICD2-N-expression does not induce changes in mitochondria and endoplasmic reticulum in motor neurons Double labelling immunofluorescence of GFP-BICD2-N with mitochondrial protein SOD2 (A), or ER-protein calreticulin (B) in ventral lumbar spinal cord sections of BN1 mouse shows similar staining in GFP-BICD-N (A3,B3) and control (A4, B4) motor neurons. Bars: A1, 50 µm; A4, 10 µm.

Chapter 5

Golgi fragmentation in ALS motor neurons precedes neuromuscular denervation and is associated with intracellular transport abnormalities

Vera van Dis[1], Marijn Kuijpers[1,2], Elize D. Haasdijk[1], Eva Teuling[1], Scott A. Oakes[3], Casper C. Hoogenraad[1,2], Dick Jaarsma[1#]

[1]Department of Neuroscience, Erasmus Medical Center, Rotterdam, The Netherlands. [2]Cell Biology, Faculty of Science, Utrecht University, Utrecht, The Netherlands

Abstract

Fragmentation of stacked cisterns of the Golgi apparatus into dispersed smaller elements is a feature associated with degeneration of neurons in amyotrophic lateral sclerosis (ALS) and some other neurodegenerative disorders. Although this is well accepted pathological hallmark, the processes of Golgi fragmentation is not well characterized. Here we show in a SOD1-ALS mouse model (low-copy Gurney G93A-SOD1 mouse) that motor neurons with Golgi fragmentation (GF neurons) are retrogradely labeled by intramuscularly injected CTB (beta subunit of cholera toxin), indicating that Golgi fragmentation precedes neuromuscular denervation and axon retraction. Golgi fragmentation also precedes the appearance of two key pathological markers, *i.e.* somatodendritic SOD1 inclusions, and the induction of ATF3 expression. We further show that Golgi fragmentation is associated with an altered dendritic organisation of the Golgi apparatus, that does not depend on intact apoptotic machinery, and is facilitated in transgenic mice with impaired retrograde dynein-dependent transport (BICD2-N mice). A linkage with altered dynein-dependent transport also is suggested by reduced expression of endosomal markers in neurons with Golgi fragmentation, a phenomenon that like Golgi fragmentation also occurs in neurons with impaired dynein function. Together the data indicate that Golgi fragmentation is a very early event in the pathological cascade in ALS that is associated with altered organization of intracellular trafficking.

Introduction

Death and disappearance of neurons is a constant hallmark of neurodegenerative disorders, such as Alzheimer's disease and other dementia's, Parkinson's disease, and amyotrophic lateral sclerosis. How the primary molecular deficits causing these disorders and ultimately lead to neuronal degeneration and death is yet poorly established for most disorders. A variety of cellular deficits and molecular pathways have been proposed to contribute, including impaired axonal transport, synaptic abnormalities, proteotoxic stress, ER stress, impaired calcium homeostasis, mitochondrial insufficiency, synaptic dysfunction, aberrant function of glia, improper activation of cell death pathways, or combinations of these events (De Vos et al., 2008; Ilieva et al., 2009; Nassif et al., 2010; Saxena and Caroni, 2011; Schon and Przedborski, 2011; Harris and Rubinsztein, 2012). Fragmentation of the Golgi apparatus, *i.e.* the transformation from a network of large stacked cisternae to dispersed ministacks composed of small element, has been identified in a subset of motor neurons in amyotrophic lateral sclerosis (ALS) (Gonatas et al., 1992; Gonatas et al., 2006; Fujita et al., 2008). Golgi fragmentation occurs in sporadic ALS patients and at least two monogenetic form of ALS, *i.e.* SOD1-ALS and optineurin-ALS (Fujita and Okamoto, 2005; Gonatas et al., 2006; Fujita et al., 2008; Ito et al., 2011), and in transgenic SOD1-ALS mice that develop a progressive motor neuron disorder, strongly resembling ALS in man (Mourelatos et al., 1996; Gonatas et al., 2006). Golgi fragmentation also has been documented in other neurodegenerative disorders including Parkinson's disease, multiple system atrophy, corticobasal degeneration, Creutzfeldt-Jakob disease Alzheimer's disease (Stieber et al., 1996; Sakurai et al., 2000; Fujita et al., 2006; Gonatas et al., 2006), but it was not found in X-linked spinal and bulbar muscular atrophy, a non-ALS motor neuron disorder (Yaguchi et al., 2003), in transgenic mice with motor neurons with massive cytoplasmic neurofilaments aggregates (Stieber et al., 2000), and in the majority of degenerating motor neurons in a DNA-repair deficient mouse model (de Waard et al., 2010). These data suggest that Golgi fragmentation is a specific event shared by multiple ALS forms and some other conditions.

The Golgi apparatus is a highly dynamic organelle involved in processing and sorting of lipids and proteins, and its morphology depends on a large variety of protein components and cellular processes (De Matteis and D'Angelo, 2007; Ngo and Ridgway, 2009; Ramirez and Lowe, 2009; Goud and Gleeson, 2010; Mironov and Beznoussenko, 2011; Sengupta and Linstedt, 2011; Xiang and Wang, 2011). Accordingly, the morphology can alter under a variety physiological conditions such as cell division, growth, and altered metabolic demands (Gardiol et al., 1999; Polishchuk and Mironov, 2004; Horton et al., 2005; Goud and Gleeson, 2010; Mironov and Beznoussenko, 2011; Sengupta and Linstedt, 2011), as well as pathological conditions, including impaired endoplasmic reticulum function, disruption of intracellular transport, altered lipid metabolism, and activation of cell death pathways (Hicks and Machamer, 2005; Gonatas et al., 2006; Nakagomi et al., 2008; Teuling et al., 2008; Nassif et al., 2010). Several of these conditions may cause Golgi fragmentation, albeit with various morphologies (Hicks and Machamer, 2005; Gonatas et al., 2006; Nakagomi et al., 2008; Xiang and Wang, 2011). Fragmentation into ministacks as

observed in ALS motor neurons also occur in cells treated with microtubule depolymerizing agent nocodazole, and cells with impaired function of the minus-end microtubule-dependent motor dynein (Burkhardt et al., 1997; Hafezparast et al., 2003; Gonatas et al., 2006; Teuling et al., 2008).

To further characterize the pathological significance of Golgi fragmentation in ALS motor neurons, in the present study we have precisely characterized the relationship between Golgi fragmentation and other early pathological events in SOD1-ALS mice. Our data show that Golgi fragmentation precede the appearance of somatodendritic SOD1 inclusions, activation of the injury transcription factor ATF3, neuromuscular denervation and axon retraction, occurs in the absence of a functional mitochondrial apoptotic pathway, is greatly facilitated in neurons with impaired dynein function, and is associated with endosomal abnormalities. The data suggest that Golgi fragmentation reflect altered organization of intracellular trafficking, perhaps in response to specific aggregated SOD1 complexes.

Materials and Methods

Transgenic mice

All animal experiments were approved by the Erasmus University animal care committee, and performed in accordance with the guidelines the "Principles of laboratory animal care" (NIH publication No. 86-23), and the European Community Council Directive (86/609/EEC). Transgenic mice expressing a human genomic SOD1 construct with the G93A mutation were originally derived from the Gurney G1 mice, but because of a reduction in the transgene copy number (8 instead of ~20 transgene copy numbers per haploid genome) show a delayed disease onset and are termed G1del mice (Gurney, 1997; Jaarsma et al., 2008; Acevedo-Arozena et al., 2011). G1del mice are maintained under standard housing conditions in a FVB/N background by mating hemizygote males with non-transgenic females, non-transgenic offspring serving as controls (Jaarsma et al., 2008).

Neuron-specific mice carrying the cDNA of G93A-mutant hSOD1 cloned into the Thy1.2 expression cassette were generated as described (Jaarsma et al., 2008). In this study we used tissue from T3hSOD1 double transgenic mice generated by crossing Thy1hSOD1-G93A mice derived from founder T3 with line N1029 wild-type hSOD1 overexpressing mice (Jaarsma et al., 2008).

BICD2-N (line BN1) mice are transgenic for GFP-BICD2-N cDNA cloned into the Thy1.2 expression vector (Teuling et al., 2008). BN1/G1del mice were obtained by intercrossing hemizygous G1del and BN1 mice as described (Teuling et al., 2008). In this study we analyzed Golgi fragmentation in G1del, G1del/BN1 and BN1 of 28 weeks of age with 5-7 mice per genotype.

For one experiment we used paraffin embedded spinal cord tissue from 90 days old high copy (fast) G1 mice (carrying ~20 hSOD1-G93A transgene copy numbers, see above) crossed with mice deficient for the mitochondrial apoptotic pathway in the central nervous system, termed DKO mice. DKO mice were Bak-null in the whole body ($Bak^{-/-}$) and Bax-null in the central nervous system ($Bax^{f/f}$/Nestin-Cre; see (Reyes et al., 2010) for details).

We analyzed archival sections from 3 mice per genotype (non-tg, DKO, G1del, G1del/DKO).

Antibodies

Primary antibodies (supplier; dilutions) used in this study are: Rabbit anti-ATF3 (Santa Cruz; IHC and IF 1:1000), goat-anti-choline acetyltransferase (ChAT, Millipore, 1:500), goat anti-Cholera toxin B subunit (CTB; List Biological laboratories, 1:5000), rabbit-anti-CGRP (Calbiochem, IF, 1:10.000), human-anti EEA1 (gift from Dr. M.J. Fritzler, IF: 1:500), mouse-anti GM130 (BD Biosciences, 1:200), rabbit-anti GM130 (antibody M07, gift from Dr. M. Lowe (Lane et al., 2002), 1:1000), mouse anti GRASP65 (gift from Dr. M. Lowe (Lane et al., 2002), 1:200), rabbit-anti-GRASP-1 (Millipore, 1:500), rat anti-Mac-2 (Cedarlane, 1:2000), mouse-anti p115 (BD Biosciences, 1:500), sheep anti-hSOD1 (Calbiochem; IF, 1:5000), rabbit-anti unfolded SOD1 (USOD, gift from Dr. A. Chakrabartty (Kerman et al., 2010), 1:1000), rabbit anti-SOD1 exposed dimer interface (SEDI, gift from Dr. J. Robertson (Rakhit et al., 2007), 1:1000), mouse anti-ubiquitin (clone FK2; Affinity BioReagents, Golden, CO; 1:2000, rabbit anti-ubiquitin (DAKO, 1:1000).
Secondary antibodies used for IF or ICC were Alexa-488, -568 or -633- conjugated goat-anti mouse or goat-anti rabbit antibodies from Molecular Probes; or FITC, Cy3 or Cy5 anti-rabbit, mouse or goat antibodies from Jackson Laboratories; all antibodies were used at 1:400. Biotinylated goat-anti-rabbit or anti-mouse IgG (Vector) were used at 1:400.

Immunocytochemical and histochemical analyses

For immunocytochemistry and immunofluorescence mice were anaesthetized with pentobarbital and perfused transcardially with 4% paraformaldehyde with or without glutaraldehyde (0.05%). The lumbar and cervical spinal cord were carefully dissected out and postfixed overnight in 4% paraformaldehyde. Routinely, spinal cord tissue was embedded in gelatin blocks (Hossaini et al., 2011), sectioned at 40 µm with a freezing microtome, and sections were processed, free-floating, using a standard avidin–biotin–immunoperoxidase complex method (ABC, Vector Laboratories, USA) with diaminobenzidine (DAB, 0.05%) as the chromogen, or single-, double- and triple-labelling immunofluorescence. Immunoperoxidase-stained sections were analysed and photographed using a Leica DM-RB microscope and a Leica DC300 digital camera. Sections stained for immunofluorescence were analyzed with a Leica DM-RB epifluorescence microscope and Zeiss LSM 510 and LSM700 confocal laser scanning microscopes.

Cholera toxin B-fragment (CTB) retrograde tracing

Mice were anaesthetized, immobilized, and Cholera toxin B-fragment (CTB) (0.5% in 2.5 µl saline) is injected in the gastrocnemic muscle of 15, 20 and 25 weeks old G1del mice and non-transgenic littermates (Fig. 5.1A). 4 days following injections mice were perfused with 4% paraformaldehyde with or without glutaraldehyde (0.05%), and their spinal cords were embedded in gelatine blocks, sectioned at 40 µm, and further processed for immunohistological procedures.

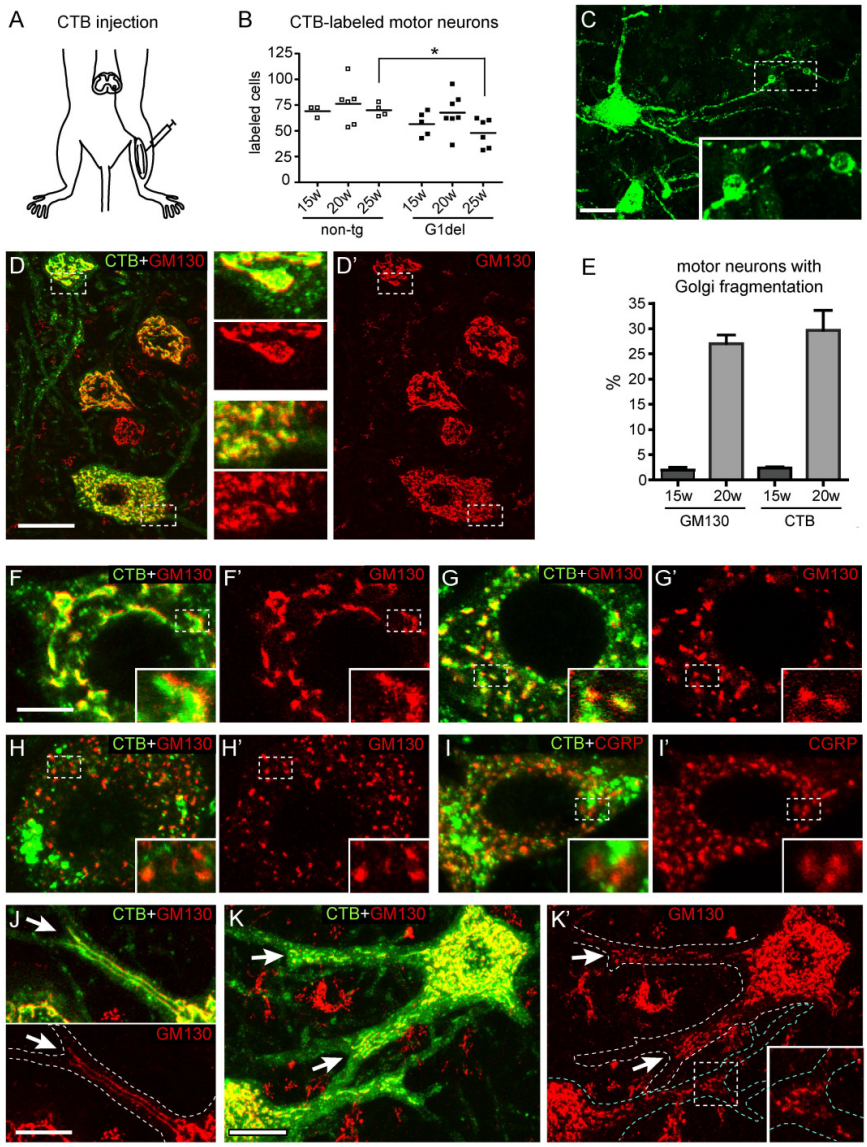

Figure 5.1. Retrograde labeling of motor neurons with Golgi fragmentation following intramuscular injections of CTB. A-C) CTB (0.5% in 2.5 µl saline) is injected in the gastrocnemic muscle to retrogradely label motor neurons (A). B) Dot plot showing the number of CTB-positive motor neurons counted in each tenth section. Note reduced number of CTB-positive cells in 25 week old G1del mice compared to age matched non-transgenic mice ($P < 0.05$, unpaired Students's *t*-test. C) Maximal projection of confocal stack (optical section 22 µm) of CTB-labeled motor neuron illustrating small vacuoles in the distal dendrite (insert). D) Double-labeling confocal image of CTB and GM130 showing cross sections of 4 retrogradely labeled motor neurons. A large proportion of CTB localizes to the Golgi apparatus. The motor neuron below has fragmented Golgi. E) Bar graph showing the proportion of motor neurons with Golgi fragmentation in all large ventral horn neurons (GM130) and the CTB labeled population. F-I) Representative images of a CTB-labeled motor neuron with normal Golgi apparatus (F), fragmented Golgi (G), and fragmented Golgi with no or little CTB (H, I). J) Representative example of a proximal motor neuron dendrite with GM130-positive ribbons that stops at the branching point (arrow). K) Two motor neurons with Golgi fragmentation showing fragmented Golgi in the proximal dendrites up to the first branching point (arrows and insert). Bars: 20 µm (C, D), 10 µm (K), 5 µm (F, J)

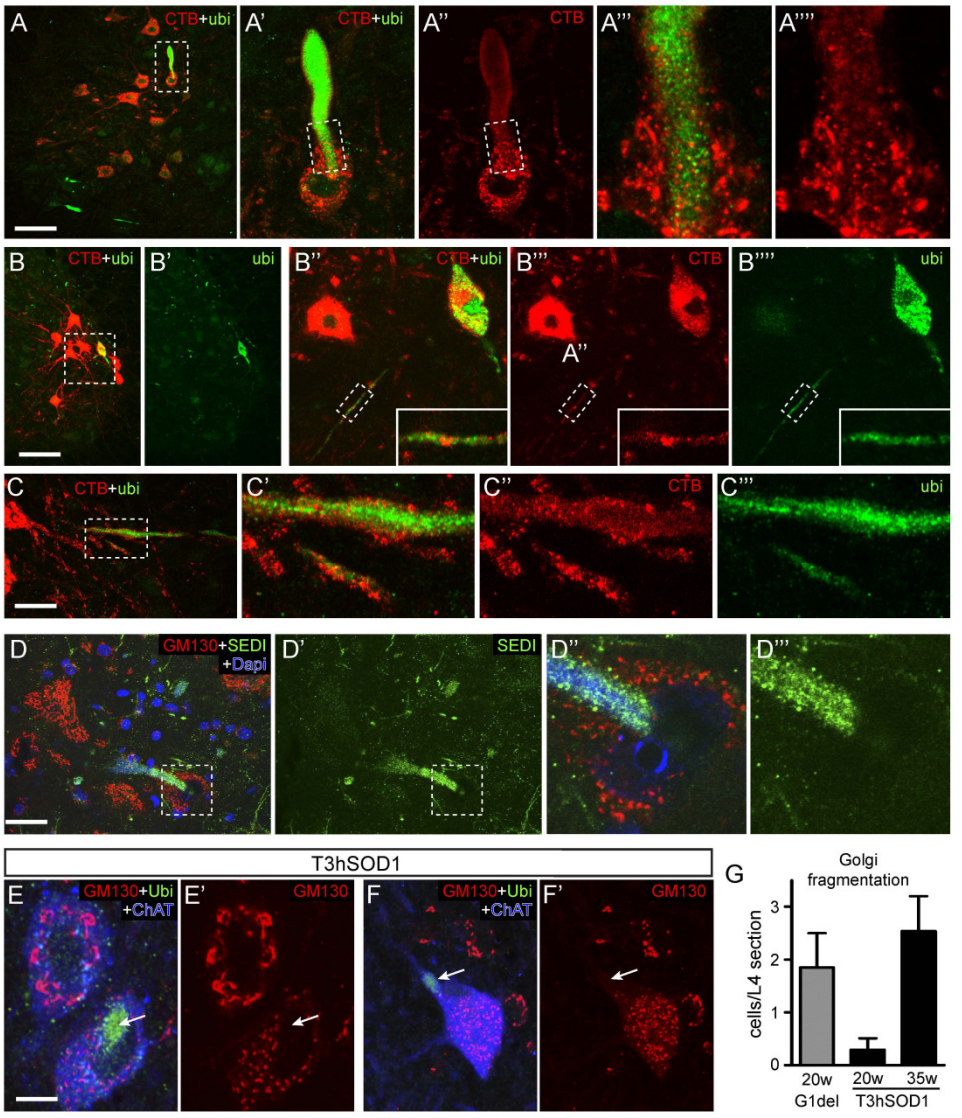

Figure 5.2. CTB tracing and Golgi fragmentation in motor neurons with ubiquitinated SOD1-inclusions

A-C) Double-labeling confocal image of CTB and ubiquitinated epitopes showing a CTB-positive motor neuron with a large inclusion in the proximal dendrite (A' and A''), a CTB-positive motor neuron with intense ubiquitin labeling throughout most of the somato-dendritic compartment (B' and B''''), and ubiquitin-labeling in distal CTB-positive dendrites (C-C''').

D) Double-labeling confocal image of GM130 and misfolded SOD1 (SEDI epitope) showing a motor neuron with fragmented Golgi and a large SEDI-immunoreactive inclusion.

E-F) Confocal image showing motor neurons labeled for ChAT with fragmented Golgi apparatus and poly-ubiquitinated epitope (arrow) in L4 lumbar spinal cord section of 20 (E) and 35 (F) weeks old T3hSOD1 mouse.

G) Bar graph showing the number of Golgi fragmented motor neurons in L4 spinal cord sections of G1del versus T3hSOD1 mice. Values represent Means ± SE from 3 mice per group. Note that no motor neurons with fragmented Golgi occur in non-transgenic, T3 and hSOD1 mice at 35 weeks of age.

Bars: 50 µm (A-C), 10 µm (D-F)

To obtain an estimate of the number of retrogradely labeled motor neurons, one in 10 sections was immunoperoxidase-DAB stained for CTB, and used for counting CTB-positive cells with the aid of a Olympus microscope fitted with a LucividTM miniature monitor and NeurolucidaTM software (MicroBrightField, Colchester, VT, USA). Only CTB-positive cells whose nucleus was partially or entirely present in the section but did not contact the surface of the sections were counted.

Quantitative analysis of immunofluorescence images

The proportion of CTB and GM130-positive motor neurons was determined in section from G1del mice of 15 (n=3) and 20 weeks (n=3), 4 sections/mouse using a Leica DM-RB epifluorescence microscope with a 63x objective. First, all large neurons (diameter >20 µm) in the ventral horn both ipsi and contralateral of the injection were scored for golgi fragmentation, and subsequently using the same sections CTB-positive cells were scored for golgi fragmentation.

The proportion of motor neurons with dendritic GM130 staining was examined in the same material using a Zeiss LSM 510 laser scanning microscope. Motor neurons were randomly selected on the basis of the presence of at least 2 dendrites that could be followed to the first branching point within the plane of the section, and subsequently confocal stacks of CTB and GM130 stacks were collected and analyzed for the presence of dendritic GM130 labeling.

For analysis of fluorescent intensities images were collected using a Zeiss LSM 510 confocal laser scanning microscope with 63x objective. Fluorescent intensities were determined using Metamorph image analysis software.

Statistical analyzes were performed with MS Excel or Graphpad Prism software using Student's t-test and one-way ANOVA.

Results

Retrograde labeling of motor neurons with Golgi fragmentation after intramuscular injection of cholera toxin B (CTB)

The present study has been mainly performed with the G1del mice (also termed G1sow) that carries 8 copies of a human G93A-mutant SOD1, and that develops develop weakness in one or more limbs from age 24-34 weeks of age and die of fatal paralysis between 30-41 weeks of age (Vlug et al., 2005; Acevedo-Arozena et al., 2011). The onset of Golgi fragmentation in G1del mice is at about 14-15 weeks of age (Vlug et al., 2005). In view of evidence that degeneration of the distal axon is an early event in SOD1-ALS mice preceding the loss of motor neurons (Frey et al., 2000; Fischer et al., 2004; Hegedus et al., 2008).

We first examined whether motor neurons with Golgi fragmentation have an intact axon. For this purpose we performed retrograde tracing of Choleratoxin B (CTB) injected in the gastrocnemic muscle (Fig. 5.1A), and double stained for CTB and the cis-Golgi matrix protein GM130 (Nakamura et al., 1995). CTB is taken up via endocytosis after binding to the ganglioside GM1 in motor nerve endings, and then retrogradely transported to the cell

bodies, where it accumulates in the trans-golgi, lysosomes, and the cytoplasm (Wan et al., 1982; Ragnarson et al., 1998). The number of CTB labeled motor neurons was the same in non-transgenic littermates as in G1del mice at 15 and 20 weeks, and was reduced in G1del mice at 25 weeks (Fig. 5.1B), consistent with the onset of motor neuron loss at this 25 weeks (Vlug et al., 2005). CTB labeling was present throughout the soma and dendrites. Typically, motor neurons of G1del mice showed small vacuolar expansions in the distal portion of the dendrites (Fig. 5.1C), reflecting vacuolated mitochondria (Jaarsma et al., 2001). A proportion of CTB-positive cells showed Golgi fragmentation (Fig. 5.1D-K). Importantly, the proportion of retrogradely CTB-labeled motor neurons with Golgi fragmentation is the same as the proportion of Golgi fragmented motor neurons in the total population of motor neurons (Fig. 5.1E). This indicates that Golgi fragmentation does not interfere with retrograde labeling.

Consistent with retrograde trafficking to the Golgi apparatus, in all CTB positive motor neurons with a normal Golgi and the majority of motor neurons with Golgi fragmentation a large proportion of CTB codistributed with GM130 (Fig. 5.1D, F, G). However, in a subset of CTB-positive motor neurons with Golgi fragmentation CTB poorly codistributed with GM130 (Fig. 5.1H). In these cells CTB was predominantly distributed to large clusters into the cell body (Fig. 5.1H), while diffuse distribution throughout the somato-dendritic compartments and dot-like codistribution with LAMP1, marking lysosomes (not shown) did not appear to be affected. The same results were obtained in sections double-labeled for CTB and CGRP (calcitonin-gene related peptide), a peptide that is present in the trans-Golgi and secretory granules of most large motor neurons (Caldero et al., 1992). Thus in the majority of CTB-positive motor neurons with Golgi fragmentation a large portion of CTB codistributed with CGRP, while in a small subset of Golgi fragmented CTB-positive cells CTB poorly colocalized with CGRP (Fig. 5.1I). Together the data show that although Golgi fragmented motor neurons are capable of taking up, retrogradely transport, and redistribute the tracer throughout the somatodendritic compartment, a subset of Golgi fragmented neurons may have compromised retrograde transport to the Golgi apparatus.

A larger proportion of dendrites with Golgi apparatus in motor neurons with Golgi fragmentation

Although the majority of dendrites of motor neurons do not show significant GM130 staining, a subset show one or more GM130-positve ribbons that enter the proximal dendrite coursing up to the first branching point, indicative of long Golgi stacks entering the proximal dendrite (Fig. 5.1J). Also motor neurons with Golgi fragmentation showed dendrites with Golgi apparatus that as in the cell body was fragmented in smaller elements (Fig. 5.1K). Analysis of motor neurons with 3 or more dendrites that could be traced to the first branching point indicated that a larger proportion of motor neurons with Golgi fragmentation showed dendritic Golgi apparatus (32% versus 79%, normal versus fragmented Golgi; mean number of dendrites 3.38 ± 0.14 versus 3.68 ± 0.25; non-significant, unpaired student's *t*-test). The proportion of dendrites with Golgi apparatus was not-significantly different (36 ± 7% versus 48 ± 5%, normal versus fragmented Golgi; non-significant in unpaired student's *t*-test). Overall Golgi apparatus occurred 3-4 times more

often in motor neurons with fragmented Golgi (12 ± 4% of dendrites versus 44 ± 5%, P < 0.0001 unpaired student's *t*-test).

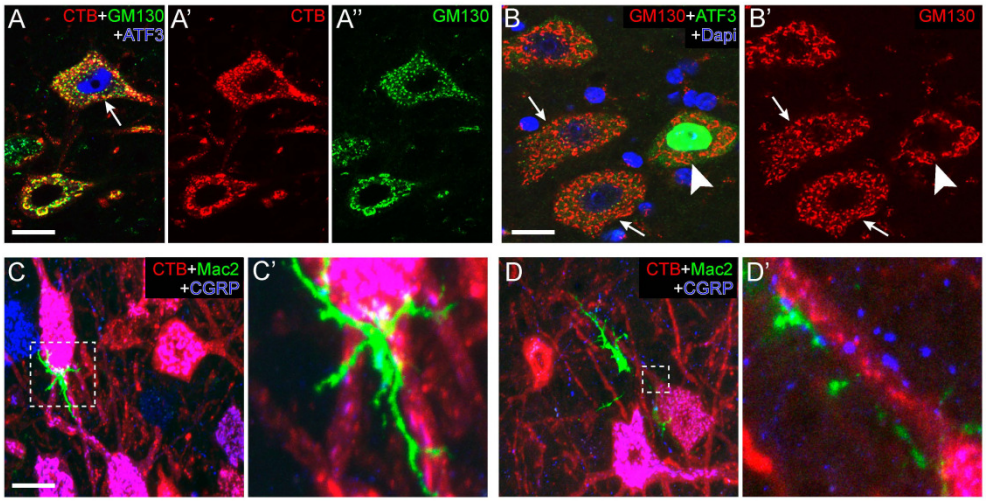

Figure 5.3. CTB tracing and Golgi fragmentation in motor neurons expressing ATF3 or contacted by phagocytosing microglia

A) Confocal image showing a CTB-positive motor neuron with fragmented Golgi and ATF3-positive nucleus (arrow). B) Confocal image of motor neurons with fragmented Golgi that are ATF3-negative (arrows) and a motor neuron with a normal Golgi apparatus that is ATF3-positive.

C, D) Maximal projections of confocal stacks showing CTB-positive motor neurons contacted by Mac-2 positive microglial cells. Calibration bars: 20 µm (A-C)

Golgi fragmentation precedes the appearance of somato-dendritic ubiquitin-positive inclusions

We previously have shown that the onset of Golgi fragmentation in G1del coincides with the onset of other pathological signs, *i.e.* the appearance of somatodendritic ubiquitinated SOD1 inclusions, the induction of stress transcription factor ATF3 expression, and signs of microglia activation (Vlug et al., 2005; Hossaini et al., 2011). For comparison, also in the high-copy fast G1 mouse the onset of Golgi fragmentation at post-natal day 30 (Mourelatos et al., 1996), coincides with the onset of ATF3 expression, signs of ER stress and microglia activation (Saxena et al., 2009). Double-labeling of CTB with antibody against ubiquitinated epitopes revealed CTB-positive motor neurons that contained ubiquitinated inclusions (Fig. 5.2), including cells with large inclusions in the proximal dendrite (Fig. 5.2A) and cells with intense ubiquitin staining throughout most of the somato-dendritic compartment (Fig. 5.2B), likely reflecting cells in a compromised state (Vlug et al., 2005). CTB also was present in the distal ubiquitinated dendrites (Fig. 5.2C). As previously reported (Vlug et al., 2005) double labeling for ubiquitination and GM130 showed that motor neurons with ubiquitinated inclusions in the proximal dendrite or cell body, all showed fragmented Golgi apparatus, but only represented a minority of motor neurons with fragmented Golgi.

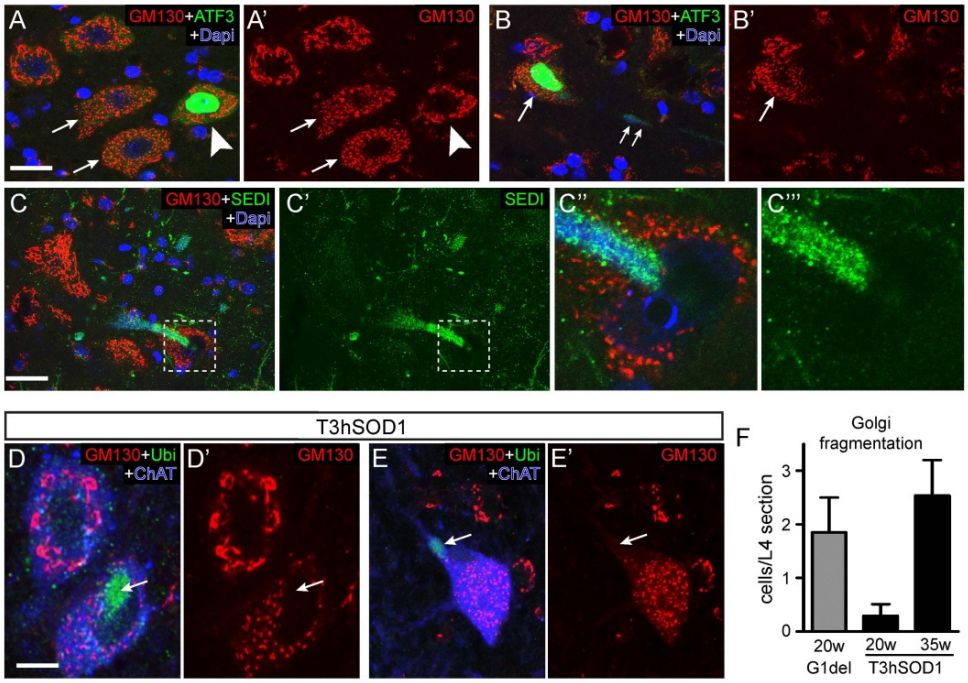

Figure 5.4. Golgi fragmentation in SOD1-ALS mice is not downstream of apoptotic pathways in apoptosis-deficient G1del mouse A, B) Confocal images of GM130 and ATF3 labeling in spinal motor neurons of a 90 day old fast SOD1-G93A mouse (G1 line) crossed into mouse deficient for BAK in all cells and BAX specifically in neurons (DKO) resulting in deficiency of the mitochondrial apoptotic pathways. Note, motor neurons with normal (A) and fragmented (B) Golgi apparatus and ATF3 expression in motor neurons with fragmented Golgi. C) G1-DKO showed a lower proportion Golgi fragmented motor neurons but this difference was not significant (Unpaired Students t-test); values are means ± SE (n=3 mouse per group).
D) Confocal image of p115 and GM130 (N-terminus) double labeling in motor neurons in 25 week old G1del mouse showing that motor neurons with fragmented Golgi (insert) show the same relative intensity of p115 staining. Calibration bars: 10 µm

To analyze the relationship between Golgi fragmentation and the accumulation of misfolded SOD1 species we performed double labeling of GM130 with antibodies against SOD1 dimer interface (SEDI, (Rakhit et al., 2007) and unfolded beta barrel domain of SOD1 (USOD, (Kerman et al., 2010). The USOD antibody mainly stained vacuolated mitochondria in the axon and distal dendrites, and, in addition, produced diffuse staining in the cell bodies of motor neurons and lightly stained ubiquitinated inclusions (not shown). The SEDI antibody, apart from light staining of vacuolated mitochondria and some background staining of astrocytic processes, selectively immunoreacted with the ubiquitinated inclusions (not shown). As with ubiquitinated epitopes, the presence of SEDI immunoreactive inclusions in proximal dendrites or cell body, in all occasions was associated with Golgi fragmentation (Fig. 5.2D).
To further establish the relationship between Golgi fragmentation and the presence of ubiquitin-positive inclusions we analyzed Golgi fragmentation in spinal cord section of T3hSOD1 mice that express a relatively low level of G93A mutant SOD1 specifically in neurons and in addition ubiquitously express high levels of wild-type SOD1 (Jaarsma et al.,

2008). T3hSOD1 mice develop signs of muscle weakness starting from 1 year of age, while dendritic ubiquitinated inclusions are already present at the age of 20 weeks (Jaarsma et al., 2008; Hossaini et al., 2011). T3hSOD1 showed fragmented Golgi apparatus in a subset of motor neurons, the number of neurons with fragmented Golgi increasing with aging, and a subset showing ubiquitin positive inclusions (Fig. 5.2E-G). Together the data point to a close relationship between the occurrence ubiquitinated inclusions and Golgi fragmentation. However, Golgi fragmentation precedes the appearance ubiquitinated inclusions, as it frequently occurs in their absence.

Golgi fragmentation precedes ATF3 expression

Double-labeling of CTB with antibody against ATF3 and activated phagocytosing microglia (Mac-2 positive, (Hossaini et al., 2011)) revealed CTB-positive motor neurons that expressed ATF3, or were contacted by phagocytosing microglia (Fig. 5.3), indicating that also these pathological signatures precede distal axon degeneration. Double-labeling of ATF3 and GM130 showed that consistent with previous data (Vlug et al., 2005) most (>80%) ATF3-positive motor neurons also have fragmented Golgi (Fig. 5.3A). Inversely, however, many motor neurons with fragmented Golgi, were ATF3-negative (Fig. 5.3B). Systematic analysis of lumbar sections in 20 weeks G1del mice (n=6) revealed ATF3 expression in 40 ± 6 % (Mean ± SE, range 25-62 %). Analysis of ATF3 and ubiquitin double labeled sections indicated that all cells with somato-dendritic ubiquitin-positive inclusions are ATF3 positive. Together these data suggest that Golgi fragmentation also precedes ATF3 expression.

Golgi fragmentation in SOD-ALS mice does not depend on apoptotic pathways

There is substantial evidence of early activation of apoptotic pathways in SOD1-ALS mice (Pasinelli et al., 2000; Guegan et al., 2001), and accordingly complete blockade of the mitochondrial apoptotic pathway through deletion of both BAX and BAK attenuated motor neuron loss and extended survival in high copy (fast) G1 mice (Reyes et al., 2010). Analysis of archival paraffin spinal cord sections from 90 weeks old G1 BAX-BAK double KO mice from this study (Reyes et al., 2010) revealed that these mice still show Golgi fragmentation (Fig. 5.4A-C), indicating that Golgi fragmentation in G1 mice is not dot downstream of mitochondrial apoptotic pathway's.

Golgi fragmentation in apoptosis may depend on caspase 3 mediated cleavage of several membrane tethering factors involved in the structural organization of the Golgi, in particular GRASP65 and p115 (Hicks and Machamer, 2005; Aslan and Thomas, 2009; Ramirez and Lowe, 2009). We therefore examined whether motor neurons with Golgi fragmentation show reduced expression of these proteins. However, there was no evidence for a relative reduction of GRASP65 (not shown) or p115 (Fig. 5.4D) expression in Golgi fragmented motor neurons. Together the data suggest no major role of apoptotic pathways in triggering Golgi fragmentation in SOD1-ALS mice.

Golgi fragmentation is facilitated in SOD1-ALS mice with reduced dynein/dynactin function

Fragmentation and dispersion of the Golgi apparatus is a well established consequence of inhibition of the dynein/dynactin microtubule motor complex (Burkhardt et al., 1997; Harada et al., 1998; Hoogenraad et al., 2001). Accordingly, we showed that impairment of dynein function via overexpression of the N-terminus of Bicaudal D2 (BICD2-N) causes Golgi fragmentation in cultured neurons and *in vivo* in motor neurons of transgenic BICD2-N mice (Teuling et al., 2008). Here we have analyzed the occurrence of Golgi fragmentation in double transgenic G1del/BICD2-N mice resulting from crossing of G1del mice with BICD2-N mice from the BN1 line. Of note, BN1 mice show expression of the BICD2-N transgene in 50-60% of the motor neurons, and show Golgi fragmentation only in a small proportion (1-15% depending on the age) of transgenic motor neurons (Teuling et al., 2008). Significantly, nearly 70% of BICD2-N-expressing motor neurons showed Golgi fragmentation in G1del/BN1 mice (Fig. 5.5), which is a much larger proportion than in BICD2-N-negative motor neurons in G1del/BN1 mice, in BICD2-N-positive motor neurons in BN1 only mice, and in motor neurons in G1del only mice (Fig. 5.5B). These data indicate that impaired dynein/dynactin function facilitates the process causing Golgi fragmentation in G1del mice or vice versa and suggest that Golgi fragmentation in G1del mice is related to impaired dynein-dynactin dependent trafficking.

Reduced levels of endosomes in cells with Golgi fragmentation

Inhibition of dynein-dynactin function, in addition to Golgi fragmentation also causes redistribution of other organelles, in particular endosomes that in cells with impaired dynein-dynactin function redistribute to the cell periphery (Burkhardt et al., 1997; Harada et al., 1998; Hoogenraad et al., 2001). We therefore studied the distribution of endosomes in motor neurons of BN1 and G1del mice using antibodies against early endosome antigen 1 (EEA1) (Mu et al., 1995) and Rab4 binding protein GRASP-1 (Stinton et al., 2005; Hoogenraad et al., 2010). Strikingly, BICD2-N-expressing motor neurons in BN1 mice rather than a redistribution of endosomes to the cell periphery showed reduced endosomal size and density in both EAA1 and GRASP1 stained sections (Fig. 5.6A-C), indicating that dynein/dynactin inhibition in neurons may cause a reduction rather than redistribution of endosomal compartments. The same was observed in motor neurons with Golgi fragmentation in G1del mice, showing reduced levels of GRASP1 staining that correlated with the severity of Golgi fragmentation (Fig. 5.6D-F). Remarkably, increased levels of GRASP1 staining occurred in inclusions in cell bodies and dendrites (Fig. 5.6G, H). Together the analyses of the endosomal markers indicate a reduction of the endosomal compartment in motor neurons with Golgi fragmentation, as well as the accumulation of endosomal markers in ubiquitinated inclusions.

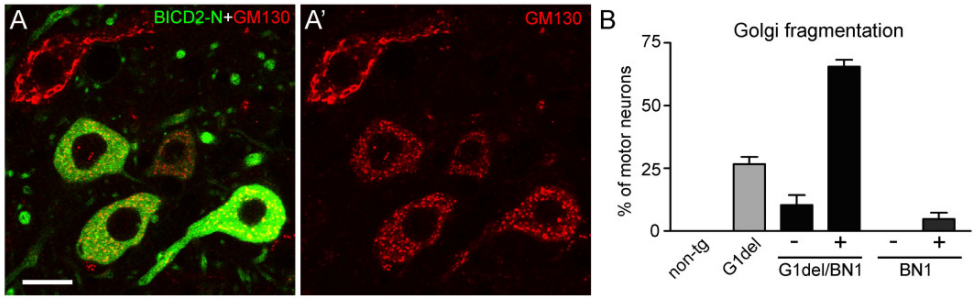

Figure 5.5. Facilitated Golgi fragmentation in mice G1del motor neurons with impaired dynein function
A) Representative confocal image of L4 lumbar motor neurons of a BN1/G1del transgenic mouse of 28 weeks of age. BN1 mice express GFP-BICD2-N in 50-60% of the motor neurons (Teuling et al., 2008). Note Golgi fragmentation in all GFP-BICD2-N neurons and normal Golgi apparatus in the other motor neurons. Bar, 20 µm. B) Bar graph showing the proportion of motor neurons with Golgi fragmentation in G1del, BN1, and G1del/BN1 mice of 28 weeks of age. Note a large proportion of Golgi fragmented motor neurons in GFP-BICD2-N-positive motor neurons of G1del/BN1 mice. GFP-BICD2-N-negative motor neurons of G1del/BN1 mice show a similar percentage of motor neurons with fragmented Golgi as motor neurons in G1del mice.

Discussion

Golgi fragmentation is a well established feature of ALS spinal and cortical motor neurons, that also occurs in some other neurodegenerative conditions, is reproduced in SOD1-ALS mice, and is not found in degenerating motor neuron in a non-ALS disorder (Yaguchi et al., 2003 and non-ALS mouse models [Stieber, 2000 #3592; de Waard et al., 2010). In sporadic ALS patients Golgi fragmentation occurs in all motor neurons with an abnormal TDP-43 distribution suggesting a relationship between Golgi fragmentation and the presence of protein aggregates (Fujita et al., 2008). Accordingly, here we show in SOD1-ALS mice that Golgi fragmentation occurs in all motor neurons with ubiquitinated SOD1 inclusions. However, the majority of motor neurons with Golgi fragmentation did not show such inclusions. This can be explained by the presence of inclusions in dendrites that were not in the plain of the section, or small aggregates that are not detectable at the light microscopic level (Prudencio and Borchelt, 2011). Alternatively, Golgi fragmentation may be caused by a process upstream of large aggregates, perhaps mediated by toxic misfolded or oligomeric SOD1 species (Shaw and Valentine, 2007; Prudencio and Borchelt, 2011). Using antibodies against misfolded and aggregated SOD1 species (USOD and SEDI, (Rakhit et al., 2007 5750 ; Kerman et al., 2010 5749) we did not detect changes that showed a consistent correlation with Golgi fragmentation.

In the present study we also show that motor neurons with Golgi fragmentation more frequently show Golgi apparatus within the proximal dendrite. Despite the limitations of our analysis, in that we only analyzed the dendrites in the transverse plane, the data indicate that the likelihood for a proximal dendrite showing Golgi apparatus is 3-4 times higher in cells with Golgi fragmentation.

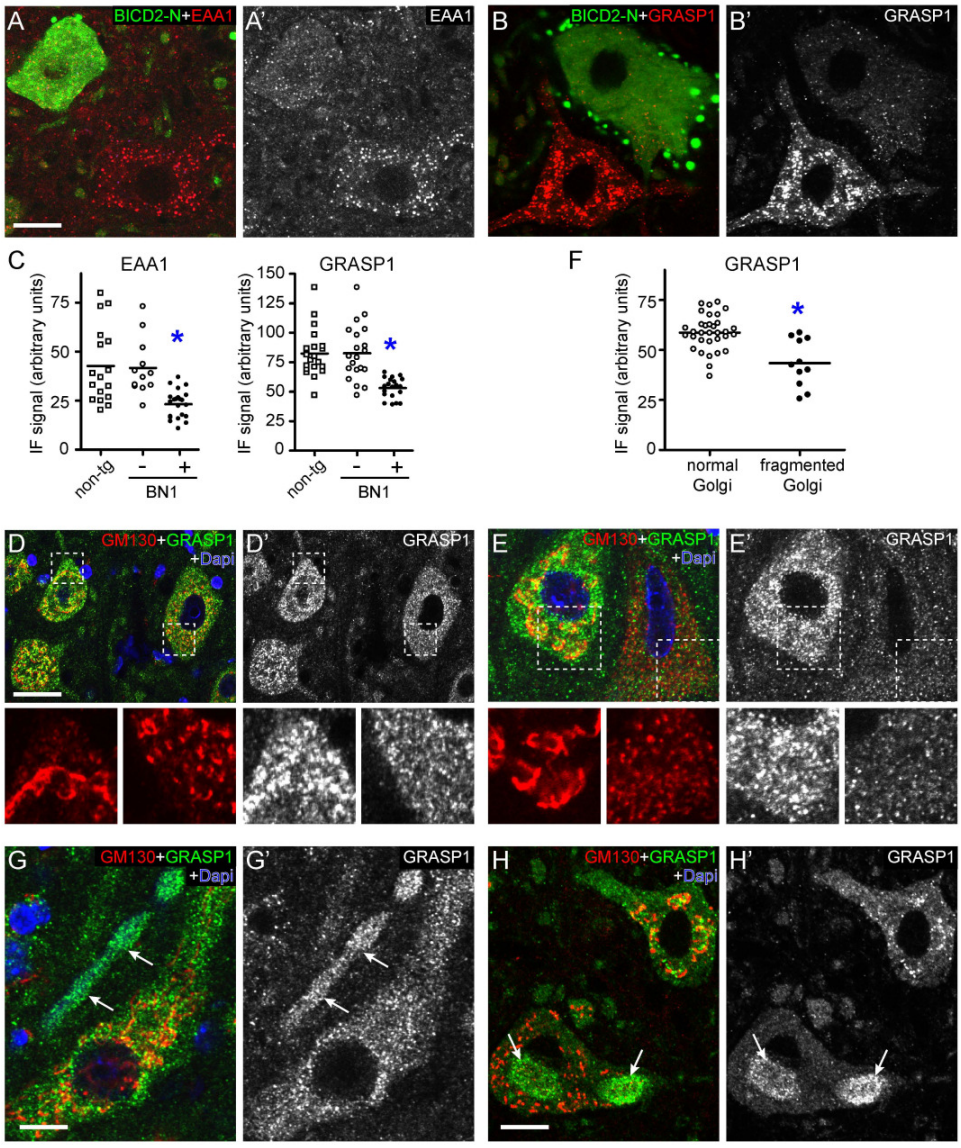

Figure 5.6. Reduced endosome levels in motor neurons with Golgi fragmentation

A, B) Confocal images of staining of the endosomal proteins EEA1 (A) and GRASP1 (B) in lumbar spinal cord sections of a BN1 transgenic mouse. Note reduced EAA1 and GRASP1 labeling in GFP-BICD2-N positive neurons. C) Analysis of fluorescent intensities of GFP-BICD2-N positive versus negative motor neurons showed reduced mean intensities in GFP-BICD2-N positive motor neurons ($P < 0.05$, unpaired Student's t-test negative versus positive neurons). Note that all values were collected from non-transgenic (n=2 mice) and BN1 (n=4) lumbar spinal cord specimen embedded in a single gelatin block and processed in the same immunorun (see material and methods).

D-F) Representative images (D, E) and quantitation (F) of GRASP1-labeling in motor neurons with normal and fragmented Golgi showing reduced GRASP1 labeling in motor neurons with fragmented Golgi ($P < 0.05$, unpaired Student's t-test, normal versus fragmented Golgi).

G, H) Confocal images of GM130 and GRASP1 double labeling showing increased GRASP1 staining in dendritic (arrows in G) and somato-dendritic (arrows in H).

Bars, 10 µm.

Data from hippocampal neurons indicate that the Golgi apparatus orients toward the longest dendrite, and that the presence of the Golgi apparatus and Golgi outposts (*i.e.* discrete compartments that are discontinuous with somatic Golgi) into dendrites relates to local secretory demands (Pierce et al., 2001; Horton et al., 2005; Sengupta and Linstedt, 2011). Thus the increased presence of Golgi apparatus in dendrites and perhaps also Golgi fragmentation may reflect may reflect a reorganization of the secretory pathway in response to increased secretory demands from specific dendrites, *e.g.* to repair dendritic damage.
Several findings suggest that Golgi fragmentation in SOD1-ALS motor neurons is associated with reorganized or aberrant trafficking: First, fragmentation into ministacks is reminiscent of Golgi fragmentation resulting from impaired dynein-dependent transport (Gonatas et al., 2006; Teuling et al., 2008). Second, a subset of neurons with Golgi fragmentation, in spite of their ability of taking up, retrogradely transport, and redistribute the CTB throughout the somatodendritic compartment, do not show accumulation of CTB in the trans-Golgi, suggestive of impaired endosome to Golgi retrograde trafficking. Third, we show a large increase in Golgi fragmentation in G1del mouse crossed with a mouse model showing impaired dynein/dynactin dependent transport, indicative of a synergistic interaction between the process causing Golgi fragmentation and dynein-dynactin dependent trafficking. Fourth, we show that motor neurons with Golgi fragmentation like motor neurons with impaired dynein/dynactin function show reduced expression of endosomal markers. Of note, the endosomal changes that we observed in motor neurons with impaired dynein/dynactin function are different from those observed in cultured non-neuronal cells with radially oriented microtubules. The differences between neurons and other cells may follow from differences in microtubule organization as well as differences in endosomal functional pathways (Soldati and Schliwa, 2006; Schmidt and Haucke, 2007).
Another finding of this study is the enrichment of the endosomal marker GRASP1 in somatodendritic inclusions. The presence of endosomal marker in the inclusions is compatible with the presence of a large amount of vesicular structures in inclusions as identified by electron microscopy (Jaarsma et al., 2008; Teuling et al., 2008). Thus a possible scenario suggested by our data is that one or more endosomal compartments are trapped in ubiquitinated SOD1 inclusions, which subsequently could impeding recycling of specific membrane compartments to the Golgi apparatus and hence trigger fragmentation.
Previous data from BICD2-N transgenic mice suggested Golgi fragmentation is not necessarily detrimental. Furthermore, we showed that G1del mice crossed with BICD2-N transgenic mice show increased life span, which combined with the finding of the present study that these mice show increased levels of Golgi fragmentation, indicates that Golgi fragmentation is not detrimental.

Together our data indicate that Golgi fragmentation reflect an early reorganization of the secretory pathway represents in response to early damage or endosomal abnormalities.
Multiple pathological events have been identified in SOD1-ALS mice models, including mitochondrial abnormalities, ER stress, proteotoxic stress, abnormal ion and glutamate homeostasis, abnormal axonal transport, axonal degeneration, and non-cell autonomous toxic events mediated by glial cells, but the relationship between these events, and the extent to which they occur in SOD1-ALS and other ALS patients remains to be established

(Ilieva et al., 2009). Golgi fragmentation is a well established feature of ALS motor neurons. In the present study we confirm that Golgi fragmentation is a very early event that precedes ATF3 induction and degeneration of the distal axon, and occurs independently of the activation of apoptosis pathways. Thus the data for instance challenge the notion that ALS primarily is a dying back axonopathy as suggested by some studies (Frey et al., 2000; Fischer et al., 2004; Hegedus et al., 2008). We propose that Golgi fragmentation is an early response to deleterious mechanism shared by several ALS forms. Further identification of the mechanisms up stream of Golgi fragmentation may therefore provide important insights in ALS pathogenesis.

Acknowledgements

This work is supported by Prinses Beatrix Fonds and Hersenstichting Nederland grants to C.C.H and D.J.

References

Acevedo-Arozena A, Kalmar B, Essa S, Ricketts T, Joyce P, Kent R, Rowe C, Parker A, Gray A, Hafezparast M, Thorpe JR, Greensmith L, Fisher EM (2011) A comprehensive assessment of the SOD1G93A low-copy transgenic mouse, which models human amyotrophic lateral sclerosis. Dis Model Mech.

Aslan JE, Thomas G (2009) Death by committee: organellar trafficking and communication in apoptosis. Traffic (Copenhagen, Denmark) 10:1390-1404.

Burkhardt JK, Echeverri CJ, Nilsson T, Vallee RB (1997) Overexpression of the dynamitin (p50) subunit of the dynactin complex disrupts dynein-dependent maintenance of membrane organelle distribution. J Cell Biol 139:469-484.

Caldero J, Casanovas A, Sorribas A, Esquerda JE (1992) Calcitonin gene-related peptide in rat spinal cord motoneurons: subcellular distribution and changes induced by axotomy. Neuroscience 48:449-461.

De Matteis MA, D'Angelo G (2007) The role of the phosphoinositides at the Golgi complex. Biochem Soc Symp:107-116.

De Vos KJ, Grierson AJ, Ackerley S, Miller CC (2008) Role of axonal transport in neurodegenerative diseases. Annu Rev Neurosci 31:151-173.

de Waard MC, van der Pluijm I, Zuiderveen Borgesius N, Comley LH, Haasdijk ED, Rijksen Y, Ridwan Y, Zondag G, Hoeijmakers JH, Elgersma Y, Gillingwater TH, Jaarsma D (2010) Age-related motor neuron degeneration in DNA repair-deficient Ercc1 mice. Acta Neuropath 120:461-475.

Fischer LR, Culver DG, Tennant P, Davis AA, Wang M, Castellano-Sanchez A, Khan J, Polak MA, Glass JD (2004) Amyotrophic lateral sclerosis is a distal axonopathy: evidence in mice and man. Exp Neurol 185:232-240.

Frey D, Schneider C, Xu L, Borg J, Spooren W, Caroni P (2000) Early and selective loss of neuromuscular synapse subtypes with low sprouting competence in motoneuron diseases. J Neurosci 20:2534-2542.

Fujita Y, Okamoto K (2005) Golgi apparatus of the motor neurons in patients with amyotrophic lateral sclerosis and in mice models of amyotrophic lateral sclerosis. Neuropathol 25:388-394.

Fujita Y, Mizuno Y, Takatama M, Okamoto K (2008) Anterior horn cells with abnormal TDP-43 immunoreactivities show fragmentation of the Golgi apparatus in ALS. J Neurol Sci 269:30-34.

Fujita Y, Ohama E, Takatama M, Al-Sarraj S, Okamoto K (2006) Fragmentation of Golgi apparatus of nigral neurons with alpha-synuclein-positive inclusions in patients with Parkinson's disease. Acta Neuropath 112:261-265.

Gardiol A, Racca C, Triller A (1999) Dendritic and postsynaptic protein synthetic machinery. J Neurosci 19:168-179.

Gonatas NK, Stieber A, Gonatas JO (2006) Fragmentation of the Golgi apparatus in neurodegenerative diseases and cell death. J Neurol Sci 246:21-30.

Gonatas NK, Stieber A, Mourelatos Z, Chen Y, Gonatas JO, Appel SH, Hays AP, Hickey WF, Hauw JJ (1992) Fragmentation of the Golgi apparatus of motor neurons in amyotrophic lateral sclerosis. Am J Pathol 140:731-737.

Goud B, Gleeson PA (2010) TGN golgins, Rabs and cytoskeleton: regulating the Golgi trafficking highways. Trends Cell Biol 20:329-336.

Guegan C, Vila M, Rosoklija G, Hays AP, Przedborski S (2001) Recruitment of the mitochondrial-dependent apoptotic pathway in amyotrophic lateral sclerosis. J Neurosci 21:6569-6576.

Gurney ME (1997) The use of transgenic mouse models of amyotrophic lateral sclerosis in preclinical drug studies. J Neurol Sci 152:S67-S73.

Hafezparast M et al. (2003) Mutations in dynein link motor neuron degeneration to defects in retrograde transport. Science 300:808-812.

Harada A, Takei Y, Kanai Y, Tanaka Y, Nonaka S, Hirokawa N (1998) Golgi vesiculation and lysosome dispersion in cells lacking cytoplasmic dynein. J Cell Biol 141:51-59.

Harris H, Rubinsztein DC (2012) Control of autophagy as a therapy for neurodegenerative disease. Nat Rev Neurol 8:108-117.

Hegedus J, Putman CT, Tyreman N, Gordon T (2008) Preferential motor unit loss in the SOD1 G93A transgenic mouse model of amyotrophic lateral sclerosis. J Physiol 586:3337-3351.

Hicks SW, Machamer CE (2005) Golgi structure in stress sensing and apoptosis. Biochim Biophysica Acta 1744:406-414.

Hoogenraad CC, Akhmanova A, Howell SA, Dortland BR, De Zeeuw CI, Willemsen R, Visser P, Grosveld F, Galjart N (2001) Mammalian Golgi-associated Bicaudal-D2 functions in the dynein-dynactin pathway by interacting with these complexes. EMBO 20:4041-4054.

Hoogenraad CC, Popa I, Futai K, Sanchez-Martinez E, Wulf PS, van Vlijmen T, Dortland BR, Oorschot V, Govers R, Monti M, Heck AJ, Sheng M, Klumperman J, Rehmann H, Jaarsma D, Kapitein LC, van der Sluijs P (2010) Neuron specific Rab4 effector GRASP-1 coordinates membrane specialization and maturation of recycling endosomes. PLoS Biol 8:e1000283.

Horton AC, Racz B, Monson EE, Lin AL, Weinberg RJ, Ehlers MD (2005) Polarized secretory trafficking directs cargo for asymmetric dendrite growth and morphogenesis. Neuron 48:757-771.

Hossaini M, Cano SC, van Dis V, Haasdijk ED, Hoogenraad CC, Holstege JC, Jaarsma D (2011) Spinal Inhibitory Interneuron Pathology Follows Motor Neuron Degeneration Independent of Glial Mutant Superoxide Dismutase 1 Expression in SOD1-ALS Mice. J Neuropathol Exp Neurol 70:662-677.

Ilieva H, Polymenidou M, Cleveland DW (2009) Non-cell autonomous toxicity in neurodegenerative disorders: ALS and beyond. J Cell Biol 187:761-772.

Ito H, Nakamura M, Komure O, Ayaki T, Wate R, Maruyama H, Nakamura Y, Fujita K, Kaneko S, Okamoto Y, Ihara M, Konishi T, Ogasawara K, Hirano A, Kusaka H, Kaji R, Takahashi R, Kawakami H (2011) Clinicopathologic study on an ALS family with a heterozygous E478G optineurin mutation. Acta Neuropathol 122: 223-229.

Jaarsma D, Teuling E, Haasdijk ED, De Zeeuw CI, Hoogenraad CC (2008) Neuron-specific expression of mutant superoxide dismutase is sufficient to induce amyotrophic lateral sclerosis in transgenic mice. J Neurosci 28:2075-2088.

Jaarsma D, Rognoni F, Van Duijn W, Verspaget H, Haasdijk ED, Holstege JC (2001) CuZn superoxide dismutase (SOD1) accumulate in vacuolated mitochondria in transgenic mice expressing amyotrophic lateral sclerosis (ALS)-linked SOD1 mutations. Acta Neuropathol 102:293-305.

Kerman A, Liu HN, Croul S, Bilbao J, Rogaeva E, Zinman L, Robertson J, Chakrabartty A (2010) Amyotrophic lateral sclerosis is a non-amyloid disease in which extensive misfolding of SOD1 is unique to the familial form. Acta Neuropathol 119:335-344.

Lane JD, Lucocq J, Pryde J, Barr FA, Woodman PG, Allan VJ, Lowe M (2002) Caspase-mediated cleavage of the stacking protein GRASP65 is required for Golgi fragmentation during apoptosis. J Cell Biol 156:495-509.

Mironov AA, Beznoussenko GV (2011) Molecular mechanisms responsible for formation of Golgi ribbon. Histol Histopathol 26:117-133.

Mourelatos Z, Gonatas NK, Stieber A, Gurney ME, Dal Canto MC (1996) The Golgi apparatus of spinal cord motor neurons in transgenic mice expressing mutant Cu,Zn superoxide dismutase becomes fragmented in early, preclinical stages of the disease. PNAS (USA) 93:5472-5477.

Mu FT, Callaghan JM, Steele-Mortimer O, Stenmark H, Parton RG, Campbell PL, McCluskey J, Yeo JP, Tock EP, Toh BH (1995) EEA1, an early endosome-associated protein. EEA1 is a conserved alpha-helical peripheral membrane protein flanked by cysteine "fingers" and contains a calmodulin-binding IQ motif. J Biol Chem 270:13503-13511.

Nakagomi S, Barsoum MJ, Bossy-Wetzel E, Sutterlin C, Malhotra V, Lipton SA (2008) A Golgi fragmentation pathway in neurodegeneration. Neurobiol Dis 29:221-231.

Nakamura N, Rabouille C, Watson R, Nilsson T, Hui N, Slusarewicz P, Kreis TE, Warren G (1995) Characterization of a cis-Golgi matrix protein, GM130. The J Cell Biol 131:1715-1726.

Nassif M, Matus S, Castillo K, Hetz C (2010) Amyotrophic lateral sclerosis pathogenesis: a journey through the secretory pathway. Antioxidants & redox signaling 13:1955-1989.

Ngo M, Ridgway ND (2009) Oxysterol binding protein-related Protein 9 (ORP9) is a cholesterol transfer protein that regulates Golgi structure and function. Mol Biol Cell 20:1388-1399.

Pasinelli P, Houseweart MK, Brown RH, Jr., Cleveland DW (2000) Caspase-1 and -3 are sequentially activated in motor neuron death in Cu,Zn superoxide dismutase-mediated familial amyotrophic lateral sclerosis. PNAS (USA) 97:13901-13906.

Pierce JP, Mayer T, McCarthy JB (2001) Evidence for a satellite secretory pathway in neuronal dendritic spines. Curr Biol 11:351-355.

Polishchuk RS, Mironov AA (2004) Structural aspects of Golgi function. Cell Mol Life Sci 61:146-158.

Prudencio M, Borchelt DR (2011) Superoxide dismutase 1 encoding mutations linked to ALS adopts a spectrum of misfolded states. Mol Neurodegener 6:77.

Ragnarson B, Ornung G, Ottersen OP, Grant G, Ulfhake B (1998) Ultrastructural detection of neuronally transported choleragenoid by postembedding immunocytochemistry in freeze-substituted Lowicryl HM20 embedded tissue. J Neurosci Methods 80:129-136.

Rakhit R, Robertson J, Vande Velde C, Horne P, Ruth DM, Griffin J, Cleveland DW, Cashman NR, Chakrabartty A (2007) An immunological epitope selective for pathological monomer-misfolded SOD1 in ALS. Nat Med 13:754-759.

Ramirez IB, Lowe M (2009) Golgins and GRASPs: holding the Golgi together. Sem Cell Dev Biol 20:770-779.

Reyes NA, Fisher JK, Austgen K, VandenBerg S, Huang EJ, Oakes SA (2010) Blocking the mitochondrial apoptotic pathway preserves motor neuron viability and function in a mouse model of amyotrophic lateral sclerosis. J Cli Invest 120:3673-3679.

Sakurai A, Okamoto K, Fujita Y, Nakazato Y, Wakabayashi K, Takahashi H, Gonatas NK (2000) Fragmentation of the Golgi apparatus of the ballooned neurons in patients with corticobasal degeneration and Creutzfeldt-Jakob disease. Acta Neuropathol 100:270-274.

Saxena S, Caroni P (2011) Selective neuronal vulnerability in neurodegenerative diseases: from stressor thresholds to degeneration. Neuron 71:35-48.

Saxena S, Cabuy E, Caroni P (2009) A role for motoneuron subtype-selective ER stress in disease manifestations of FALS mice. Nat Neurosci 12:627-636.

Schmidt MR, Haucke V (2007) Recycling endosomes in neuronal membrane traffic. Biol Cell 99:333-342.

Schon EA, Przedborski S (2011) Mitochondria: the next (neurode)generation. Neuron 70:1033-1053.

Sengupta D, Linstedt AD (2011) Control of organelle size: the Golgi complex. Annu Review Cell Dev Biol 27:57-77.

Shaw BF, Valentine JS (2007) How do ALS-associated mutations in superoxide dismutase 1 promote aggregation of the protein? Trends Biochem Sci 32:78-85.

Soldati T, Schliwa M (2006) Powering membrane traffic in endocytosis and recycling. Nat Rev Mol Cell Biol 7:897-908.

Stieber A, Mourelatos Z, Gonatas NK (1996) In Alzheimer's disease the Golgi apparatus of a population of neurons without neurofibrillary tangles is fragmented and atrophic. Am J Pathol 148:415-426.

Stieber A, Gonatas JO, Collard J, Meier J, Julien J, Schweitzer P, Gonatas NK (2000) The neuronal Golgi apparatus is fragmented in transgenic mice expressing a mutant human SOD1, but not in mice expressing the human NF-H gene. J Neurol Sci 173:63-72.

Stinton LM, Selak S, Fritzler MJ (2005) Identification of GRASP-1 as a novel 97 kDa autoantigen localized to endosomes. Clin Immunol 116:108-117.

Teuling E, van Dis V, Wulf PS, Haasdijk ED, Akhmanova A, Hoogenraad CC, Jaarsma D (2008) A novel mouse model with impaired dynein/dynactin function develops amyotrophic lateral sclerosis (ALS)-like features in motor neurons and improves lifespan in SOD1-ALS mice. Hum Mol Gen 17:2849-2862.

Vlug AS, Teuling E, Haasdijk ED, French P, Hoogenraad CC, Jaarsma D (2005) ATF3 expression precedes death of spinal motoneurons in amyotrophic lateral sclerosis-SOD1 transgenic mice and correlates with c-Jun phosphorylation, CHOP expression, somato-dendritic ubiquitination and Golgi fragmentation. Eur J Neurosci 22:1881-1894.

Wan XC, Trojanowski JQ, Gonatas JO (1982) Cholera toxin and wheat germ agglutinin conjugates as neuroanatomical probes: their uptake and clearance, transganglionic and retrograde transport and sensitivity. Brain Res 243:215-224.

Xiang Y, Wang Y (2011) New components of the Golgi matrix. Cell Tissue Res 344:365-379.

Yaguchi M, Hashizume Y, Yoshida M, N KG, Okamoto K (2003) Reduction of the size of the Golgi apparatus of spinal anterior horn cells in patients with X-linked spinal and bulbar muscular atrophy. Amyotroph Lateral Scler Other Motor Neuron Disord 4:17-21.

Chapter 6

Amyotrophic lateral sclerosis (ALS)-associated VAPB-P56S inclusions represent a reversible ER quality control compartment in motor neurons

Vera van Dis[1], Marijn Kuijpers[1,2], Elize D. Haasdijk[1], Wiep Scheper[3,4], Casper C. Hoogenraad[1,2], Dick Jaarsma[1#]

[1]Department of Neuroscience, Erasmus Medical Center, Rotterdam, The Netherlands. [2]Cell Biology, Faculty of Science, Utrecht University, Utrecht, The Netherlands, [3]Department of Genome Analysis, Academic Medical Center, University of Amsterdam, The Netherlands, [4]Department of Neurology, Academic Medical Center, University of Amsterdam, The Netherlands

Abstract

The P56S mutant form of vesicle-associated membrane protein (VAMP)-associated protein B (VAPB) is associated with motor neuron disorder amyotrophic lateral sclerosis type 8 (ALS8). VAPB-P56S proteins aggregate and form multiple inclusions in cellular and invertebrate model systems. To examine the role of VAPB inclusions in motor neurons and their significance in ALS pathogenesis, we generated transgenic mice expressing human VAPB-P56S under the control of the Thy1.2 neuron-specific promoter. In three independent transgenic lines VAPB-P56S accumulates into intracellular inclusions consisting of smooth ER-like tubular profiles. The inclusions are observed in young motor neurons, their number and size is unaffected by aging and does not correlate with signs of axonal and neuronal degeneration, while axotomy causes their gradual disappearance within 1-2 weeks. The VAPB-P56S inclusions are strongly immunoreactive for ubiquitinated epitopes and factors that operate in the ER associated degradation (ERAD) pathway, including Derlin-1 and p97/VCP. Inhibition of the proteasome and knockdown of the ER membrane chaperone Bap31 increased the size of mutant VAPB inclusions in cultured primary neurons. Mutant forms of seipin that also cause ER-derived inclusions partially codistribute with VAPB-P56S inclusions. Together the data indicate that the VAPB-P56S inclusions represent a reversible ER quality control compartment that is formed when the amount of mutant VAPB exceeds the capacity of the ERAD pathway in motor neurons.

Introduction

Protein aggregation is a central feature of many neurodegenerative disorders, including Alzheimer's disease and other dementias, Parkinson's disease, Huntington's disease and amyotrophic lateral sclerosis (ALS). The events triggering protein aggregation can be mutations increasing the aggregation propensity of proteins, increased expression of aggregation-prone proteins (*e.g.* gene duplication), aberrant post-translation modifications (oxidative modifications, aberrant phosphorylation), failure of the protein quality control machinery, or combinations of these factors (Chiti and Dobson, 2006; Rubinsztein, 2006; Aguzzi and O'Connor, 2010; Buchberger et al., 2010; *GAD*ad et al., 2011). In multiple disorders aggregating proteins accumulate into discrete micrometer-scale structures that are termed inclusions, inclusion bodies, aggregates or have disease or morphology specific names (*e.g.* Lewy bodies, Pick bodies, neurofibrilary tangles). Not only the protein composition, but also the morphologies, as well as (sub) cellular and regional distributions of inclusions can be correlated to specific disorders and subtypes of disorders (Skovronsky et al., 2006; Cohen et al., 2011; Hart et al., 2012). Depending on the type of disorder and inclusion, inclusions may be either neuroprotective, neutral or detrimental structures (Kaganovich et al., 2008; Tyedmers et al., 2010).

A peculiar inclusion, ultrastructurally characterized by the presence of membranous profiles continuous with the ER, occurs in cellular and invertebrate models of a rare familial amyotrophic lateral sclerosis (ALS)-like disorder designated ALS8 (Teuling et al., 2007; Tsuda et al., 2008; Fasana et al., 2010; Papiani et al., 2012). ALS8 is caused by mutations in VAPB (Nishimura et al., 2004; Chen et al., 2010 6767; Funke et al., 2010; Millecamps et al., 2010), a small tail-anchored ER membrane protein that is member of a highly conserved VAP (VAMP/synaptobrevin-associated proteins) family of proteins. VAP proteins are characterized by an N-terminal MSP (major sperm protein) domain, a coiled-coil motif, and a C-terminal transmembrane region, and in mammals consists of two genes, VAPA and VAPB, yielding at least three gene products VAPC being a splice variant of VAPB lacking the C-terminal transmembrane domain (Nishimura et al., 1999; Lev et al., 2008; Nachreiner et al., 2010). The MSP domain (named after C. elegans MSPs) contains a binding site for the FFAT (diphenylalanine [FF] in an acidic tract) or FFAT-like motifs that are present in a variety of proteins in particular lipid transfer proteins (Loewen and Levine, 2005; Mikitova and Levine, 2012). In addition the MSP domain may function as a secreted ligand after cleavage from the transmembrane domain (Han et al., 2012). VAPs have been implicated in diverse processes, including non-vesicular transfer of lipids and membrane trafficking (Loewen and Levine, 2005; Kawano et al., 2006; Perry and Ridgway, 2006; Peretti et al., 2008), ER-organelle and cytoskeleton interaction (Amarilio et al., 2005; Rocha et al., 2009), neurite extension [Saita, 2009; De Vos et al., 2011; Stefan et al., 2011), ER stress (Kanekura et al., 2006; Gkogkas et al., 2008; Suzuki et al., 2009), and (at least in invertebrates) homeostatic and signaling functions at the neuromuscular synapse (Pennetta et al., 2002; Chai et al., 2008; Ratnaparkhi et al., 2008; Han et al., 2012).

To date, two mutations, P56S (Nishimura et al., 2004; Funke et al., 2010; Millecamps et al., 2010) and T46I (Chen et al., 2010) both localized in the MSP domain have been associated

with an ALS-like motor neuron disorder in man. The mutations do not perturb post-translational insertion into ER membrane (Fasana et al., 2010), but disrupt FFAT-motif binding and cause rapid oligomerization and aggregation of mutant VAPB, resulting in multiple dot-like inclusions (Nishimura et al., 2004; Kanekura et al., 2006; Teuling et al., 2007; Kim et al., 2010; Papiani et al., 2012). The presence of wild-type VAPB in the inclusions and data from mutant invertebrates indicate that VAPB-P56S may act in a dominant negative way by recruiting wild-type VAPB into aggregates (Pennetta et al., 2002; Teuling et al., 2007; Chai et al., 2008; Ratnaparkhi et al., 2008; Han et al., 2012). In addition, mutant VAPB aggregates may disrupt normal ER structure and function (Teuling et al., 2007; Chen et al., 2010; Papiani et al., 2012; Tran et al., 2012); or interfere with ER protein quality control systems (Kanekura et al., 2006; Moumen et al., 2011).

In this study we generated and characterized P56S-mutant VAPB transgenic mice to examine the effect of long-term expression motor neurons in motor neurons *in vivo*, in a mammalian model. The main finding of our study is that mutant VAPB inclusions that occur in motor neurons of our transgenic mice are non-toxic structures and represent an ER quality control compartment that is formed when the amount of substrate exceeds the capacity of the ERAD pathway of the cell.

Materials and Methods

Transgenic mice

Animals were housed and handled in accordance with the "Principles of laboratory animal care" (NIH publication No. 86-23) and the guidelines approved by the Erasmus University animal care committee

Transgenic VAPB mice were generated using the cDNAs of wild-type or P56S-mutant human VAPB were cloned into the Thy1.2-expression module. The VAPB-constructs also contain an HA-tag to enable easy visualization of transgenic VAPB by immunocytochemical approaches. Experiments in transfected cells have shown that the HA-tag does not alter the biochemical characteristics of wild-type and mutant VAPB.

A selected group of all transgenic lines was allowed to age for 2 years. The mice were weighed and inspected for signs of muscle weakness once per to weeks using a set of simple tests: mice were examined for their ability to extend their hindlimbs when suspended in the air by their tail and their ability to hang upside down on a grid for 60 s (Jaarsma et al., 2008). In addition, at specific ages animals were subjected to an accelerating rotarod test as described (van Woerden et al., 2007). The mice were killed when they developed motor problems or when they reached 2 years of age. Mice developing tumors were excluded from the study. Selected mice were analyzed for neuromuscular denervation and pathological abnormalities in the spinal cord (e.g motor neuron loss, gliosis).

Axotomy of the sciatic nerve

Six week old VM1 mice and their non-transgenic littermates were anesthetized and the sciatic nerve was exposed. Than bound with suture and cut at mid thigh level. After

various intervals mice were perfused transcardially with 4% paraformaldehyde and processed for immunocytochemistry. 8 weeks old BN1 and non-transgenic animals were anaesthetized, the sciatic nerve was exposed, bound with suture and cut just above the division of the sciatic nerve into the tibial and common peroneal nerves. A 2 mm-piece of the nerve was removed. Animals were left to recover for 12 or 24 hours. Following transection, animals were perfused transcardially with 4% paraformaldehyde and processed for immunohistochemistry as described before with antibodies against ATF3.

Primary neuron cultures and transfection

Primary hippocampal cultures were prepared from embryonic day 18 (E18) rat brains (Hoogenraad et al., 2010). Cells were plated on coverslips coated with poly-L- lysine (30 μg/ml) and laminin (2 μg/ml) at a density of 75,000/well. Hippocampal cultures were grown in Neurobasal medium (NB) supplemented with B27, 0.5 mM glutamine, 12.5 μM glutamate and penicillin/streptomycin. Hippocampal neurons were transfected using Lipofectamine 2000 (Invitrogen). The following mammalian expression constructs and shRNA were used: HA- and myc-tagged VAPB-wt and VAPB-P56S constructs (Teuling et al., 2007); myc-tagged seipin-wt, seipin-N88S and seipin-S90L constructs (Ito et al., 2012); and BAP31 shRNA construct (Wang et al., 2008). DNA (3.6 μg /well) was mixed with 3 μl of Lipofectamine 2000 in 200 μl of NB, incubated for 30 min, and then added to the neurons in NB at 37°C in 5% CO2 for 45 min. Next, neurons were washed with NB and transferred in the original medium at 37°C in 5% CO2. After 2-4 days of transfection, neurons were fixed with 4% paraformaldehyde/4% sucrose in PBS, washed three times in PBS for 10 min and incubated with the indicated primary antibodies in GDB buffer (0.2% BSA, 0.8 M NaCl, 0.5% Triton X-100, 30 mM phosphate buffer, pH 7.4) overnight at 4°C. Neurons were then washed three times in PBS for 30 min and incubated with secondary antibodies in GDB for 1hr at room temperature and washed three times in PBS for 30 min. Slides were mounted using Vectashield mounting medium (Vector laboratories). Images for co-localization measurements were acquired using a Nikon microscope equipped with a 100x oil objectives. Confocal images were acquired using a LSM510 confocal microscope (Zeiss) with 40× or 63× oil objectives.

Antibodies

Primary antibodies reported in this study are: mouse anti-actin (1:5000; Millipore, Temecula, CA), rabbit anti-ATF3 (Santa Cruz; IHC and IF 1:1000), rabbit anti-Bap31 rabbit (from M. Tagaya; Tokyo University of Pharmacy and Life Sciences (Wakana et al., 2008)), rabbit anti-BiP/GRP78 (1:500; Stressgen Biotechnologies, San Diego, CA), rabbit anti-calreticulin (1:1000; Affinity BioReagents), goat-anti-choline acetyltransferase (ChAT, Chemicon, IF 1:500), rabbit-anti-CGRP (Calbiochem, IF 1:10.000), rabbit anti-Derlin-1 (D4443, Sigma-Aldrich, IF 1:1000), rabbit anti-GFAP (DAKO, IF 1:5000), mouse-anti GM130 (BD Biosciences, IF 1:1000), rabbit anti-HA (Santa Cruz), rat anti-HA, mouse anti-HA (1:500; Roche, Indianapolis, IN), rabbit anti KDEL (Stressgen), rabbit anti-myc (1:500; Cell Signaling Technology, Beverly, MA), mouse anti-myc (1:500; Santa Cruz Biotechnology, Santa Cruz, CA), chicken anti-neurofilament M (Millipore), rabbit anti-NIR2, rabbit anti-ORP9 (gift from Neale Ridgway, Dalhousie University, Canada), rabbit

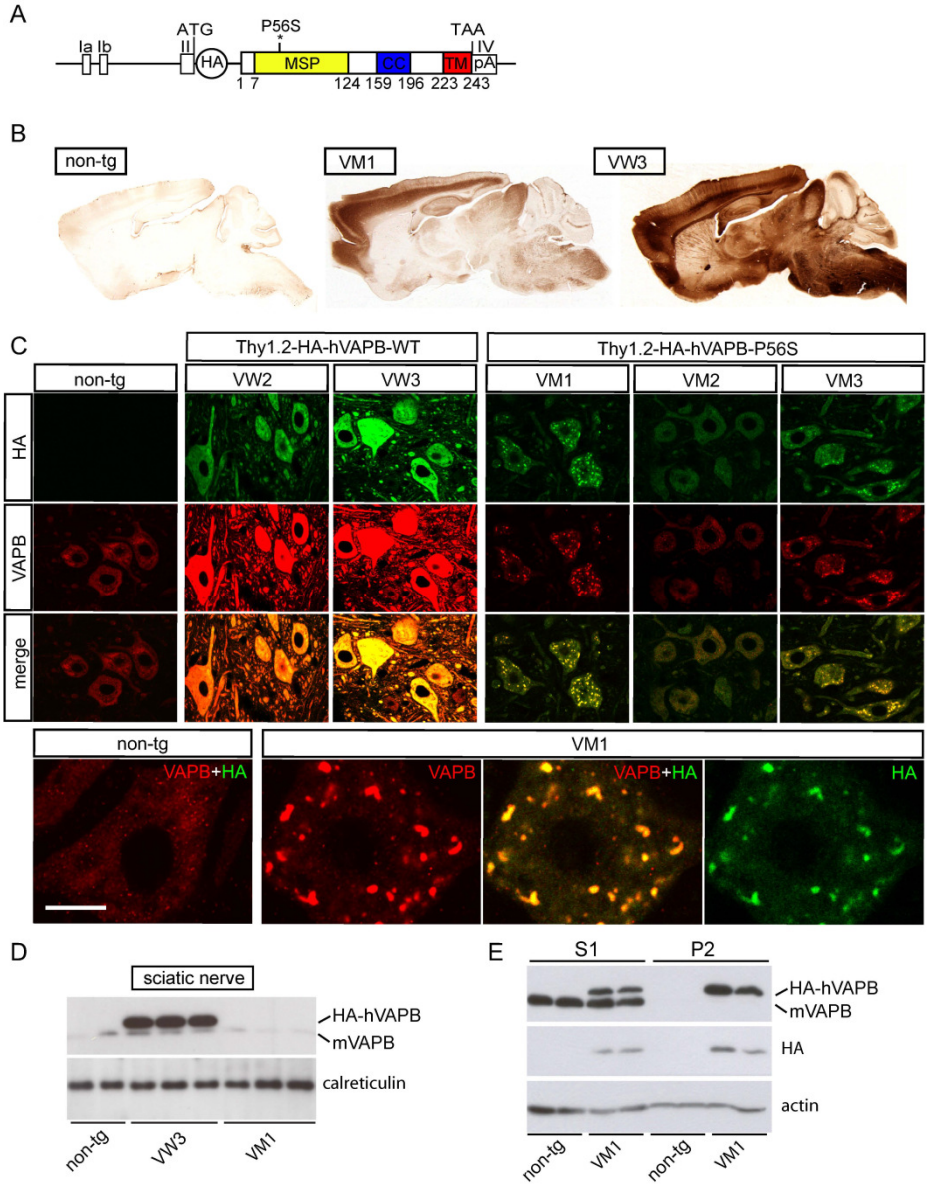

Figure 6.1. VAPB-P56S transgenic mice develop inclusions in motor neurons

A) To generate VAPB transgenic mice the cDNAs of wild-type or P56S-mutant human VAPB coupled to HA were cloned into the Thy1.2-expression casette.

B, C) Pro-nuclear injections yielded 4 Thy1.2-hVAPB-P56S (VM1, VM2, VM3, VM5) and 3 Thy1.2-hVAPB-WT (VW1, VW2, VW3) founders that showed Mendelian transmission of the transgene and widespread transgene expression in the nervous system as identified by anti HA immunohistochemistry (B) and confocal immunofluorescence for HA and VAPB (C). Note that 3 of 4 Thy1.2-hVAPB-P56S lines (VM1, VM3, VM5 [not shown]) develop multiple small spherical intensely HA and VAPB-immunoreactive inclusions in motor neurons. Also note higher HA staining intensities in wild-type compared to mutant lines and the absence of HA staining in non-transgenic mice (B and C). Bar in C, 10 µm.

D) Western blot of sciatic nerve homogenate of wild-type (line VW3) and mutant (line VM1) transgenic mice showing a high level of transgenic VAPB (running in a higher molecular weight band because of the HA-tag) in wild-type VAPB sciatic nerve, and no transgenic VAPB in mutant VAPB sciatic nerve.
E) Western blot of whole homogenates (S1), and Nonidet P40-insoluble fraction (P2) of spinal cord mutant VAPB (line VM1) and non transgenic mice showing the accumulation of mutant VAPB in the P2 fraction.

anti-ORP2, rabbit anti-ORP3, rabbit anti-ORP6 (gift from Vesa Olkkonen, Institute for Molecular Medicine Finland), Man anti-P0, Rabbit anti-phosphoS6 (Cell Signalling), mouse anti ubiquitin (FK2; 1:300; Biomol, Plymouth Meeting, PA), rabbit anti-VAPB variable central domain of VAPB (#1006-02) and the whole cytosolic domain of VAPB (#1006-00), guinea pig anti-VAChT, mouse anti-VCP (Ma3-004; Thermo Scientific; 1:200).
Secondary antibodies: For avidin-biotin-peroxidase immunocytochemistry biotinylated secondary antibodies from Vector Laboratories diluted 1:200 were used. FITC-, Cy3-, and Cy5-conjugated secondary antibodies raised in donkey (Jackson Immunoresearch, USA), Alexa488, 568 or 633 conjugated antibodies raised in goat were used for immunofluorescence. For Western blots, HRP-conjugated goat-anti mouse or goat-anti rabbit IgG were used at 1:5000 (DAKO, 1:5000).

Immunohistochemical and histopathological procedures

For immunocytochemistry and immunofluorescence mice were anaesthetised with pentobarbital and perfused transcardially with 4% paraformaldehyde. The lumbar and cervical spinal cord were carefully dissected out and post-fixed overnight in 4% paraformaldehyde. Routinely, spinal cord tissue was embedded in gelatin blocks, sectioned at 40 µm with a freezing microtome and sections were processed, free floating, employing a standard avidin-biotin-immunoperoxidase complex method (ABC, Vector Laboratories, USA) with diaminobenzidine (0.05%) as the chromogen, or single, double and triple-labelling immunofluorescence (Jaarsma et al., 2008). Immunoperoxidase-stained sections were analyzed and photographed using a Leica DM-RB microscope and a Leica DC300 digital camera. Sections stained for immunofluorescence were mounted on coverslips, placed on glass slides with Vectashield mounting medium, and were examined with Zeiss LSM 510 and LSM 700 confocal laser scanning microscopes.
For analysis of neuromuscular denervation medial gastrocnemius muscle from 4% paraformaldehyde fixed mice were dissected, embedded into gelatin blocks and sectioned at 80µm with a freezing microtome. Sections were immunolabeled, free floating for guinea pig anti-VAChT and chicken-anti-NFM followed by Cy3 anti-goat and Cy5 anti-chicken or anti-rabbit secondaries, and motor endplates were labeled with FITC-bungarotoxin (1:500, Molecular Probes). For quantitative analyses, muscle sections were examined under a Leica DM-RB fluorescence microscope, end-plates being scored as 'innervated' in case of complete overlap between bungarotoxin and VAChT labeling, 'partially denervated' in case of partial overlap, and 'denervated' in case of the absence of VAChT labeling at the end-plate. Per muscle all endplates within three sections were analyzed.

Quantitative analysis of immunofluorescence images

Fluorescent intensities were determined using Metamorph image analysis software. Images were collected using Zeiss LSM 510 confocal laser scanning microscope with 63x Plan apo oil immersion objective. Stacks of 1 µm thick sections were collected from the first 4 µm facing the coverslip, and the optical section 2 µm below the surface was used for density measurements. Material from non-transgenic and transgenic mice always is imbedded in a single gelatin block to minimalize variability in staining intensity resulting from the sectioning and immunostaining procedure. Per mouse, motor neurons from 3 randomly selected L4 sections (yielding 4-12 cells/sections) were measured.

Analyses of sciatic nerves

Sciatic nerves were carefully dissected from perfused mice, post-fixed in 4% paraformaldehyde with 0.2% glutaraldehyde, extensively rinsed in 0.1M PB, post-fixed in 1% osmium, dehydrated, embedded in Durcupan, sectioned transversely at 500 nm with an Ultratome, and stained with toluidine blue.

Electron Microscopy

For electron microscopy, mice were perfused transcardially with 4% paraformaldehyde with 0.2% (post-embedding immunogold electron microscopy) or 1% (standard transmission electron microscopy) glutaraldehyde. Specimens were sectioned with a Vibratome and further processed using standard methods as described before (Jaarsma et al., 2001; Jaarsma et al., 2008). For standard transmission electron microscopy Vibratome sections (60-100 µm thick) were post-fixed in 1% osmium, dehydrated and embedded in Durcupan. Ultrathin sections (50–70 nm) were contrasted with uranyl acetate and lead citrate, and analyzed in a Phillips CM100 electron microscope at 80 kV. Post-embedding immunogold labelling was performed on 50–70 nm thick thin sections from 4% paraformaldefyde and 0.2% glutaraldehyde fixed brain and spinal cord sections as described before (Jaarsma et al., 2008) using the rat-anti-HA antibody at 1:100.

Statistical analyses

Statistical analyzes were performed with MS Excel or Graphpad Prism software (San Diego, USA). Means from different age groups, and different transgenic mouse lines were compared using Student's t-test, or one-way ANOVA and Tukey's post test.

Results

Motor neurons of VAPB-P56S transgenic mice develop VAPB inclusions depending on transgene expression level

Transgenic VAPB mice were generated using a construct of human VAPB cDNA with or without the P56S mutation cloned into the Thy1.2 expression cassette (Fig. 6.1A) that drives transgene expression in neurons throughout the CNS, including spinal motor neurons (Feng et al., 2000; Jaarsma et al., 2008). The transgenes incorporated an HA-tag at the N-terminus to enable the efficient localization of transgenic protein at the light and

ultrastructural level (Kushner et al., 2005). On the basis of Western blot and immunohistochemistry with antibodies against the HA-tag, we selected 4 lines of hVAPB-P56S (VM1, VM2, VM3, VM5) and 3 lines of wild-type (wt)-hVAPB (VW1, VW2, VW3) transgenic mice. All lines showed Mendelian inheritance of the transgene and expression of the transgene in neurons throughout the central nervous system including cortex, hippocampus, cerebellum, brain stem and spinal cord (Fig. 6.1B). Transgene expression levels in motor neurons were considerable higher in wt-hVAPB compared to hVAPB-P56S expressing lines (Fig. 6.1C). Another difference was the presence of a high level transgenic VAPB in axons in wild-type but not mutant lines. The presence of high levels of transgenic VAPB in axons of wild-type transgenic mice was confirmed by Western blot of sciatic nerve homogenates (Fig. 6.1D). In all lines the transgene was expressed in the majority of motor neurons as determined by double-labeling immunofluorescence with antibodies against HA and the motor neuronal marker choline acetyl transferase. In all lines the onset of transgene protein expression was present before post-natal day 7. There was no detectable HA signal in glial cells (not shown), nor was there HA signal in various non-CNS tissues including heart, skeletal muscle, liver, and kidney.

In 3 of 4 hVAPB-P56S expressing lines (VM1, VM3, VM5), very intense HA and VAPB-immunoreactivity occurred in small spherical and ellipsoid inclusion-like structures (Fig. 6.1D). The structures were distributed throughout the cell bodies of the majority of motor neurons, and resembled the inclusions previously documented in transfected cells (Nishimura et al., 2004; Teuling et al., 2007). The inclusions also occurred in other populations of neurons, including large spinal interneurons, and large neurons in brain stem and the cerebellar nuclei. Comparison of different lines suggests that the frequency of inclusions grossly correlates with transgene expression levels, occurring at higher frequencies in lines VM1 and VM5 that express relatively high levels of mutant protein, show larger numbers of inclusions per motor neuron, and a higher proportion of motor neurons with inclusions (about 70 % of motor neurons; see also below) as compared to line VM3 (about 50-60% of motor neurons has inclusions). Mice from line VM2, showed the lowest transgene expression levels, which may explain the absence of detectable inclusions.

Western blot analysis showed that a large proportion of transgenic mutant VAPB accumulated in a non-ionic detergent (Nonidet P40) insoluble (P2) fraction, indicative of reduced solubility and aggregation of mutant VAPB (Fig. 6.1E). Endogenous murine VAPB was not detectable in the insoluble fraction of spinal cord homogenate of mutant VAPB mice, suggesting that it does not coaggregate with transgenic mutant VAPB (Fig. 6.1E).

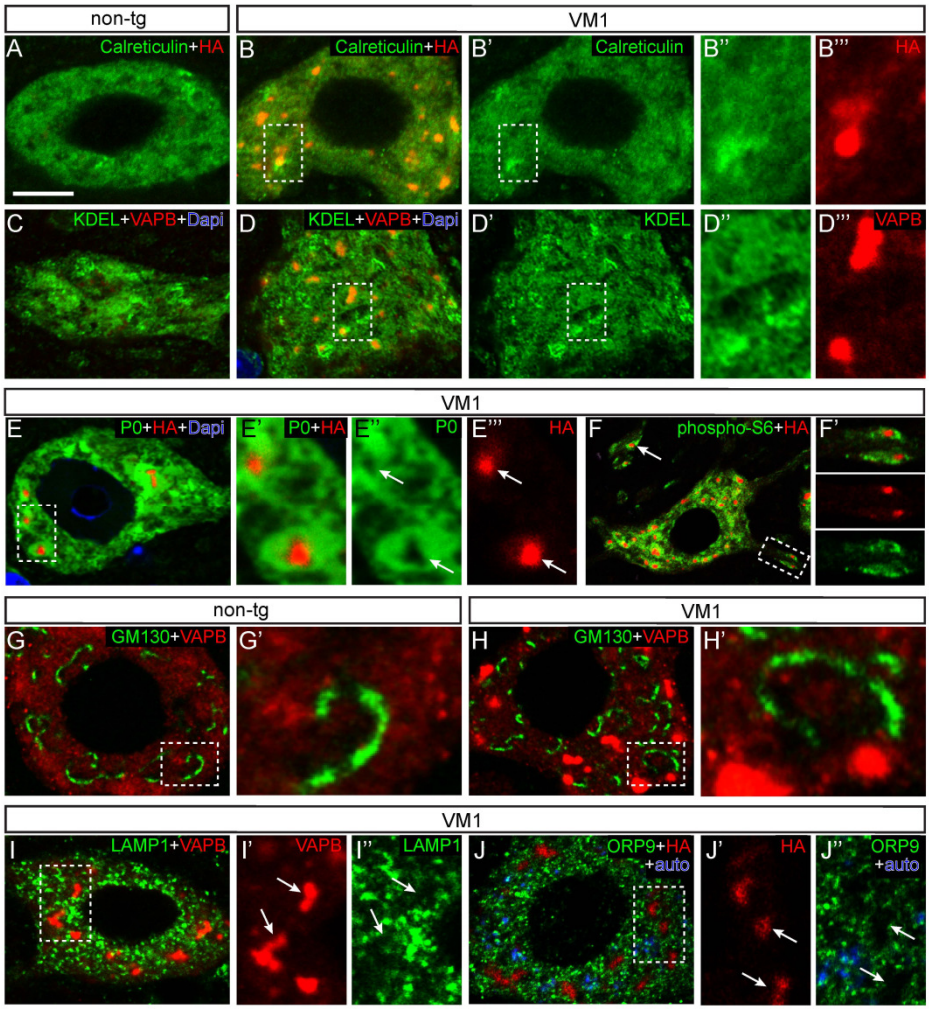

Figure 6.2. VAPB Inclusions in VAPB-P56S transgenic motor neurons are immunoreactive for ER markers and are surrounded by ribosome rich areas

A-D) Confocal immunofluorescence of non-transgenic (A, C), or mutant VAPB (line VM1; B, D) spinal motor neurons double-labeled for VAPB labeled with either anti-HA (specific for transgenic VABP; A, B) or anti-VAPB (labels endogenous and transgenic VAPB; C, D) and antibodies against luminal ER proteins, *i.e.* calreticulin (A, B) or KDEL-motif proteins (C, D); calreticulin and KDEL-immunoreactivities are diffusely distributed throughout the cytoplasm of bo th non-transgenic (A, C) and mutant VAPB (B', D') expressing motor neurons irrespective of the presence of VAPB inclusions.

E, F) Double labeling for HA and the ribosomal proteins P0 (E) or phosphorylated-S6 (F) shows that mutant VAPB inclusions are P0 and phospho-S6-immunonegative, but the surrounding cytoplasm is always intensely P0 (arrows in E) and phospho S6-positive (F). Arrow and insert in F show that also dendritic VAPB inclusions are surrounded by high levels of ribosomes.

G-J) Double of VAPB and HA, with antibodies against the cis-Golgi protein GM130 (G, H), lysosomal protein LAMP1 (I), and the FFAT-motif protein ORP9 (J), shows that VAPB inclusions (arrow is I and J) are immunonegative for these proteins. Note the presence of autofluorescent structures, representing lipofuscin (aging pigment) in the motor neuron shown in J which is from a 70 week old VM1 mouse. Bar in C, 10 µm

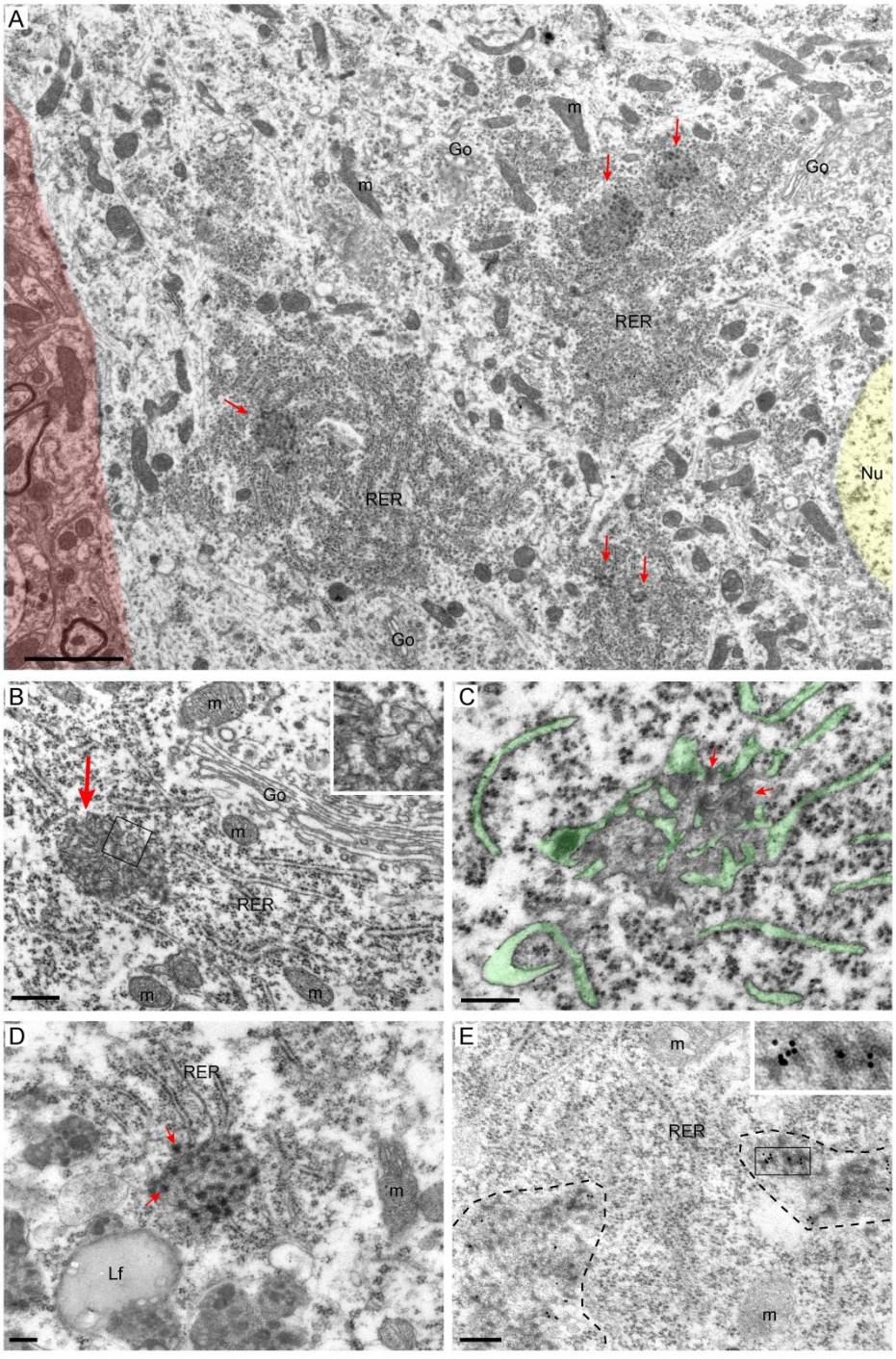

Figure 6.3. VAPB inclusions consist of smooth ER-like tubular profiles intermingled with electron dense material

Figure 6.3. VAPB inclusions consist of smooth ER-like tubular profiles intermingled with electron dense material

A-D) Transmission electron photomicrographs of mutant VAPB inclusions in spinal motor neurons of a 6 weeks old VM1 (A, B), a 6 week old VM3 (C), and a 70 weeks old VM1 x VM5 mouse (D). Note in A that the inclusions (red arrows) are localized within normal appearing rough ER (RER). Other organelles such as Golgi apparatus (Go) and mitochondria (m) are unaltered (A, B). In C the ER lumen is accentuated in green to outline the continuity of tubular smooth ER like profiles in the inclusions with the surrounding rough ER cisterns. Note in C and D that the electron dense material in the inclusions has a patchy appearance (red arrows).

E) Post-embedding immunogold electron microscopy with anti-HA antibody showing that HA-labeling is preferentially associated with the electron dense material in the inclusions (see insert). The dashed lines outline two distinct inclusions.

Color overlay in A: red, area outside the motor neuron; yellow, nucleus; green, lumen of ER.

Scale bars: 2 µm (A), 500 nm (B), 200 nm (C, D, E)

VAPB inclusions consist of smooth ER-like tubular profiles intermingled with electron dense material

To further characterize the inclusions in motor neurons of VAPB-P56S transgenic mice we double stained for HA or VAPB and a variety of cellular markers. Double labeling with antibodies against calreticulin (a luminal ER sugar-binding protein) and KDEL (a C-terminal tetrapeptide motif shared by several ER chaperones), showed that the mutant VAPB inclusions were immunoreactive for these ER markers (Fig. 6.2A-D). However calreticulin and KDEL staining was not enriched in the inclusions; the same staining intensity is observed in the inclusions as compared to the surrounding area. Accordingly, the calreticulin and KDEL staining in motor neurons with inclusions was indistinguishable from that in non-transgenic motor neurons (*e.g.* compare Figs. 6.2A and C with Figs 6.2B' and D'). Double labeling with antibodies against ribosomal protein P0 and phosphorylated ribosomal protein S6 showed that while the inclusions were immunonegative for P0 and phospho-S6, the area around the inclusions contains a high density of ribosomes (Fig. 6.2E, F). The specific association of mutant VAPB inclusions within ribosome-rich areas was particularly clear in motor neuronal dendrites showing focal areas of intense phospho-S6 staining. Analysis of dendritic VAPB inclusions (> 100) indicated that in all occasions they are present within an area of intense phospho-S6 staining (Fig. 6.2F'). Mutant VAPB did not codistribute with Golgi apparatus markers such as GM130 (Fig. 6.1G, H) and CGRP (not shown). The presence of inclusions did not have a detectable effect on the Golgi apparatus morphology as identified by GM130 immunofluorescence (Fig. 6.2G, H). Also markers for lysosomes (LAMP1, Fig 6.2I) and endosomes (EAA1, not shown) did not codistribute with inclusions and showed unaltered distributions in motor neurons with inclusions. Finally we screened antibodies against a variety of FFAT-motif containing proteins, representing a major class of VAPB interacting proteins (Loewen et al., 2003; Kaiser et al., 2005; Teuling et al., 2007), to determine whether these proteins accumulate in the inclusions. Consistent labeling in motor neurons was observed with antibodies against NIR2 and ORP9 both of which are potential VAPB interacting proteins as determined by immunoprecipitation and pull down experiments (Wyles and Ridgway, 2004; Amarilio et al., 2005; Lehto et al., 2005; Teuling et al., 2007). However, no ORP9 (Fig. 6.2J) nor NIR2 (data not shown) accumulated in the mutant VAPB inclusions, consistent with our

observation that the P56S mutation disrupts the FFAT-motif binding domain of VAPB (Teuling et al., 2007).

The above data indicate that the mutant VAPB inclusions are positive for luminal ER proteins and are surrounded by ribosome-rich areas. Consistently, transmission electron microscopy revealed abnormal structures containing smooth ER-like tubular profiles that were situated within the rough endoplasmatic reticulum (RER) of motor neurons in the VAPB-P56S transgenic mice (Fig. 6.3). The tubular profiles in many occasions were continuous with profiles of surrounding rough ER cisterns (Fig. 6.3A-D). The inclusions, in addition to the tubular profiles, consisted of diffuse electron dense material.

Typically the electron dense material was not homogeneously distributed throughout the inclusion, but showed a patchy appearance, suggestive of some degree of organization into smaller clusters (Fig. 6.3C, D). Post-embedding immunogold electron microscopy with anti-HA antibody, showed that HA-labeling was specifically associated with the inclusions (Fig. 6.3E; 78.40 ± 16.98 particles/μm^2 [10 inclusions] versus 0.32 ± 0.14 gold particles/μm^2 in the surrounding cytoplasm and 0.24 ± 0.08 particles/μm^2 in non-transgenic motor neuron, n = 10 cells) but not in any other structure. Immunogold labeling was preferentially associated with the electron dense material in the inclusions, suggesting that the electron dense material at least in part represent aggregated VAPB (Fig. 6.3E).

Comparison of different lines of VAPB-P56S transgenic mice, showed that the ultrastructural characteristics of the inclusions were the same in all lines showing inclusions at the light microscopic level (VM1, VM3 and VM5), while they do not occur in line VM2 (see Table 1) consistent with immunofluorescence data. Also in double mutant mice generated by crossing VM1 and VM5 mice to increase transgene expression levels (see below) the ultrastructural characteristics of the inclusions were the same as in other lines. The ultrastructural characteristics of the inclusions also were the same in old (70-90 weeks) transgenic mice (Fig. 6.3D), indicating no effect of aging on their morphology. Importantly, the RER around the inclusions and other organelles in the same cells in all instances showed a normal appearance, suggesting that the inclusions do not have a deleterious effect on other cellular organelles. Finally, the inclusions showed the same appearance in spinal interneurons (not shown), indicating that the ultrastructure of inclusions does not depend on specific features of the ER in motor neurons.

Stacked ER cisterns in wt-hVAPB motor neurons

Motor neurons of wt-hVAPB mice did not show the ER-inclusions as observed in VAPB-P56S transgenic mice, indicating that these inclusions are a specific consequence of mutant VAPB. A subset of motor neurons, however, showed another abnormalitiy, *i.e.* stacked ER, consisting of flat or circular arrays of parallel narrow cisterns separated by a 17.2 ± 1.6 nm thick layer (Fig. 6.4A). These stacked ER cisterns resembled previously reported stacked ERs (also termed organized smooth ER [OSER], or crystaloid ER)
observed in cells coexpressing VAPB together with FFAT-motif protein (Amarilio et al., 2005; Lehto et al., 2005), cells expressing high levels of certain ER membrane proteins (Takei et al., 1994; Snapp et al., 2003), and knock-down of specific proteins (Dykstra et al., 2010 6736). Usually the ER stacks were localized in the RER bodies, the superficial cisterns being continuous with rough ER cisterns (Fig. 6.5A). Occasionally, stacked ER

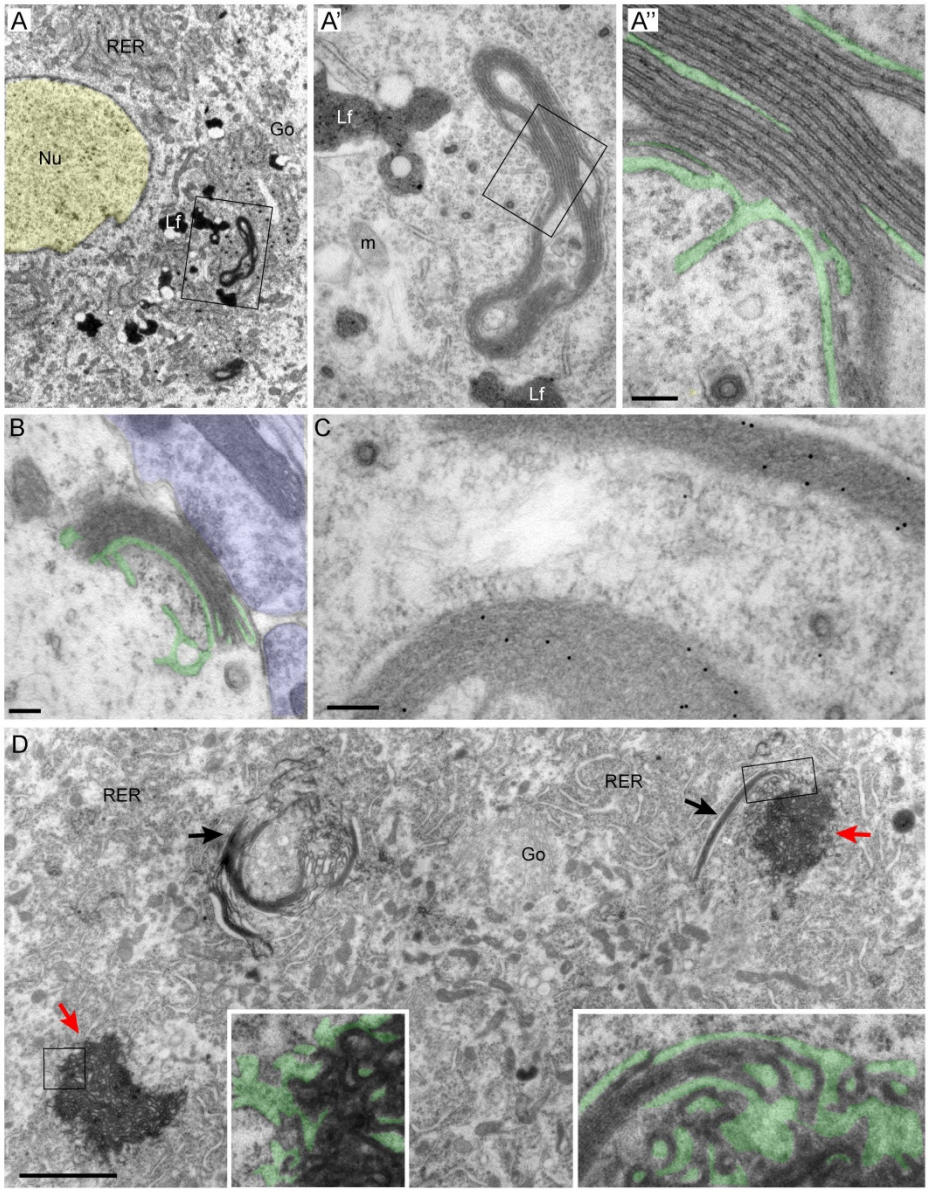

Figure 6.4. Stacked ER in motor neurons of wild-type VAPB overexpressing mice A, B) Transmission electron photomicrographs showing stacked ER in motor neurons from a 30 week old wild-type VAPB overexpressing mouse (line VW3). The ER cisterns in the stacks are thin, while the cytosolic faces of the cisternal membranes are separated by a 17.2 ± 1.6 nm thick layers (A). In A" the ER lumen is accentuated in green to outline the continuity of lumen of stacked cisterns with the surrounding ER cisterns. B illustrates stacked ER also next to a C-type synapse characterized by the presence of subsynaptic ER cisterns. C) Post-embedding ant-HA immunogold electron photomicrographs, showing that transgenic wild-type VAPB is concentrated in the stacked ER. D) Transmission electron photomicrograph of a motor neuron of an 8 week old mouse from line VW1 showing a variant of stacked ER, consisting of curved more irregular ER cisterns, and electron dense intra-cisternal spaces (inserts in D). Color overlay: yellow, nucleus (A); purple, presynaptic bouton (B); green, lumen of ER (B and D). Scale bars: 2 µm (D), 500 nm (B), 100 nm (A", C) Both the 'regular' and the electron-dense irregular variant of stacked ER were never observed in VAPB-P56S transgenic mice.

also occurred at C-type synapses (Fig. 6.4B) which in non-transgenic mice are characterized by the presence of subsurface ER cisterns (Hellstrom et al., 2003). Immunogold labeling showed increased anti-HA immunoreactivity within stacks (Fig. 6.4C). Remarkably, in one line of wt-hVAPB mice (line VW1) we noted a variant of stacked ER, where ER cisterns were curved, the lumen of the cisternae was expanded and the space linking cisterns together was considerably more electron dense (Fig. 6.4D). This electron dense form of stacked ER was continuous with both 'regular' ER stacks and RER profiles (inserts in Fig. 6.4D).

Only a few VAPB-P56S transgenic mice display motor axon degeneration

Together our confocal and electron microscopic analyses show that mutant VAPB in motor neurons of VAPB-P56S transgenic mice accumulates in unique ER containing inclusions. To determine whether these inclusions or the presence of mutant VAPB per se in the long term are detrimental for motor neurons and cause an ALS-like disorder, 10-13 mice from each line (VM1, VM2, VM3 and VM5) were allowed to age and tested for the development of motor abnormalities Moreover, we increased the levels of mutant VAPB by generating double transgenic mutant VAPB mice through intercrossing VM1 and VM5. Almost all VAPB-P56S transgenic mice (46 mice) reached the age of 2 years without developing signs of motor deficits as measured by accelerating rotarod, hanging wire and hind limb extension tests, while 2 mice developed progressive motor impairment. The mice that survived without signs of motor abnormalities included all mice of VM1 and VM5 lines showing high levels of VAPB inclusions in motor neurons (Fig. 6.5A). In these mice there was no evidence for increased astrocyte or microglia activation or increased neuromuscular denervation and motor neuron loss. The mice with a motor phenotype (MP) included a mouse from line VM3 (mouse MP1, onset 61 weeks) and line VM1xVM5 (mouse MP2, onset 74 weeks). The mice were killed when they were unable to hang for more than 1s and started to show > 20% weight loss at the age 65 (mouse MP1) and 78 (mouse MP2) weeks. At the time of killing the mice were still capable of moving their hind limbs, but they were unable to extend them and use them properly for locomotion (Fig. 6.5B). Both mice showed mild astrocytosis and microgliosis in the spinal cord ventral horn. Interestingly, while the motor neurons showed a relatively healthy appearance, a large proportion throughout the spinal cord showed the expression of ATF3 (Fig. 6.5C, D), a stress transcription factor that is expressed in motor neurons following multiple pathological conditions (Tsujino et al., 2000; Vlug et al., 2005; de Waard et al., 2010). Remarkably, double labeling with anti-HA antibody showed that ATF3 expressing motor neurons in mouse MP1 and MP2 both showed diffuse HA-immunoreactivity in the cytoplasm instead of the HA-positive inclusions (Fig. 6.5E).

Analysis of the sciatic nerve revealed profiles of degenerating axons (Fig. 6.5F). Together the data indicate that only a few VAPB-P56S transgenic mice (<5% - MP1 and MP2) show axonal degeneration and develop progressive motor abnormalities. Although the total number of transgenic mice with motor neuron abnormalities is too low to conclusively link the phenotype to VAPB-P56S expression, the data do suggest a correlation between ATF3 expression, axonal degeneration and the absence of VAPB inclusions.

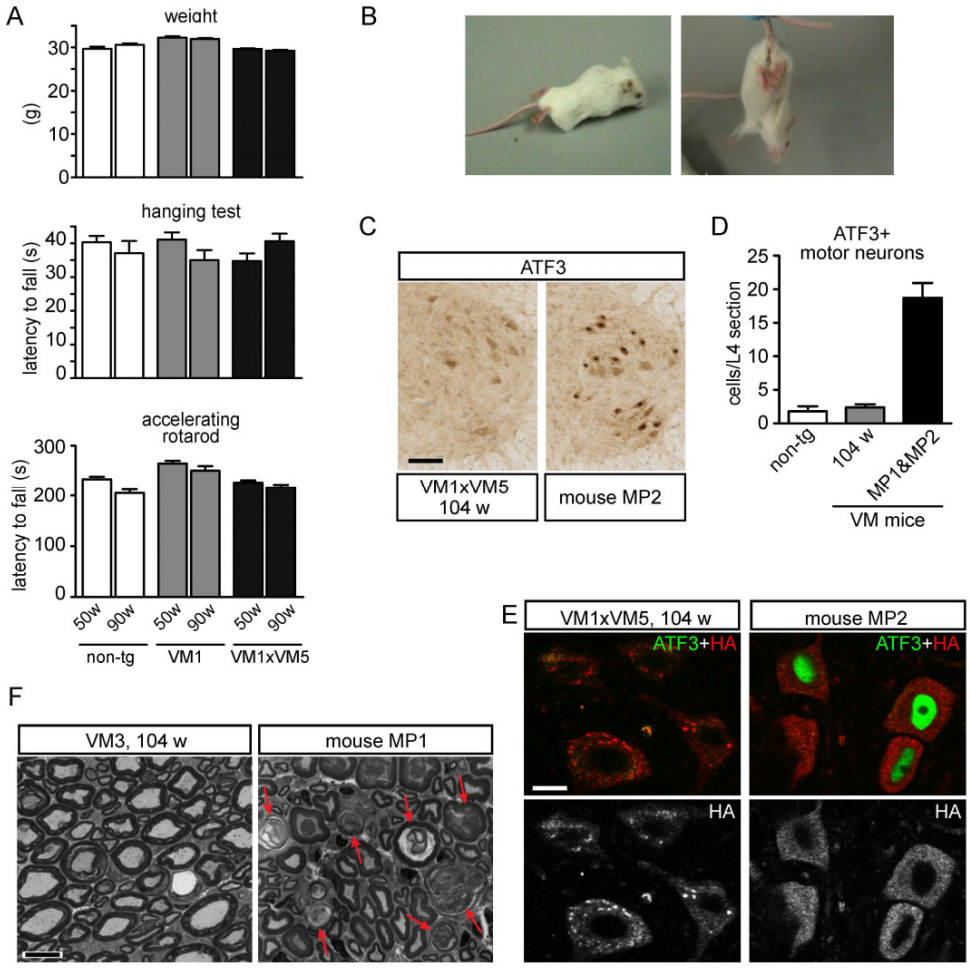

Figure 6.5. ATF3 activation and motor axon degeneration in 2 of 46 VAPB-P56S transgenic mice

A) Bar graphs showing weight, and motor performance in hanging grid and accelerating rotarod tests of mutant VAPB transgenic mice (line VM1 and VM1xVM5 mice) and non-transgenic littermates. VAPB transgenic mice showed the same weight and motor performance as non-transgenic littermates. Numbers in bars represent the number of mice tested per group. B) Mutant VAPB mouse (mouse MP2, line VM1xVM5, age 78 weeks) that developed muscle weakness resulting in impaired locomotion and inability to extend the hind limbs when lifted by the tail. C, D) Representative images (C) and bar graph (D) showing high levels of ATF3 expression in spinal motor neurons of mutant VAPB mice that developed muscle weakness (Mouse MP1 and MP2).

E) Confocal images of motor neurons double-labeled for HA and ATF3 showing both the absence of VAPB inclusions as well as ATF3 expression in motor neurons of the mutant VAPB mouse MP2.

F) Semithin (0.5 µm) toluidine blue-stained sciatic nerve sections of mutant VAPB mice (line VM3) showing degenerating axons (red arrows) in mouse MP, a VM3 mouse that developed muscle weakness.

Scale bars: 250 µm (A), 10 µm (B), 2 µm (C).

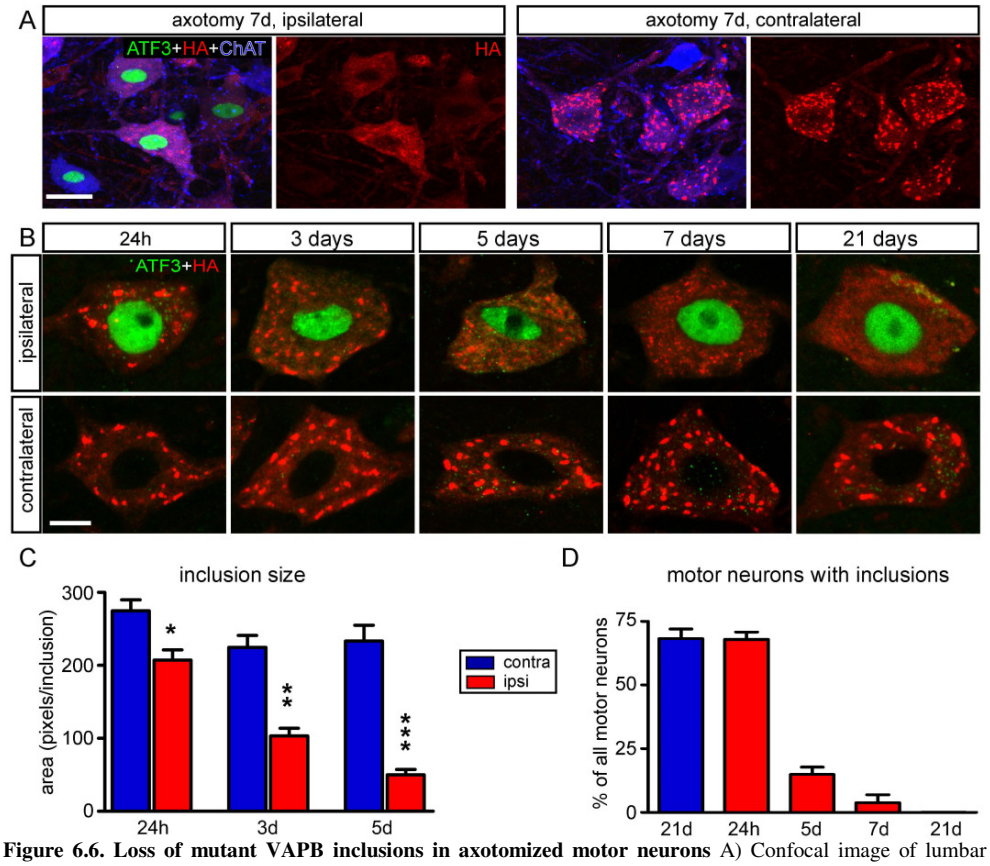

Figure 6.6. Loss of mutant VAPB inclusions in axotomized motor neurons A) Confocal image of lumbar motor neurons of a VM1 mutant VAPB mouse, 7 days after sciatic nerve transection, showing that axotomized motor neurons identified by ATF3 expression (ipsilateral) have no or very small VAPB inclusions as compared to control (contralateral) VM1 motor neurons. B) Representative images of axotomized motor neurons (ipsilateral, ATF3 positive) from VM1 mice killed at different time points after axotomy. Note the gradual reduction of the size of VAPB inclusion following post-axotomy, ultimately leading to diffuse perikaryal HA staining 2-3 weeks post-axotomy. C, D) Bar graphs showing the inclusion size expressed as the number of pixels in a 1 µm thick optical section (C), and the percentage of HA-labeled motor neurons with inclusions (D). Values in C represent means ± SE from more than 50 motor neurons from 2-3 mice. *, **, ***: $P < 0.05$, $P < 0.01$, $P < 0.001$ compared to contralateral (unpaired Student's t-test). Scale Bars: 25 µm (A), 10 µm (B).

Loss of mutant VAPB inclusions in axotomized motor neurons

To further investigate the connection between ATF3 expression, axonal damage and the absence of VAPB inclusions, we examined the effect of axotomy on in sciatic nerve motor neurons of VM1 mice. Axotomy results in a strong induction of ATF3 expression in motor neurons, within 12 hours, which lasts for more than 5 weeks post transection (Tsujino et al., 2000; Teuling et al., 2008). Analysis of inclusions in axotomized VM1 spinal cord revealed a gradual reduction of the size of inclusions starting within 24 hours post-axotomy, and a reduction of the number of motor neurons with inclusions 3-5 days post-axotomy, resulting in the total absence of inclusions and diffuse HA labeling 2-3 weeks post-axotomy (Fig. 6.6).

The diffuse HA labeling in 2-3 weeks axotomized VM1 motor neurons strongly resembled HA-labeling of MP1 and MP2 motor neurons indicating that the absence of mutant VAPB inclusions in MP1/MP2 mice can be explained as a secondary phenomenon following ATF3 expression/axonal injury. Importantly, the level of HA-labeling in 2-3 weeks axotomized VM1 motor neurons is considerable higher than in VM2 motor neurons, indicating that the absence of inclusions cannot simply be explained by reduced VAPB-P56S expression levels.

VAPB inclusions are an ER associated degradation (ERAD) quality control compartment

The above data indicate that mutant VAPB inclusions in motor neurons of VAPB-P56S transgenic mice represent reversible structures. Being a misfolded ER membrane protein, VAPB- P56S is likely to be degraded by the ERAD-C pathway, *i.e.* ER associated degradation (ERAD) for ER substrates exposing a misfolded domain into the cytoplasm (Claessen et al., 2012; Wolf and Stolz, 2012). This pathway like other ERAD pathways involves ubiquitination of the substrate, followed by extraction from the ER membrane for delivery to the proteasome. Studies in Drosophila and mammalian cells have documented that P56S-VAPB can be poly-ubiquitinated, and that mutant VAPB inclusions are immunostained with antibodies against poly-ubiquitinated epitopes (Kanekura et al., 2006; Ratnaparkhi et al., 2008; Papiani et al., 2012), although in our hands VAPB-P56S inclusions in transfected HeLa cells were relatively weakly positive for ubiquitin-epitopes as compared to inclusion formed by mutant huntingtin (Supplementary Fig. 2A of (Teuling et al., 2007)). Using monoclonal antibody FK2 that immunoreacts with mono- and poly-ubiquitinated epitopes, inclusions of our VAPB-P56S transgenic mice showed intense staining (Fig. 6.7A), consistent with ubiquitination of mutant VAPB in the inclusions. Interestingly, motor neurons without inclusions showed a diffuse increase of FK2-immunostaining throughout the cytoplasm as compared to motor neurons from non-transgenic mice processed in the same immunorun. This was observed in 2 independent experiments with spinal cord sections from both VM1 and VM3 mice and their respective non-transgenic littermates (Fig. 6.7B-D). These data raise the possibility that also diffuse mutant VAPB which is not in the inclusions may be ubiquitinylated.

We next stained for other ERAD components, such as Valosin-containing protein (VCP/p97, cdc48 in yeast) a hexameric AAA ATPase that is an essential ERAD component by providing the mechanical force for ER extraction (Wolf and Stolz, 2012). In wild-type motor neurons VCP-immunoreactivity was present in the nucleus and the perykaryon, with higher staining intensities of the nucleus (Fig. 6.7I). Motor neurons with mutant VAPB inclusions showed the same overall staining, but in addition showed intense VCP staining within the inclusions, indicative of an accumulation of VCP in the inclusions (Fig. 6.7E). Staining for Derlin-1, an ER membrane spanning protein that plays a role in ERAD of many substrates, including tail-anchored proteins (Claessen et al., 2010), showed that VAPB inclusions also were immunoreactive for Derlin-1 (Fig. 6.7F). However, unlike VCP, Derlin-1 immunoreactivity was not specifically enriched in the inclusions, showing the same overall distribution in non-transgenic motor neurons and motor neurons with inclusions (compare Fig. 6.7F'and H). Finally, we stained for Bap31 an ER membrane

chaperone that may play a role in ERAD (Wakana et al., 2008 4512; Wang et al., 2008), and is enriched in mutant VAPB inclusions in transfected HeLa cells (Fasana et al., 2010). Accordingly, we found a marked enrichment of Bap31 immunoreactivity in mutant VAPB inclusions in our transgenic mice (Fig. 6.7G). Together the data indicate that mutant VAPB inclusions are a region of increased ERAD activity.

To further study the relationship between the ERAD pathway and the mutant VAPB inclusion we moved to primary cultured hippocampal neurons. Like VAPB inclusions in transgenic mice, VAPB inclusions in hippocampal neurons transfected with myc- or HA-tagged P56S-VAPB were enriched in ubiquitinylated epitopes, VCP, Bap-31 and Derlin-1 immunoreactivity (Fig. 6.7J-M). Inhibition of the ERAD pathway by inhibiting the proteasome with MG-132 resulted in the formation of larger inclusions (Fig. 6.8). Also shRNA-mediated knockdown of Bap31 resulted in larger inclusions (Fig. 6.8C, D). Together these data indicate that the sizes of the inclusions depend on ERAD activity, compromised ERAD resulting in larger inclusions.

VAPB-P56S inclusions are not ERPO, an ER protective organelle associated with luminal ERAD substrates

Together the data raise the possibility that VAPB-P56S clusters in motor neurons of our P56S-VAPB transgenic mice represent a defensive cell response aimed at protecting cells from a level of mutant ER membrane protein that exceeds the capacity of ER associated degradation. A recent study documented a protective ER compartment termed ERPO (ER protective organelle) in neurons of mice expressing mutated forms of seipin, an ER protein associated with an autosomal dominant motor neuron disease (Yagi et al., 2011; Ito et al., 2012). To determine whether overlapping mechanisms operate in the formation of mutant seipin and VAPB inclusions we coexpressed VAPB-P56S with wild-type or mutant seipin forms. Consistent with previous reports expression of seipin-S90L and seipin-N88S resulted in the formation of small spherical in hippocampal neurons (not shown). The sizes of seipin inclusion were in the same range as VAPB inclusions. In most cells expressing mutant seipin and VAPB-P56S, the mutated proteins accumulated in distinct inclusions (Fig. 6.9B, C). However, a few cells developed larger inclusions that contained both high levels of both mutant seipin and VAPB (Fig. 6.9D). These data indicate that VAPB inclusions are different from ERPO, but that in some conditions these ER quality control compartments may fuse.

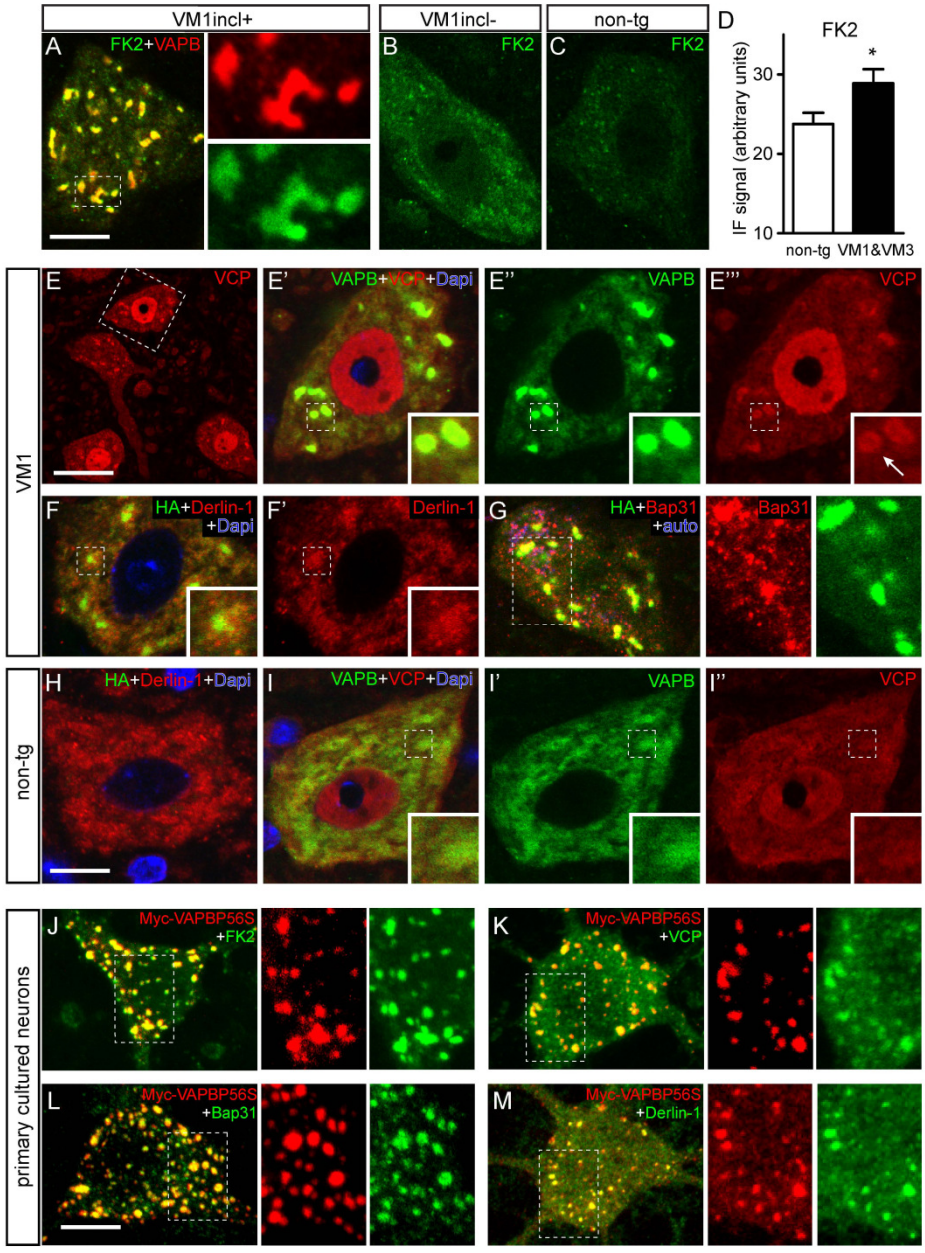

Figure 6.7. Mutant VAPB inclusions are ubiquitin-positive and enriched in ERAD components

A-C) Representative confocal images of the distribution of ubiquitinated epitopes labeled with the FK2 antibody in motor neurons of mutant VAPB line VM1 with (A) or without (B) inclusions, and non-transgenic littermates (C). Note high level of FK2-immunoreactivity in inclusions (A) and diffuse increase as compared to non-transgenic motor neurons in VM1 motor neurons without inclusions (B).

D) Bar graph of FK2-immunofluoresence signal in non-transgenic versus VM1 and VM3 motor neurons without inclusions. Values are means ± SE and are from lumbar L4 segments from 4 non-transgenic, 2 VM1 and 2 VM3 mice imbedded in a single gelatin block (see methods).

E-I) Confocal image of mutant VAPB (line VM1, E-G) or non-transgenic (H, I) spinal motor neurons double-labeled for VAPB or HA and ERAD components, *i.e.* VCP/p97 E, I), derlin-1 (F, H), and Bap31 (G).

J-M) Maximal projections of confocal stacks of primary cultured hippocampal neurons transfected with Myc-VAPB-P56S mutant VAPB, showing high levels of ubiquitinated epitopes, VCP/p97, derlin-1, and Bap31 in mutant VAPB inclusions.

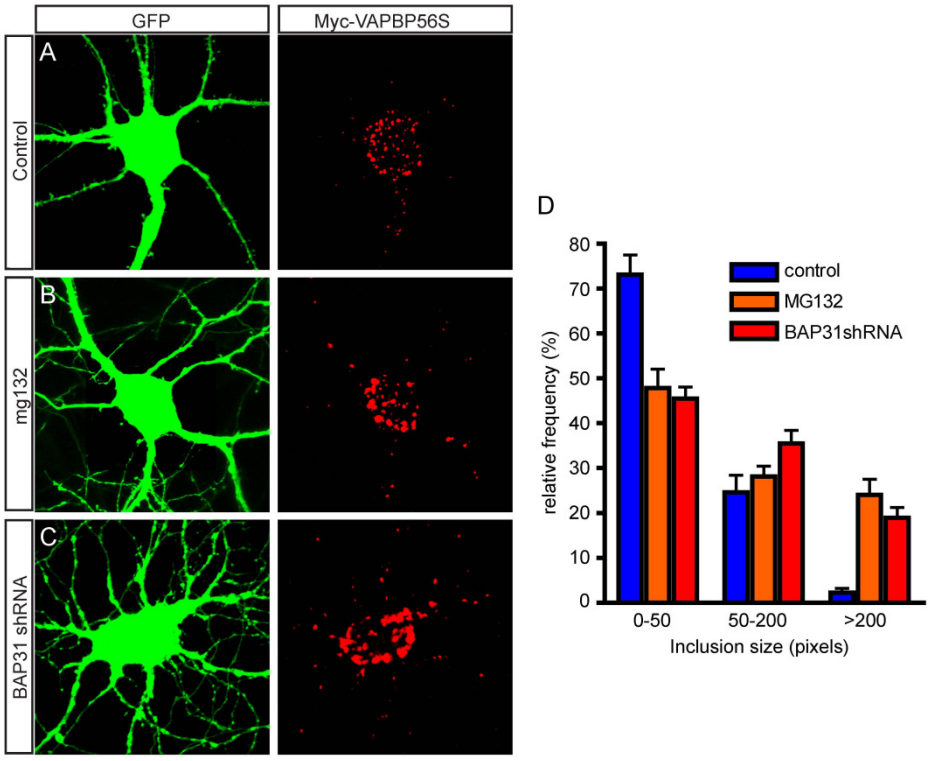

Figure 6.8. Increased size of mutant VAPB inclusions after proteasome inhibition or BAP31 knockdown
A-C) Incubation of GFP and Myc-VAPB-P56S transfected primary cultured hippocampal neurons with Mg132 to inhibit proteasome (B), or BAP31 shRNA construct to down regulate BAP31 expression (C) result in increased size of mutant VAPB inclusions as compared to untreated cultures (A).
D) Frequency distribution of inclusion size in Myc-VAPB-P56S expressing neurons. The inclusion size is expressed in pixel in a maximal projection of a stack encompassing the entire thickness of the cultured neurons (5-10 µm).

Discussion

Inclusions in motor neurons of transgenic VAPB-P56S mice may represent an ER quality control compartment

In the present study we show that transgenic mice expressing the ALS8-linked mutant form of VAPB develop a novel type of inclusion that is localized within the rough ER and consists of smooth ER-like tubular profiles surrounded by electron dense material. Several lines of evidence raise the possibility that this mutant VAPB inclusion represents an ER protein quality control compartment: First, the presence of the inclusions was not associated with signs of neuronal malfunction or neuronal pathology. Second, the inclusions are reversible as they gradually disappear following axonal transection. Third,the inclusions are strongly immunoreactive for factors that operate in the ER associated

degradation (ERAD) pathway, including p97/VCP, Derlin-1 and the ER membrane chaperone Bap31. And forth, inhibition of ERAD increased the size of the inclusions. Therefore we propose that the inclusions in motor neurons of our mutant VAPB transgenic mice, represent an ER quality control compartment that arises, when the amount of substrate exceeds the capacity of the ER associated degradation (ERAD) pathways, reminiscent of aggresomes that may form in condition of excess cytoplasmatic misfolded protein (Bagola and Sommer, 2008; Tyedmers et al., 2010).

Compatible with this idea, mutant VAPB inclusions do not occur in motor neurons of low-expressing mutant VAPB transgenic mice (line VM2).Several studies have reported on ER-derived inclusion-like structures that are formed after expression of specific mutated ER proteins in yeast or mammalian cells, and may have cytoprotective properties (Huyer et al., 2004; Granell et al., 2008; Yagi et al., 2011; Ito et al., 2012). An ER-derived structure termed ERPO (ER protective organelle) has been identified as a protective ER compartment in cells expressing the serpin α1-antitrypsin with a E342K mutation, associated with liver disease in children (Granell et al., 2008). A recent study showed that mutant forms of seipin (N88S and S90L), that cause an autosomal dominant motor neuron disease and accumulate into inclusions in transfected cells and neurons in transgenic mice (Yagi et al., 2011), codistribute with α1-antitrypsin in ERPO in double transfected cells (Ito et al., 2012). These data suggest that ERPO may represent an ER quality control pathway for multiple ER substrates. However, our data show that mutant VAPB and mutant seipin predominantly accumulate in different inclusions when coexpressed, suggesting that the mechanisms that operate in the formation of VAPB inclusions differ from those underlying the formation of ERPO. In view of the presence of multiple ERAD subpathways that are specific for different classes of ER proteins (*e.g.* ERAD-L, ERAD-M and ERAD-C for luminal, intermembrane, and cytoplasmatic misfolded domains, respectively), it is conceivable that there are also multiple ER protective compartments that may form in conditions of overload of specific ERAD-subpathways. Interestingly, an ER derived compartment termed ERAC (ER associated compartment) that is formed in yeast expressing a misfolded multispanning membrane protein (Ste6p) shows ultrastructural resemblance to the mutant VAPB inclusions (Huyer et al., 2004).Further studies are needed to determine whether a compartment similar to ERAC exists in mammalian cells, to characterize the molecular machinery underlying the formation of mutant VAPB inclusions, and to determine whether there are additional proteins that use the same machinery and accumulate in the same inclusions. These studies will also reveal to what extent the formation of ER quality control compartments represent an integral cellular complement to ERAD. These pathways may represent an alternative for unfolded protein response (UPR), a set of well characterized molecular pathways that are activated by conditions of ER proteolytic stress and result in down regulation of transcription and upregulation of ER chaperones (Buchberger et al., 2010; Ronzoni et al., 2010; Smith et al., 2011).

The formation of a specialized ER quality control compartment may be favorable in conditions of overload of a single mutated protein, while the UPR may be activated in more generalized conditions causing the accumulation of multiple substrates. The presence of an alternative for UPR in conditions of ERAD overload may explain the variability in the literature on the activation UPR in cells expressing VAP-P56S (Suzuki et al., 2009;

Moumen et al., 2011). Preliminary data indicate that there is no UPR activation in spinal cord and brain homogenates from our VAPB-P56S transgenic mice.

Wild-type VAPB overexpression causes stacked ER

The ultrastructure of the mutant VAPB inclusions in motor neurons resemble the ultrastructure of VAPB inclusion in non-neuronal mammalian cells (Teuling et al., 2007) and drosophila neurons (Tsuda et al., 2008). However, recent work of Borghese and co-workers (Fasana et al., 2010; Papiani et al., 2012) suggests that VAPB-P56S inclusions in non-neuronal mammalian cells predominantly consist of a special form of stacked ER, made of two tightly apposed smooth-surfaced ER cisternae separated by an electron-dense layer (Fasana et al., 2010; Papiani et al., 2012). This bilayered stacked ER resembled bi- and tri-layered ER stacks documented in 'control' COS cells transfected with salmon sperm cDNA (Takei et al., 1994), suggesting that this type of ER abnormality is not necessarily linked to mutant VAPB expression. We did not observe bi- or trilaminar stacked ER, nor any other form of stacked ER in neurons of our mutant VAPB expressing lines. Instead stacked ER occurred in motor neurons of our wild-type VAPB expressing transgenic mice. Stacked ER is a well documented phenomenon in cells that coexpress wild-type VAPB and FFAT-motif proteins, and it has been proposed that they are formed as a result of heterotypic interaction between VAPB and FFAT-motif proteins (Amarilio et al., 2005; Lehto et al., 2005). Hence, stacked ER in motor neurons of wild-type VAPB overexpressing mice may result from excessive VAPB interacting with endogenous FFAT-motif protein. Remarkably, in one line of wild-type VAPB overexpressing mice we observed a variant of stacked ER where the cytosolic space linking the cisterns together was considerably more electron dense. These data indicate that stacked ER in some conditions is irreversible, which contrasts with the notion that stacked ER is a relatively harmless and reversible phenomenon (Takei et al., 1994; Snapp et al., 2003).

Does mutant VAPB cause a motor axonopathy?

Recently, another study has reported on mutant VAPB transgenic mice (Tudor et al., 2010). Consistent with our data, their mice developed mutant VAPB inclusions in motor neurons, but did not develop signs of motor neuron degeneration (Tudor et al., 2010 6705), further indicating that the VAPB inclusions are harmless or protective to motor neurons. Within our cohort of mutant mice that was allowed to age up to 2 years, however, there were two (of 46) mice that developed progressive motor deficits that, albeit milder, resembled motor deficits in SOD1-ALS mice (Vlug et al., 2005; Jaarsma et al., 2008). These two mice showed remarkably intact cell bodies of motor neurons, while significant axonal degeneration occurred in the sciatic nerve. The total number of transgenic mice with motor neuron abnormalities is too low to conclusively link the phenotype to mutant VAPB expression. However, a low-penetrant clinical phenotype would be compatible with the variability of clinical phenotypes in patients with the VAPB-P56S mutation (Marques et al., 2006 6652; Marques and Marques, 2008). Furthermore, also the preferential axonal pathology would be compatible with data from patients, showing axonal abnormalities in nerve biopsies (Marques et al., 2006 6652).

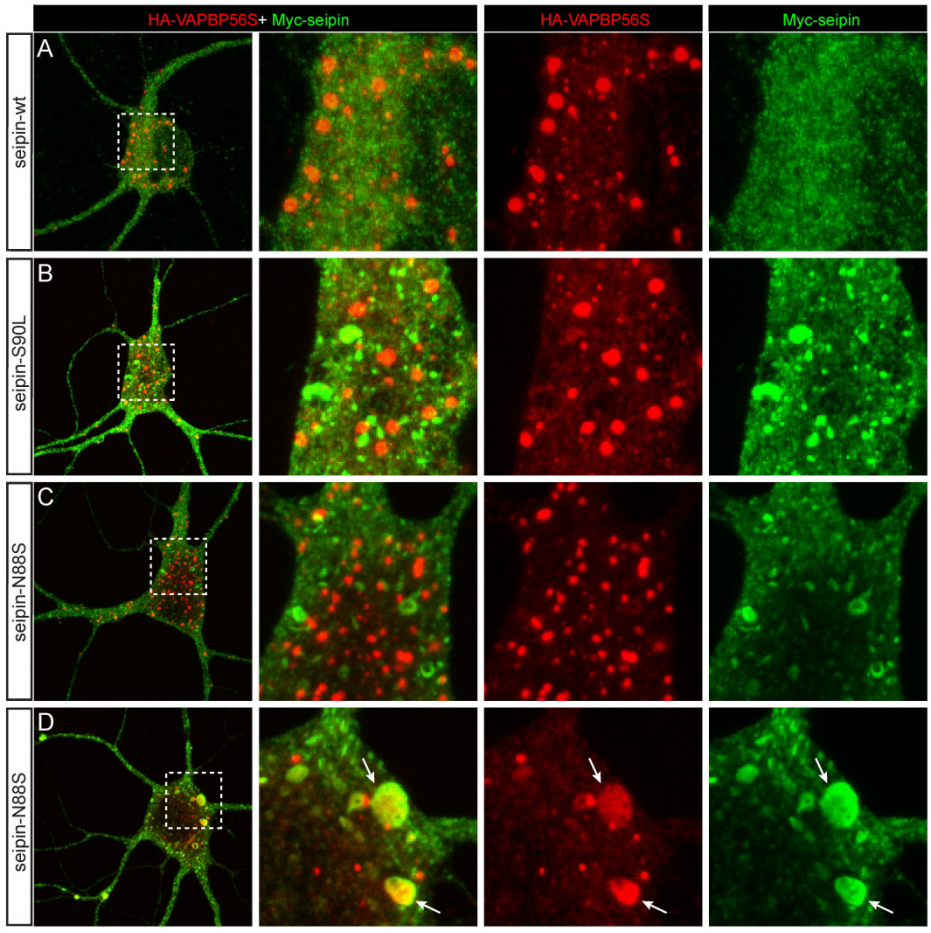

Figure 6.9. Mutant VAPB inclusions poorly colocalize with mutant seipin inclusions
Primary cultured hippocampal neurons cotransfected with HA-VAPB-P56S and myc-tagged seipin constructs. Wild-type seipin shows a diffuse cytoplasic distribution, but seipin-S90L and seipin-N88S accumulate in inclusions (B-D) designated ER protective organelle (ERPO, (Ito et al., 2012)). In most cells HA-VAPB-P56S does not accumulate in seipin-positive inclusions (B and C). However, some cells show large inclusion like structures that are positive for both mutant seipin and VAPB-HA (arrows in D).

Significantly, our data also showed that VAPB-P56S, in contrast to wild-type transgenic VAPB, did not distribute to axons in our transgenic mice. Thus a toxic mechanism involving the axon of motor neurons can not be explained by a direct toxic action VAPB-P56S within the axon, but would imply an indirect toxic mechanism at the level of the cell body. At this point all options, *i.e.* haploinsufficiency, a gained toxic activity, or a dominant-negative effect, are still open. Studies with VAPB deficient mice may reveal to what extent VAPB has a role in axonal maintenance and whether mutant VAPB mediated toxicity can be explained by a haplo-insufficient or dominant-negative mechanism. Interestingly there is an increasing number of long axon axonopathies that result from mutations in proteins involved in ER structure and function, including receptor accessory protein 1 (REEP1), atlastin-1 (ATL1), spastin (SPAST), and reticulon 2 (RTN2) (Renvoise

and Blackstone, 2010 6744; Ramirez and Couve, 2011 6743; Montenegro et al., 2012 6747; O'Sullivan et al., 2012 6748).

In summary, in this study we obtained evidence that inclusions formed by ALS8-mutant VAPB in motor neurons in transgenic mice represent a protective ER compartment. The data suggest that motor neurons are able to handle misfolded ER membrane protein levels that exceed the capacity of the ERAD systems. The data do not support pathogenic pathways involving toxic ER stress signaling or chronic proteotoxic stress proposed for sporadic and SOD1-ALS (Lautenschlaeger et al., 2011).

References

Aguzzi A, O'Connor T (2010) Protein aggregation diseases: pathogenicity and therapeutic perspectives. Nat Rev Drug Discov 9:237-248.

Amarilio R, Ramachandran S, Sabanay H, Lev S (2005) Differential regulation of endoplasmic reticulum structure through VAP-Nir protein interaction. J Biol Chem 280:5934-5944.

Bagola K, Sommer T (2008) Protein quality control: on IPODs and other JUNQ. Curr Biol 18:R1019-1021.

Buchberger A, Bukau B, Sommer T (2010) Protein quality control in the cytosol and the endoplasmic reticulum: brothers in arms. Mol Cell 40:238-252.

Chai A, Withers J, Koh YH, Parry K, Bao H, Zhang B, Budnik V, Pennetta G (2008) hVAPB, the causative gene of a heterogeneous group of motor neuron diseases in humans, is functionally interchangeable with its Drosophila homologue DVAP-33A at the neuromuscular junction. Hum Mol Genet 17:266-280.

Chen HJ, Anagnostou G, Chai A, Withers J, Morris A, Adhikaree J, Pennetta G, de Belleroche JS (2010) Characterization of the properties of a novel mutation in VAPB in familial amyotrophic lateral sclerosis. J Biol Chem 285:40266-40281.

Chiti F, Dobson CM (2006) Protein misfolding, functional amyloid, and human disease. Annu Rev Biochem 75:333-366.

Claessen JH, Kundrat L, Ploegh HL (2012) Protein quality control in the ER: balancing the ubiquitin checkbook. Trends Cell Biol 22:22-32.

Claessen JH, Mueller B, Spooner E, Pivorunas VL, Ploegh HL (2010) The transmembrane segment of a tail-anchored protein determines its degradative fate through dislocation from the endoplasmic reticulum. J Biol Chem 285:20732-20739.

Cohen TJ, Lee VM, Trojanowski JQ (2011) TDP-43 functions and pathogenic mechanisms implicated in TDP-43 proteinopathies. Trends Mol Med.

De Vos KJ, Morotz GM, Stoica R, Tudor EL, Lau KF, Ackerley S, Warley A, Shaw CE, Miller CC (2011) VAPB interacts with the mitochondrial protein PTPIP51 to regulate calcium homeostasis. Hum Mol Genet.

de Waard MC, van der Pluijm I, Zuiderveen Borgesius N, Comley LH, Haasdijk ED, Rijksen Y, Ridwan Y, Zondag G, Hoeijmakers JH, Elgersma Y, Gillingwater TH, Jaarsma D (2010) Age-related motor neuron degeneration in DNA repair-deficient Ercc1 mice. Acta Neuropathol 120:461-475.

Dykstra KM, Pokusa JE, Suhan J, Lee TH (2010) Yip1A structures the mammalian endoplasmic reticulum. Mol Biol Cell 21:1556-1568.

Fasana E, Fossati M, Ruggiano A, Brambillasca S, Hoogenraad CC, Navone F, Francolini M, Borgese N (2010) A VAPB mutant linked to amyotrophic lateral sclerosis generates a novel form of organized smooth endoplasmic reticulum. Faseb J 24:1419-1430.

Feng G, Mellor RH, Bernstein M, Keller-Peck C, Nguyen QT, Wallace M, Nerbonne JM, Lichtman JW, Sanes JR (2000) Imaging neuronal subsets in transgenic mice expressing multiple spectral variants of GFP. Neuron 28:41-51.

Funke AD, Esser M, Kruttgen A, Weis J, Mitne-Neto M, Lazar M, Nishimura AL, Sperfeld AD, Trillenberg P, Senderek J, Krasnianski M, Zatz M, Zierz S, Deschauer M (2010) The p.P56S mutation in the VAPB gene is not due to a single founder: the first European case. Clin Genet 77:302-303.

*GAD*ad BS, Britton GB, Rao KS (2011) Targeting Oligomers in Neurodegenerative Disorders: Lessons from alpha-Synuclein, Tau, and Amyloid-beta Peptide. J Alzheimers Dis 24:223-232.

Gkogkas C, Middleton S, Kremer AM, Wardrope C, Hannah M, Gillingwater TH, Skehel P (2008) VAPB interacts with and modulates the activity of ATF6. Hum Mol Genet.

Granell S, Baldini G, Mohammad S, Nicolin V, Narducci P, Storrie B, Baldini G (2008) Sequestration of mutated alpha1-antitrypsin into inclusion bodies is a cell-protective mechanism to maintain endoplasmic reticulum function. Mol Biol Cell 19:572-586.

Han SM, Tsuda H, Yang Y, Vibbert J, Cottee P, Lee SJ, Winek J, Haueter C, Bellen HJ, Miller MA (2012) Secreted VAPB/ALS8 major sperm protein domains modulate mitochondrial localization and morphology via growth cone guidance receptors. Dev Cell 22:348-362.

Hart MP, Brettschneider J, Lee VM, Trojanowski JQ, Gitler AD (2012) Distinct TDP-43 pathology in ALS patients with ataxin 2 intermediate-length polyQ expansions. Acta Neuropathol.

Hellstrom J, Oliveira AL, Meister B, Cullheim S (2003) Large cholinergic nerve terminals on subsets of motoneurons and their relation to muscarinic receptor type 2. J Comp Neurol 460:476-486.

Hoogenraad CC, Popa I, Futai K, Sanchez-Martinez E, Wulf PS, van Vlijmen T, Dortland BR, Oorschot V, Govers R, Monti M, Heck AJ, Sheng M, Klumperman J, Rehmann H, Jaarsma D, Kapitein LC, van der Sluijs P (2010) Neuron specific Rab4 effector GRASP-1 coordinates membrane specialization and maturation of recycling endosomes. PLoS Biol 8:e1000283.

Huyer G, Longsworth GL, Mason DL, Mallampalli MP, McCaffery JM, Wright RL, Michaelis S (2004) A striking quality control subcompartment in Saccharomyces cerevisiae: the endoplasmic reticulum-associated compartment. Mol Biol Cell 15:908-921.

Ito D, Yagi T, Ikawa M, Suzuki N (2012) Characterization of inclusion bodies with cytoprotective properties formed by seipinopathy-linked mutant seipin. Hum Mol Genet 21:635-646.

Jaarsma D, Teuling E, Haasdijk ED, De Zeeuw CI, Hoogenraad CC (2008) Neuron-specific expression of mutant superoxide dismutase is sufficient to induce amyotrophic lateral sclerosis in transgenic mice. J Neurosci 28:2075-2088.

Jaarsma D, Rognoni F, Van Duijn W, Verspaget H, Haasdijk ED, Holstege JC (2001) CuZn superoxide dismutase (SOD1) accumulate in vacuolated mitochondria in transgenic mice expressing amyotrophic lateral sclerosis (ALS)-linked SOD1 mutations. Acta Neuropathol 102:293-305.

Kaganovich D, Kopito R, Frydman J (2008) Misfolded proteins partition between two distinct quality control compartments. Nature 454:1088-1095.

Kaiser SE, Brickner JH, Reilein AR, Fenn TD, Walter P, Brunger AT (2005) Structural basis of FFAT motif-mediated ER targeting. Structure 13:1035-1045.

Kanekura K, Nishimoto I, Aiso S, Matsuoka M (2006) Characterization of amyotrophic lateral sclerosis-linked P56S mutation of vesicle-associated membrane protein-associated protein B (VAPB/ALS8). J Biol Chem 281:30223-30233.

Kawano M, Kumagai K, Nishijima M, Hanada K (2006) Efficient trafficking of ceramide from the endoplasmic reticulum to the Golgi apparatus requires a VAMP-associated protein-interacting FFAT motif of CERT. J Biol Chem 281:30279-30288.

Kim S, Leal SS, Ben Halevy D, Gomes CM, Lev S (2010) Structural requirements for VAP-B oligomerization and their implication in amyotrophic lateral sclerosis-associated VAP-B(P56S) neurotoxicity. J Biol Chem 285:13839-13849.

Kushner SA, Elgersma Y, Murphy GG, Jaarsma D, van Woerden GM, Hojjati MR, Cui Y, LeBoutillier JC, Marrone DF, Choi ES, De Zeeuw CI, Petit TL, Pozzo-Miller L, Silva AJ (2005) Modulation of presynaptic plasticity and learning by the H-ras/extracellular signal-regulated kinase/synapsin I signaling pathway. J Neurosci 25:9721-9734.

Lautenschlaeger J, Prell T, Grosskreutz J (2011) Endoplasmic reticulum stress and the ER mitochondrial calcium cycle in amyotrophic lateral sclerosis. Amyotroph Lateral Scler 13:166-177.

Lehto M, Hynynen R, Karjalainen K, Kuismanen E, Hyvarinen K, Olkkonen VM (2005) Targeting of OSBP-related protein 3 (ORP3) to endoplasmic reticulum and plasma membrane is controlled by multiple determinants. Exp Cell Res 310:445-462.

Lev S, Ben Halevy D, Peretti D, Dahan N (2008) The VAP protein family: from cellular functions to motor neuron disease. Trends Cell Biol 18:282-290.

Loewen CJ, Levine TP (2005) A highly conserved binding site in vesicle-associated membrane protein-associated protein (VAP) for the FFAT motif of lipid-binding proteins. J Biol Chem 280:14097-14104.

Loewen CJ, Roy A, Levine TP (2003) A conserved ER targeting motif in three families of lipid binding proteins and in Opi1p binds VAP. Embo J 22:2025-2035.

Marques VD, Marques W, Jr. (2008) Neurophysiological findings of the late-onset, dominant, proximal spinal muscular atrophies with dysautonomia because of the VAPB PRO56SER mutation. J Clin Neurophysiol 25:233-235.

Marques VD, Barreira AA, Davis MB, Abou-Sleiman PM, Silva WA, Jr., Zago MA, Sobreira C, Fazan V, Marques W, Jr. (2006) Expanding the phenotypes of the Pro56Ser VAPB mutation: proximal SMA with dysautonomia. Muscle Nerve 34:731-739.

Mikitova V, Levine TP (2012) Analysis of the key elements of FFAT-like motifs identifies new proteins that potentially bind VAP on the ER, including two AKAPs and FAPP2. PLoS One 7:e30455.

Millecamps S, Salachas F, Cazeneuve C, Gordon P, Bricka B, Camuzat A, Guillot-Noel L, Russaouen O, Bruneteau G, Pradat PF, Le Forestier N, Vandenberghe N, Danel-Brunaud V, Guy N, Thauvin-Robinet C, Lacomblez L, Couratier P, Hannequin D, Seilhean D, Le Ber I, Corcia P, Camu W, Brice A, Rouleau G, LeGuern E, Meininger V (2010) SOD1, ANG, VAPB, TARDBP, and FUS mutations in familial amyotrophic lateral sclerosis: genotype-phenotype correlations. J Med Genet 47:554-560.

Montenegro G, Rebelo AP, Connell J, Allison R, Babalini C, D'Aloia M, Montieri P, Schule R, Ishiura H, Price J, Strickland A, Gonzalez MA, Baumbach-Reardon L, Deconinck T, Huang J, Bernardi G, Vance JM, Rogers MT, Tsuji S, De Jonghe P, Pericak-Vance MA, Schols L, Orlacchio A, Reid E, Zuchner S (2012) Mutations in the ER-shaping protein reticulon 2 cause the axon-degenerative disorder hereditary spastic paraplegia type 12. J Clin Invest 122:538-544.

Moumen A, Virard I, Raoul C (2011) Accumulation of wildtype and ALS-linked mutated VAPB impairs activity of the proteasome. PLoS One 6:e26066.

Nachreiner T, Esser M, Tenten V, Troost D, Weis J, Kruttgen A (2010) Novel splice variants of the amyotrophic lateral sclerosis-associated gene VAPB expressed in human tissues. Biochem Biophys Res Commun 394:703-708.

Nishimura AL, Mitne-Neto M, Silva HC, Richieri-Costa A, Middleton S, Cascio D, Kok F, Oliveira JR, Gillingwater T, Webb J, Skehel P, Zatz M (2004) A Mutation in the Vesicle-Trafficking Protein VAPB Causes Late-Onset Spinal Muscular Atrophy and Amyotrophic Lateral Sclerosis. Am J Hum Genet 75:822-831.

Nishimura Y, Hayashi M, Inada H, Tanaka T (1999) Molecular cloning and characterization of mammalian homologues of vesicle-associated membrane protein-associated (VAMP-associated) proteins. Biochem Biophys Res Commun 254:21-26.

O'Sullivan NC, Jahn TR, Reid E, O'Kane CJ (2012) Reticulon-like-1, the Drosophila ortholog of the Hereditary Spastic Paraplegia gene reticulon 2, is required for organization of endoplasmic reticulum and of distal motor axons. Hum Mol Genet.

Papiani G, Ruggiano A, Fossati M, Raimondi A, Bertoni G, Francolini M, Benfante R, Navone F, Borgese N (2012) Restructured Endoplasmic Reticulum, Generated by Mutant, Amyotrophic Lateral Sclerosis-Linked VAPB, is Cleared by the Proteasome. J Cell Sci.

Pennetta G, Hiesinger PR, Fabian-Fine R, Meinertzhagen IA, Bellen HJ (2002) Drosophila VAP-33A directs bouton formation at neuromuscular junctions in a dosage-dependent manner. Neuron 35:291-306.

Peretti D, Dahan N, Shimoni E, Hirschberg K, Lev S (2008) Coordinated lipid transfer between the endoplasmic reticulum and the Golgi complex requires the VAP proteins and is essential for Golgi-mediated transport. Mol Biol Cell 19:3871-3884.

Perry RJ, Ridgway ND (2006) Oxysterol-binding protein and vesicle-associated membrane protein-associated protein are required for sterol-dependent activation of the ceramide transport protein. Mol Biol Cell 17:2604-2616.

Ramirez OA, Couve A (2011) The endoplasmic reticulum and protein trafficking in dendrites and axons. Trends Cell Biol 21:219-227.

Ratnaparkhi A, Lawless GM, Schweizer FE, Golshani P, Jackson GR (2008) A Drosophila model of ALS: human ALS-associated mutation in VAP33A suggests a dominant negative mechanism. PLoS ONE 3:e2334.

Renvoise B, Blackstone C (2010) Emerging themes of ER organization in the development and maintenance of axons. Curr Opin Neurobiol 20:531-537.

Rocha N, Kuijl C, van der Kant R, Janssen L, Houben D, Janssen H, Zwart W, Neefjes J (2009) Cholesterol sensor ORP1L contacts the ER protein VAP to control Rab7-RILP-p150 Glued and late endosome positioning. J Cell Biol 185:1209-1225.

Ronzoni R, Anelli T, Brunati M, Cortini M, Fagioli C, Sitia R (2010) Pathogenesis of ER storage disorders: modulating Russell body biogenesis by altering proximal and distal quality control. Traffic 11:947-957.

Rubinsztein DC (2006) The roles of intracellular protein-degradation pathways in neurodegeneration. Nature 443:780-786.

Skovronsky DM, Lee VM, Trojanowski JQ (2006) Neurodegenerative diseases: new concepts of pathogenesis and their therapeutic implications. Annu Rev Pathol 1:151-170.

Smith MH, Ploegh HL, Weissman JS (2011) Road to ruin: targeting proteins for degradation in the endoplasmic reticulum. Science 334:1086-1090.

Snapp EL, Hegde RS, Francolini M, Lombardo F, Colombo S, Pedrazzini E, Borgese N, Lippincott-Schwartz J (2003) Formation of stacked ER cisternae by low affinity protein interactions. J Cell Biol 163:257-269.

Stefan CJ, Manford AG, Baird D, Yamada-Hanff J, Mao Y, Emr SD (2011) Osh proteins regulate phosphoinositide metabolism at ER-plasma membrane contact sites. Cell 144:389-401.

Suzuki H, Kanekura K, Levine TP, Kohno K, Olkkonen VM, Aiso S, Matsuoka M (2009) ALS-linked P56S-VAPB, an aggregated loss-of-function mutant of VAPB, predisposes motor neurons to ER stress-related death by inducing aggregation of co-expressed wild-type VAPB. J Neurochem 108:973-985.

Takei K, Mignery GA, Mugnaini E, Sudhof TC, De Camilli P (1994) Inositol 1,4,5-trisphosphate receptor causes formation of ER cisternal stacks in transfected fibroblasts and in cerebellar Purkinje cells. Neuron 12:327-342.

Teuling E, van Dis V, Wulf PS, Haasdijk ED, Akhmanova A, Hoogenraad CC, Jaarsma D (2008) A novel mouse model with impaired dynein/dynactin function develops amyotrophic lateral sclerosis (ALS)-like features in motor neurons and improves lifespan in SOD1-ALS mice. Hum Mol Genet 17:2849-2862.

Teuling E, Ahmed S, Haasdijk E, Demmers J, Steinmetz MO, Akhmanova A, Jaarsma D, Hoogenraad CC (2007) Motor neuron disease-associated mutant vesicle-associated membrane protein-associated protein (VAP) B recruits wild-type VAPs into endoplasmic reticulum-derived tubular aggregates. J Neurosci 27:9801-9815.

Tran D, Chalhoub A, Schooley A, Zhang W, Ngsee JK (2012) Amyotrophic Lateral Sclerosis Mutant VAPB Causes a Nuclear Envelope Defect. J Cell Sci.

Tsuda H, Han SM, Yang Y, Tong C, Lin YQ, Mohan K, Haueter C, Zoghbi A, Harati Y, Kwan J, Miller MA, Bellen HJ (2008) The amyotrophic lateral sclerosis 8 protein VAPB is cleaved, secreted, and acts as a ligand for Eph receptors. Cell 133:963-977.

Tsujino H, Kondo E, Fukuoka T, Dai Y, Tokunaga A, Miki K, Yonenobu K, Ochi T, Noguchi K (2000) Activating transcription factor 3 (ATF3) induction by axotomy in sensory and motoneurons: A novel neuronal marker of nerve injury. Mol Cell Neurosci 15:170-182.

Tudor EL, Galtrey CM, Perkinton MS, Lau KF, de Vos KJ, Mitchell JC, Ackerley S, Hortobagyi T, Vamos E, Leigh PN, Klasen C, McLoughlin DM, Shaw CE, Miller CC (2010) Amyotrophic lateral sclerosis mutant vesicle-associated membrane protein-associated protein-B transgenic mice develop TAR-DNA-binding protein-43 pathology. Neuroscience.

Tyedmers J, Mogk A, Bukau B (2010) Cellular strategies for controlling protein aggregation. Nat Rev Mol Cell Biol 11:777-788.

van Woerden GM, Harris KD, Hojjati MR, Gustin RM, Qiu S, de Avila Freire R, Jiang YH, Elgersma Y, Weeber EJ (2007) Rescue of neurological deficits in a mouse model for Angelman syndrome by reduction of alphaCaMKII inhibitory phosphorylation. Nat Neurosci 10:280-282.

Vlug AS, Teuling E, Haasdijk ED, French P, Hoogenraad CC, Jaarsma D (2005) ATF3 expression precedes death of spinal motoneurons in amyotrophic lateral sclerosis-SOD1 transgenic mice and correlates with c-Jun phosphorylation, CHOP expression, somato-dendritic ubiquitination and Golgi fragmentation. Eur J Neurosci 22:1881-1894.

Wakana Y, Takai S, Nakajima KI, Tani K, Yamamoto A, Watson P, Stephens DJ, Hauri HP, Tagaya M (2008) Bap31 Is an Itinerant Protein that Moves between the Peripheral ER and a Juxtanuclear Compartment Related to ER-associated Degradation. Mol Biol Cell.

Wang B, Heath-Engel H, Zhang D, Nguyen N, Thomas DY, Hanrahan JW, Shore GC (2008) BAP31 interacts with Sec61 translocons and promotes retrotranslocation of CFTRDeltaF508 via the derlin-1 complex. Cell 133:1080-1092.

Wolf DH, Stolz A (2012) The Cdc48 machine in endoplasmic reticulum associated protein degradation. Biochim Biophys Acta 1823:117-124.

Wyles JP, Ridgway ND (2004) VAMP-associated protein-A regulates partitioning of oxysterol-binding protein-related protein-9 between the endoplasmic reticulum and Golgi apparatus. Exp Cell Res 297:533-547.

Yagi T, Ito D, Nihei Y, Ishihara T, Suzuki N (2011) N88S seipin mutant transgenic mice develop features of seipinopathy/BSCL2-related motor neuron disease via endoplasmic reticulum stress. Hum Mol Genet 20:3831-3840.

Chapter 7

General Discussion

The studies in this thesis were aimed to gain a better understanding of the disease mechanisms underlying ALS. The work focussed on pathological and interventional approaches in transgenic mice that model two forms of ALS, *i.e.* SOD1-ALS and VAPB-ALS. In this chapter common principles learned from these studies that are relevant for other forms of ALS and other late onset progressive neurodegenerative disorders, such as Parkinson's disease and dementia are discussed. The central theme is the role of protein aggregation and the formation of intracellular inclusions in neuronal degeneration. One topic is the regional and cellular specificity of protein aggregation and neuronal degeneration. In addition we discuss the role of trafficking, endoplasmic reticulum and Golgi apparatus in ALS.

7.1 Neuroanatomy of ALS

A key feature of most neurodegenerative diseases is the non-uniform distribution of neurodegenerative changes, while the disease causing proteins usually show ubiquitous expression. Furthermore, pathological and clinical data indicate that at onset pathological changes occur focally in specific populations of neurons and subsequently progress in a relatively predictable way to other brain regions and neuronal populations. The stereotyped progression of pathological or neurodegenerative changes in sporadic Alzheimer's and Parkinson's disease has led to disease staging schemes based on topographic extent of the lesions, the earliest stages occurring long before clinical diagnosis (Braak and Del Tredici, 2009; Braak et al., 2011). These findings also have led to the hypothesis that disorders such as Alzheimer's disease are 'connectopathies', in which the pathological process initiated in a small population of neurons, subsequently spreads via interconnected neurons.

The concept of connectopathy also may apply to ALS, as it by definition requires the involvement of two populations of topographically distant neurons that are synaptically connected: lower motor neurons (LMN, *i.e.* the α-motor neurons in the spinal cord and the brain stem) and upper motor neurons (UMN, *i.e.* neurons in the motor cortex). However, the relative involvement of LMN and UMN is variable among patients, and many neuropathological and neurophysiological studies have suggested a poor topographic correlation between UMN and LMN symptoms (Ravits and La Spada, 2009). In an attempt to reconcile the controversy in the literature it has been proposed that there is a linkage between upper and lower motor symptoms in initial stages of disease when symptoms manifest focally in discrete parts of the body, while this linkage is lost in later stages of the disease, as the degenerative process also may spread to adjacent regions, independent of connectivity (Ravits and La Spada, 2009). This hypothesis implies two types of transcellular disease propagation: 1) via axonal connections such as between LMNs and UMNs; and 2) to neighboring cells which causes local progression and contiguous spread of pathology (Ravits and La Spada, 2009). Such a local spreading of pathology may explain the involvement of glial cells in ALS and other neurodegenerative disease (see below). Importantly, the fact that cells interconnected or contiguous to afflicted cells develop degenerative changes more readily than other cells points to the occurrence of non-cell autonomous disease mechanisms that contribute to or facilitate the degenerative process (see below).

The availability of transgenic mouse models, such as SOD1-ALS mice, that reproduce an ALS-like progressive motor neuron disease enable the precise characterization of neuropathological changes at every stage of disease. It is important to note, however, that the organization and connectivity of UMNs is different between rodents and men (Lemon, 2008). In particular, UMNs in mice do not provide direct synaptic input to LMN, but project to premotor spinal interneurons. This has implications for the propagation of the pathology via UMN axons. In fact, SOD1-ALS mice, despite early and abundant LMN pathology, show no or very limited UMN pathology. This indirectly supports a disease model for SOD1-ALS, in which the disease starts in LMNs and retrogradely spreads to UMNs. Consistent with a retrograde spreading of pathology to neurons that innervate LMNs, in **chapter 2** we show that in SOD1-ALS mice pathological changes (*i.e.* ubiquitin and SOD1-immunoreactive inclusions) appear first in LMN and subsequently in spinal interneurons. Interestingly, the onset of degenerative changes in interneurons preceded the onset of the bulk of motor neuron loss and abnormalities in motor behaviour.

As in ALS patients, motor symptoms in SOD1-ALS mice typically appear asymmetrically in one body part, and subsequently spread to other body parts (Jaarsma et al., 2008). The severity of LMN loss grossly correlates with the region of symptom onset (Jaarsma et al., 2008), indicating that α-motor neuron degeneration occurs non-uniformly. Longitudinal physiological and histological analyses showed that muscle denervation starts before symptom onset (Pun et al., 2006; Hegedus et al., 2008). Different types of LMN display different vulnerability to the disease: the axons from the largest motor neurons that innervate type IIB muscle fibres and form the forceful fast-fatigable (FF) units degenerate first, followed by fast fatigue–resistant (FR) motor neurons, while slow (S) motor neurons innervating type I muscle fibres are relatively resistant to the disease, and are responsible for the bulk of compensatory sprouting (Pun et al., 2006; Hegedus et al., 2008). The absence of obvious motor symptoms despite FF axon denervation and severe loss of maximum muscle strength presumably occurs because FF motor neurons are only recruited during the most forceful tasks. The onset of the clinical phase coincides with the degeneration of FR axons. Together the data indicate that the disease in SOD1-ALS mice starts in FF motor neurons and subsequently involves other motor neurons, and at the same time the spinal interneurons. The early involvement of interneurons, raises the possibility that their degeneration further contributes to the degeneration of motor neurons. For instance, degeneration of inhibitory interneurons is facilitating excitotoxic stress, which is one of the potential factors contributing to motor neuron degeneration in SOD1-ALS (see **chapter 2**).

The data from SOD1-ALS mice discussed above are consistent with data from patients indicating that SOD1-ALS is predominantly an LMN first disorder (Andersen and Al-Chalabi, 2011). In contrast, Alsin-deficient mice develop distal axonal degeneration of UMNs without obvious defects in the LMNs (Deng et al., 2007), which is also compatible with data from ALS2 patients, that in general develop UMN first or UMN only symptoms (Andersen and Al-Chalabi, 2011). Transgenic mice and rats overexpressing wild-type or ALS-mutant TDP-43 in general show short life span and neurodegenerative changes in UMN, LMN, and in other populations of neurons (Tsao et al., 2012). The relevance of these models for ALS has been questioned as LMN loss is relatively limited, and the TDP-43

models do not reproduce a key pathological feature observed in ALS motor neurons, *i.e*. cytoplasmic mislocalization of TDP-43, while developing pathological features that do not occur in ALS patients (Tsao et al., 2012). The presence of pathology in multiple regions, however, is compatible with the presence of TDP-43 pathology in multiple disorders. Analysis of the distribution of TDP-43 pathology in ALS patients shows that, although this pathology preferentially occurs in motor cortex and spinal cord, also other areas are affected (Geser et al., 2008; Nishihira et al., 2008). Interestingly, patients could be classified in two groups on the basis of patterns of distributions of TDP-43 pathology: one group with limited pathology in the non-motor area, the other group with severe non-motor pathology in particular in the fronto-temporal cortex (Geser et al., 2008; Nishihira et al., 2008). These data are compatible with the recent notion that ALS at least in part is mechanistically related to FTD. An interesting possibility would be that the two groups would represent LMN onset ALS, with subsequent spread to UMN, and UMN onset ALS with spread to LMN as well as connected and adjacent cortical areas. Of note, even patients that clinically present with pure LMN symptoms show pathology in motor cortex and other brain areas, albeit limited (Geser et al., 2011). Recent pathological studies have started to identify subtle pathological differences in TDP-43 pathology and other pathological features in genetically distinct ALS forms, *i.e.* ALS with C9ORF72 expansion, and ALS with ataxin-2 intermediate-length polyQ expansions (Hart et al., 2012; Stewart et al., 2012). Further pathological characterisation of ALS forms may uncover the mechanisms underlying TDP-43 abnormalities and their role in ALS pathogenesis.

7.2 A role for cell-to-cell transmission of protein aggregation in ALS

The data discussed above suggest that SOD1-ALS and perhaps other forms of ALS show features of a connectopathy and a nextopathy, implying that cells interconnected or adjacent to afflicted regions develop degenerative changes more readily than other cells. Pointing to the occurrence of non-cell autonomous disease mechanisms that mediate the spreading of the pathological process. A number of mechanisms could explain the disease propagation: disruption of the circuitry resulting in altered synaptic input and trophic support, toxic factors released by activated astrocytes and microglia, diffusion of toxic factors released by dying neurons. There is evidence for a role of glial abnormalities SOD1-ALS (Ilieva et al., 2009); see below). An alternative mechanism that could explain the spread of pathology is transcellular transmission of protein aggregation (Aguzzi and Rajendran, 2009). This mechanism poses that aggregates released from cells are taken up by neighbouring cells, where they enter and facilitate or initiate aggregation in a way reminiscent of spreading of prion protein toxicity (Aguzzi and Rajendran, 2009). Seeding aggregates may be released in the extracellular space as a consequence of cell death, or released via exosomes or exocytosis. Alternatively aggregates might cross synapses, which could explain propagation along interconnected neurons. Evidence favoring transcellular transmission of protein aggregation has been obtained for several neurodegenerative disorders (table 7.1), in particular α-synucleinopathies and tauopathies (Aguzzi and Rajendran, 2009). Most significantly, the importance in human disease is illustrated by the spreading of α-synuclein aggregation to grafted cells in Parkinson's disease patients.

Furthermore, the phenomenon provides a scientific basis for considering antibody based therapeutic approaches, which could operate by scavenging extracellular aggregates.
Compelling evidence favoring a role of a transcellular prion-like seeding mechanism in ALS has been obtained in cellular models of SOD1 aggregation. These studies showed efficient cell to cell transfer of SOD1 aggregates and the ability to transferred SOD1 aggregates to initiate aggregation of soluble mutant SOD1 (Chia et al., 2010; Grad et al., 2011; Münch and Bertolotti, 2011; Münch et al., 2011). Importantly, transcellular seeding can fully explain our pathological data obtained in SOD1-ALS mice which suggest trans-synaptic retrograde spreading of SOD1-aggregation from spinal motor neurons to spinal interneurons in an early preclinical disease phase (**chapter 2**). No data are yet available for cell-to cell transmission of TDP-43 and FUS aggregation, but at least for TDP-43 it is well established that seeds greatly facilitate aggregation and trigger the onset of aggregation in some conditions (Pesiridis et al., 2011; Polymenidou and Cleveland, 2011). Proof for a role for cell-to-cell transmission of protein aggregation in ALS awaits further experiments in cell culture and mice models.

7.3 The role of glial pathology in ALS

Although clinical deficits and irreversible damage mostly are a consequence of neuronal degeneration, in several neurodegenerative disorders inclusions, degenerative changes, and other abnormalities occur in astrocytes or oligodendrocytes (table 7.2). The presence of glial inclusions raise questions about the relationship between inclusion formation in neurons versus glia, and about the contribution of glial pathology to neuronal malfunction and clinical symptoms. High level glial inclusions occur in multiple system atrophy, an atypical parkinsonian disorder characterized by a high density of α-synuclein-positive inclusions in oligodendrocytes (Fellner et al., 2011), and in four repeat tauopathies such as progressive supranuclear palsy and corticobasal degeneration which are characterized by a high level of tau aggregates in astrocytes and oligodendrocytes (Kouri et al., 2011).
In line with a pathogenic role of glial inclusions in these α-synucleopathies and tauopathies, transgenic mice that express α-synuclein or tau selectively in oligodendrocytes or astrocytes, not only develop glial inclusions resembling those observed in the respective human disorders, but also recapitulate aspects of neurodegenerative and clinical changes (Dabir et al., 2004; Forman et al., 2005; Shults et al., 2005). A role for protein aggregation in glia in causing neurological symptoms is also provided by Alexander's disease, which is caused by mutations in the astrocyte specific GFAP (glial fibrilary acidic protein) protein leading to filamentous GFAP aggregates in astrocytes in association with a variable spectrum of neurological abnormalities (Balbi et al., 2010). Glial inclusions also occur in ALS (table 7.2). Cytoplasmatic TDP-43 inclusions have been documented in sporadic, TDP-43, and C9ORF72-expansion ALS (Murray et al., 2011). Frequent oligodendrocytic aggregates also occur in a subset of FUS-ALS patients (Mackenzie et al., 2011). Interestingly, these aggregates that were intensely positive for FUS were associated with a benign slowly progressing form of disease, while absent in patients with rapidly progressing disease, indirectly suggesting a minor role of oligodendrocytic aggregates in FUS-ALS. In contrast, a prominent role for glial pathology has been proposed for SOD1-

ALS (Ilieva et al., 2009). Astrocytic SOD1 inclusions have been documented in a subset of SOD1-ALS patients (Watanabe et al., 2001); and in SOD1-ALS transgenic rodents (Ilieva et al., 2009) (see **chapter 3**). Evidence pointing to a pathogenic role of astrocytic inclusions in SOD1-ALS rodents include the correlation between the presence of astrocytic inclusions and signs of astrocytic malfunction and death and the demonstration that SOD1-ALS mice with reduced expression of mutant SOD1 show prolonged survival (Ilieva et al., 2009; Wang et al., 2011).

Table7.1; prion like properties of aggregation prone proteins

protein	disease	cell to cell	Seeding	evidence	references
SOD1	ALS	yes	Yes	Induction of aggregates of both mutant and wild type protein. Spread of aggregation from cell to cell in cell culture.	1, 2, 3
TDP-43	ALS, FTD		Yes	Seeding of aggregation in vitro and cultured cells	4, 5, 6
FUS/TLS	ALS, FTD			Aggregation prone in vitro.	8
Amyloid β protein	Alzheimer's disease	yes	Yes	Extracellular amyloid β plaques in Amyloid Precursor Protein transgenic mice after injection with brain homogenates of Alzheimer's disease patients. Induction of tau aggregation local and to distant areas of neuronal projections in tau overexpressing mice injected with beta-amyloid protein.	9, 10, 11
tau	tauopathies	yes	Yes	Seeding, aggregates of mutant and wild type protein and spread of pathology to regional areas and to areas of neuronal projections.	12, 13, 14, 15, 16
α-synuclein	Synuclein-opathies	yes	yes	Spread of pathololgy both in vitro and in vivo. Induce pathology in a young synucleinopathy mouse model after injecting brain homogenate from symptomatic synucleinopathy mice.	17, 18, 19, 20, 21, 22
Huntingtin with poly Q repeat	Huntington's disease		yes	Seeding of aggregates in vitro. Striatum specific expression can result in motor abnormalities in a huntington's disease mouse model	23, 24, 25
Prion protein	transmissible sponiform encepha-lopahies	yes	yes	In vitro aggregation with non-pathological protein. Mice develop disease after intracerebral injection with prion protein.	26, 27, 28

Review: (Aguzzi and Rajendran, 2009; Polymenidou and Cleveland, 2011; Aguzzi and Falsig, 2012)
References: 1) Chia et al., 2010; 2) Grad et al., 2011; 3) Münch et al., 2011; 4) Johnson et al., 2009; 5) Furukawa et al., 2011; 6) Guo et al., 2011; 7) Sun et al., 2011; 8) Kahle et al., 2002; 9) Meyer-Luehmann et al., 2006; 10) Bolmont et al., 2007; 11) Eisele et al., 2010; 12) Clavaguera et al., 2009; 13) Nonaka et al., 2010; 14) Guo and Lee, 2011; 15) de Calignon et al., 2012;16) Liu et al., 2012; 17) Kordower et al., 2008; 18) Li et al., 2008; 19) Desplats et al., 2009; 20) Nonaka et al., 2010; 21) Hansen et al., 2011; 22) Mougenot et al., 2012; 23) Gu et al., 2005; 24) Brown et al., 2008; 25) Ren et al., 2009; 26) Saborio et al., 2001; 27) Castilla et al., 2005; 28) Wang et al., 2010

Several lines of evidence indicate that the appearance of astrocytic inclusions and their contribution to the pathogenesis is secondary to neuronal pathology. First, the distribution of astrocytic inclusions is spatially restricted to the brain regions developing neuronal

pathology, and, although not yet fully documented, seemingly develop at a later time point (Jaarsma et al., 2008). Second, neuron-specific expression of mutant SOD1 is sufficient to cause neuronal SOD1 inclusions, and trigger motor neuron degeneration (Jaarsma et al., 2008); **Chapter 2**), while astrocyte-specific expression of mutant SOD1, although causing significant astrocytic hypertrophy and increased GFAP reactivity, does not cause astrocytic SOD1 inclusions or motor neuron pathology (Gong et al., 2000). Third, astrocytic inclusions have been documented for human SOD1-patients with a prolonged clinical course, which could indicate that their formation depends on the chronic astrocytic reaction following neuronal degeneration (Ilieva et al., 2009).

Table 7.2: glial pathology in neurodegerative disease

	astrocyte			oligodendrocyte	
	Inclu-sions	Glio-sis	remarks	Inclu-sions	remarks
Physio-logical role			Blood brain barrier, glycogen storage,modulating synaptic activity, glutamate uptake from synaptic cleft, produce trophic factors (Kandell et al., 2000)		myelination (Kandell et al., 2000)
TDP-43 ALS	+	?	TDP-43 positive inclusions (Murray et al., 2011)	+	cytoplasmic TDP-43 inclusions (Neumann et al., 2007)
FUS/TLS ALS	?	?		+	tangle like inclusions in late-onset cases (Mackenzie et al., 2011)
SOD1 ALS	+	+	hyaline inclusions (Gong et al., 2000; Pardo et al., 2006; Forsberg et al., 2011; Vargas and Johnson, 2010) . *Functional:* mutant SOD1 depletion in astrocyte results in slower disease progression (Clement et al., 2003; Lepore et al., 2008a; Yamanaka et al., 2008a, 2008b)		SOD1 inclusions (Lee et al., 2012).
C9ORF72 ALS	+	?	TDP-43 positive inclusions (Murray et al., 2011)	+	TDP-43 positive aggregates (Brettschneider et al., 2012).
sALS	+	+	hyaline inclusions (Gong et al., 2000; Pardo et al., 2006; Forsberg et al., 2011).	+	
Tauopathy FTD	+		Filamentous tau and ubiqutin positive inclusions, pick bodies (Komori, 1999; Lin et al., 2003a; Dabir et al., 2006). *Functional:* tau expression selectively in astrocytes can induce neurodegenerative disease (Forman et al., 2005).	+	Filamentous tau inclusions, coiled bodies (Lin et al., 2003a). *Funtional:* tau expression selectively in oligodendrocytes can induce neurodegenerative disease (Higuchi et al., 2005).
Tauopathy Alzheimer's disease	?	+	Gliosis, predominantly as a component of neuritic plaques (Marshak et al., 1991).	-	Increased proliferation of NG2 oligodendrocyte progenitor cells (Kang et al., 2010).
tauopathy CBD	+	+	Astrocytic plaques, thorny astrocytes.(Komori, 1999)	+	Coiled bodies, glial threads.

table continues on next page

Table 7.2: glial pathology in neurodegerative disease; continued					
	astrocyte			oligodendrocyte	
	Inclu-sions	Glio -sis	remarks	Inclu-sions	remarks
Tauopathy PSP	+	+	Tau positive, thorny, tufted astrocytes (Yamada et al., 1992a; Komori, 1999; Togo and Dickson, 2002; Ito et al., 2008).	+	Coiled bodies, glial threads (Chin and Goldman, 1996).
Synuclein-opathy MSA	+	+	α-synuclein and ubiquitin positive glial inclusions, gliosis (Ishizawa et al., 2008; Song et al., 2009).	+	α-synuclein, ubiquitin and tau positive inclusions (Papp et al., 1989; Tu et al., 1998). *Functional:* oligendendrocyte specific expression of α-synuclein results in myelin and neuronal damage (Shults et al., 2005).
Synuclein-opathy LBD	?	+	Thufted astrocytes, close to αβ plaques (Hishikawa et al., 2005; Mrak and Griffin, 2007).	+	Coil like inclusions.
Synuclein-opathie Parkinson 's disease	+	+	α-synuclein inclusions; lewy bodies (Knott et al., 1999; Braak et al., 2007; Power and Blumbergs, 2009).	+	α-synuclein positive inclusions, activated oligodendrocytes (Yamada et al., 1992b; Wakabayashi et al., 2000)
Huntingtin Huntington' s disease	?	+	Gliosis, observed early in a huntington's disease mouse model (Burke, 1980; Reddy et al., 1998; Lin et al., 2001). *Functional:* glial expression of mutant huntingtin increases pathology in neuronal huntingtin mice (Bradford et al., 2010).	?	Oligodendrocyte proliferation, non-myeling producing oligodendrocytes (Gunčová et al., 2011).
GFAP Alexander 's disease	+	+	Rosenthal fibers (accumulation of GFAP) in cytoplasm of hypertrophied astrocytes. Reduced GLT-1 expression (Brenner et al., 2001; Tian et al., 2010).	_	Loss of oligodendrocytes (Tian et al., 2010).

FTD = Frontotemporal dementia CBD = Corticobasal degeneration, PSP = Progressive Supranuclear Palsy, MSA = Multiple System Atrophy, LBD = Lewy Body Dementia. Review by (Barres, 2008; De Keyser et al., 2008)

Beside astrocytes and oligodendrocytes, also microglia have been proposed to have a role in ALS as well as other neurodegenerative disease. Microglia activation is a common feature of neurodegenerative diseases, both in man and mice (Alexianu et al., 2001; Ishizawa and Dickson, 2001; Sapp et al., 2001; Hagemann et al., 2005; Mrak and Griffin, 2007; Bellucci et al., 2011). Mutant SOD1 has the ability to activate microglia (Ezzi et al., 2007; Zhao et al., 2010), which in turn are neurotoxic to neurons in co-cultures (Xiao et al., 2007). Mutant SOD1 in microglia alone does not induce a MN phenotype (Beers et al., 2006). However, as with astrocytes, deleting expression of mutant SOD1 from microglia, resulted in a slowing of disease progression (Beers et al., 2006; Boillée et al., 2006). Noticeably, in Alzheimer's disease blocking microglia accumulation increases plaque formation and enhances disease progression (Wyss-Coray et al., 2002; El Khoury et al., 2007). In conclusion, in SOD1-ALS microglia have a role in disease progression, whereas in Alzheimer's disease, they control plaque size and therefore disease progression. Showing a disease specific role for microglia activation.

In **chapter 3** we show that increasing proteotoxic stress in astrocytes of SOD1-ALS mice by crossing them with astrocyte-specific tau mice has a marginal effect on survival, despite abundant tau-pathology in addition to SOD1-aggregates. These data indicate that astrocytic pathology does not have a major role in disease progression. Another finding from this study is that the double transgenic mice develop a high level of tau-pathology in symptomatic mice (*i.e.* at age 25-40 weeks) which is considerably earlier than in tau only mice (**Chapter 3**). This suggests that the neurodegenerative context as observed in SOD1-ALS mice facilitates accumulation of hyperphosphorylated and aggregation prone tau in astrocytes. Preliminary data not documented in **chapter 3** indicate that astrocytes in double transgenic mice despite stressful conditions (*i.e.* high levels of tau and GFAP) do not show earlier appearance of SOD1 aggregates, while showing increased levels of SOD1 aggregation in late stages of disease. Together the data indicate a synergistic deleterious pathological interplay between mutant SOD1 and excessive tau expression, but only after the onset of neurodegenerative changes supporting the notion that glial pathology is secondary to neuronal pathology. It has been proposed that spinal injections of non-mutant astrocytes may be beneficial in SOD1-ALS patients (Lepore et al., 2008b, 2011; Boucherie et al., 2009). According to our data such a treatment at best may have a limited beneficial effect.

Table 7.3, diseases associated with dynein/dynactin mutations

	protein	mutation	Phenotype	references
classical lissencephaly (Miller-Dieker syndrome)	Dync1h1	E1518K, H3822P	Intellectual disability, epilepsy, hypotony and spasticity. Cortical malformation.	1, 2
Charcot-Marie-Tooth disease	Dync1h1	H306R	Motor and sensory neuropathy, mostly affecting the lower limbs.	3
Spinal Muscular Atrophy	Dync1h1	I584L, K617E, Y970C	Early childhood onset of proximal leg weakness with muscle atrophy. No sensory loss.	4
Distal Spinal and Bulbar Muscular Atrophy	DCTN1, p150 glued	P150 glued-G59S	Slowly progressive vocal fold paralysis, progressive weakness and muscle atrophy in the hands and the face, later in the distal lower extremities. Inclusions of dynein/dynactin complex components in motor neurons.	5, 6
Perry syndrome	DCTN1, p150 glued	G71R, G71E, G71A, T72P and Q74P	Parkinsonism, depression, weight loss and hypoventilation. Dopaminergic neuron degeneration, TDP-43 positive neuronal inclusions.	7
ALS	DCTN1, p150 glued	T1249I, M571T, R785W, R1101K	Slowly progressive lower motor neuron disease.	8, 9
Parkinson's disease	DCTN1, p150 glued	R785Q, A1230T, 1288-10C>T	Dopaminergic neuronal degeneration, motor symptoms and as the disease progresses, cognitive symptoms.	10

Reference:s 1) Vissers et al., 2010; 2) Willemsen et al., 2012; 3) Weedon et al., 2011 4) Harms et al., 2012; 5) Puls et al., 2003; 6) Puls et al., 2005; 7) Farrer et al., 2009; 8) Münch et al., 2004; 9) Münch et al., 2005; 10) Vilariño-Güell et al., 2009

7.4 The role of intracellular transport abnormalities in ALS

Chapter 4 describes how inhibition of dynein/dynactin dependent cellular transport via the overexpression of BICD2-N results in ALS-like pathology without cell death (Teuling et al., 2008). The dynein/dynactin protein complex mediates retrograde axonal transport via microtubules. Microtubules in axons are polarized with their plus end towards the synapse and their minus end to the cell body. Transport towards the synapse is mediated by motors of the kinesin superfamily. Kinesins mostly mediate plus-end-directed, where the dynein motor mostly mediates minus-end-directed transport. Retrograde transport in the axon provides a way of maintenance and repair of the axon, but also mediates retrograde signalling, mRNA localization, neurofilament transport, neuronal migration, and protein recycling and degradation.

The dynein/dynactin complex is build up from various subunits. The actual motor protein, dynein, is composed of two heavy chains with a head for ATP-binding and force production, and multiple light, light intermediate and intermediate chains.

Mutations affecting the dynein/dynactin complex, resulting in disease, are loss of function mutations (Willemsen et al., 2012). Table 7.3 shows human disease associated with dynein/dynactin mutations. These diseases are characterized by neuronal death and migration deficits. As in the mouse models (table 7.4), not only the motor neurons are affected. Sensory (Weedon et al., 2011) and dopaminergic neurons (Farrer et al., 2009; Vilariño-Güell et al., 2009) can be affected by these mutations as well.

As shown in Table 7.4, mutations in dynein/dynactin are associated with various neurodegenerative abnormalities. Three mouse models with mutations affecting dynein heavy chain were created, two of which used N-ethyl-N-nitrosourea-induced mutations from independent experiments; *loa* (Legs at odd angles) and the *cra1* (Crawler1) mouse. Homozygous mouse are unable to move and die shortly after birth. Heterozygous mouse develop progressive motor disease (Hafezparast et al., 2003). The third model, was made using radiation induced mutations; Swl (Sprawling), develop sensory neuron loss (Chen et al., 2007). Furthermore, a dynein heavy chain knockout mouse was developed. Homozygous knockout is lethal and the heterozygous animals do not develop a phenotype (Harada et al., 1998).

A mouse model expressing a mutation in one of the dynein light intermediate chains was also developed. These mice develop, beside behavioural abnormalities, defects in neuronal migration and outgrowth, an impairment in endosome trafficking and in Golgi assembly (Banks et al., 2011). Indicating the importance of a well functioning dynein motor.

Mutations in the dynactin complex can disrupt retrograde transport as well. The best know mutation is the G59S mutation in the p150glued subunit associated with lower motor neuron disease (Puls et al., 2003). This mutation is located at the cytoskeleton-associated protein-glycine-rich (CAP-gly) domain, resulting in a disruption of microtubule binding and an impairment of dynactin function (Levy et al., 2006). Various mouse models expressing this mutation, either transgenic (Laird et al., 2008), or knock-in (Lai et al., 2007), were developed. And they all resulted in neurodegenerative disease and protein aggregation. A knock-out of p150glued is embryonically lethal and the heterozygous animals show no phenotype (Lai et al., 2007).

Table 7.4, dynein/dynactin mutations in animal models				
	protein	Mutation	phenotype	references
Legs at odd angels (*Loa)*	Dync1h1	F580Y	Homozygous lethal. Heterozygous: α-MN decrease, lewy like inclusions. SOD1, neurofilament and ubiquitin containing inclusions, reduced fast axonal transport.	1, 2
Crawler 1 *(Cra1)*	Dync1h1	Y1055C	Homozygous lethal, Heterozygous α-MN decrease, lewy like inclusion. SOD1, neurofilament and ubiquitin containing inclusions.	1
Sprawling (Swl)	Dync1h1	9 bp deletion	Homozygous embryonic lethal, Heterozygous early onset sensory neuropathie with muscle spindle deficiency, depletion of ganglion neurons.	3, 4
Dynein heavy chain knock-out	Dynein heavy chain	Dynein heavy chain	Homozygous embryonic lethal. Heteozygous no phenotype.	5
transgenic $P150^{glued}$ G59S	DCTN1, $p150^{glued}$	transgene $P150^{glued}$ G59S	MN disease, vesicular transport defects, neuro muscular junction degeneration, axonal swelling.	6
Knock-in $P150^{glued}$ G59S	DCTN1, $p150^{glued}$	$P150^{glued}$ G59S	Homozygous embryonic lethal, Heterozygous motor neuron disease. Accumulation of vesicular and cytoskeletal proteins at the neuro muscular junction, loss of motor neurons.	7
Knock-out $P150^{glued}$	DCTN1, $p150^{glued}$	$P150^{glued}$	Homozygous embryonic lethal. Heterozygous no phenotype.	7
Dynamitin (p50)	dynamitin	transgenic dynamitin P50 subunit	MN degeneration, NF accumulation, inhibited retrograde transport.	8
dynein	dynein light intermediate chain	N235Y	Increased anxiety, neuronal migration defect.	9

References: 1) Hafezparast et al., 2003; 2) Teuchert et al., 2006; 3) Duchen and Scaravilli, 1977; 4) Chen et al., 2007; 5) Harada et al., 1998; 6) Laird et al., 2008; 7) Lai et al., 2007; 8) LaMonte et al., 2002; 9) Banks et al., 2011

Overexpression of the p50, dynamitin subunit of dynactin destabilizes the complex via the connection of p150glued to Arp1. The p50 overexpressing mouse develop late onset progressive motor neuron degeneration, neurofilament accumulation and a inhibition of retrograde transport (LaMonte et al., 2002). The above models show that dynein/dynactin dependent transport is highly important for neuronal integrity.

In our BICD2-N mice we observe fragmentation of the Golgi apparatus and massive accumulations of neurofilament (NF) (Teuling et al., 2008; **chapter 4**). NF inclusions are an important and well described feature in ALS (Delisle and Carpenter, 1984; Xiao et al., 2006). Even thought a causative link could be expected, in NF heavychain overexpressing mice that develop massive NF accumulations, no Golgi fragmentation was observed (Stieber et al., 2000).

Table 7.5a. GF in disease		
	morphology	references
cell division	Reduction in golgi size during metaphase. Dissapearance of labelling. Reappearing of Golgi structure in telophase	1, 2
apoptosis	Golgi fragmentation, retrograde transport of golgi proteins to the ER.	2
axonal damage	Axonal avulsion: GF into small disconnected elements, Axonal axotomy: no GF	3
sporadic ALS	GF in small, round disconnected profiles. associated with bunina bodies, however no colocalization, basophilic inclusions,	4, 5, 6, 7
SOD1 G93A ALS	GF associated with sod1 aggregates.	4, 5, 6, 7
TDP-43 ALS	GF associated with loss of nuclear TDP-43	8
Optineurin ALS	GF before loss of nuclear TDP-43.	10
Parkinson's disease	GF associated with pale bodies.	11
Multiple system atrophy	GF associated with α-synuclein inclusions, reduced labelling, fragmented Golgi accumulated perinuclear.	12
Creutzfelt Jacob disease	In ballooned neurons; reduced golgi labeling, fragmented Gogli accumulated perinuclear	13
Olivary hypertrophy	Small, disconnected Golgi profiles.	14
Corticobasal degeneration	In ballooned neurons; reduced Golgi labeling, fragmented Golgi accumulated around the nucleus.	13
Niemann Pick disease	GF in cerebellar purkinje cells and cerebral cortical neurons.	15
Alzheimer's disease	GF associated with mitochondria abnormalities, NFT present: GA appears deformed and displaced by NFT no GF. No NFT: small, round disconnected ànd dispersed elements.	16, 17
X-linked spinal and bulbar muscular atrophy	no GF	18

References: 1) Robbins and Gonatas, 1964; 2) Sesso et al., 1999; 3) Fujita et al., 2011; 4) Gonatas et al., 1992; 5) Mourelatos et al., 1994; 6) Stieber et al., 1998; 7) Fujita et al., 1999; 8) Fujita et al., 2000; 9) Fujita et al., 2008; 10) Ito et al., 2011; 11) Fujita et al., 2006; 12) Sakurai et al., 2002; 13) Sakurai et al., 2000; 14) Takamine et al., 2000; 15) Walkley and Suzuki, 2004; 16) Stieber et al., 1996; 17) Baloyannis, 2006; 18) Fujita et al., 2006

7.5 Abnormalities of the ER and the secretory pathways in ALS

Early onset Golgi fragmentation (GF) is one of the hallmarks of ALS and other neurodegenerative diseases, as described in table 7.5a. Animal models of disease recapitulate this phenomenon (Table 7.5b). The significance of this phenomenon is not entirely understood. Nakagomi and collegues describe that excitotoxicity (stimulating NMDA glutamate receptors), reactive oxygen or nitrogen species, and ER stress can induce GF (Nakagomi et al., 2008). Some believe GF is a sign of apoptosis, a process of cell death regulated by caspases. Caspases are known to cleave specific proteins important in Golgi structure, resulting in GF (Machamer, 2003). However, neurons with GF in ALS mouse models do not have other characteristics of apoptosis; *e.g.* eccentric nuclei, and dystrophic neurites (Gonatas et al., 2006). Furthermore the morphology of these fragmented Golgi stacks is not specific for GF in apoptosis. GF in ALS resembles Golgi mini stacks instead

of pinched off vesicles from the cisternae as described in apoptosis (Stieber et al., 1998; Sesso et al., 1999). Other evidence is the absence of a correlation between apoptotic markers and GF both in ALS models (Stieber et al., 2004) and tau expressing cells (Liazoghli et al., 2005). Also *in vitro* studies using cells expressing tau or α-synuclein failed to show a link between GF and apoptosis (Gosavi et al., 2002; Yoshiyama et al., 2003).
The Golgi apparatus is highly important in sorting and targeting proteins from the ER. If the fragmentation of the Golgi apparatus affects this function is not known. A role for ER stress was described in GF. ER stress is an early feature of ALS and a reaction to the accumulation of protein aggregates. A majority of cells expressing ER stress markers show GF and inhibiting ER stress also reduces GF. (Vlug et al., 2005; Nakagomi et al., 2008; Lautenschlaeger et al., 2012).

Table 7.5b. GF in mouse models

	morphology	references
SOD1 ALS	Small, round disconnected golgi profiles, associated with ubiquitinated aggregates. Associated with ATF3, CHOP and p C-JUN upregulation.	1, 2, 3,4
Neurofilament light chain	No GF, in despite of NF accumulation	3
Neurofilament heavy chain	No GF, in despite of NF accumulation	4
tau , JNPL3	Small, round disconnected and dispersed profiles. GF associated with accumulation of hyperphophorylted tau and ballooned neurons	5, 6
BICD2-N	Small, round disconnected golgi profiles in high overexpressing cells.	7
Loa/Loa	Impaired rebuilding of Golgi after nocodazole induced GF.	8
NPC -/- mice	GF similar to Niemann pick's disease patients.	9
ercc delta/-	ATF3 and p53 related golgi redistribution.	10

References: 1) Mourelatos et al., 1996; 2) Stieber et al., 1998; 3) Stieber et al., 2000; 4) Vlug et al., 2005; 5) Lin et al., 2003b; 6) Liazoghli et al., 2005; 7) Teuling et al., 2008; 8) Hafezparast et al., 2003; 9) Walkley and Suzuki, 2004; 10) de Waard et al., 2010.

It is known that the Golgi structure is dependent on an intact microtubule network. Furthermore, intact dynein/dynactin dependent transport is important for Golgi structure. Cells expressing mutant SOD1 showed altered cellular localization of dynein and developed GF (Ligon et al., 2005). Also, inhibition of intracellular transport is described in SOD1 G93A mice (Ligon et al., 2005; Bilsland et al., 2010). We have shown that inhibiting retrograde transport by overexpressing truncated BICD2 in G1del mice results in a an increase of cells with GF to nearly 70% (compared to 1-15%) in these mice (**Chapter 4**; (Teuling et al., 2008), indicating that Golgi morphology is highly dependent on functional cellular transport.
Inhibiting retrograde transport can attenuate disease in mutant SOD1 mice. Breeding the Loa and Cra1 mice to SOD1 G93A mice leads to milder disease phenotypes (Kieran et al., 2005; Teuchert et al., 2006). However, breeding the Swl mice or p150 glued G59S mice with SOD G93A mice does not delay the disease progression (Chen et al., 2007; Lai et al., 2007). In **chapter 4** we observe longer survival of G1del mice when bred with our BICD2-

N mice. The effect of inhibiting transport in SOD1-ALS mice seems to be dependent on the specific mutation and the affected cell type.
One mechanism for this observation might be a delay of signalling axonal damage and therefore delaying a neuronal stress response. An early defect in anterograde transport was described in SOD1 G93A mice (Williamson and Cleveland, 1999; De Vos et al., 2007, 2008), Loa/SOD1 G93A show a restoration of the balance in retrograde and anterograde transport (Kieran et al., 2005). Furthermore distribution of mitochondria is altered in mutant SOD1 expressing cells, there number is reduced in the axon (De Vos et al., 2007; Marinkovic et al., 2012). Possibly a reduced retrograde transport results in increased presence of mitochondria in the axon, resulting in maintenance of energy delivery.
Disrupting axonal transport and GF potentially has a protective effect in ALS pathology, that may be due to a delay in the signalling cascade eventually leading to cell death.

7.6 Quality control in the ER: ERAD, ERPO, ERAC

The cell is equipped with appropriate machinery to defend itself against pathological aggregates. One of the first quality control systems is located in the ER. Chaperones from the heat shock protein family, like HSP70, can detect the misfolded protein. After this detection the cell tries to properly fold the protein. When proper folding fails, the ER associated degradation (ERAD) system is activated to prevent overload of the ER. The misfolded protein is dislocated from the ER, ubiquitinated and recruited to the proteasome system for degradation, using various heat shock proteins and other chaperones such as BIP, to assist in the translocation, from the ER and prevent aggregation.
ERAD is a system that recognizes misfolded proteins and targets them for the proteasomes. Generally, misfolded proteins are recognized and translocated via an ubiqutin ligase complex, like Derlin1 and sec61. The protein is than tagged with ubiquitin and recruited to the proteasome by VCP/P79 and its cofactors UFD1 and NPL4 (Wakana et al., 2008; Smith et al., 2011; Claessen et al., 2012). There are 3 types of ERAD, classified by the localization of the misfolded region (table 7.6). These 3 pathways converge to the VCP /p79 complex and the proteasome.

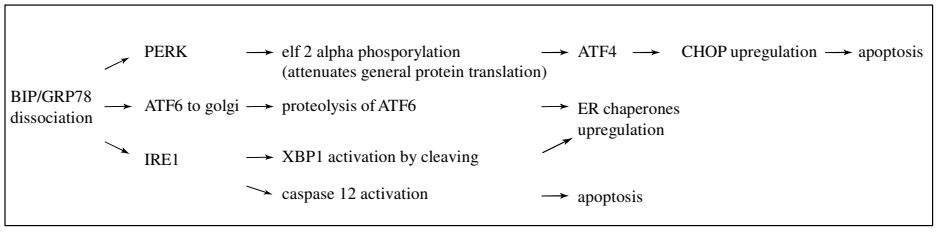

Figure 7.1 ER stress pathway

When ERAD fails, accumulation of misfolded protein leads to ER stress. This is a cell stress response first attenuating transcription, and then eventually leading to apoptosis. There are three known pathways (Fig 7.1). IRE1, ATF6 and PERK are inactivated via an associating with BIP. After BIP dissociation these proteins activate the ER stress cascade. VAPB enhances splicing of XBP1 by IRE1. Mutant VAPB loses this function. Making the cell more vulnerable to ER stress (Kanekura et al., 2009; Chen et al., 2010). Other defense

mechanisms, when ERAD is not able to cope with the misfolded protein, consist in forming an ER protective organelle (ERPO) (Ito and Suzuki, 2009; Yagi et al., 2011; Ito et al., 2012), or an ER associated compartment (ERAC) (Huyer et al., 2004; Fu and Sztul, 2009). ERAC targets proteins for degradation by autophagy. Another example are the Russel bodies, which are dilated cisternae of ER loaded with mutant immunoglobulin (Kopito and Sitia, 2000; Mattioli et al., 2006; Ronzoni et al., 2010) (Table 7.6).

The precise role of these ER compartments is not sure. They contain aggregate-prone proteins, preventing these proteins to form aggregates in the cytosol. In our mutant VABP mouse model we observe ER linked compartments, resembling ERAC. This observation might means that mutant VAPB is contained in this compartment. Other evidence pointing in this direction is the fact that cellular stress results in disappearing of these aggregates, enabling mutant VAPB to exert its toxic effects.

Table 7.6. specialized ER compartments

	role	markers	references
ER stress	Attenuate transcription, activate apoptotic pathways via caspase 12.	BIP/GRP 78, pIRE1, pPERK, ATF6, CHOP	1
ERAD-L	Recruit misfolded proteins in the ER lumen to the proteasome.	recognition: EDEM, EDEM2. Translocation: hrd1, Derlin1, VIMP. Ubiquitin ligase: hrd1, gp78 Ubiquitin-dependent protein degradation: VCP/p97	2, 3, 4
ERAD-M	Recruit misfolded ER membrane proteins to the proteasome.	recogniton: EDEM,EDEM2, ubiquitin ligase:hrd1, gp78, sel1 Ubiquitin-dependent protein degradation: VCP/p97	2, 3, 4
ERAD-C	Recruit ER membrane proteins with a misfolded cytosolic domain to the proteasome	recognition: EDEM, EDEM2 ubiquitin ligase: teb4 Ubiquitin-dependent protein degradation: VCP/p97	2, 3, 4
ERPO	ER derived, separate from the main ER with cytoprotective properties.	overexpressing α1-antitrypsin Z E342K or the ER membrane protein Seipin N88S	5, 6, 7
ERAC	ER related compartment targeting proteins for degradation by autophagy.	Pre-autophagosome: Ape1P, ER markers: Kar2p/Bip, ste14p, ste24p	8, 9
Russell body	Failure of ERAD, compartment where the mutant immunoglobulin is contained.	ER membrane protein: calnexin, ribosomes, ER golgi intermediate compartment (ergic-53)	10, 11, 12

References: 1) Lin et al., 2008; 2) Vashist and Ng, 2004; 3) Carvalho et al., 2006; Yoshida and Tanaka, 2010; 4) Kario et al., 2011; 5) Ito and Suzuki, 2009; 6) Yagi et al., 2011; 7) Ito et al., 2012; 8) Huyer et al., 2004; 9) Fu and Sztul, 2009; 10) Kopito and Sitia, 2000; 11) Mattioli et al., 2006; 12) Ronzoni et al., 2010.

7.7 The heterogenic features of aggregates

As shown by the previous chapters, aggregates are a very important feature of various neurodegenerative diseases. The cell has many protective pathways to prevent toxicity from the pathological aggregates, *e.g.* GF and various protein degradation pathways. These protective mechanisms can be overloaded or even change into a toxic agent on their own.

Recent evidence in Huntington's disease utilizing primary neuronal cultures showed that mutant Huntingtin (Htt) harbouring a polyQ region in inclusion bodies are protective to the cell. They showed that more inclusion bodies are correlated with increased cell survival and that the diffuse, cytosolic staining of mutant Htt was decreased. Therefore it was speculated that these inclusion bodies protect the cell from the toxic properties of mutant Htt (Arrasate

et al., 2004). Furthermore, the survival of the neurons is dependent on the level of mutant Htt and the formation of inclusion bodies, indicating the inclusions represent a defensive mechanism (Miller et al., 2010). In conclusion, inclusion bodies are an adaptive mechanism to prevent toxic aggregates. This notion is confirmed by showing that converting mutant Seipin into ERPO, an ER membrane protein, resulted in a lower cytosolic seipin concentration, attenuating the ER stress response and increased cell survival (Ito et al., 2012). In mutant Ataxin-7 overexpressing mice, ubiquitinated aggregates develop after the onset of neurodegenerative disease, indicating that the aggregates themselves do not trigger the disease (Yoo et al., 2003). In our mutant VAPB overexpressing mice, we observed that the MNs in mice that developed a MN phenotype and ATF3 upregulation, indicating cellular stress, showed no mutant VAPB aggregates. Why these aggregates disappear, possibly increasing the cytosolic levels of mutant VAPB, is not known. The ER compartment could be overloaded, resulting in a total disruption of ER integrity.

In other forms of ALS and neurodegenerative disease characterized by aggregate formation, a direct link between the appearance of ubiquitinated aggregates and disease can be made (Cleveland and Liu, 2000; Deng et al., 2006) Furthermore the distinct upregulation of activated microglia and astrocytes around αβ plaques (Marshak et al., 1991; Bamberger and Landreth, 2001; Streit, 2004), indicates these inclusions can induce neuroinflamation, and have toxic features.

It appears that cells have the ability to prevent the formation of toxic aggregates by containing them in ER specific aggregates. These aggregates will appear numerous throughout the cell and have a protective effect. The disappearing of these aggregates leads to an increase of cytosolic mutant protein, resulting in pathology.

A connection between ALS and various other neurodegenerative diseases can be made. These are usually characterized by protein aggregates as well. Aggregates from different mutant proteins have different characteristics and are handled differently by different neuronal types. These diseases are very dynamic, and pathology can spread progressively throughout the central nervous system.

In the past few years, huge progress was made uncovering many new ALS associated genes, all with specific pathological and clinical features. Showing ALS may not be one disease, but a spectrum of neurodegenerative diseases, with different causative agents.

References

Aguzzi A, Falsig J (2012) Prion propagation, toxicity and degradation. Nature neuroscience 15:936–939.

Aguzzi A, Rajendran L (2009) The transcellular spread of cytosolic amyloids, prions, and prionoids. Neuron 64:783–790.

Alexianu ME, Kozovska M, Appel SH (2001) Immune reactivity in a mouse model of familial ALS correlates with disease progression. Neurology 57:1282–1289.

Andersen PM, Al-Chalabi A (2011) Clinical genetics of amyotrophic lateral sclerosis: what do we really know? Nature reviews Neurology 7:603–615.

Arrasate M, Mitra S, Schweitzer ES, Segal MR, Finkbeiner S (2004) Inclusion body formation reduces levels of mutant huntingtin and the risk of neuronal death. Nature 431:805–810.

Balbi P, Salvini S, Fundarò C, Frazzitta G, Maestri R, Mosah D, Uggetti C, Sechi G (2010) The clinical spectrum of late-onset Alexander disease: a systematic literature review. Journal of neurology 257:1955–1962.

Baloyannis SJ (2006) Mitochondrial alterations in Alzheimer's disease. Journal of Alzheimer's disease : JAD 9:119–126.

Bamberger ME, Landreth GE (2001) Microglial interaction with beta-amyloid: implications for the pathogenesis of Alzheimer's disease. Microscopy research and technique 54:59–70.
Banks GT et al. (2011) Behavioral and other phenotypes in a cytoplasmic Dynein light intermediate chain 1 mutant mouse. The Journal of neuroscience : the official journal of the Society for Neuroscience 31:5483–5494.
Barres BA (2008) The mystery and magic of glia: a perspective on their roles in health and disease. Neuron 60:430–440.
Beers DR, Henkel JS, Xiao Q, Zhao W, Wang J, Yen AA, Siklos L, McKercher SR, Appel SH (2006) Wild-type microglia extend survival in PU.1 knockout mice with familial amyotrophic lateral sclerosis. Proceedings of the National Academy of Sciences of the United States of America 103:16021–16026.
Bellucci A, Bugiani O, Ghetti B, Spillantini MG (2011) Presence of reactive microglia and neuroinflammatory mediators in a case of frontotemporal dementia with P301S mutation. Neuro-degenerative diseases 8:221–229.
Bilsland LG, Sahai E, Kelly G, Golding M, Greensmith L, Schiavo G (2010) Deficits in axonal transport precede ALS symptoms in vivo. Proceedings of the National Academy of Sciences of the United States of America 107:20523–20528.
Boillée S, Yamanaka K, Lobsiger CS, Copeland NG, Jenkins NA, Kassiotis G, Kollias G, Cleveland DW (2006) Onset and progression in inherited ALS determined by motor neurons and microglia. Science (New York, NY) 312:1389–1392.
Bolmont T, Clavaguera F, Meyer-Luehmann M, Herzig MC, Radde R, Staufenbiel M, Lewis J, Hutton M, Tolnay M, Jucker M (2007) Induction of tau pathology by intracerebral infusion of amyloid-beta -containing brain extract and by amyloid-beta deposition in APP x Tau transgenic mice. The American journal of pathology 171:2012–2020.
Boucherie C, Schäfer S, Lavand'homme P, Maloteaux J-M, Hermans E (2009) Chimerization of astroglial population in the lumbar spinal cord after mesenchymal stem cell transplantation prolongs survival in a rat model of amyotrophic lateral sclerosis. Journal of neuroscience research 87:2034–2046.
Braak H, Del Tredici K (2009) Neuroanatomy and pathology of sporadic Parkinson's disease. Advances in anatomy, embryology, and cell biology 201:1–119.
Braak H, Sastre M, Del Tredici K (2007) Development of alpha-synuclein immunoreactive astrocytes in the forebrain parallels stages of intraneuronal pathology in sporadic Parkinson's disease. Acta neuropathologica 114:231–241.
Braak H, Thal DR, Ghebremedhin E, Del Tredici K (2011) Stages of the pathologic process in Alzheimer disease: age categories from 1 to 100 years. Journal of neuropathology and experimental neurology 70:960–969.
Bradford J, Shin J-Y, Roberts M, Wang C-E, Sheng G, Li S, Li X-J (2010) Mutant huntingtin in glial cells exacerbates neurological symptoms of Huntington disease mice. The Journal of biological chemistry 285:10653–10661.
Brenner M, Johnson AB, Boespflug-Tanguy O, Rodriguez D, Goldman JE, Messing A (2001) Mutations in GFAP, encoding glial fibrillary acidic protein, are associated with Alexander disease. Nature genetics 27:117–120.
Brettschneider J, Toledo JB, Van Deerlin VM, Elman L, McCluskey L, Lee VM-Y, Trojanowski JQ (2012) Microglial activation correlates with disease progression and upper motor neuron clinical symptoms in amyotrophic lateral sclerosis. PloS one 7:e39216.
Brown TB, Bogush AI, Ehrlich ME (2008) Neocortical expression of mutant huntingtin is not required for alterations in striatal gene expression or motor dysfunction in a transgenic mouse. Human molecular genetics 17:3095–3104.
Burke R (1980) Motor unit types: functional specializations in motor control. Trends in Neurosciences 3:255–258.
Carvalho P, Goder V, Rapoport TA (2006) Distinct ubiquitin-ligase complexes define convergent pathways for the degradation of ER proteins. Cell 126:361–373.
Castilla J, Saá P, Hetz C, Soto C (2005) In vitro generation of infectious scrapie prions. Cell 121:195–206.
Chen H-J, Anagnostou G, Chai A, Withers J, Morris A, Adhikaree J, Pennetta G, de Belleroche JS (2010) Characterization of the properties of a novel mutation in VAPB in familial amyotrophic lateral sclerosis. The Journal of biological chemistry 285:40266–40281.
Chen X-J, Levedakou EN, Millen KJ, Wollmann RL, Soliven B, Popko B (2007) Proprioceptive sensory neuropathy in mice with a mutation in the cytoplasmic Dynein heavy chain 1 gene. The Journal of neuroscience : the official journal of the Society for Neuroscience 27:14515–14524.
Chia R, Tattum MH, Jones S, Collinge J, Fisher EMC, Jackson GS (2010) Superoxide dismutase 1 and tgSOD1 mouse spinal cord seed fibrils, suggesting a propagative cell death mechanism in amyotrophic lateral sclerosis. PloS one 5:e10627.
Chin SS, Goldman JE (1996) Glial inclusions in CNS degenerative diseases. Journal of neuropathology and experimental neurology 55:499–508.
Claessen JHL, Kundrat L, Ploegh HL (2012) Protein quality control in the ER: balancing the ubiquitin checkbook. Trends in cell biology 22:22–32.

Clavaguera F, Bolmont T, Crowther RA, Abramowski D, Frank S, Probst A, Fraser G, Stalder AK, Beibel M, Staufenbiel M, Jucker M, Goedert M, Tolnay M (2009) Transmission and spreading of tauopathy in transgenic mouse brain. Nature cell biology 11:909–913.

Clement AM, Nguyen MD, Roberts EA, Garcia ML, Boillée S, Rule M, McMahon AP, Doucette W, Siwek D, Ferrante RJ, Brown RH, Julien J-P, Goldstein LSB, Cleveland DW (2003) Wild-type nonneuronal cells extend survival of SOD1 mutant motor neurons in ALS mice. Science (New York, NY) 302:113–117.

Cleveland DW, Liu J (2000) Oxidation versus aggregation - how do SOD1 mutants cause ALS? Nature medicine 6:1320–1321.

Dabir DV, Robinson MB, Swanson E, Zhang B, Trojanowski JQ, Lee VM-Y, Forman MS (2006) Impaired glutamate transport in a mouse model of tau pathology in astrocytes. The Journal of neuroscience : the official journal of the Society for Neuroscience 26:644–654.

Dabir DV, Trojanowski JQ, Richter-Landsberg C, Lee VM-Y, Forman MS (2004) Expression of the small heat-shock protein alphaB-crystallin in tauopathies with glial pathology. The American journal of pathology 164:155–166.

de Calignon A, Polydoro M, Suárez-Calvet M, William C, Adamowicz DH, Kopeikina KJ, Pitstick R, Sahara N, Ashe KH, Carlson GA, Spires-Jones TL, Hyman BT (2012) Propagation of tau pathology in a model of early Alzheimer's disease. Neuron 73:685–697.

De Keyser J, Mostert JP, Koch MW (2008) Dysfunctional astrocytes as key players in the pathogenesis of central nervous system disorders. Journal of the neurological sciences 267:3–16.

De Vos KJ, Chapman AL, Tennant ME, Manser C, Tudor EL, Lau K-F, Brownlees J, Ackerley S, Shaw PJ, McLoughlin DM, Shaw CE, Leigh PN, Miller CCJ, Grierson AJ (2007) Familial amyotrophic lateral sclerosis-linked SOD1 mutants perturb fast axonal transport to reduce axonal mitochondria content. Human molecular genetics 16:2720–2728.

De Vos KJ, Grierson AJ, Ackerley S, Miller CCJ (2008) Role of axonal transport in neurodegenerative diseases. Annual review of neuroscience 31:151–173.

de Waard MC, van der Pluijm I, Zuiderveen Borgesius N, Comley LH, Haasdijk ED, Rijksen Y, Ridwan Y, Zondag G, Hoeijmakers JHJ, Elgersma Y, Gillingwater TH, Jaarsma D (2010) Age-related motor neuron degeneration in DNA repair-deficient Ercc1 mice. Acta neuropathologica 120:461–475.

Delisle MB, Carpenter S (1984) Neurofibrillary axonal swellings and amyotrophic lateral sclerosis. Journal of the neurological sciences 63:241–250.

Deng H-X, Shi Y, Furukawa Y, Zhai H, Fu R, Liu E, Gorrie GH, Khan MS, Hung W-Y, Bigio EH, Lukas T, Dal Canto MC, O'Halloran TV, Siddique T (2006) Conversion to the amyotrophic lateral sclerosis phenotype is associated with intermolecular linked insoluble aggregates of SOD1 in mitochondria. Proceedings of the National Academy of Sciences of the United States of America 103:7142–7147.

Deng H-X, Zhai H, Fu R, Shi Y, Gorrie GH, Yang Y, Liu E, Dal Canto MC, Mugnaini E, Siddique T (2007) Distal axonopathy in an alsin-deficient mouse model. Human molecular genetics 16:2911–2920.

Desplats P, Lee H-J, Bae E-J, Patrick C, Rockenstein E, Crews L, Spencer B, Masliah E, Lee S-J (2009) Inclusion formation and neuronal cell death through neuron-to-neuron transmission of alpha-synuclein. Proceedings of the National Academy of Sciences of the United States of America 106:13010–13015.

Duchen LW, Scaravilli F (1977) Quantitative and electron microscopic studies of sensory ganglion cells of the Sprawling mouse. Journal of neurocytology 6:465–481.

Eisele YS, Obermüller U, Heilbronner G, Baumann F, Kaeser SA, Wolburg H, Walker LC, Staufenbiel M, Heikenwalder M, Jucker M (2010) Peripherally applied Abeta-containing inoculates induce cerebral beta-amyloidosis. Science (New York, NY) 330:980–982.

El Khoury J, Toft M, Hickman SE, Means TK, Terada K, Geula C, Luster AD (2007) Ccr2 deficiency impairs microglial accumulation and accelerates progression of Alzheimer-like disease. Nature medicine 13:432–438.

Ezzi SA, Urushitani M, Julien J-P (2007) Wild-type superoxide dismutase acquires binding and toxic properties of ALS-linked mutant forms through oxidation. Journal of neurochemistry 102:170–178.

Farrer MJ et al. (2009) DCTN1 mutations in Perry syndrome. Nature genetics 41:163–165.

Fellner L, Jellinger KA, Wenning GK, Stefanova N (2011) Glial dysfunction in the pathogenesis of α-synucleinopathies: emerging concepts. Acta neuropathologica 121:675–693.

Forman MS, Lal D, Zhang B, Dabir DV, Swanson E, Lee VM-Y, Trojanowski JQ (2005) Transgenic mouse model of tau pathology in astrocytes leading to nervous system degeneration. The Journal of neuroscience : the official journal of the Society for Neuroscience 25:3539–3550.

Forsberg K, Andersen PM, Marklund SL, Brännström T (2011) Glial nuclear aggregates of superoxide dismutase-1 are regularly present in patients with amyotrophic lateral sclerosis. Acta neuropathologica 121:623–634.

Fu L, Sztul E (2009) ER-associated complexes (ERACs) containing aggregated cystic fibrosis transmembrane conductance regulator (CFTR) are degraded by autophagy. European journal of cell biology 88:215–226.

Fujita Y, Mizuno Y, Takatama M, Okamoto K (2008) Anterior horn cells with abnormal TDP-43 immunoreactivities show fragmentation of the Golgi apparatus in ALS. Journal of the neurological sciences 269:30–34.

Fujita Y, Ohama E, Takatama M, Al-Sarraj S, Okamoto K (2006) Fragmentation of Golgi apparatus of nigral neurons with alpha-synuclein-positive inclusions in patients with Parkinson's disease. Acta neuropathologica 112:261–265.

Fujita Y, Okamoto K, Sakurai A, Amari M, Nakazato Y, Gonatas NK (1999) Fragmentation of the Golgi apparatus of Betz cells in patients with amyotrophic lateral sclerosis. Journal of the neurological sciences 163:81–85.

Fujita Y, Okamoto K, Sakurai A, Gonatas NK, Hirano A (2000) Fragmentation of the Golgi apparatus of the anterior horn cells in patients with familial amyotrophic lateral sclerosis with SOD1 mutations and posterior column involvement. Journal of the neurological sciences 174:137–140.

Fujita Y, Watabe K, Ikeda K, Mizuno Y, Okamoto K (2011) Morphological changes of Golgi apparatus in adult rats after facial nerve injuries. Neuropathology : official journal of the Japanese Society of Neuropathology 31:42–47.

Furukawa Y, Kaneko K, Watanabe S, Yamanaka K, Nukina N (2011) A seeding reaction recapitulates intracellular formation of Sarkosyl-insoluble transactivation response element (TAR) DNA-binding protein-43 inclusions. The Journal of biological chemistry 286:18664–18672.

Geser F, Brandmeir NJ, Kwong LK, Martinez-Lage M, Elman L, McCluskey L, Xie SX, Lee VM-Y, Trojanowski JQ (2008) Evidence of multisystem disorder in whole-brain map of pathological TDP-43 in amyotrophic lateral sclerosis. Archives of neurology 65:636–641.

Geser F, Stein B, Partain M, Elman LB, McCluskey LF, Xie SX, Van Deerlin VM, Kwong LK, Lee VM-Y, Trojanowski JQ (2011) Motor neuron disease clinically limited to the lower motor neuron is a diffuse TDP-43 proteinopathy. Acta neuropathologica 121:509–517.

Gonatas NK, Stieber A, Gonatas JO (2006) Fragmentation of the Golgi apparatus in neurodegenerative diseases and cell death. Journal of the neurological sciences 246:21–30.

Gonatas NK, Stieber A, Mourelatos Z, Chen Y, Gonatas JO, Appel SH, Hays AP, Hickey WF, Hauw JJ (1992) Fragmentation of the Golgi apparatus of motor neurons in amyotrophic lateral sclerosis. The American journal of pathology 140:731–737.

Gong YH, Parsadanian AS, Andreeva A, Snider WD, Elliott JL (2000) Restricted expression of G86R Cu/Zn superoxide dismutase in astrocytes results in astrocytosis but does not cause motoneuron degeneration. The Journal of neuroscience : the official journal of the Society for Neuroscience 20:660–665.

Gosavi N, Lee H-J, Lee JS, Patel S, Lee S-J (2002) Golgi fragmentation occurs in the cells with prefibrillar alpha-synuclein aggregates and precedes the formation of fibrillar inclusion. The Journal of biological chemistry 277:48984–48992.

Grad LI, Guest WC, Yanai A, Pokrishevsky E, O'Neill MA, Gibbs E, Semenchenko V, Yousefi M, Wishart DS, Plotkin SS, Cashman NR (2011) Intermolecular transmission of superoxide dismutase 1 misfolding in living cells. Proceedings of the National Academy of Sciences of the United States of America 108:16398–16403.

Gu X, Li C, Wei W, Lo V, Gong S, Li S-H, Iwasato T, Itohara S, Li X-J, Mody I, Heintz N, Yang XW (2005) Pathological cell-cell interactions elicited by a neuropathogenic form of mutant Huntingtin contribute to cortical pathogenesis in HD mice. Neuron 46:433–444.

Gunčová I, Látr I, Mazurová Y (2011) The neurodegenerative process in a neurotoxic rat model and in patients with Huntington's disease: histopathological parallels and differences. Acta histochemica 113:783–792.

Guo JL, Lee VM-Y (2011) Seeding of normal Tau by pathological Tau conformers drives pathogenesis of Alzheimer-like tangles. The Journal of biological chemistry 286:15317–15331.

Guo W et al. (2011) An ALS-associated mutation affecting TDP-43 enhances protein aggregation, fibril formation and neurotoxicity. Nature structural & molecular biology 18:822–830.

Hafezparast M et al. (2003) Mutations in dynein link motor neuron degeneration to defects in retrograde transport. Science (New York, NY) 300:808–812.

Hagemann TL, Gaeta SA, Smith MA, Johnson DA, Johnson JA, Messing A (2005) Gene expression analysis in mice with elevated glial fibrillary acidic protein and Rosenthal fibers reveals a stress response followed by glial activation and neuronal dysfunction. Human molecular genetics 14:2443–2458.

Hansen C, Angot E, Bergström A-L, Steiner JA, Pieri L, Paul G, Outeiro TF, Melki R, Kallunki P, Fog K, Li J-Y, Brundin P (2011) α-Synuclein propagates from mouse brain to grafted dopaminergic neurons and seeds aggregation in cultured human cells. The Journal of clinical investigation 121:715–725.

Harada A, Takei Y, Kanai Y, Tanaka Y, Nonaka S, Hirokawa N (1998) Golgi vesiculation and lysosome dispersion in cells lacking cytoplasmic dynein. The Journal of cell biology 141:51–59.

Harms MB, Ori-McKenney KM, Scoto M, Tuck EP, Bell S, Ma D, Masi S, Allred P, Al-Lozi M, Reilly MM, Miller LJ, Jani-Acsadi A, Pestronk A, Shy ME, Muntoni F, Vallee RB, Baloh RH (2012) Mutations in the tail domain of DYNC1H1 cause dominant spinal muscular atrophy. Neurology 78:1714–1720.

Hart MP, Brettschneider J, Lee VMY, Trojanowski JQ, Gitler AD (2012) Distinct TDP-43 pathology in ALS patients with ataxin 2 intermediate-length polyQ expansions. Acta neuropathologica 124:221–230.

Hegedus J, Putman CT, Tyreman N, Gordon T (2008) Preferential motor unit loss in the SOD1 G93A transgenic mouse model of amyotrophic lateral sclerosis. The Journal of physiology 586:3337–3351.

Higuchi M, Zhang B, Forman MS, Yoshiyama Y, Trojanowski JQ, Lee VM-Y (2005) Axonal degeneration induced by targeted expression of mutant human tau in oligodendrocytes of transgenic mice that model glial

tauopathies. The Journal of neuroscience : the official journal of the Society for Neuroscience 25:9434–9443.
Hishikawa N, Hashizume Y, Yoshida M, Niwa J-I, Tanaka F, Sobue G (2005) Tuft-shaped astrocytes in Lewy body disease. Acta neuropathologica 109:373–380.
Huyer G, Longsworth GL, Mason DL, Mallampalli MP, McCaffery JM, Wright RL, Michaelis S (2004) A striking quality control subcompartment in Saccharomyces cerevisiae: the endoplasmic reticulum-associated compartment. Molecular biology of the cell 15:908–921.
Ilieva H, Polymenidou M, Cleveland DW (2009) Non-cell autonomous toxicity in neurodegenerative disorders: ALS and beyond. The Journal of cell biology 187:761–772.
Ishizawa K, Dickson DW (2001) Microglial activation parallels system degeneration in progressive supranuclear palsy and corticobasal degeneration. Journal of neuropathology and experimental neurology 60:647–657.
Ishizawa K, Komori T, Arai N, Mizutani T, Hirose T (2008) Glial cytoplasmic inclusions and tissue injury in multiple system atrophy: A quantitative study in white matter (olivopontocerebellar system) and gray matter (nigrostriatal system). Neuropathology : official journal of the Japanese Society of Neuropathology 28:249–257.
Ito D, Suzuki N (2009) Seipinopathy: a novel endoplasmic reticulum stress-associated disease. Brain : a journal of neurology 132:8–15.
Ito D, Yagi T, Ikawa M, Suzuki N (2012) Characterization of inclusion bodies with cytoprotective properties formed by seipinopathy-linked mutant seipin. Human molecular genetics 21:635–646.
Ito H, Fujita K, Nakamura M, Wate R, Kaneko S, Sasaki S, Yamane K, Suzuki N, Aoki M, Shibata N, Togashi S, Kawata A, Mochizuki Y, Mizutani T, Maruyama H, Hirano A, Takahashi R, Kawakami H, Kusaka H (2011) Optineurin is co-localized with FUS in basophilic inclusions of ALS with FUS mutation and in basophilic inclusion body disease. Acta neuropathologica 121:555–557.
Ito K, Arai K, Yoshiyama Y, Kashiwado K, Sakakibara Y, Hattori T (2008) Astrocytic tau pathology positively correlates with neurofibrillary tangle density in progressive supranuclear palsy. Acta neuropathologica 115:623–628.
Jaarsma D, Teuling E, Haasdijk ED, De Zeeuw CI, Hoogenraad CC (2008) Neuron-specific expression of mutant superoxide dismutase is sufficient to induce amyotrophic lateral sclerosis in transgenic mice. The Journal of neuroscience : the official journal of the Society for Neuroscience 28:2075–2088.
Johnson BS, Snead D, Lee JJ, McCaffery JM, Shorter J, Gitler AD (2009) TDP-43 is intrinsically aggregation-prone, and amyotrophic lateral sclerosis-linked mutations accelerate aggregation and increase toxicity. The Journal of biological chemistry 284:20329–20339.
Kahle PJ, Neumann M, Ozmen L, Muller V, Jacobsen H, Spooren W, Fuss B, Mallon B, Macklin WB, Fujiwara H, Hasegawa M, Iwatsubo T, Kretzschmar HA, Haass C (2002) Hyperphosphorylation and insolubility of alpha-synuclein in transgenic mouse oligodendrocytes. EMBO reports 3:583–588.
Kandell ER, Schwartz JH, Jessel TM (2000) Principles of neural Science. McGraw-Hill Compagnies.
Kanekura K, Suzuki H, Aiso S, Matsuoka M (2009) ER stress and unfolded protein response in amyotrophic lateral sclerosis. Molecular neurobiology 39:81–89.
Kang SH, Fukaya M, Yang JK, Rothstein JD, Bergles DE (2010) NG2+ CNS glial progenitors remain committed to the oligodendrocyte lineage in postnatal life and following neurodegeneration. Neuron 68:668–681.
Kario E, Amar N, Elazar Z, Navon A (2011) A new autophagy-related checkpoint in the degradation of an ERAD-M target. The Journal of biological chemistry 286:11479–11491.
Kieran D, Hafezparast M, Bohnert S, Dick JRT, Martin J, Schiavo G, Fisher EMC, Greensmith L (2005) A mutation in dynein rescues axonal transport defects and extends the life span of ALS mice. The Journal of cell biology 169:561–567.
Knott C, Wilkin GP, Stern G (1999) Astrocytes and microglia in the substantia nigra and caudate-putamen in Parkinson's disease. Parkinsonism & related disorders 5:115–122.
Komori T (1999) Tau-positive glial inclusions in progressive supranuclear palsy, corticobasal degeneration and Pick's disease. Brain pathology (Zurich, Switzerland) 9:663–679.
Kopito RR, Sitia R (2000) Aggresomes and Russell bodies. Symptoms of cellular indigestion? EMBO reports 1:225–231.
Kordower JH, Chu Y, Hauser RA, Freeman TB, Olanow CW (2008) Lewy body-like pathology in long-term embryonic nigral transplants in Parkinson's disease. Nature medicine 14:504–506.
Kouri N, Whitwell JL, Josephs KA, Rademakers R, Dickson DW (2011) Corticobasal degeneration: a pathologically distinct 4R tauopathy. Nature reviews Neurology 7:263–272.
Lai C, Lin X, Chandran J, Shim H, Yang W-J, Cai H (2007) The G59S mutation in p150(glued) causes dysfunction of dynactin in mice. The Journal of neuroscience : the official journal of the Society for Neuroscience 27:13982–13990.
Laird FM, Farah MH, Ackerley S, Hoke A, Maragakis N, Rothstein JD, Griffin J, Price DL, Martin LJ, Wong PC (2008) Motor neuron disease occurring in a mutant dynactin mouse model is characterized by defects in vesicular trafficking. The Journal of neuroscience : the official journal of the Society for Neuroscience 28:1997–2005.

LaMonte BH, Wallace KE, Holloway BA, Shelly SS, Ascaño J, Tokito M, Van Winkle T, Howland DS, Holzbaur ELF (2002) Disruption of dynein/dynactin inhibits axonal transport in motor neurons causing late-onset progressive degeneration. Neuron 34:715–727.

Lautenschlaeger J, Prell T, Grosskreutz J (2012) Endoplasmic reticulum stress and the ER mitochondrial calcium cycle in amyotrophic lateral sclerosis. Amyotrophic lateral sclerosis : official publication of the World Federation of Neurology Research Group on Motor Neuron Diseases 13:166–177.

Lee Y, Morrison BM, Li Y, Lengacher S, Farah MH, Hoffman PN, Liu Y, Tsingalia A, Jin L, Zhang PW, others (2012) Oligodendroglia metabolically support axons and contribute to neurodegeneration. Nature.

Lemon RN (2008) Descending pathways in motor control. Annual review of neuroscience 31:195–218.

Lepore AC, Dejea C, Carmen J, Rauck B, Kerr DA, Sofroniew MV, Maragakis NJ (2008a) Selective ablation of proliferating astrocytes does not affect disease outcome in either acute or chronic models of motor neuron degeneration. Experimental neurology 211:423–432.

Lepore AC, O'Donnell J, Kim AS, Williams T, Tuteja A, Rao MS, Kelley LL, Campanelli JT, Maragakis NJ (2011) Human glial-restricted progenitor transplantation into cervical spinal cord of the SOD1 mouse model of ALS. PloS one 6:e25968.

Lepore AC, Rauck B, Dejea C, Pardo AC, Rao MS, Rothstein JD, Maragakis NJ (2008b) Focal transplantation-based astrocyte replacement is neuroprotective in a model of motor neuron disease. Nature neuroscience 11:1294–1301.

Levy JR, Sumner CJ, Caviston JP, Tokito MK, Ranganathan S, Ligon LA, Wallace KE, LaMonte BH, Harmison GG, Puls I, Fischbeck KH, Holzbaur ELF (2006) A motor neuron disease-associated mutation in p150Glued perturbs dynactin function and induces protein aggregation. The Journal of cell biology 172:733–745.

Li J-Y, Englund E, Holton JL, Soulet D, Hagell P, Lees AJ, Lashley T, Quinn NP, Rehncrona S, Björklund A, Widner H, Revesz T, Lindvall O, Brundin P (2008) Lewy bodies in grafted neurons in subjects with Parkinson's disease suggest host-to-graft disease propagation. Nature medicine 14:501–503.

Liazoghli D, Perreault S, Micheva KD, Desjardins M, Leclerc N (2005) Fragmentation of the Golgi apparatus induced by the overexpression of wild-type and mutant human tau forms in neurons. The American journal of pathology 166:1499–1514.

Ligon LA, LaMonte BH, Wallace KE, Weber N, Kalb RG, Holzbaur ELF (2005) Mutant superoxide dismutase disrupts cytoplasmic dynein in motor neurons. Neuroreport 16:533–536.

Lin CH, Tallaksen-Greene S, Chien WM, Cearley JA, Jackson WS, Crouse AB, Ren S, Li XJ, Albin RL, Detloff PJ (2001) Neurological abnormalities in a knock-in mouse model of Huntington's disease. Human molecular genetics 10:137–144.

Lin JH, Walter P, Yen TSB (2008) Endoplasmic reticulum stress in disease pathogenesis. Annual review of pathology 3:399–425.

Lin W-L, Lewis J, Yen S-H, Hutton M, Dickson DW (2003a) Filamentous tau in oligodendrocytes and astrocytes of transgenic mice expressing the human tau isoform with the P301L mutation. The American journal of pathology 162:213–218.

Lin W-L, Lewis J, Yen S-H, Hutton M, Dickson DW (2003b) Ultrastructural neuronal pathology in transgenic mice expressing mutant (P301L) human tau. Journal of neurocytology 32:1091–1105.

Liu L, Drouet V, Wu JW, Witter MP, Small SA, Clelland C, Duff K (2012) Trans-synaptic spread of tau pathology in vivo. PloS one 7:e31302.

Machamer CE (2003) Golgi disassembly in apoptosis: cause or effect? Trends in cell biology 13:279–281.

Mackenzie IRA, Ansorge O, Strong M, Bilbao J, Zinman L, Ang L-C, Baker M, Stewart H, Eisen A, Rademakers R, Neumann M (2011) Pathological heterogeneity in amyotrophic lateral sclerosis with FUS mutations: two distinct patterns correlating with disease severity and mutation. Acta neuropathologica 122:87–98.

Marinkovic P, Reuter MS, Brill MS, Godinho L, Kerschensteiner M, Misgeld T (2012) Axonal transport deficits and degeneration can evolve independently in mouse models of amyotrophic lateral sclerosis. Proceedings of the National Academy of Sciences of the United States of America 109:4296–4301.

Marshak DR, Pesce SA, Stanley LC, Griffin WS (1991) Increased S100 beta neurotrophic activity in Alzheimer's disease temporal lobe. Neurobiology of aging 13:1–7.

Mattioli L, Anelli T, Fagioli C, Tacchetti C, Sitia R, Valetti C (2006) ER storage diseases: a role for ERGIC-53 in controlling the formation and shape of Russell bodies. Journal of cell science 119:2532–2541.

Meyer-Luehmann M, Coomaraswamy J, Bolmont T, Kaeser S, Schaefer C, Kilger E, Neuenschwander A, Abramowski D, Frey P, Jaton AL, Vigouret J-M, Paganetti P, Walsh DM, Mathews PM, Ghiso J, Staufenbiel M, Walker LC, Jucker M (2006) Exogenous induction of cerebral beta-amyloidogenesis is governed by agent and host. Science (New York, NY) 313:1781–1784.

Miller J, Arrasate M, Shaby BA, Mitra S, Masliah E, Finkbeiner S (2010) Quantitative relationships between huntingtin levels, polyglutamine length, inclusion body formation, and neuronal death provide novel insight into huntington's disease molecular pathogenesis. The Journal of neuroscience : the official journal of the Society for Neuroscience 30:10541–10550.

Mougenot A-L, Nicot S, Bencsik A, Morignat E, Verchère J, Lakhdar L, Legastelois S, Baron T (2012) Prion-like acceleration of a synucleinopathy in a transgenic mouse model. Neurobiology of aging 33:2225–2228.

Mourelatos Z, Gonatas NK, Stieber A, Gurney ME, Dal Canto MC (1996) The Golgi apparatus of spinal cord motor neurons in transgenic mice expressing mutant Cu,Zn superoxide dismutase becomes fragmented in early, preclinical stages of the disease. Proceedings of the National Academy of Sciences of the United States of America 93:5472–5477.

Mourelatos Z, Hirano A, Rosenquist AC, Gonatas NK (1994) Fragmentation of the Golgi apparatus of motor neurons in amyotrophic lateral sclerosis (ALS). Clinical studies in ALS of Guam and experimental studies in deafferented neurons and in beta,beta'-iminodipropionitrile axonopathy. The American journal of pathology 144:1288–1300.

Mrak RE, Griffin WST (2007) Dementia with Lewy bodies: Definition, diagnosis, and pathogenic relationship to Alzheimer's disease. Neuropsychiatric disease and treatment 3:619–625.

Münch C, Bertolotti A (2011) Self-propagation and transmission of misfolded mutant SOD1: prion or prion-like phenomenon? Cell cycle (Georgetown, Tex) 10:1711.

Münch C, O'Brien J, Bertolotti A (2011) Prion-like propagation of mutant superoxide dismutase-1 misfolding in neuronal cells. Proceedings of the National Academy of Sciences of the United States of America 108:3548–3553.

Münch C, Rosenbohm A, Sperfeld A-D, Uttner I, Reske S, Krause BJ, Sedlmeier R, Meyer T, Hanemann CO, Stumm G, Ludolph AC (2005) Heterozygous R1101K mutation of the DCTN1 gene in a family with ALS and FTD. Annals of neurology 58:777–780.

Münch C, Sedlmeier R, Meyer T, Homberg V, Sperfeld AD, Kurt A, Prudlo J, Peraus G, Hanemann CO, Stumm G, Ludolph AC (2004) Point mutations of the p150 subunit of dynactin (DCTN1) gene in ALS. Neurology 63:724–726.

Murray ME, DeJesus-Hernandez M, Rutherford NJ, Baker M, Duara R, Graff-Radford NR, Wszolek ZK, Ferman TJ, Josephs KA, Boylan KB, Rademakers R, Dickson DW (2011) Clinical and neuropathologic heterogeneity of c9FTD/ALS associated with hexanucleotide repeat expansion in C9ORF72. Acta neuropathologica 122:673–690.

Nakagomi S, Barsoum MJ, Bossy-Wetzel E, Sütterlin C, Malhotra V, Lipton SA (2008) A Golgi fragmentation pathway in neurodegeneration. Neurobiology of disease 29:221–231.

Neumann M, Kwong LK, Truax AC, Vanmassenhove B, Kretzschmar HA, Van Deerlin VM, Clark CM, Grossman M, Miller BL, Trojanowski JQ, Lee VM-Y (2007) TDP-43-positive white matter pathology in frontotemporal lobar degeneration with ubiquitin-positive inclusions. Journal of neuropathology and experimental neurology 66:177–183.

Nishihira Y, Tan C-F, Onodera O, Toyoshima Y, Yamada M, Morita T, Nishizawa M, Kakita A, Takahashi H (2008) Sporadic amyotrophic lateral sclerosis: two pathological patterns shown by analysis of distribution of TDP-43-immunoreactive neuronal and glial cytoplasmic inclusions. Acta neuropathologica 116:169–182.

Nonaka T, Watanabe ST, Iwatsubo T, Hasegawa M (2010) Seeded aggregation and toxicity of alpha-synuclein and tau: cellular models of neurodegenerative diseases. The Journal of biological chemistry 285:34885–34898.

Papp MI, Kahn JE, Lantos PL (1989) Glial cytoplasmic inclusions in the CNS of patients with multiple system atrophy (striatonigral degeneration, olivopontocerebellar atrophy and Shy-Drager syndrome). Journal of the neurological sciences 94:79–100.

Pardo AC, Wong V, Benson LM, Dykes M, Tanaka K, Rothstein JD, Maragakis NJ (2006) Loss of the astrocyte glutamate transporter GLT1 modifies disease in SOD1(G93A) mice. Experimental neurology 201:120–130.

Pesiridis GS, Tripathy K, Tanik S, Trojanowski JQ, Lee VM-Y (2011) A "two-hit" hypothesis for inclusion formation by carboxyl-terminal fragments of TDP-43 protein linked to RNA depletion and impaired microtubule-dependent transport. The Journal of biological chemistry 286:18845–18855.

Polymenidou M, Cleveland DW (2011) The seeds of neurodegeneration: prion-like spreading in ALS. Cell 147:498–508.

Power JHT, Blumbergs PC (2009) Cellular glutathione peroxidase in human brain: cellular distribution, and its potential role in the degradation of Lewy bodies in Parkinson's disease and dementia with Lewy bodies. Acta neuropathologica 117:63–73.

Puls I, Jonnakuty C, LaMonte BH, Holzbaur ELF, Tokito M, Mann E, Floeter MK, Bidus K, Drayna D, Oh SJ, Brown RH, Ludlow CL, Fischbeck KH (2003) Mutant dynactin in motor neuron disease. Nature genetics 33:455–456.

Puls I, Oh SJ, Sumner CJ, Wallace KE, Floeter MK, Mann EA, Kennedy WR, Wendelschafer-Crabb G, Vortmeyer A, Powers R, others (2005) Distal spinal and bulbar muscular atrophy caused by dynactin mutation. Annals of neurology 57:687–694.

Pun S, Santos AF, Saxena S, Xu L, Caroni P (2006) Selective vulnerability and pruning of phasic motoneuron axons in motoneuron disease alleviated by CNTF. Nature neuroscience 9:408–419.

Ravits JM, La Spada AR (2009) ALS motor phenotype heterogeneity, focality, and spread: deconstructing motor neuron degeneration. Neurology 73:805–811.

Reddy PH, Williams M, Charles V, Garrett L, Pike-Buchanan L, Whetsell WO, Miller G, Tagle DA (1998) Behavioural abnormalities and selective neuronal loss in HD transgenic mice expressing mutated full-length HD cDNA. Nature genetics 20:198–202.

Ren P-H, Lauckner JE, Kachirskaia I, Heuser JE, Melki R, Kopito RR (2009) Cytoplasmic penetration and persistent infection of mammalian cells by polyglutamine aggregates. Nature cell biology 11:219–225.
Robbins E, Gonatas NK (1964) The ultrastructure of a mammalian cell during the mitotic cycle. The Journal of cell biology 21:429–463.
Ronzoni R, Anelli T, Brunati M, Cortini M, Fagioli C, Sitia R (2010) Pathogenesis of ER storage disorders: modulating Russell body biogenesis by altering proximal and distal quality control. Traffic (Copenhagen, Denmark) 11:947–957.
Saborio GP, Permanne B, Soto C (2001) Sensitive detection of pathological prion protein by cyclic amplification of protein misfolding. Nature 411:810–813.
Sakurai A, Okamoto K, Fujita Y, Nakazato Y, Wakabayashi K, Takahashi H, Gonatas NK (2000) Fragmentation of the Golgi apparatus of the ballooned neurons in patients with corticobasal degeneration and Creutzfeldt-Jakob disease. Acta neuropathologica 100:270–274.
Sakurai A, Okamoto K, Yaguchi M, Fujita Y, Mizuno Y, Nakazato Y, Gonatas NK (2002) Pathology of the inferior olivary nucleus in patients with multiple system atrophy. Acta neuropathologica 103:550–554.
Sapp E, Kegel KB, Aronin N, Hashikawa T, Uchiyama Y, Tohyama K, Bhide PG, Vonsattel JP, DiFiglia M (2001) Early and progressive accumulation of reactive microglia in the Huntington disease brain. Journal of neuropathology and experimental neurology 60:161–172.
Sesso A, Fujiwara DT, Jaeger M, Jaeger R, Li TC, Monteiro MM, Correa H, Ferreira MA, Schumacher RI, Belisário J, Kachar B, Chen EJ (1999) Structural elements common to mitosis and apoptosis. Tissue & cell 31:357–371.
Shults CW, Rockenstein E, Crews L, Adame A, Mante M, Larrea G, Hashimoto M, Song D, Iwatsubo T, Tsuboi K, Masliah E (2005) Neurological and neurodegenerative alterations in a transgenic mouse model expressing human alpha-synuclein under oligodendrocyte promoter: implications for multiple system atrophy. The Journal of neuroscience : the official journal of the Society for Neuroscience 25:10689–10699.
Smith MH, Ploegh HL, Weissman JS (2011) Road to ruin: targeting proteins for degradation in the endoplasmic reticulum. Science (New York, NY) 334:1086–1090.
Song YJC, Halliday GM, Holton JL, Lashley T, O'Sullivan SS, McCann H, Lees AJ, Ozawa T, Williams DR, Lockhart PJ, Revesz TR (2009) Degeneration in different parkinsonian syndromes relates to astrocyte type and astrocyte protein expression. Journal of neuropathology and experimental neurology 68:1073–1083.
Stewart H, Rutherford NJ, Briemberg H, Krieger C, Cashman N, Fabros M, Baker M, Fok A, DeJesus-Hernandez M, Eisen A, Rademakers R, Mackenzie IRA (2012) Clinical and pathological features of amyotrophic lateral sclerosis caused by mutation in the C9ORF72 gene on chromosome 9p. Acta neuropathologica 123:409–417.
Stieber A, Chen Y, Wei S, Mourelatos Z, Gonatas J, Okamoto K, Gonatas NK (1998) The fragmented neuronal Golgi apparatus in amyotrophic lateral sclerosis includes the trans-Golgi-network: functional implications. Acta neuropathologica 95:245–253.
Stieber A, Gonatas JO, Collard J, Meier J, Julien J, Schweitzer P, Gonatas NK (2000) The neuronal Golgi apparatus is fragmented in transgenic mice expressing a mutant human SOD1, but not in mice expressing the human NF-H gene. Journal of the neurological sciences 173:63–72.
Stieber A, Gonatas JO, Moore JS, Bantly A, Yim H-S, Yim MB, Gonatas NK (2004) Disruption of the structure of the Golgi apparatus and the function of the secretory pathway by mutants G93A and G85R of Cu, Zn superoxide dismutase (SOD1) of familial amyotrophic lateral sclerosis. Journal of the neurological sciences 219:45–53.
Stieber A, Mourelatos Z, Gonatas NK (1996) In Alzheimer's disease the Golgi apparatus of a population of neurons without neurofibrillary tangles is fragmented and atrophic. The American journal of pathology 148:415–426.
Streit WJ (2004) Microglia and Alzheimer's disease pathogenesis. Journal of neuroscience research 77:1–8.
Sun Z, Diaz Z, Fang X, Hart MP, Chesi A, Shorter J, Gitler AD (2011) Molecular determinants and genetic modifiers of aggregation and toxicity for the ALS disease protein FUS/TLS. PLoS biology 9:e1000614.
Takamine K, Okamoto K, Fujita Y, Sakurai A, Takatama M, Gonatas NK (2000) The involvement of the neuronal Golgi apparatus and trans-Golgi network in the human olivary hypertrophy. Journal of the neurological sciences 182:45–50.
Teuchert M, Fischer D, Schwalenstoecker B, Habisch H-J, Böckers TM, Ludolph AC (2006) A dynein mutation attenuates motor neuron degeneration in SOD1(G93A) mice. Experimental neurology 198:271–274.
Teuling E, van Dis V, Wulf PS, Haasdijk ED, Akhmanova A, Hoogenraad CC, Jaarsma D (2008) A novel mouse model with impaired dynein/dynactin function develops amyotrophic lateral sclerosis (ALS)-like features in motor neurons and improves lifespan in SOD1-ALS mice. Human molecular genetics 17:2849–2862.
Tian R, Wu X, Hagemann TL, Sosunov AA, Messing A, McKhann GM, Goldman JE (2010) Alexander disease mutant glial fibrillary acidic protein compromises glutamate transport in astrocytes. Journal of neuropathology and experimental neurology 69:335–345.
Togo T, Dickson DW (2002) Tau accumulation in astrocytes in progressive supranuclear palsy is a degenerative rather than a reactive process. Acta neuropathologica 104:398–402.

Tsao W, Jeong YH, Lin S, Ling J, Price DL, Chiang P-M, Wong PC (2012) Rodent models of TDP-43: Recent advances. Brain research 1462:26–39.

Tu PH, Galvin JE, Baba M, Giasson B, Tomita T, Leight S, Nakajo S, Iwatsubo T, Trojanowski JQ, Lee VM (1998) Glial cytoplasmic inclusions in white matter oligodendrocytes of multiple system atrophy brains contain insoluble alpha-synuclein. Annals of neurology 44:415–422.

Vargas MR, Johnson JA (2010) Astrogliosis in amyotrophic lateral sclerosis: role and therapeutic potential of astrocytes. Neurotherapeutics : the journal of the American Society for Experimental NeuroTherapeutics 7:471–481.

Vashist S, Ng DTW (2004) Misfolded proteins are sorted by a sequential checkpoint mechanism of ER quality control. The Journal of cell biology 165:41–52.

Vilariño-Güell C et al. (2009) Characterization of DCTN1 genetic variability in neurodegeneration. Neurology 72:2024–2028.

Vissers LELM, de Ligt J, Gilissen C, Janssen I, Steehouwer M, de Vries P, van Lier B, Arts P, Wieskamp N, del Rosario M, van Bon BWM, Hoischen A, de Vries BBA, Brunner HG, Veltman JA (2010) A de novo paradigm for mental retardation. Nature genetics 42:1109–1112.

Vlug AS, Teuling E, Haasdijk ED, French P, Hoogenraad CC, Jaarsma D (2005) ATF3 expression precedes death of spinal motoneurons in amyotrophic lateral sclerosis-SOD1 transgenic mice and correlates with c-Jun phosphorylation, CHOP expression, somato-dendritic ubiquitination and Golgi fragmentation. The European journal of neuroscience 22:1881–1894.

Wakabayashi K, Hayashi S, Yoshimoto M, Kudo H, Takahashi H (2000) NACP/alpha-synuclein-positive filamentous inclusions in astrocytes and oligodendrocytes of Parkinson's disease brains. Acta neuropathologica 99:14–20.

Wakana Y, Takai S, Nakajima K-I, Tani K, Yamamoto A, Watson P, Stephens DJ, Hauri H-P, Tagaya M (2008) Bap31 is an itinerant protein that moves between the peripheral endoplasmic reticulum (ER) and a juxtanuclear compartment related to ER-associated Degradation. Molecular biology of the cell 19:1825–1836.

Walkley SU, Suzuki K (2004) Consequences of NPC1 and NPC2 loss of function in mammalian neurons. Biochimica et biophysica acta 1685:48–62.

Wang F, Wang X, Yuan C-G, Ma J (2010) Generating a prion with bacterially expressed recombinant prion protein. Science (New York, NY) 327:1132–1135.

Wang L, Gutmann DH, Roos RP (2011) Astrocyte loss of mutant SOD1 delays ALS disease onset and progression in G85R transgenic mice. Human molecular genetics 20:286–293.

Watanabe M, Dykes-Hoberg M, Culotta VC, Price DL, Wong PC, Rothstein JD (2001) Histological evidence of protein aggregation in mutant SOD1 transgenic mice and in amyotrophic lateral sclerosis neural tissues. Neurobiology of disease 8:933–941.

Weedon MN, Hastings R, Caswell R, Xie W, Paszkiewicz K, Antoniadi T, Williams M, King C, Greenhalgh L, Newbury-Ecob R, Ellard S (2011) Exome sequencing identifies a DYNC1H1 mutation in a large pedigree with dominant axonal Charcot-Marie-Tooth disease. American journal of human genetics 89:308–312.

Willemsen MH, Vissers LEL, Willemsen MAAP, van Bon BWM, Kroes T, de Ligt J, de Vries BB, Schoots J, Lugtenberg D, Hamel BCJ, van Bokhoven H, Brunner HG, Veltman JA, Kleefstra T (2012) Mutations in DYNC1H1 cause severe intellectual disability with neuronal migration defects. Journal of medical genetics 49:179–183.

Williamson TL, Cleveland DW (1999) Slowing of axonal transport is a very early event in the toxicity of ALS-linked SOD1 mutants to motor neurons. Nature neuroscience 2:50–56.

Wyss-Coray T, Yan F, Lin AH-T, Lambris JD, Alexander JJ, Quigg RJ, Masliah E (2002) Prominent neurodegeneration and increased plaque formation in complement-inhibited Alzheimer's mice. Proceedings of the National Academy of Sciences of the United States of America 99:10837–10842.

Xiao Q, Zhao W, Beers DR, Yen AA, Xie W, Henkel JS, Appel SH (2007) Mutant SOD1(G93A) microglia are more neurotoxic relative to wild-type microglia. Journal of neurochemistry 102:2008–2019.

Xiao S, McLean J, Robertson J (2006) Neuronal intermediate filaments and ALS: a new look at an old question. Biochimica et biophysica acta 1762:1001–1012.

Yagi T, Ito D, Nihei Y, Ishihara T, Suzuki N (2011) N88S seipin mutant transgenic mice develop features of seipinopathy/BSCL2-related motor neuron disease via endoplasmic reticulum stress. Human molecular genetics 20:3831–3840.

Yamada T, McGeer PL, McGeer EG (1992a) Appearance of paired nucleated, Tau-positive glia in patients with progressive supranuclear palsy brain tissue. Neuroscience letters 135:99–102.

Yamada T, McGeer PL, McGeer EG (1992b) Lewy bodies in Parkinson's disease are recognized by antibodies to complement proteins. Acta neuropathologica 84:100–104.

Yamanaka K, Boillee S, Roberts EA, Garcia ML, McAlonis-Downes M, Mikse OR, Cleveland DW, Goldstein LSB (2008a) Mutant SOD1 in cell types other than motor neurons and oligodendrocytes accelerates onset of disease in ALS mice. Proceedings of the National Academy of Sciences of the United States of America 105:7594–7599.

Yamanaka K, Chun SJ, Boillee S, Fujimori-Tonou N, Yamashita H, Gutmann DH, Takahashi R, Misawa H, Cleveland DW (2008b) Astrocytes as determinants of disease progression in inherited amyotrophic lateral sclerosis. Nature neuroscience 11:251–253.

Yoo SY, Pennesi ME, Weeber EJ, Xu B, Atkinson R, Chen S, Armstrong DL, Wu SM, Sweatt JD, Zoghbi HY (2003) SCA7 knockin mice model human SCA7 and reveal gradual accumulation of mutant ataxin-7 in neurons and abnormalities in short-term plasticity. Neuron 37:383–401.

Yoshida Y, Tanaka K (2010) Lectin-like ERAD players in ER and cytosol. Biochimica et biophysica acta 1800:172–180.

Yoshiyama Y, Zhang B, Bruce J, Trojanowski JQ, Lee VM-Y (2003) Reduction of detyrosinated microtubules and Golgi fragmentation are linked to tau-induced degeneration in astrocytes. The Journal of neuroscience : the official journal of the Society for Neuroscience 23:10662–10671.

Zhao W, Beers DR, Henkel JS, Zhang W, Urushitani M, Julien J-P, Appel SH (2010) Extracellular mutant SOD1 induces microglial-mediated motoneuron injury. Glia 58:231–243.

Summary

Amyotrophic Lateral Sclerosis (ALS) is a neurodegenerative disease resulting in progressive muscle paralysis, leading to inevitable death within 3 to 5 year after diagnosis. ALS is characterized by dying of neurons that innervate the muscles; the motorneurons (MN). They are located in the spinalcord, the lower MN, and in the cerebral motorcortex, the upper MN. Both groups of MN can be affected in ALS, resulting in muscle weakness, muscle atrophy and muscle twitches when the lower MN are affected. Or showing symptoms of spasticity, muscle weakness and increased tendon reflexes when the upper MN develop pathology. Symptoms usually start in a distal limb, or the head and neck area, and spread progressively to adjacent or anatomically connected areas.
Most patients develop sporadic ALS (sALS). However, about 10 % of the patients have a family history of disease, *e.g.* familial ALS (fALS). There are about 16 genes found associated with ALS patients. In 1993 mutations in Superoxide Dismutase (SOD1) were discovered. About 20% of the fALS cases are linked to SOD1 mutations. In total over 160 mutations throughout the gene are now described. SOD1 converts superoxide radicals to water and hydrogen peroxide. Mutant SOD1 is proposed to cause disease via a gain of function.
An important discovery was the presence of Tar DNA-binding protein 43 (TDP-43) in aggregates of both sALS and non-SOD1 fALS. TDP-43 is a nuclear protein important in RNA regulation. When pathological, it translocates to the cytosol where it forms ubiquitinated, hyperphosporylated aggregates of abnormally cleaved protein. TDP-43 pathology is not only observed in ALS, also in frontal temporal dementia, Alzheimer's disease, Lewy Body dementia, and Huntington's disease the TDP-43 pathology was found. Mouse models expressing mutant and wild type TDP-43 develop pathological neurological features, however the characteristic TDP-43 cytoplasmic inclusions are rare.
A very recent discovery was an expanded GGGGCC repeat in the C9ORF72 as a major ALS gene in both fALS; up to 39%, and sALS; almost 8%. This is also highly associated with frontotemporal dementia patients.

In this thesis we focus on two mouse models. One is the model overexpressing mutant SOD1. Mouse models expressing mutant SOD1 develop a progressive MN disease, resembling the human disease. Since this phenotype in mice is very robust and predictable, they are an excellent tool to unravel the pathological features of SOD1-ALS at various disease stages. The other model expresses mutant VAPB. This protein is located in the endoplasmic reticulum (ER). The ER is important in the proper folding of proteins. Mutant VAPB was linked to ALS in 2004 and expression in either cellular cultures or mouse models result in protein aggregates highly associated with the ER.

ALS is characterized by intracellular cytoplasmic protein inclusions of misfolded protein. Even though the disease is a MN disease, other neuronal types and non-neuronal cells are affected as the disease progresses. Mutant SOD1 inclusions in interneurons, neurons having important regulatory roles on MN, are observed before the onset of symptomatic disease in

mice. Loss of interneurons specifically in the ventral horn, the area of MN, is observed from symptom onset.
Another cell type involved in ALS disease are glial cells. These are the supportive cells of the central nervous system, consisting of astrocytes, forming the blood brain barrier, modulate synapses and having a nurturing role for neurons, the microglia, the immune cells of the nervous system and oligodendrocytes, forming myelin around axons in the central nervous system.
Astrocyte activation and the appearance of mutant SOD1 aggregates in astrocytes is a late event in disease. Crossing mice with astrocyte specific expression of aggregate prone tau with an ALS mouse model shows that astrocytes are highly sensitive to aggregate prone tau in an environment of neurodegeneration. Which is shown by the formation of inclusions of pathological tau species. Even though there is evidence that astrocytes have an effect on disease progression, we did not observe a change in survival in double transgenic animals.
These data together show that the major determinants of ALS disease are the MNs, and secondary disease is spreading to neighboring cells, either anatomically or synaptically.

Another pathological feature of ALS is the slowing of intracellular transport. Mutations in dynein/dynactin, *i.e.* the motor regulating transport from the synapse back to the cell body, results in neurodegenerative disease both in mice and man. By overexpressing the N-terminus of Bicaudal 2 (BICD2-N), we inhibit dynein/dynactin function. In the BICD2-N mice no neuronal death or motor abnormalities were observed. However, pathological features, characteristic of ALS such as reduced retrograde axonal transport, axonal neurofilament swellings and Golgi fragmentation are observed in these mice. Notably, inhibiting dynein/dynactin dependent transport in an ALS-mouse model increases their life span. Possibly by attenuating signaling of damage from the axon, and postponing cellular stress reactions.
We also observed a high increase of cells with Golgi fragmentation (GF) in these mice. GF is another hallmark of ALS, however its role in disease is not clear. We show GF is an early disease phenomenon, preceding neuromuscular denervation and upregulation of the cellular stress marker, ATF3. Even though cells with GF can still take up and transport the β subunit of cholera toxin to the cell body, the distribution of this protein is altered in cells with severe GF. Furthermore, a decrease in the expression of endosomal markers is observed in cells with GF. Indicating GF is associated with altered organization of intracellular trafficking and a defect in the sorting machinery of the cell.

In mutant VAPB overexpressing mice we observe aggregates associated with the ER. These inclusions are observed in young neurons and their size and numbers do not change with ageing. However, when cellular stress is induced via axotomy of the sciatic nerve, these mutant VAPB aggregated disappear over 1 to 2 weeks. This was also observed in a minority of mutant VAPB animals that showed expression of ATF3 in MN at high age. VAPB is a protein located in the membrane of the endoplasmatic reticulum (ER). The ER is important in the proper folding of proteins, and harbors multiple defense mechanisms for misfolded proteins, that otherwise accumulate in the ER, leading to ER stress. One example is ER associated degradation (ERAD). Inhibiting the ERAD in neuronal cell cultures results

in an increased size of the mutant VAPB inclusions. Furthermore, the misfolded protein can be shielded from the rest of the cell in special ER compartments. Mutant VAPB inclusions seem to be accumulated in one of these compartments. The precise role of these inclusions is not clear, but evidence points to a protective effect by shielding the mutant protein from the rest of the cell in specific ER compartments.

ALS is a disease of the MN, progressively spreading throughout the central nervous system to other neuronal cell types and to glia. Inclusions in ALS and other neurodegenerative disease are hallmarks of these diseases. These inclusions can both have toxic and protective effects, showing ALS is a multifactorial disease.

Samenvatting

Amyotrofische Laterale Sclerose (ALS) is een ziekte van de motorneuronen, die onontkoombaar leidt tot progressieve spierverlamming en overlijden binnen 3 tot 5 jaar na diagnose. De belangrijkste parameter van de ziekte is het verdwijnen van de cellen die de spieren aansturen; de motorneuronen. Deze cellen zijn gelokaliseerd in het ruggenmerg, die direct de spieren aansturen, en in de motorcortex van de grote hersenen, die de activiteit van de motorneuronen in het ruggenmerg controleren. Deze beide groepen kunnen aangedaan zijn in ALS. Symptomen van de lagere motorneuronen zijn verzwakking en atrofie van de spieren en fasciculaties, ofwel spiertrekkingen en bij ziekte in de motorneuronen in de grote hersenen passen klachten van spastische verlamming, spierzwakte en verhoogde peesreflexen.
De meeste patiënten hebben geen familie geschiedenis van ALS, dit wordt sporadische ALS genoemd (sALS). Ongeveer 10% hebben wel familieleden met ALS in de familie (fALS). Er zijn tot nu toe 16 genen geassocieerd met de ziekte. In 1993 is een mutatie in het gen voor superoxide dismutase (SOD1) ontdekt in een familie met ALS, geassocieerd met ongeveer 20% van de fALS patiënten. SOD1 is een eiwit belangrijk voor het omzetten van toxische zuurstofradicalen naar zuurstof en waterstof peroxide. Het pathologische effect lijkt te komen door een versterkte SOD1 functie. Een grote ontdekking in het ALS veld was het voorkomen van Tar DNA-binding protein-43 (TDP-43) in inclusies in sALS en fALS patiënten. TDP-43 is belangrijk in het reguleren van RNA. Ook patiënten met frontotemporale dementie en andere neurondegeneratieve ziekten hebben deze TDP-43 inclusies. TDP-43 komt gewoonlijk tot expressie in de celkern, echter, in ziekte verplaatst het van de kern, naar het cytoplasma, waar het ophoopt in ubiquitine positieve aggregaten met pathologisch vervormd TDP-43. Muis modellen die mutant en gewoon TDP-43 tot overexpressie brengen ontwikkelen wel neuronale pathologie en zelfs tekenen van spierzwakte, maar de pathologische inclusies in het cytoplasma zijn zeer zeldzaam.
In 2011 is een zeer belangrijke mutatie in het C9ORP72 gen ontdekt, waarbij een verlenging van een GGCCCC repeat wordt gevonden. Een grote groep fALS (39%) en sALS (bijna 8%) patiënten dragen deze verlenging. Daarbij wordt een sterke correlatie gezien met patiënten die ook cognitieve problemen hebben; frontotemporale dementie.

In dit proefschrift focussen we op twee muismodellen. Het eerste model heeft een hoge expressie van mutant SOD1. Verschillende muismodellen die mutant SOD1 tot expressie brengen ontwikkelen progressieve spierzwakte en pathologie, die sterk lijkt op de pathologie van ALS patiënten. Deze muizen zijn dan ook een zeer waardevol model om de pathologie van SOD1-ALS op verschillende tijdstippen te bestuderen.
Het andere model heeft een hoge expressie van mutant VAPB. Mutaties in dit eiwit zijn ontdekt in ALS patiënten in 2004. VAPB is een eiwit in het endoplasmatisch reticulum (ER) en vormt zowel in cellulaire modellen als in muismodellen typische eiwit ophopingen in het ER.

De pathologie van ALS wordt gekenmerkt door intracellulaire eiwit inclusies van misvormde eiwitten. Hoewel ALS een ziekte is van de motorneuronen komen deze

aggregaten ook in andere neuronale types voor, zoals de interneuronen en in niet- neuronale cellen in het centrale zenuwstelsel.
De interneuronen hebben een belangrijke rol in het reguleren van de vuursterkte van motorneuronen. In deze cellen zien we pathologische inclusies voordat de muis symptomen van spierzwakte ontwikkeld. Echter, pas nadat deze aggregaten zich in motorneuronen hebben ontwikkeld. Na het begin van symptomen in de muis, met name in het gebied waar de motorneuronen zich bevinden, zien we celdood van de interneuronen.
Andere celtypen die aangedaan zijn, zijn de glia cellen. Dit zijn astrocyten, de steuncellen van het centrale zenuwstelsel met een belangrijke rol in het onderhouden van neuronen, microglia, de afweercellen van het centrale zenuwstelsel en oligodendrocyten, belangrijk in het vormen van myeline; een isolatielaag om axonen binnen het centrale zenuwstelsel.
Astrocyt activatie is een kenmerk van neurodegeneratieve ziekten. Daarnaast zien we aggregaten van mutant SOD1 in deze cellen in een laat stadium van de ziekte. Door SOD1-ALS muizen te kruisen met muizen die astrocyt specifieke tau expressie hebben, een eiwit zeer vatbaar voor aggregatie, kunnen we zien dat astrocyten erg vatbaar zijn voor aggregatie van pathologisch tau in een omgeving van neurodegeneratie. Hoewel wij geen verschil zagen in overleving tussen de verschillende muizen, is er bewijs dat astrocyten een effect hebben op de progressie van de ziekte.
Dit tezamen laat zien dat motorneuronen de eerst aangedane cellen in de ziekte zijn en dat de ziekte zich daarna verspreidt naar andere celsoorten in de buurt of via synaptische contacten.

Een ander kenmerk van de ziekte is het verslechteren van het intracellulaire transport. Mutaties in dyneine/dynactine, een eiwit belangrijk voor transport van de synaps naar het cellichaam, veroorzaken neurodegeneratieve ziekte zowel in patiënten als in muis modellen. Door de N-terminus van het eiwit Bicaudal D (BICD2-N) hoog tot expressie te brengen wordt de motorfunctie van dyneine/dynactine verstoord.
In muizen met overexpressie van BICD2-N zien we geen celdood of tekenen van spierzwakte. We zien op eiwitniveau wel karakteristieken van ALS: fragmentatie van het Golgi apparaat, axonale zwellingen met neurofilament en een vertraagd cellulair transport. Wanneer we dit muismodel kruisen met SOD1-ALS muizen, zien we dat het ziekte proces vertraagt en de muis langer leeft. Mogelijk door een vertraging in de signalering van axonale schade en daardoor een uitstel van de cellulaire stress respons. Daarnaast zien we een vermeerdering van het aantal cellen met Golgi fragmentatie.
Golgi fragmentatie is een ander kenmerk van ALS dat al vroeg in de ziekte wordt gezien, maar de rol hiervan is niet helemaal duidelijk. Wij laten zien dat in de SOD1 muis, Golgi fragmentatie al ontstaat voor het kapot gaan van axonen en voor de detectie van een cellulaire stress marker; ATF3. En hoewel cellen met Golgi fragmentatie nog steeds de niet toxische β-subunit van het cholera toxine kunnen opnemen en transporteren naar het cellichaam, verandert de distributie hiervan in cellen met ernstige Golgi fragmentatie. Dit laat zien dat cellen met Golgi fragmentatie een stoornis in de eiwitverdeling en het -transport hebben.

In muizen met overexpressie van mutant VAPB zien we inclusies die aankleuren met endoplasmatisch reticulum (ER) markers. Deze inclusies zien we al in jonge muizen en zowel het formaat als het aantal verandert niet bij veroudering. Maar, als we cel-stress veroorzaken door het axon door te snijden, dan verdwijnen deze inclusies in 1 tot 2 weken. Hetzelfde zagen we in een paar oude mutant VAPB muizen die ATF3 expressie hadden in motorneuronen.
VAPB is een eiwit dat in het ER membraan zit. Het ER is zeer belangrijk in het vormen van eiwitten. Als dit niet goed lukt, heeft het ER verschillende manier om het op te lossen en niet verstopt te raken met misvormd eiwit. Dit leidt tot ER stress. Een voorbeeld van een ER stress mechanisme is het ER geassocieerde degeneratie (ERAD). Ook kan het misvormde eiwit in speciale ER compartimenten geplaatst worden en zo is de rest van de cel beschermd tegen het gemuteerde eiwit. De VAPB inclusies lijken in een beschermd ER compartiment te zitten. Als ERAD geremd wordt in gekweekte neuronen, zien we dat het formaat van de inclusies toeneemt, wat laat zien dat de VAPB inclusies een nauwe relatie met ERAD hebben.
De precieze rol van deze ER compartimenten is niet geheel duidelijk, maar ze lijken een beschermend effect te hebben door het gemuteerde eiwit weg te houden van de rest van de cel.

ALS is een ziekte van de motorneuronen, die zich progressief verspreidt door het centrale zenuwstelsel naar andere soorten neuronen en glia cellen. Inclusies zijn een van de belangrijkste kenmerken van ALS en andere neurodegeneratieve ziekten. Deze inclusies kunnen zowel toxisch als beschermend zijn, en laten dus zien dat ALS een ziekte is met meerdere oorzaken en specifieke pathologische beelden.

Curriculum Vitae

Personal details:

Name:	Vera van Dis
Adress:	
Date of Birth	Februay 2nd 1985
Place of Birth:	Rotterdam

Education:

1997-2003:	GSG Helinium Profiel: Natuur en Gezondheid 27 juni 2003; Vwo-diploma
2003-2007:	Erasmus University, Rotterdam Geneeskunde 31 Augustus 2007; Doctoraal
2006-2008:	Erasmus University, Rotterdam Master of Neuroscience 25 augustus 2008; Master of Science
2011-present	Erasmus University, Rotterdam Geneeskunde Co-schappen

Work:

2008-2012	Phd student Department of Neuroscience supervisor: Dr. Dick Jaarsma Promotor: prof. Chris de Zeeuw The role of inclusions in ALS pathogenesis
2009- 2010	Support Karin Boekhoorn (Postdoc in the lab of Casper C. Hoogenraad) The characterization of Stathmin family proteins

Workshops, teaching and courses:

2008-2011	-Ondersteuning onderwijs voor dr. D. Jaarsma vaardigheidsonderwijs embryologie, placenta en het oog -Practicle guidence for several students from: Master of Neuroscience Rotterdam, Master Molecular Medicine Rotterdam, HLO Rotterdam, Master of Neurscience Utrecht, Bachelor Biologie Amsterdam.
Oktober 2008	Article 9 course
April 2009	Boerhave Course: Transgenesis, Gene Targeting and in vivo Imaging
May 2009	cursus boerhave: Signal transduction pathways regulating aging and disease

June 2009	MGC workshop Brugge
2009 and 2010	Tutor of a group of students from Geneeskunde Rotterdam
February 2010	Workshops: high resolution and deconvolution
June 2010	MGC workshop Cologne

Publications:

*Hossaini M, Cano SC, **van Dis V**, Haasdijk ED, Hoogenraad CC, Holstege JC, Jaarsma D (2011) Spinal Inhibitory Interneuron Pathology Follows Motor Neuron Degeneration Independent of Glial Mutant Superoxide Dismutase 1 Expression in SOD1-ALS Mice. J Neuropathol Exp Neurol 70:662-677.

*Teuling E, **van Dis V**, Wulf PS, Haasdijk ED, Akhmanova A, Hoogenraad CC, Jaarsma D (2008) A novel mouse model with impaired dynein/dynactin function develops amyotrophic lateral sclerosis (ALS)-like features in motor neurons and improves lifespan in SOD1-ALS mice. Hum Mol Genet.

Posterpresentation

***Vera van Dis**, Elize D. Haasdijk, Mark S. Forman, Casper C. Hoogenraad, & Dick Jaarsma; 6th international conference on frontotemporal dementias 2008: Neuronal degeneration facilitates the formation of pathological inclusions in surrounding astrocytes in SOD1-ALS mice

***Vera van Dis**, Karin Boekhoorn, Elize D. Haasdijk, Marc S. Forman, Casper C. Hoogenraad & Dick Jaarsma; ENP 2009 8th Dutch Endo-Neuro-Psycho Meeting; Neuronal degeneration facilitates the formation of pathological inclusions in surrounding astrocytes in SOD1-ALS mice

***Vera van Dis**, Elize D, Haasdijk, Casper C. Hoogenraad & Dick Jaarsma**;** FENS Abstr. vol 5, 136.20, 2010 Golgi fragmentation in amyotrophic lateral sclerosis (ALS) motor neurons precedes neuromuscular denervation and is associated with intracellular transport abnormalities

***Vera van Dis**, Elize D, Haasdijk, Casper C. Hoogenraad & Dick Jaarsma**;** MGC workshop cologne 2010; Golgi fragmentation in amyotrophic lateral sclerosis (ALS) motor neurons precedes neuromuscular denervation and is associated with intracellular transport abnormalities

Oral Presentations

***Vera. van Dis**, Elize D. Haasdijk, Casper C. Hoogenraad, Marc S. Forman, Dick Jaarsma; ENP 2008 7th Dutch Endo-Neuro-Psycho Meeting; Neuronal degeneration in SOD1-ALS mice facilitates aggregate formation in surrounding astrocytes

*__Vera van Dis__, Karin Boekhoorn, Lukas C. Kapitein, Casper C. Hoogenraad; Intercity young scientist meeting 2010; The tubulin binding protein Stathmin has a function in dendritic branching

* __V. van Dis__, Elize D. Haasdijk, Casper C. Hoogenraad, Marc S. Forman, Dick Jaarsma; Second Neuroscience Retreat 2009; Glial protein aggregation is facilitated by neuronal degeneration in a SOD1-ALS mouse model

Dankwoord

Na 4,5 jaar op de afdeling Neurowetenschappen kan ik eindelijk een dankwoord schijven. In de afgelopen jaren heb ik veel leuke dingen gedaan, veel mensen ontmoet en samengewerkt. Ik zal proberen het een beetje kort te houden. Ik hoop dat ik niemand vergeet.
Waarschijnlijk lijkt het na het lezen van dit dankwoord dat ik mijn tijd op de afdeling vooral heb volgemaakt met borrelen, kletsen en koffie drinken. Gelukkig ligt voor u het bewijs dat ik ook nog aardig wat uren op het lab en achter de microscoop heb doorgebracht. Hoewel ik echt een fantastische tijd heb gehad, is nu toch de tijd gekomen dat ik mijn studie geneeskunde af moet ronden. Wat daarna komt, zal alleen de tijd kunnen leren.

Als afdelingshoofd en promotor kan **Chris de Zeeuw** niet ontbreken. Na het voltooien van mijn master kon ik dankzij u op de afdeling blijven en beginnen aan het avontuur dat ik nu aan het afsluiten ben.

Mijn tweede promotor, **Casper Hoogenraad**. Inmiddels gesetteld in Utrecht om daar een eigen afdeling te leiden. Het bespreken van het werk met Marijn en Dick was altijd erg gezellig en verrassend genoeg ook productief. De afdeling is waarschijnlijk nog immer aan het groeien en ik twijfel er niet aan dat er nog aardig wat Cell en Science papers uit zullen voortvloeien.

Dick, als ontwetende masterstudent begon ik in 2007 in jou groepje. Hoewel je vond dat ik teveel met sport bezig was, hoop ik dat ik toch genoeg data geproduceerd heb. Als student heb ik ontzettend veel geleerd van je, hoewel ik soms tussen de regels door moest luisteren. Ik heb altijd het idee gehad dat je zoveel weet, dat het er soms niet helemaal duidelijk uit komt. Ook is je werk met confocal plaatjes zó goed, dat op de een of andere manier zijn mijn plaatjes nooit zo mooi als die van jou. Etentjes en besprekingen waren ontzettend gezellig. Zonder jou briljante ideeën zou dit boekje er absoluut niet zijn.

Mijn leescommissie: **Prof.dr. J.M. Kros, Prof. dr. P.A.E. Sillevis Smitt en Prof.dr. D.N. Meijer** wil ik bedanken voor het lezen en goedkeuren van dit proefschrift. Helaas kunnen Prof.dr. J.M. Kros, Prof. dr. P.A.E. Sillevis Smitt niet in mijn grote commissie plaatsnemen, toch ben ik blij dat u tijd voor mijn proefschrift heeft willen vrijmaken

Natuurlijk kan ook hier mijn grote commissie niet ontbreken. **Joost Jongen**, leuk dat u af toe een kamergenoot was. De combinatie neuroloog en wetenschapper lijkt mij een moeilijke. Ik vind het zeer bewonderingswaardig hoe u beide zaken combineert. **Joan Holstege**, ik moet altijd erg lachen om uw humor en tijdens de gesprekjes over mijn onderzoek wist u toch altijd de juiste vraag te stellen. **Gerard Borst**, gelukkig had u altijd wel tijd voor een kort praatje bij het koffieapparaat. **Rob Willemsen** Ik wil jullie allen bedanken dat jullie tijd vrij maken om mij het vuur aan de schenen te leggen.

De meeste tijd heb ik doorgebracht op het immer gezellige histolab. Mijn paranymfen, **Elize,** al gewend om Dickiaans te lezen, wat een enorme hulp was. Bij issues met lab en leven kon ik altijd bij je terecht. En natuurlijk ook voor pindarotsjes, en heerlijke taarten. Als drijvende kracht achter de borrel zorg je voor veel gezelligheid en binding op de afdeling. Zonder jou hulp met muizen en kleuringen had ik het allemaal niet gered
Erika, mijn buurvrouw op het lab. Eerlijk en glashelder, soms wat kort door de bocht, maar dan weet ik precies waar ik aan toe ben. Tussen het spoelen door was er altijd wel tijd om even te babbelen over de verbouwing van het huis, de schoolissues van Job en natuurlijk mannen issues. In mijn co-schappen let ik toch wat beter op mijn kleding en dan heb ik toch vaak jouw commentaar in mijn achterhoofd als steuntje.
Fellow Histolab inhabitants, always time for a chat and exchanging histology tips and trics: **Aram, Liron, Shoista, Zineb, Sheena, Behdokht, Malik, John, Ru, Lucia, Haibo, Thijs, Carolien.** Thank you all for an amazing time.

Groep Dick, door de jaren zeer van samenstelling verandert, maar de rode draad is toch dat Dick zich graag omringt met vrouwen. **Suzan**, toen bezig met de afstudeerstage, je hebt mij de eerste stapjes van het immuno doen geleerd. Studenten die bij Dick onderzoek kwamen doen: **Brenda, Lucas, Ilse, Mani** (succes met de bin, vergeet vooral niet om zo enthousiast te blijven!). Ik hoop dat jullie een leuke tijd hebben gehad. **Filipa**, I hope you are able to use your lab skills from the masters in your future career. I hope you can be at my defense. **Cindy**, je aanwezigheid op de afdeling zal altijd zichtbaar blijven in het em-snijhok. En ik zal er altijd toch weer om moeten grinniken. Ben blij dat je mijn enthousiasme over het werk deelt, dat kom je toch niet vaak tegen.

En de verschillende mensen met wie Dick samenwerkte: **Monique Mulder**, helaas was statine injecteren in muizen niet succesvol. **Monique de Waard** en **Yvonne Rijksen**; Tussen de bedrijven door was het altijd gezellig op het histolab. Ik ben blij dat ik altijd AT8 antibody kon gebruiken. **Wiep Scheper**, ook al hebben we elkaar nooit ontmoet, Ik ben blij dat we een goede negatieve controle hebben kunnen leveren voor ER-stress experimenten. And **Elisa**, Thanks so much for reading and correcting parts of my thesis. And for your hard work bringing the department closer together.

Ook heb ik wat tijd op het mollab doorgebracht. In het algemeen wil ik jullie bedanken voor de gezellige BBQs, de leuke weekendjes, de gezellige gesprekken en borrels. **Karin**, ik heb een jaartje voor je gewerkt. Zo heb ik kunnen proeven van het kloneren en omgaan met celkweek. Hoewel mijn experimenten niet altijd vlekkeloos gingen, hoop ik dat je er toch nog een mooi artikel van kan maken. In die tijd heb ik gezellig een bench gedeeld met **Robert**, gelukkig wilde je altijd de bovenste plankjes gebruiken en alle hoge dingen voor mij pakken. **Phebe**, voor het altijd klaar staan met hulp en advies bij experimenten. Ook **Nanda**, voor het helpen met de yeast -2 hybrid screens, en natuurlijk voor het maken van neuronen. **E***, altijd tijd voor een praatje. En natuurlijk voor de chocolaatjes en vooral de gedichtjes met sinterklaas. **Marijn**, naast al je andere projecten, werkte je gelukkig ook aan VAPB. Het artikel is zeer mooi aan het worden, mede door jouw experimenten. Ook heb je een paar bijzonder leuke restaurants uitgezocht in Utrecht voor onze maandelijkse paper

besprekingen. **Carol**, you started as a student of Eva and we quickly became friends. I love the Chinese food and all the nice drinks and dinners we have. **Eva**, toen ik begon bij Dick heb jij mij de eerste truukjes van het blotten en metamorph geleerd. Ook het pcr-en en handelen van de muizen En ook nu, in het laatste stukje van mijn PhD heb je bijgedragen door mijn discussie en inleiding door te lezen. Heel veel geluk in Groningen en het begrijpelijk maken van wetenschap voor het grote publiek.
Daarnaast waren de vrijdag ochtend besprekingen altijd zeer nuttig. Waarbij ik natuurlijk **Anna Akhmanova** en haar groep niet kan weglaten. Anna, it is amazing how you always know all new literature and all proteins and their function. The other members of the group: **Babet, Ilya, Max, Kah Wai, Myrrhe, Lukas, Martha, Benjamin, Kai, Renu, Mariella, Andrea, Chris (van Esther).** Thanks to all for the useful Friday mornings and drinks/chats/help/cakes/dinners/parties.

De omgeving van mijn kamerje was ook altijd druk met kleurrijke mensen, die het werk nog weer leuker maakten. Buurman **Hans**, je klusvaardigheid en kennis zijn een gemis op de afdeling. **Tom**, je anatomishe kennis en de kennis van tracers is van onschatbare waarde. Helaas ben je niet aanwezig bij mijn verdediging, ik had het een eer gevonden als je in mijn commissie had gezeten. **Rogerio,** je belevenissen zorgden voor interessante gesprekken.

Mijn werk had ik niet kunnen doen zonder de muizen. Voor de goede zorgen en het altijd beantwoorden van mijn vragen wil ik graag **Ineke Maas** en haar collega's bedanken. **Mandy**, door je zorgzame instelling kon ik altijd bij je terecht, voor muizen issues of als mijn taq weer eens op was. Ook heb ik goed gebruik gemaakt van de verschillende confocal microscopen, waarvoor mijn dank uit gaat naar het oic. **Gert van Cappellen, Alex Nigg** en **Adriaan Houtsmuller** voor het onderhoud en hulp als er weer eens wat vastliep. **Ype,** inmiddels Professor Elgersma en **Geeske**, doordat ik de rotarod wekelijks kon gebruiken heb ik mooie data kunnen verzamelen.

Ook de dames van het secretariaat kan ik hier niet vergeten. **Loes, Edith** en **Suzan**. De koekjes van Edith, en de altijd goed gevulde snoeppot waren een welkome afwisseling van mijn boterhammetjes. Ik keek toch altijd even met een schuin oog of er nog wat lekkers lag als ik langs jullie kantoor liep. Ook kon ik natuurlijk altijd terecht voor hulp bij e-mail problemen, pedel, en andere zaken. En natuurlijk gewoon een praatje over alledag. Wat soms ook hard nodig was.
Kenneth en **Annette**, nooit te beroerd voor een feestje, maar gelukkig ook altijd behulpzaam bij bestellingen en budgetnummer.

Tijdens de lunch in de koffiekamer was het immer gezellig. Elize, Erika, Tom, **Marcel**, Sheena, **Lucia,** en de overige mensen die regelmatig aanschoven aan tafel. Het gaf even een momentje rust tijdens een drukke dag.
And off course a lot of people that I didn't mention yet. But who made a round to the coffee machine a social event and the Friday drinks a good end of the week (even continuing outside the department), **Milly**, **Thijs**. **Taf, Lieke, Corstiaan, Aleksandra, Susan, Jeanette, Arman, Jolet.**

Petra, buiten je expertise op het lab kan ik gelukkig altijd bij jou terecht voor een drankje en een dansje. Hopelijk heb ik daar straks weer meer tijd voor. **Linde,** op verschillende meetings hebben we kamers gedeeld. Je nuchtere kijk op de wereld is erg prettig. Jouw baas zit in mijn commissie, gaat mijn baas dan ook in jouw commissie?

Dan zijn er natuurlijk nog een hoop vrienden bij wie ik terecht kon om mijn frustraties over het schrijven te uiten. Danwel begrip toonden als ik niet mee kon gaan stappen. Ik vind het geweldig dat iedereen zo begripvol en trots is! **Inez** en **Charlotte**, inmiddels kan ik gelukkig steeds beter de medisch getinte gesprekken volgen. **Barry,** hoewel we elkaar niet vaak zien, is het toch altijd weer gezellig. **Andreea**, ik ben enorm gevleid dat ik je paranimf mag zijn. Ik ga mijn uiterste best doen je te helpen waar ik kan. (een dag co-schap missen kan gelukkig wel). **Bo. Esther, Machiel (en Jori en Kian)**, **Kor en vele anderen.** Ik voel me aardig schuldig dat ik zo lang niks heb laten horen. Hier voor je hebben jullie de oorzaak liggen (en mijn excuus). **Kevin**, ik ben bang dat het niet meer gaat lukken voor je trouwen af te spreken, maar 21 september ben ik zeker van de partij. **JanWillem** en **Heleen,** jullie huisje begint steeds mooier te worden, ben benieuwd naar de hot-tub, ik wil hem graag uitproberen! Mijn co-groepje, ik hoop veel van jullie ze zien op mijn feestje!

Sporten is altijd erg belangrijk voor me. Ik kan helaas niet iedereen bij naam noemen, maar vul jezelf gerust hier in als je vind dat je erbij hoort. **Willeke,** ik blijf trots op 'onze' zwarte band. Ik ben heel benieuw hoe Deventer gaat bevallen. En ik blij dat je nu tijd vrijmaakt om mijn samenvattingen nog eens kritisch te lezen. **Jerry,** je kwam precies op het juiste moment aanlopen bij EDS. Ik hoop dat we komend ETDS een mooie show kunnen neerzetten!

Constance en **Frans,** ik voelde me vanaf het begin thuis bij jullie, nu echt als een deel van het gezin. Ik vind het erg leuk dat jullie aanwezig zijn bij de verdediging en de feestelijkheden. **Jeroen**, ook al heb ik de layout uitendelijk niet met LaTex gemaakt, je bereidheid om te helpen was zeer welkom.

Als laatste dan eindelijk mijn familie. **Pap** en **Mam,** helaas kunnen jullie niet bij mijn verdediging aanwezig zijn. Gelukkig is er nu dit boek, een blijvende herinnering aan mijn prestatie. Ik ben trots op wie ik ben en wat ik doe, mede dankzij jullie betrokkenheid en doordat jullie me steunen in al mijn keuzes. **Mirte, Elise** Ik ben blij dat we als zussen zo een goede band hebben. Dat lijkt met toch iets bijzonders. **Frank**, ik kan je inmiddels wel mijn zwager noemen. Ik kom graag snel weer koffie drinken en ik moet nog steeds een 3D film kijken op jullie mega-scherm. Als laatste **Michiel**, ik heb je eindelijk in pak gekregen! (moeten we nog wel gaan kopen, dus ik hoop dat het doorgaat). Je hebt heel wat scheldpartijen en frustratie momenten moeten doorstaan. Je doet zoveel voor me, ik zou niet weten waar ik moet beginnen met bedanken. Je hulp bij mijn kaft, je geweldige kookkunst, het bouwen van kapstokken en banken, reparaties uitvoeren, marktplaats afstruinen voor mij; en meer, echt te veel om op te noemen. Zonder jou steun had ik dit echt nooit gered